DESIGN AND CHARACTERISATION OF EDIBLE BIOPOLYMER MIXTURES FOR USE IN ADDITIVE MANUFACTURING

by

ELEANOR LUCY WARNER

A thesis submitted to

The University of Birmingham

for the degree of

DOCTOR OF PHILOSOPHY

School of Chemical Engineering

College of Engineering and Physical Sciences

The University of Birmingham

April 2019

ABSTRACT

Recent interest in personalisation of food through additive manufacturing has identified a need for more information on the formulation and printability of potential ingredients. Fused deposition modelling is a type of additive manufacturing technique which uses a thermal extrusion process in order to create objects in a layer by layer method. Key challenges posed for the creation of formulations using this additive manufacturing technique include the need for the material to be thermoreversible, shear thinning during extrusion, but then have the ability to retain its shape after extrusion. The majority of research of edible manufacturing using this technique have thus far only been investigated at single temperatures and predominately on materials that only maintain their shape due to a yield stress, reducing the amount of available materials. Therefore, the aim of this work was to develop novel edible material feedstocks for the creation of objects through the use of an additive manufacturing process.

Initially, the printability of a mixture of two food hydrocolloids, gelatin and kappa-carrageenan, were investigated. Design rules were established in order to determine if the materials fit the requirements of the process. The gelling temperatures of the systems were established, then, the rheological characteristics including: flow profiles, evolution of elastically dominated structures and frequency dependent behaviour were examined. The mixtures were subsequently printed at two temperatures, just above and much greater than, the gelling temperatures. It was observed that the rheological behaviours accompanying the coil-helix transitions of the systems were key to printing in a well-defined way. Printing resolution could be described by the changes in elastic modulus, where rapid formation of an elastic network gave rise to highly defined shapes with the ability to self-support under multiple layers.

The printability of the mixtures of gelatin and kappa-carrageenan were then further probed by changing the properties of the printer, including the nozzle diameter, printing temperature and printing speed. Alteration of these properties affected the viscosity of the material during extrusion, which affected the behaviour of the material and altered the printability. The viscosity of the formulations at various speeds and temperatures was established, and these were related to the printability. Further design rules were established in order to deepen the understanding of the properties necessary for a material to possess in order to be printable. It was also shown that with the materials that met the design rule criteria, a range of mechanical properties could be produced using these two biopolymers, just by altering the properties of the printer.

Finally, it was demonstrated that the design rules established held for formulations of gelatin and other secondary biopolymers (gellan and agar). Relevant testing, including establishing the gelling temperature, and investigation of the rheological characteristics including the frequency sweeps was undertaken in order to determine the material properties of the new formulations. The formulations that met the design rules produced defined printed objects, whereas the formulations which did not meet the design rules did not. Complex structures, including a ring and a star were able to be printed using several of the formulations.

Overall, this thesis demonstrates the range of formulations which can be printed, as well as exhibiting some of the exciting structures that can be produced using an additive manufacturing technique.

ACKNOWLEDGEMENTS

I would firstly like to express my gratitude to my supervisors, Dr. Tom Mills and Professor Ian Norton for all of their help and guidance throughout my research time. I will always be grateful for this opportunity and for all of your encouragement along the way.

I would also like to thank Dr. Vadodaria and the other research associates for all of their support and assistance with my project. The many conversations about my work and the help provided within the lab were invaluable.

To all of the academics and industrial partners of the Centre of Innovative Manufacturing in Food (CIM), thank you for all for the thought provoking discussion during the annual conferences and other meetings.

I am very appreciative of the funding provided by the Engineering and Physical Sciences Research Council (EPSRC) and for the University of Birmingham for allowing me to complete this work.

A special thanks to the encouragement that I have received from the support staff including Lynn Draper and Chris Dickinson who have always been there for any question, big or small.

My time at the University of Birmingham would not have been the same without the network of friends that I have made during my time here. They have helped me through the good and the bad times of the PhD and my time here would not have been the same without them.

Finally, I would like to say a massive thank you to my family, especially Mum, Dad, Lyzzie and Granna. This would have not been possible without your unwavering support and constant encouragement. Thank you.

TABLE OF CONTENTS

LIST OF FIGURES

LIST OF TABLES

LIST OF EQUATIONS

NOMENCLATURE

Rheology

G’	Elastic or Storage modulus (Pa)
G”	Viscous or Loss modulus (Pa)
G*	Complex modulus
k	Cross time constant (s)
LVR	Liner Viscoelastic Region
η	Viscosity (Pa.s)
r	Radius (m)
R	Radius of measurement geometry (m)
τ	Shear stress (Pa)
δ	Phase shift (˚)
v	Velocity ($m.s^{-1}$)
$\dot{\gamma}$	Shear rate (s^{-1})
ω	Angular velocity ($rad.s^{-1}$)
ϑ	Angle of cone (˚)
Γ	Torque (Nm)

µDSC (Micro differential scanning calorimetry)

T_g	Glass transition temperature (˚C)
T_c	Crystallisation temperature (˚C)

T_m Melting temperature (˚C)

TA (Texture Analyser)

ε_E Engineering strain

H Height (m)

ε_H True strain

σ_E Engineering stress (Pa)

F Compression force (N)

A_0 Area (m^2)

σ_H True stress (Pa)

Printing

d_p Print moves distance (mm)

d_{np} Non-print moves distance (mm)

Q Flow rate ($m^3.s^{-1}$)

R Radius of the nozzle (mm)

S_p Speed of print moves ($mm.s^{-1}$)

S_{np} Speed of non-print moves ($mm.s^{-1}$)

T_g Gelation temperature (˚C)

t_{tot} Total printing time (s)

t_p Time for the print moves (s)

T_p Printing temperature (˚C)

t_{np} Time for non-print moves (s)

V Volume of the printed part (m^3)

Abbreviations

2/3D Two/Three dimensional

ABS Acrylonitrile butadiene styrene

AM Additive Manufacturing

ASTM American Society for Testing and Materials

CAD Computer Automated Design

DSC Differential scanning calorimetry

EMF Extrusion multiplier factor

FDM Fused deposition modelling

GRAS Generally regarded as safe

HDPE High density polyethylene

HIPS High impact polystyrene

IP Intellectual property

PA Polymaide

PC Polycarbonate

PLA Polylactic acid

RP Rapid Prototyping

STL Stereolithography

CHAPTER 1. INTRODUCTION

1.1 Motivation and Background

Additive Manufacturing (AM) refers to the mass manufacturing process of making an object through the deposition of materials layer upon layer, as opposed to subtractive manufacturing or injection moulding in order to create an object (ASTM Standard, 2012). Being able to design and control the microstructure within food products through the addition of materials, could have a huge impact on the food industry. It would enable the production of food with detailed ingredient distribution meaning a highly efficient use of the materials (Diaz et al., 2014). Additively manufactured food could also lead to the creation of products with predefined textural and release properties, which could be tailored to the individual consumer's requirements. In order for the additive manufacturing of edible substances to become sustainable in the modern world, the process has to deliver new food products which can be commercialised or an increase in the flexibility of current food manufacturing method, with a significant time or cost benefit (Wegrzyn et al., 2012).

A priority with the creation of an AM produced object is ensuring that the printed objects are precise and accurate compared to the desired shape. Liu et al. (2017) determined that there are several key aspects which are involved in the creation of a precise and accurate printed part. These include:

- Additive manufacturing technique- material extrusion, binder jetting etc.;
- Material properties- rheological properties, gelling and melting transition temperatures etc.;
- Processing factors- nozzle height, diameter and extrusion speed etc.;
- Post-processing treatments.

Within this work, each of these areas have been investigated and an assessment has been presented within the following chapters.

Compared with other substances, such as metals and plastics, AM has been slow to move into the food industry, as the complex nature of foods pose many challenges: multi-component, controlled microstructures for sensory attributes, multiple thermal transitions and polymorphs *etc*. The majority of current research into additive manufacturing of food is based on creating aesthetically pleasing shapes. Although these novel creations have a place in the culinary world and are introducing consumers to the ideas of additively manufactured food, the relevance to the wider food community as well as the material science development is rather limited. The full potential of AM of food is much wider and encompasses the ability to create personalised food products with respect to composition and texture (Noort et al., 2017).

Edible materials requiring constructs with intrinsically high viscosities lend themselves well to extrusion based AM techniques; as the print head can be controlled to withstand higher pressures. The majority of reports on AM of food have therefore used an extrusion process. Some gel-like edible materials have prohibitively high stiffness at ambient temperature for extrusion. However, a subset of these materials go through a gel-sol transition at higher temperatures, i.e. their viscosity and elasticity falls within the range of processability. Of these materials, gelatin was chosen for its high strength, high viscosity and thermoreversibility. The secondary biopolymers, kappa-carrageenan, gellan and agar where chosen to increase the gelling temperature, speed of gelation and further increase the strength.

Overall, the main aim of this project was to develop novel edible material feedstocks for the use in an additive manufacturing process. In order to design these products, the microstructural approach to food formulation engineering was applied, with a schematic representation shown in Figure 1.1 (Norton and Foster, 2002). This approach recognises that the process and

ingredients are linked, forming the microstructure, which in turn dictates the material properties and then the consumer response.

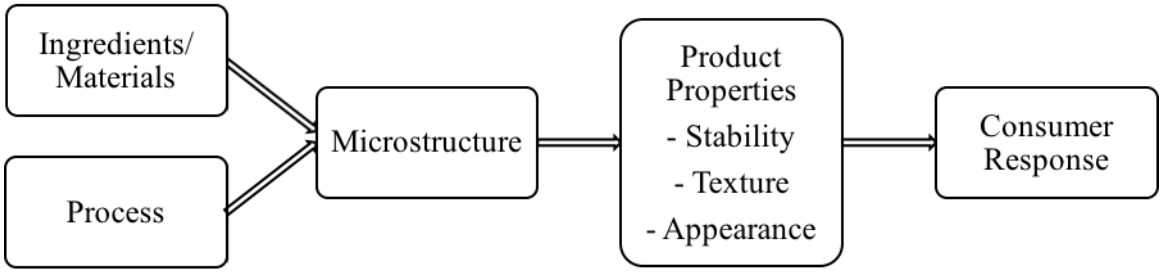

Figure 1.1. Schematic representation of the approach taken in the design of food microstructures, linking the ingredients and processing parameters with the sensory response to the consumers. Adapted from Norton and Foster (2002).

For this work, this diagram can be altered in order to give a more specific approach to how this study was undertaken. This looks at a more dynamic approach, representing how each of the areas are linked and through knowledge of two of the sections can lead to a better prediction of the third section. Initially the materials were chosen and their characteristics were investigated in order to determine the microstructure. These materials were then printed and the printability was related back to the material characteristics, which were then optimised using the changes in microstructure of formulation, in order to achieve a well-defined printed object. An effective feedback loop was established between the printing results and the material properties in order to achieve a greater range of printable materials.

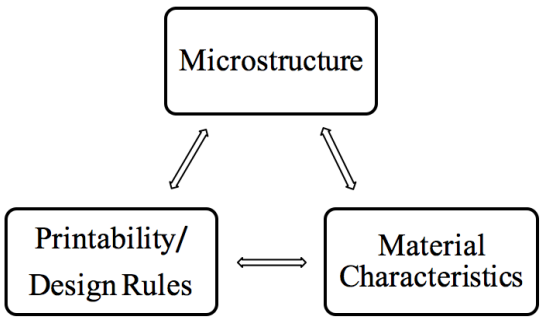

Figure 1.2. Schematic representation of the altered design approach for the printability of edible formulations.

1.2 Objectives

The ultimate goal of this project was to develop novel edible material feedstocks which could be used in an extrusion based additive manufacturing process. The focus was directed towards gaining a better understanding of what is required from a material in order for the material to print defined objects. The key research objectives included:

- To determine the suitable raw materials to be used for the AM technique;
- To investigate the thermal and mechanical properties of a temperature dependent solution and then correlate these properties with the printability of the material;
- To expand the knowledge and understanding of the effects that the AM processing conditions have upon material feedstock;
- To determine design rules for the printability of edible feedstocks.

1.3 Thesis layout

Chapter 2 consists of a critical literature review of work in the areas of additive manufacturing specifically looking at the different types of additive manufacturing and how each of these have been used with regards to edible substances. As well as this, an overview into the background knowledge of hydrocolloids has been provided and an investigation of how hydrocolloids have been printed in other industries has been conducted;

Chapter 3 provides a detailed description of the materials and method used within this work, including detailed descriptions of the different pieces of analytical equipment used;

Chapter 4 contains the results of the finding from initial material characterisation of mixtures of gelatin and kappa-carrageenan and their subsequent printability. Preliminary design rules are established in order to determine how well these formulations will print. This chapter has been

published in a peer reviewed journal under the title: "*Comparing the viscoelastic properties of gelatin and different concentrations of kappa-carrageenan mixtures for additive manufacturing applications*" (Warner et al., 2019);

Chapter 5 presents a more comprehensive investigation into how some of the printing properties including nozzle diameter, printing temperature and printing speed affect the printability of formulations of gelatin and kappa-carrageenan. The results of the printability of these formulations have then been used in order to create a more detailed set of design rules to be used for materials which undergo similar transitions;

Chapter 6 uses the design rules found from the two previous chapters and determines if these rules can be used for gelatin with a different secondary biopolymer (gellan and agar), which use the same gelling mechanism;

Finally, **Chapter 7** summarises all of the main findings within the research and highlights potential areas for future work in order to improve the developed rules.

1.4 Publications and presentations

Results obtained throughout this study have been published and presented as follows:

Publications

- **Warner, E.L.**, Norton, I.T., Mills, T.B., (2019) Comparing the viscoelastic properties of gelatin and different concentrations of kappa-carrageenan mixtures for additive manufacturing applications. *Journal of Food Engineering.*

Oral Presentations (Speaker in bold)

- **Warner, E.L.**, Norton, I.T., Mills, T.B., Comparing the viscoelastic properties of gelatin and kappa-carrageenan mixtures to their printability, 14th International Hydrocolloids Conference, China, 2018.
- **Warner, E.L.**, Norton, I.T., Mills, T.B., Comparing the viscoelastic properties of gelatin and kappa-carrageenan mixtures to their printability, CIM in Food 4th Annual Conference, Nottingham, 2018.
- **Warner, E.L.**, Norton, I.T., Mills, T.B., The formulation and characterisation of edible based filaments, CIM in Food 3rd Annual Conference, Birmingham, 2017.

Poster Presentations

- **Warner, E.L.**, Norton, I.T., Mills, T.B., Comparing the viscoelastic properties of gelatin and kappa-carrageenan mixtures to their printability, CIM in Food 4th Annual Conference, Nottingham, 2018.
- **Warner, E.L.**, Norton, I.T., Mills, T.B., The formulation and characterisation of edible based filaments, CIM in Food 3rd Annual Conference, Birmingham, 2017.
- **Warner, E.L.**, Norton, I.T., Mills, T.B., The formulation and characterisation of edible based filaments, KTN Early Career Researchers in Food Event, Manchester, 2016.
- **Warner, E.L.**, Norton, I.T., Mills, T.B., Creation of a gelatin based edible filament for use in fused deposition modelling, CIM in Food 2nd Annual Conference, Loughbourgh, 2016.

CHAPTER 2. LITERATURE REVIEW

2.1 Introduction

This chapter provides a critical literature review of the work in the areas of additive manufacturing, closely investigating the areas looking into additive manufacturing of edible materials. After this, there is a detailed investigation into hydrocolloids, focusing on the hydrocolloids used within this work and their mixtures.

2.2 Additive Manufacturing

It is widely acknowledge that the first form of additive manufacturing was stereolithography (SLA), invented by Charles Hull in 1987 (Wohlers and Gornet, 2012). Initially Hull used SLA for the rapid prototyping (RP) of plastic parts in order to speed up the design cycle for the creation of new parts (Hull, 2015). These first printed parts were 'rough' looking objects which were slow and expensive to print and, due to the size of the machine, only small objects could be created (Rayna and Striukova, 2016). However, with the advancement of technology, which led to an increase in the speed, accuracy and quality of the product, additive manufacturing is beginning to find its use in the production of final-use products. As well as this, expiration of early patents and cheap hardware has encouraged hobbyists to take up AM, which has led to a relatively quick understanding of how they work and spurred the rapid growth in the consumer-grade 3D printer market (Hoy, 2013). Through use of open access websites such as the RepRap wiki forum or thingiverse, enthusiasts are able to create new designs for printers or adapt designs other users have shared.

The term 'printability' has been coined by many researchers and hobbyists using AM techniques. Although there is no specific definition of the term 'printable', it is generally used

to describe how close to the desired shape the printed object is, how easily the material can be printed and how reproducible the printing of the object is (Derossi et al., 2018, Li et al., 2016).

There are 7 defined categories of additive manufacturing techniques (AM) commercially available, all of which use the principle of creation through the addition of material (ASTM, 2012). Each of the techniques have their own advantages as well as restrictions, however one of the current limiting factors of all of these techniques is the limited range of materials available. Research into novel and existing materials has been driven by application, for example AM of metals are of interest to engineering companies (GE, 2016, Wang and Liu, 2014), whereas biomaterials are of interest to medical applications (He et al., 2016, Melchels et al., 2010) in order to minimise material usage and reduce cost. The 7 different categories can be classified according to the main material used for the printing: solid, liquid or powder. An outline of the different categories can be seen in Figure 2.1, adapted from Petrie (2018).

These techniques all work in slightly different ways, but most require information from a computer-aided design (CAD) model of the desired object as the starting input (Wong and Hernandez, 2012). Computer software is then employed, which ‘slices’ the object into a set number of layers and approximates the path of each layer with the use of triangles. The path for the entire object is then saved as a stereolithography (.STL) file which the printer interprets and uses as the guide for the creation of the object. An outline of the basic principles can be seen in the left image of Figure 2.2 (Ligon et al., 2017), while the right image shows an example of an .STL file of a two-layered ring, used for a Fused Deposition Modelling technique. The yellow and red lines indicate where the nozzle head follows and extrudes material, whereas the lighter blue lines highlight where the nozzle moves, but does not extrude material.

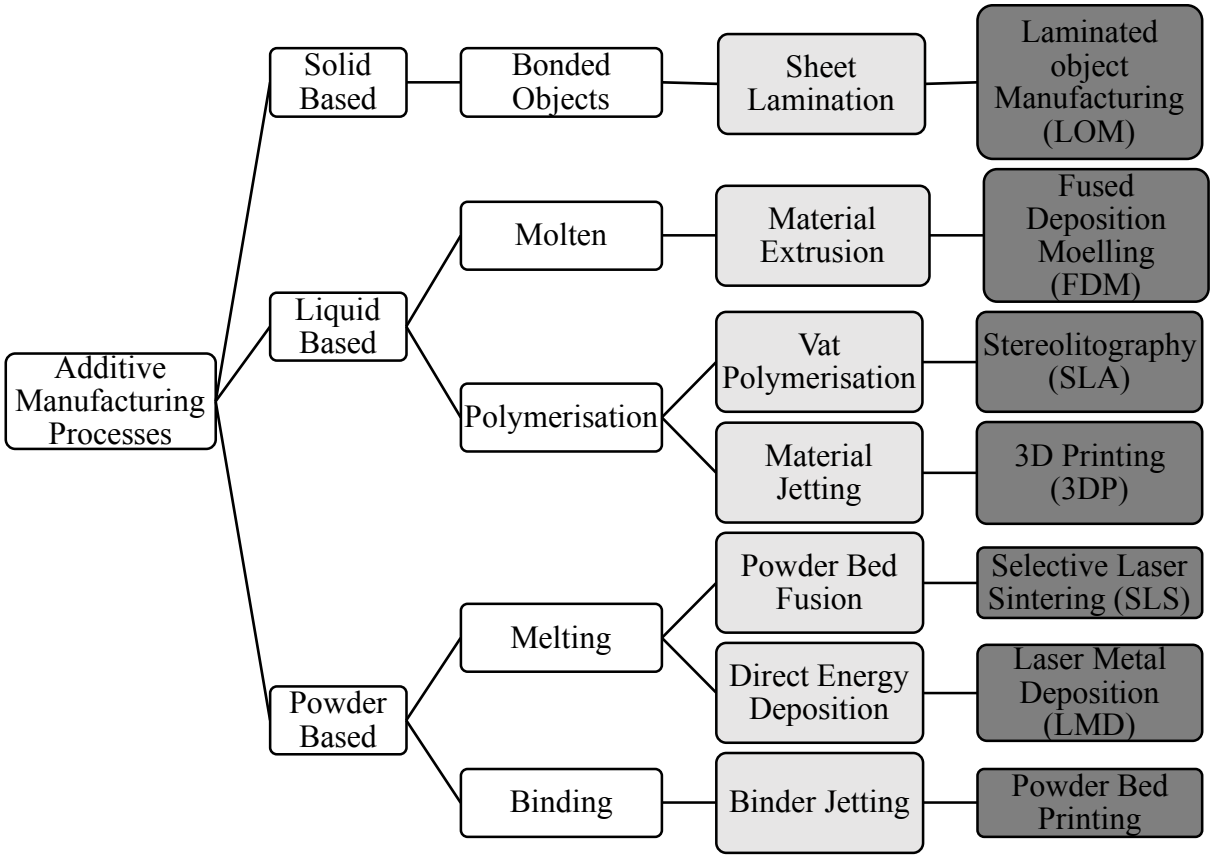

Figure 2.1: Classification of AM categories according to the main material. The most common process is highlighted in light grey and an example of their technologies is highlighted in dark grey. Adapted from Petrie (2018).

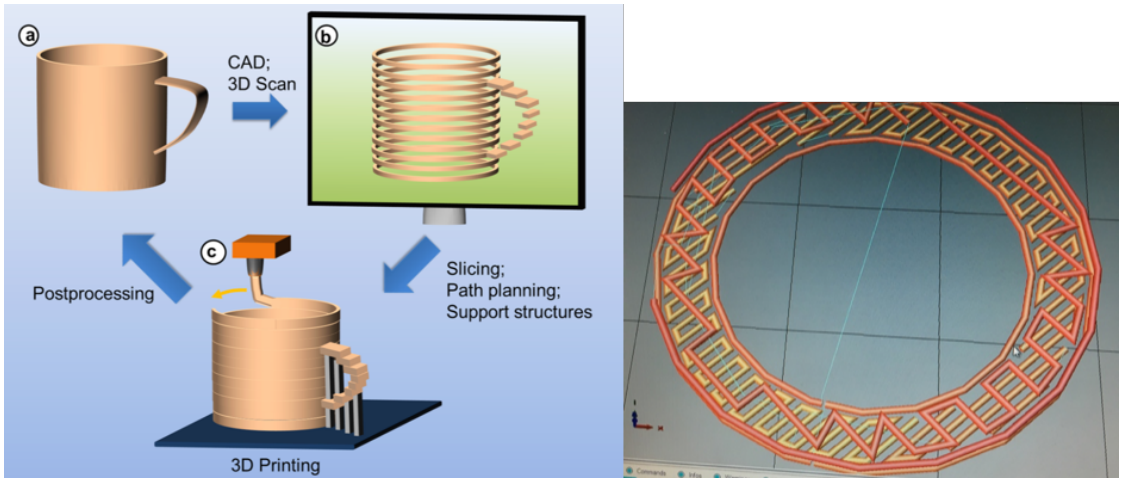

Figure 2.2. An outline of the basic principles of additive manufacturing (Ligon et al., 2017) (Left), .STL file of a two layer ring (right).

A brief summary of each of the different categories of AM, including an outline of the process, pros and cons and some of the materials currently in use has been given in Table 2.1.

Table 2.1. Brief summary of the different categories of additive manufacturing (Petrie, 2018, AMRG, 2018).

Category	Outline of process	Pros/ Cons	Materials	Schematic
Sheet lamination	Material is placed on the bed and bonded with the previous layer using an adhesion method (glue, thermal, clamping etc.). The required shape is then cut from layer by either knife or laser. Major applications include: creation of large parts and tooling.	Low cost materials; Allows for combination of different materials with relative ease. Hard to produce complex geometries; Less accurate than other AM techniques.	Metal; Paper; Film; Foil.	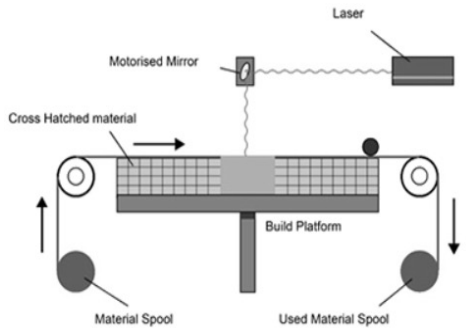
Material Extrusion	Nozzle heated and deposits a semi-molten material where required onto the cross-sectional area of the first layer. Following layers are added on top of the previous layer. Fusion happens between layers as material solidifies. Major applications include: prototyping and office manufacturing.	Widespread and inexpensive process; Multiple materials can be used for printing and support. Nozzle radius limits and reduces final print quality; Relatively slow compared to other AM techniques.	Variety of thermoplastics including: ABS; PLA; PC; HDPE.	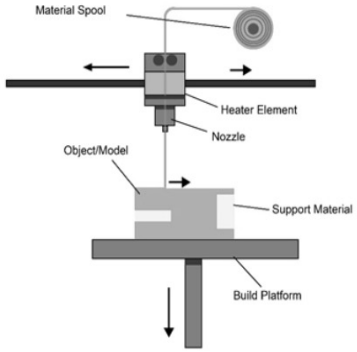

Category	Outline of process	Pros/ Cons	Materials	Schematic
Vat Polymerisation	A liquid photopolymer is deposited into a vat and then 1 layer is selectively cured by light activated polymerization. The bed is then lowered, to allow fresh resin onto the build platform and another layer is cured, in order to build up the object. Major applications include: prototyping, consumer toys and electronics.	Can be used to create virtually any design; Relatively quick process; High level of accuracy; High cost of both machine and resin; Lengthy post-processing time and removal of resin.	UV-curable photopolymer resins.	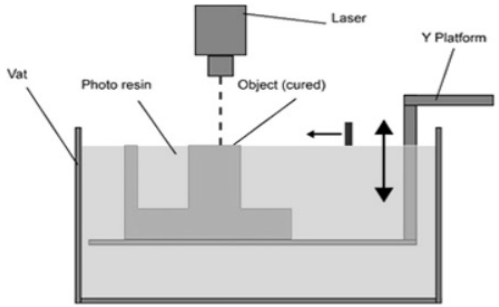
Material Jetting	Material is jetted onto a platform, from a nozzle which moves horizontally across the platform. Once on the platform, the materials solidify and the object is then built up layer by layer. Major applications include: high resolution prototypes, circuit boards and other electronics.	Good surface finish; High resolution; Enables multiple materials; Parts have relatively low strength and durability; Support materials are often required.	Polymers and plastics including: HDPE; ABS; HIPS.	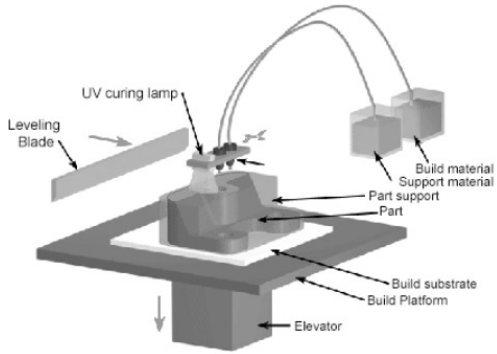

Category	Outline of process	Pros/ Cons	Materials	Schematic
Powder Bed Fusion	A layer of powder material is spread across the bed, typically 0.1 mm thick and a laser fuses the material of the first layer. A new layer is spread across the bed and further layers are fused to create the object. Major applications include: aerospace, automotive, medical implants.	Relatively inexpensive; Unsintered powder acts as a support during printing and is easily removed post-printing. Relatively slow speed; Finish is dependent on the grain size of the powder.	Can use any powder based material. Common metals include: Titanium; Stainless steel.	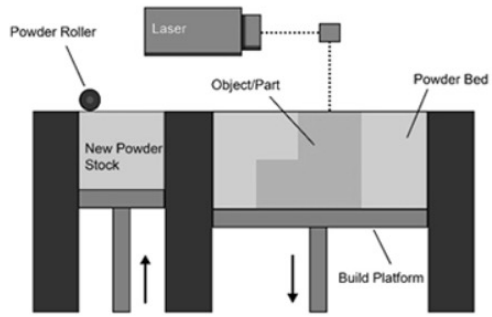
Direct Energy Deposition	Nozzle rotates around object. Materials, in either wire or powder form is deposited from the nozzles onto the bed. Material is melted using an electron beam or laser. Further material is added layer by layer and solidified, creating a new object. Major applications include: repair or build-up of large parts.	Can operate in open air; Multiple materials can be used; Large parts can be produced; Expensive equipment; Final machining is often required.	Metals: Cobalt chrome; Titanium.	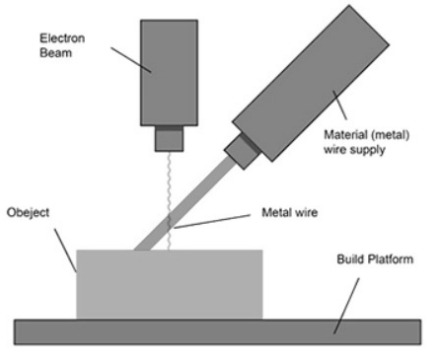

Category	Outline of process	Pros/ Cons	Materials	Schematic
Binder Jetting	A thin layer of powder is rolled across the printing platform. The printer head then sprays a liquid adhesive binder in order to fuse the powder particles together. The bed is the lowered down by the models' layer thickness and another layer of powder is rolled across the platform and the process is repeated. Major applications include: prototyping and tooling.	Low waste; Relatively fast; Uses a wide range of materials. Rough surface finish can lead to additional post processing, increasing the overall processing time.	Metals: Stainless Steel; Polymers: ABS, PA; Ceramics: Glass;	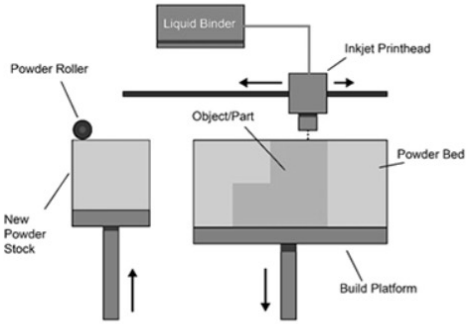

2.2.1 Additive Manufacturing of Edible Substances

From the 7 different categories of AM, currently only 3 of them have been utilised in order to print edible substances (material extrusion, powder bed fusion and binder jetting).

There are currently no documented applications of AM of edible substances through sheet lamination techniques. Due to the nature of this process and the way the layers are bound together using adhesives it is unlikely that this technique will take off with edible substances. Most food substances are delicate, compared to materials currently used within this technique and as intricate shapes cannot easily be created, there is little benefit from using this method to hand crafting food into layers and then creating the desired shape, where a person can handle the food with care.

Within the vat polymerisation technique, UV curable monomers and photoinitator molecules are used in order to fuse the objects together. Although there are a few photoinitators which are generally regarded as safe (GRAS) or FDA approved, the list is very scarce, meaning creating edible UV ink formulations is challenging (Clark et al., 2017). Therefore, this approach of AM is unlikely to flourish for the creation of edible substances.

Material jetting originally used very low viscosity ink formulations in order to create structures, which was an issue as many food products produce viscous solutions even at relatively low concentrations. However, as technology and understanding further advances within this area of AM it is likely that this technology will see a break through into the food industry. A number of patents already exist for edible inks with the potential of using this (Croker et al., 1998, Shastry et al., 2009).

Direct energy deposition was specifically created for the creation of 3D metals powders and enables the creation of parts by melting the material as it is being deposited (Gibson et al.,

2015). This technique is very similar to that of powder bed fusion, which is already in use with edible materials, therefore, it is hard to envisage how the direct energy deposition technique would produce better objects, however, there is scope for it to be used in the future.

Of the 3 techniques that are suitable and have already been utilised for printing of edible substances, a substantial effort has been made in order to pre-process materials suitable for AM and currently the available material can be classified into two categories based on their printability (Sun et al., 2015a):

- Natively printable materials - such as hydrogel, cheese, cake frosting and chocolate, which can be extruded easily from a syringe;
- Non-printable, traditional food materials - such as meat, rice, fruit and vegetables, which are consumed by people daily, but are not printable by nature.

An overview of each of the techniques currently used for edible printing as well as the materials which have been used is detailed below.

2.2.1.1 Material Extrusion of edible substances

AM of edible substances through the use of material extrusion has thus far proved to be the most common, with several groups already investigating the possibility of producing food objects using this technique. The 'Fab@Home' machine was considered one of the first AM machines to use food based products. The 'Fab@Home' machine was created by Hod Lipson and Evan Malone at Cornell University, New York, and was an experiment in order to bring rapid prototyping to people at a low cost (Molitch-Hou, 2014). The machine used a syringe based deposition technique to extrude any liquid material. Using a 'Fab@Home' Model 1 machine, a student from Manual High School, Louisville created a low-temperature heated

syringe which was suitable for the deposition of chocolate (Malone and Lipson, 2007). An image of the chocolate which was printed can be seen in Figure 2.3.

Figure 2.3. Image of printed chocolate printed by Noy Schaal (Lipson and Kurman, 2013).

The creators of the 'Fab@Home' machine have now begun a collaboration with 'The French Culinary Institute' and are currently trying to create a designated food printer (Segall, 2014).

Another group, within Cornell University have used the 'Fab@home' machine to print gelatin and xantham gum in order to determine the mouth feel of different combinations of these two materials (Cohen et al., 2009). The group determined that they could stimulate a broad range of mouth feels, ranging from systems with sensory attributes for chocolate through to risotto using these two components. This group believed that AM of food could change the culinary domain by providing a new artistic capacity for the fine dining field as well as extending mass-customisation abilities to the industrial culinary sector (Cohen et al., 2009).

The idea of eating insects is repulsive to some people, however the team at 'Insects au gratin' have begun to consider using a printer in order to extrude materials such as icing butter and cream cheese with ground up insect powder mixed inside (Soares, 2011). It has been found that

100 kg of feed could produce around 40 kg of crickets, whereas that amount would only produce about 10 kg of beef (Soares, 2011), thus, insects could be a good source of protein in the future. The team are looking for new ways to encourage people to eat insects by making them more aesthetically pleasing to look at. Images of some of the objects produced by the team can be seen in Figure 2.4. The object within the picture was made through an FDM machine with a syringe nozzle extruding the material. Although a similar object could have been made by hand, it would not be able to be this elaborate and would have needed a very skilled hand.

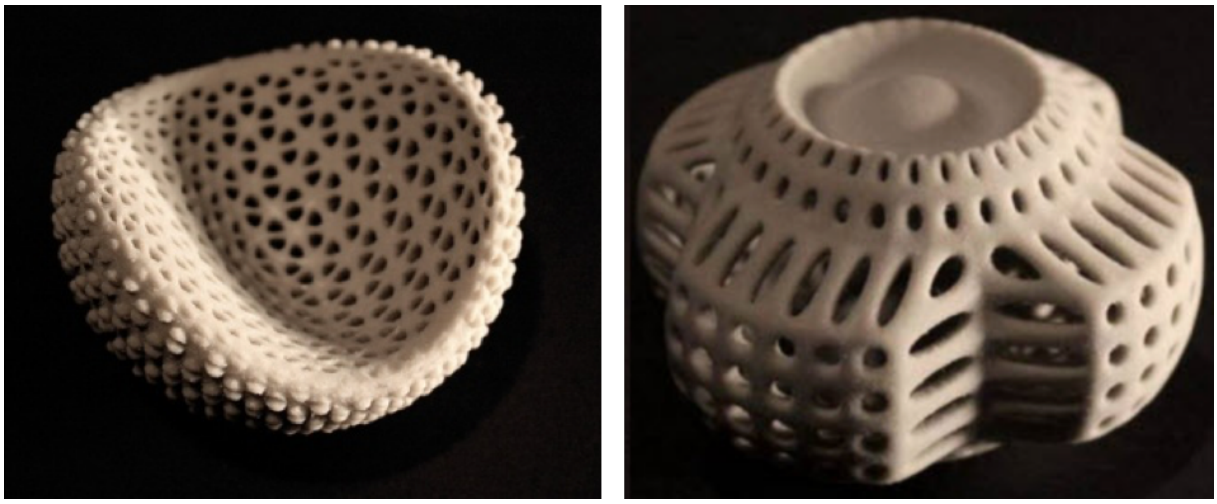

Figure 2.4. 3D printed insect food prototypes created with insect powder through a FDM machine (Soares, 2011).

Yang et al. (2018) developed an FDM machine in order to determine the optimum printing parameters for the extrusion of lemon juice gel. In order to ensure that the desired geometry was achieved from the printed shape, Yang and his team investigated different printing parameters, including nozzle height, diameter and movement speed in order to determine their optimum values. These parameters were assessed by printing lines and cylinders while varying the parameters and then visually observing which had printed closest to the target geometry. They determined that a storage modulus (G') of ca. 5 kPa, nozzle height and diameter of 1 mm and a nozzle moving speed of 30 $mm.s^{-1}$ enabled the printing of the most precise shapes.

A group in the Netherlands, from TNO (Netherlands Organisation for Applied Scientific Research, Netherlands), has been looking at creating intricate shapes from edible substances. Collaboration with a Michelin star chef led the group to print a chocolate dessert (shown in the top frame of Figure 2.5) with different fillings that were linked to a highlighted continent on the globe. Further collaboration with Barilla, led to the development of a pasta printer, which was capable of printing a small amount of high quality, uniquely shaped pasta shapes (shown in the bottom frame of Figure 2.5) (Noort et al., 2017).

Figure 2.5. Printed chocolate dessert with fillings (top) and printed pasta shapes (bottom) (Noort et al., 2017).

The intricacies of both of these shapes indicate the possibilities available with AM, which would not be capable of producing in any other way.

2.2.1.2 Powder Bed Fusion of edible substances

The range of CandyFab printers (4000, 5000 and 6000) were built as hobby projects by two scientists from Evil Mad Scientist Laboratories (Oskay and Edman, 2014). These machines were capable of printing large objects from pure sugar by using a narrow, directed, low-velocity beam of hot air to melt sugar grains. A single layer of sugar was placed on a bed, the desired shape was etched out using the hot air, and then the bed was lowered and another layer of sugar was placed on top and the process was repeated until a three-dimensional object was built. When the build had finished, the object was removed from the bed, and the excess sugar was reclaimed in order to use for the next object. The reason that they chose to use the powder bed method was due to the relative inexpense and ease of cleaning of this method, as well as the ability to print over hanging parts, that would not be possible in a material extrusion method (Oskay and Edman, 2014). Photographs of a printed object immediately after printing, and after the excess sugar had been removed created by the CandyFab 4000 machine can be seen in Figure 2.6.

Figure 2.6. Photograph of the CandyFab machine immediately after printing, with the excess sugar surrounding the printed object (left) and the final object, once the excess sugar has been removed (right) (Oskay and Edman, 2014).

The intricate shape which has been printed would not been possible to make in any other way thus showing some of the impressive abilities of AM.

As well as their work on material extrusion, TNO have applied for a patent which uses selective laser sintering using edible compositions (Diaz et al., 2014). They have worked with a number of ingredients, including NesQuik powder, and a mixture of sugars and fats in order to produce objects such as chain links and company badges (Gray, 2010). An example of a chain printed by this group can be seen in Figure 2.7.

Figure 2.7. Photograph of a chain printed from NesQuik (Wegrzyn et al., 2012).

2.2.1.3 Binder jetting of edible substances

3D Systems is a company in South Carolina which designs, manufactures and sells 3D printers, co-founded by Charles Hull (inventor of SLA). Through an acquisition of The Sugar Lab, 3D Systems have now created a Colour Jet Printer which has been adapted for sugar printing. Unlike CandyFab, which uses hot air to bind sugar, 3D systems use an edible binder, which is fully food safe. Some examples of sugar detailing of a wedding cake and intricately printed shapes in multiple colours printed in sugar by Systems (2018) can be seen in Figure 2.8. The variety of colours were created by using different flavourings within the sugar.

Figure 2.8. Detailing of a wedding cake (left) and intricate shapes (right), printed from sugar by Systems (2018).

Researchers at the University of Nottingham have investigated the recrystallization of cellulose powders through the use of a binder jetting technique using xantham gum as the 'ink' component (Holland et al., 2018). Through the deposition of an aqueous binder and a post-process heating step, amorphous cellulose particles could be selectively recrystallized in order to create a structure. Further investigation discovered that a composite powder bed of cellulose and glycans resulted in better 3D structures. Photographs of a lattice and star structure printed using a composite bed material of cellulose and konjac glucomannan can be seen in Figure 2.9.

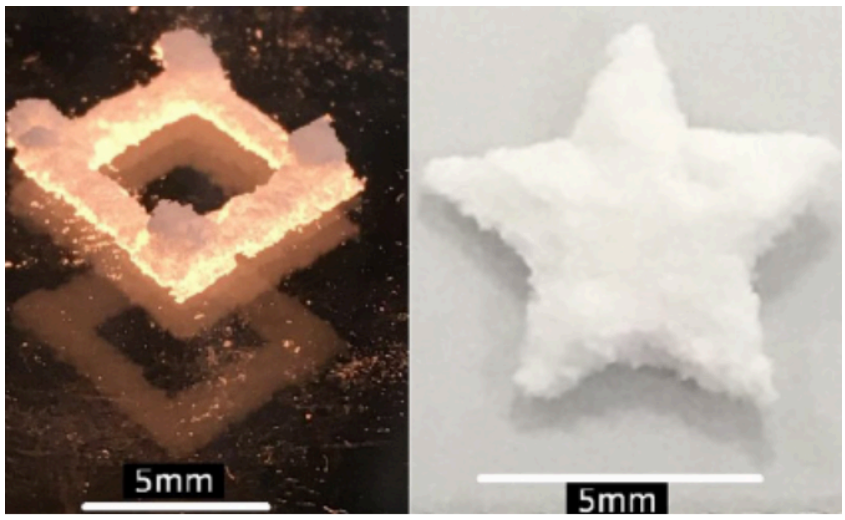

Figure 2.9. Lattice and star structure of a formulation of 9:1 cellulose/konjac glucomannan (Holland et al., 2018).

2.2.2 Additive Manufacturing of Hydrocolloids in other industries

The printing of hydrocolloids is also being investigated in the medical industry for use in biomedical research. Researchers at Zhejiang University, China, have assessed the printability of gelatin with sodium alginate for bioprinting in order to mimic organ structures (He et al., 2016). He and his team used a syringe based FDM machine in order to determine the relationship between the properties of the printer (such as feedrate, printing distance, etc.) to the quality of the printed part (He et al., 2016). The team determined that the viscosity of a mixture, in order for it to be printable, should be between 0.3-30 Pa.s. A lower viscosity resulted in the mixture smearing out instead of printing in a line and a higher viscosity resulted in the motor failure as it tried push out the material.

The brain is a complex organ and current research has modelled the brain using a two-dimensional technique. However, researchers from the University of Wollongong, Australia, have demonstrated a new method of bioprinting a 3D brain-like structure using peptide modified gellan gums substrates (Lozano et al., 2015). It is hoped that the brain-like structures may be able to improve the understanding of neurodegenerative diseases and brain injuries.

A lab in Slovenia have investigated the development of a "Vitaprint" extruder for use in bioprinting (Banović and Vihar, 2018). Having developed the extruder, they printed a scaffold of a human nose using a blend on 10 % gelatin and 1 % sodium alginate, shown in Figure 2.10.

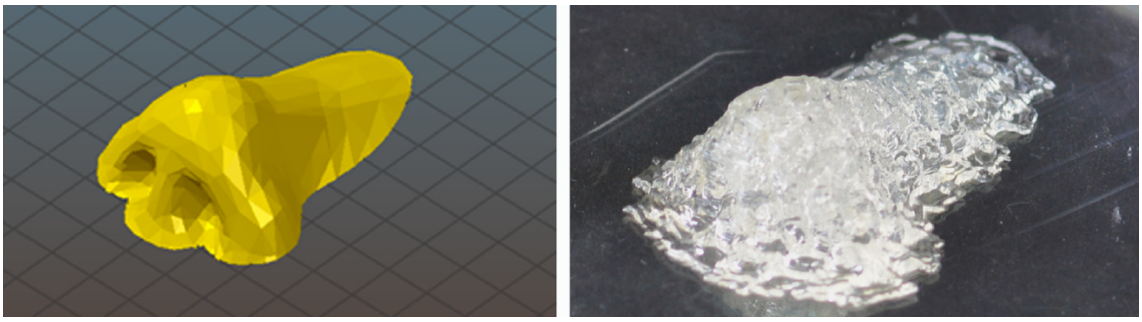

Figure 2.10. A 3D model of a human nose (left) and a printed version of the nose (right) (Banović and Vihar, 2018).

Although this technology is not currently completely reliable, the ability to print organs could in the future change the face of medicine. The organ could either be printed beforehand, so that the surgeon could practice the operation to come, or potentially use the printed part as part of the operation, by inserting a custom-made organ.

2.2.3 Potential problems with AM of Edible Substances

Although AM is an exciting prospect, there are still many challenges which need to be overcome before it comes into everyday usage. Some of these challenges are highlighted below.

One of the main issues which needs to be addressed when considering AM of edible substances is that of speed of the creation of an object. Currently, printing of food takes a long time, compared to mass producing the objects, which would preclude major commercial manufacturers utilising it. Although AM may be more likely to find a place in the production of small batch high-end products, research still needs to concentrate on trying to increase the speed, while not affecting the accuracy of the printed object.

Distributed manufacturing, where products are created in multiple sites (Hu, 2018), could be a commercial option when creating products through additive manufacturing, reducing the need for large a centralised plant. This could also help at the point of sale, when the customer could customise the product that they wanted. However, it is important that the products of distributed manufacturing are of the same quality, therefore it will be very important that the additive manufacturing machines are extremely consistent to ensure that a consumer could go to any site and get the same product.

There is also the issue of intellectual property (IP) and how it can be protected by the designer. A consumer has the potential to scan a friend's printed object and then print their own version, or put it on the internet meaning everyone else has access to it (Kietzmann et al., 2015).

Presently, there is no way to avoid this, and this will put some designers off from creating anything which can be printed. Therefore, determining a way to protect people's IP will be necessary for 3D printing to succeed.

Trying to get consumers to purchase and eat the additively manufactured food will be something which needs to be addressed. A survey completed by Gyton (2015) indicated that only 39 % would consider eating 3D printed meat. Although this result may change as AM food becomes better known, it will be important to find out why people do not want to eat this type of food and explore ways of transforming their attitudes.

Finally, there is a lack of characterised edible feed stocks available for the use in AM. The majority of literature to date has focused on non-edible feed stocks, such as plastics, metals and ceramics. Although all of the above issues need to be addressed, this current work focusses on creating a greater knowledge of the necessary properties for edible material to be printable.

2.3 Hydrocolloids

Hydrocolloid is the term commonly given to describe a range of polysaccharides and proteins that have found use in a wide variety of industrial sectors including food (Dickinson, 2003, Saha and Bhattacharya, 2010), pharmaceutical (Wong et al., 2002, Sriamornsak et al., 2004) and cosmetics (Dakia et al., 2008, Cernasov et al., 2004). Polysaccharides are complex carbohydrates which are formed by the linking of multiple monosaccharides by glucosidic linkage (Sharon, 1975, Berg et al., 2002). Different polysaccharides are derived from different origins and include trees, plants, seaweeds, microbial and animal sources (Phillips and Williams, 2009b). Hydrocolloids are hydrophilic compounds due to the presence of a large number of (-OH) groups, leading to an increased affinity for the hydrocolloids to bind water molecules (Saha and Bhattacharya, 2010).

Hydrocolloids perform a number of functions, including modifying the rheology of a material (through thickening and gelling), emulsion stabilisation and suspensions of solids (Burey et al., 2008, Milani and Maleki, 2012). Hydrocolloids also offer several health benefits, including replacing fats or modifying the texture of products such as mayonnaise or milk based drinks (Liu et al., 2007). The high demand for ready-to eat-meals, coupled with consumer awareness of the need to consume healthier meals will ensure that hydrocolloids will continue to be in demand (McKenna, 2003).

Some hydrocolloids form a thermoreversible gel, whereas others form non-thermoreversible gels. The mechanism of gelation of different hydrocolloids exhibit a wide range of structures from random coils to helices, to the egg box model (Phillips and Williams, 2009b). This wide variety of structuring and different interactions leads to a diverse range of physical and rheological properties. Figure 2.11 depicts a qualitative comparison of the range of textures which are produced by different hydrocolloids.

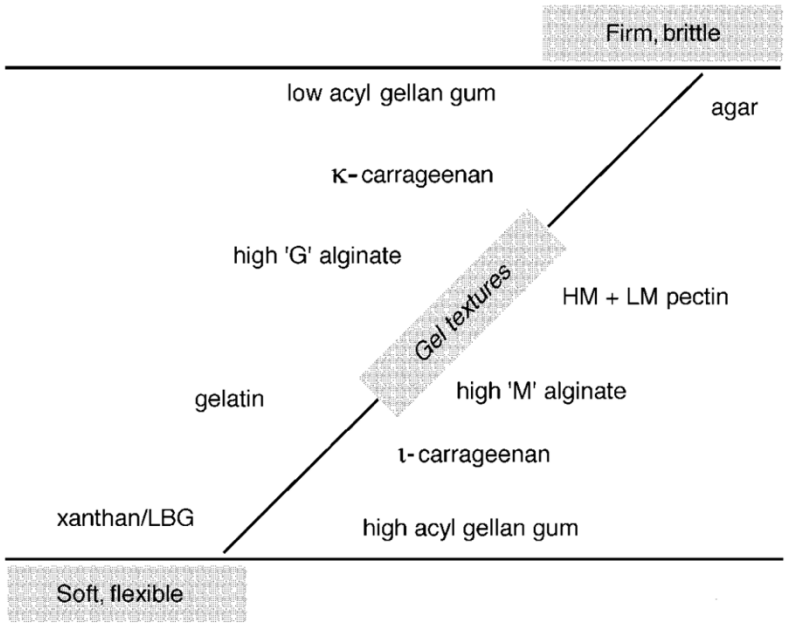

Figure 2.11. A schematic of a qualitative comparison of the different textures of gels produced by different hydrocolloids (Phillips and Williams, 2009b).

Gelation of a hydrocolloid only occurs above a critical minimum concentration, C_o, which is specific for each hydrocolloid (Phillips and Williams, 2009a). Below this concentration, the polymer chains have the ability to move independently of one another without interpenetration, and is referred to as the 'dilute region'. The viscosity within this region increases upon the collective volume occupied by the polymer chains within the solution. As the concentration of the polymer is increased, the first detection of entanglement is referred to as the critical overlap concentration, C* (Harding, 1998). Above this concentration, the polymer chains are forced to overlap, therefore a sharp increase in viscosity with increasing polymer concentration occurs (Nickerson et al., 2003). A schematic representation of increase in viscosity above and below C* can be seen in Figure 2.12.

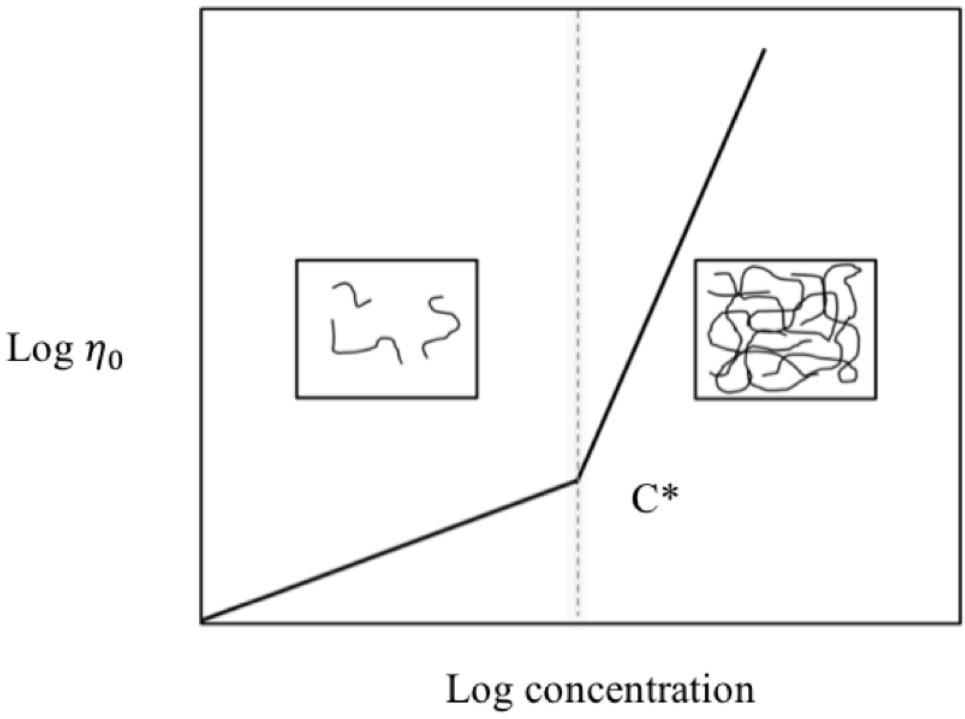

Figure 2.12. Schematic representation of the log of the zero-shear viscosity as a function of the polymer concentration. Adapted from Phillips and Williams (2009b).

Novel rheological characteristics of food products can be created through the mixing of hydrocolloids. For example, the addition of locust beam gum to xantham to form elastic, cohesive gels (Wüstenberg, 2015). The nature of the synergy of two different hydrocolloid molecules can be due to association or phase separation (Phillips and Williams, 2009b). If association occurs between the two hydrocolloids, then either precipitation or gelation can occur. Association can occur with oppositely charged hydrocolloids and forms either soluble or insoluble complexes. More commonly, if the two hydrocolloids do not associate then either a single phase (generally with low concentrations of polymer) or two phase liquid (generally at higher concentrations) will be acquired. When the polymers phase separate, 'water-in-water' emulsions are formed, with droplets which are enriched in one of the hydrocolloids, which is dispersed in a continuous phase which is enriched in the other hydrocolloid (Phillips and Williams, 2009b). Generally the rheological properties of the mixture will be governed by the continuous phase (Bourriot et al., 1999). The way in which the hydrocolloids are dispersed, either the continuous or the dispersed phase depends on the concentrations of each of the components. If either one or both of the hydrocolloids are able to form a gel independently, then gelation and phase separation can occur simultaneously. The characteristics of the resulting gel will depend on the concentration of each of the hydrocolloid and the way in which they have gelled. With careful consideration of hydrocolloid type and concentration, it is possible to create a wide range of gel textures (Phillips and Williams, 2009b). A schematic of the ways in which two hydrocolloids can interact is shown in Figure 2.13.

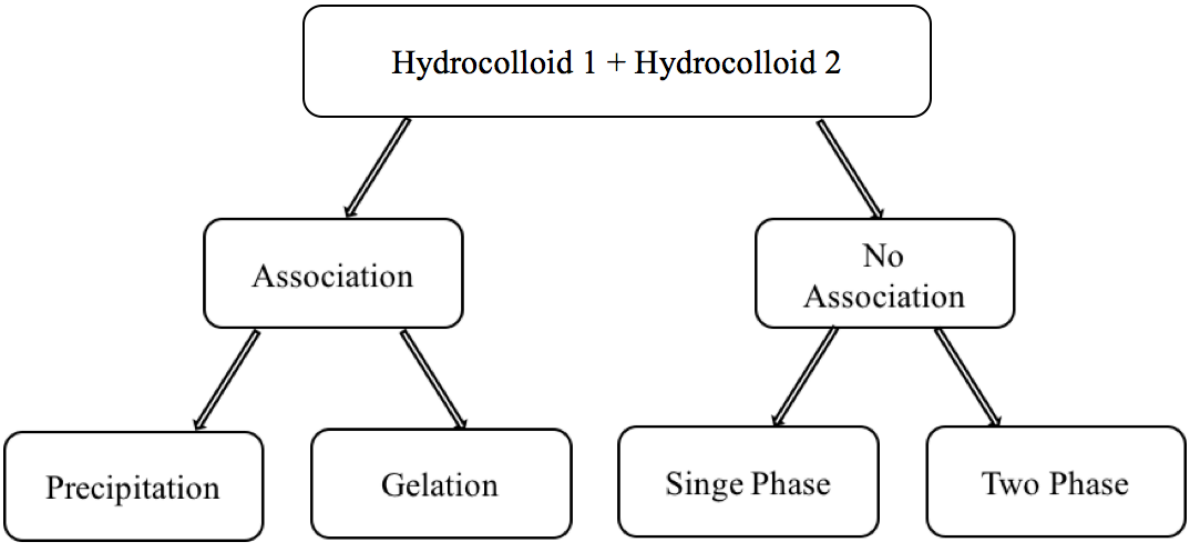

Figure 2.13. Schematic representation of mixture of hydrocolloids and the interactions that can occur. Adapted from (Phillips and Williams, 2009b).

A number of mixed hydrocolloid systems have been used within this study due to their use in food products and related research projects. A more detailed description of each of the hydrocolloids have been given below.

2.3.1 Gelatin

Gelatin is a product that is obtained by the partial hydrolysis of collagen, which is derived from animal skin, bones and white connective tissue (Morrison et al., 1999). Common sources of gelatin include pig skin (porcine), cow skin (bovine) and fish (marine). Gelatin is a very important material which is utilised in many different industries, including: pharmaceutical (e.g., hard and soft medical capsules), biomedical (e.g., three-dimensional tissue regeneration) and food industry (e.g., foaming and gelling agents) (Karim and Bhat, 2008). After starch, gelatin is the most used hydrocolloid globally (Phillips and Williams, 2009a).

Depending on the process of manufacture, two different types (Type-A and Type-B) of gelatin are available. Type-A gelatin is obtained by an acidic treatment of collagen (generally from porcine sources), while Type-B is obtained via an alkaline hydrolysis of collagen (generally

from animal bones) (Kommareddy et al., 2007). Commercially available gelatines are graded and sold according to their viscosity and the Bloom test. The Bloom test gives an indication of consistency, compressibility and firmness of the gelatin and is evaluated through how much load is required to produce a depression in the gel (Kempka et al., 2014). Bloom indexes for gelatin usually run between 125g to 250g, with the higher the Bloom number indicating a stiffer gelatin gel (Anon, 2006). These two physical constants have to be reproducible within 1 % and indicate the suitability of the gelatin for a given use (Considine, 2012). Figure 2.14 depicts a schematic of the basic chemical structure of gelatin (Kommareddy et al., 2007).

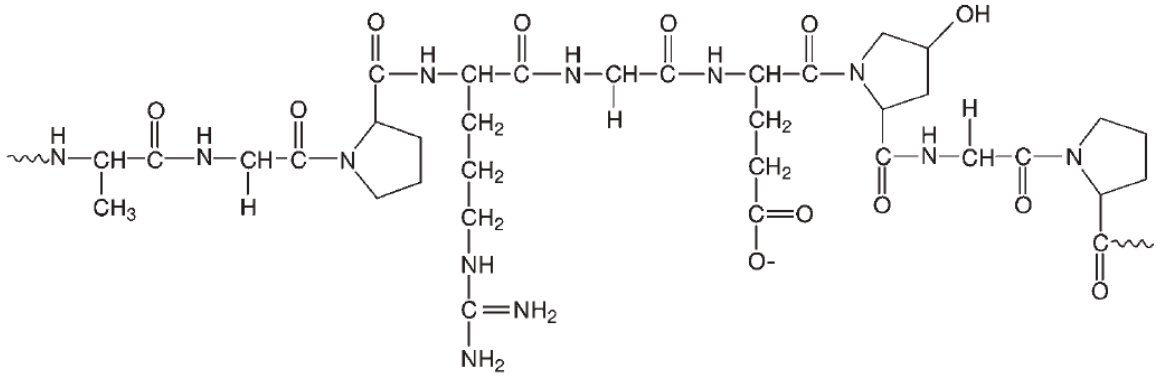

Figure 2.14. Schematic of the basic chemical structure of gelatin (Kommareddy et al., 2007).

Gelatin occurs in the form of brittle, vitreous yellow granules and when these granules are soaked in cold water they hydrate into discrete, swollen particles (GMIA, 2012). When heated, these swollen particles then dissolve in order to form a solution. When cooled to below approximately 36 ˚C, the gelatin will undergo a thermoreversible coil-helix transition as shown in Figure 2.15 (Haug and Draget, 2000). With regards to the food industry, gelatin is the preferred gelling agent in sugar confectionaries (e.g. marshmallows and wine gums), yoghurt product and dairy mousses (Phillips and Williams, 2009a).

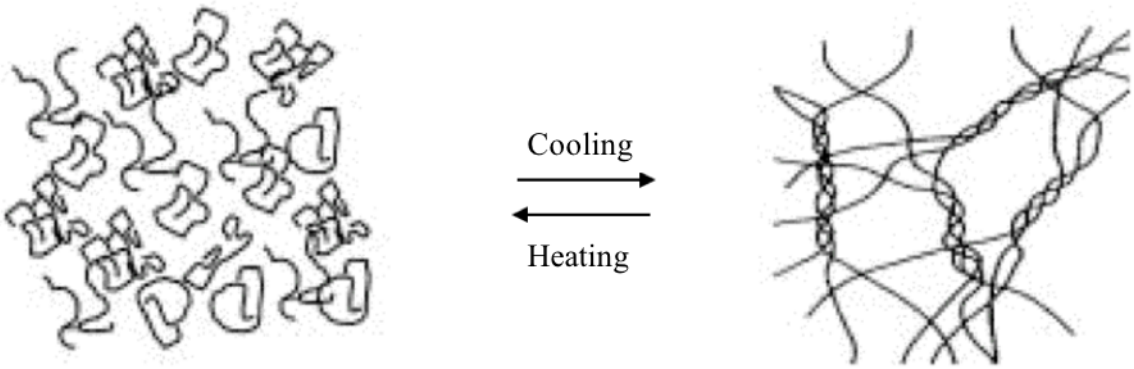

Figure 2.15. Schematic representation of the thermoreversible coil-helix gelling process of gelatin. Adapted from Haug and Draget (2000).

Due to the outbreak of BSE ('mad cow disease') in the 80s (Haug et al., 2004) and the increasing number of people choosing not to eat meat (especially pig) due to religious or personal reasons (Rasli and Sarbon, 2014), alternatives to mammalian gelatins, such as fish gelatins (Ninan et al., 2014) have been investigated. However, the key property of mammalian gelatins is the melting at relatively low temperature, which gives mammalian gelatins the melt-in-the-mouth property (Phillips and Williams, 2009a), which thus far has not been replicated with fish gelatins or any other hydrocolloid. Therefore, mammalian gelatins are still in abundant current use. Other important properties, which account for mammalian gelatins being used in so many different industries include their thermoreversibility, viscosity and high strength of film (Considine, 2012). Due to these reasons, for this study, porcine gelatin (a mammalian gelatin) was chosen as the main biopolymer due to these unique properties that it possesses.

One of the main restrictions of using gelatin is the slow gelation rate, therefore it is sometimes necessary to modify gelatin with a gelator (Derkach et al., 2015). Modification with cross-linking agents such as formaldehyde have shown to improve the mechanical properties of gelatin gels (de Carvalho and Grosso, 2004), however such cross-linking agents are prohibited in the food industry. Therefore, other methods of manipulating the properties of gelatin have

been investigated such as the addition of other hydrocolloids, which has been expanded upon below.

2.3.2 Kappa-carrageenan

Carrageenan is a collective name for a family of polysaccharides of high molecular weight, which are extracted from red seaweed of the class Rhodophyceae (Paquin, 2009). Carrageenans are sulfated linear galactans, with basic structural disaccharides units, which consist of alternating β-1,3- and α-1,4-linked galactose residues (Yermak et al., 2017). There are three main used forms of carrageenan: kappa (κ), iota (ι) and lambda (λ) (Paquin, 2009). These different forms are distinguished by the extent of sulphation of the disaccharide repeating unit: kappa-carrageenan has one repeating unit, iota-carrageenan has two sulphates per disaccharide and lambda-carrageenan has three sulphate groups per disaccharide (Knutsen et al., 1994). Figure 2.16 displays an idealised unit structure of kappa-carrageenan (Dul et al., 2015).

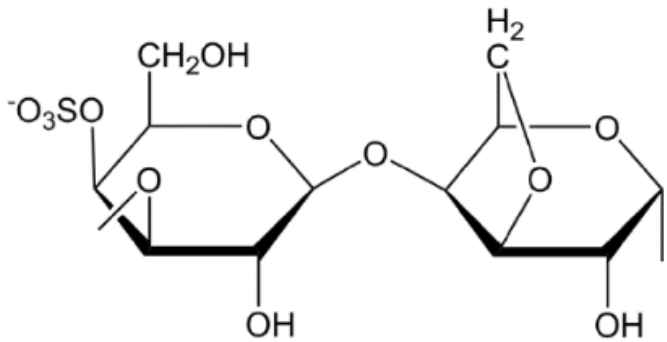

Figure 2.16. Idealised unit structure of kappa-carrageenan (Dul et al., 2015).

Native carrageenans contain a mixture of the three forms and the species of the red seaweed as well as the extraction process will determine which of the three forms is more dominant (Paquin, 2009). Initially the seaweed is washed in order to remove sand and stone and then it undergoes an alkali treatment in order to extract the carrageenan (Imeson, 2000). Each of the different forms exhibit different properties and strength in their gel form. Extracts with a high

amount of kappa-carrageenan form strong, thermoreversible gels, with a relatively high melting point, while iota rich carrageenan forms more compliant, weaker gels and lambda-carrageenans do not gel at all, but can still be used as thickeners (Smith and Hong-Shum, 2011).

All carrageenans appear as a white to yellow powder and carrageenan gels are prepared by dispersing the powder in hot (around 80 ˚C) water for at least 10 minutes in order to hydrate the polysaccharide (Smith and Hong-Shum, 2011). On cooling, the carrageenans set between 40 to 60 ˚C, depending on the type of carrageenan and salt content, and form a range of gel textures (Imeson, 2000). Gelation of kappa-carrageenan has been attributed to the double helix formation which involves regular sequences between kink point on two adjacent chains (Rees, 1972). These helices then aggregate together in order to form a gel (shown in Figure 2.17). Robinson et al. (1980) were the first to report this behaviour and it is known as the 'domain' model.

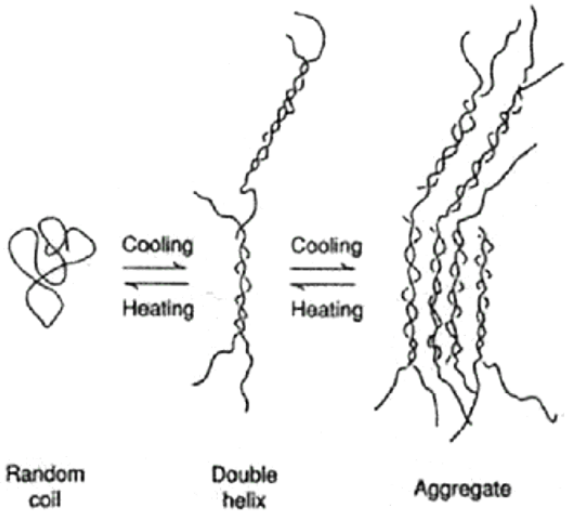

Figure 2.17. Schematic representation of the 'domain' model, the coil-helix-aggregate transition of kappa-carrageenan (Phillips and Williams, 2009a).

Kappa-carrageenan has widely been used within the food industry as a gelling and thickening agent in foods such as water-based jellies and dairy products, in order to modify their texture

(Morris and Chilvers, 1983). Carrageenans are also used in meat products, such as cooked ham, where the carrageenans stabilise the injected water (Wüstenberg, 2015). One of the major features of kappa-carrageenans was that they formed a thermoreversible gel (Rochas and Rinaudo, 1984).

Upon the addition of kappa-carrageenan to gelatin, there occurs an interaction between the positively charged amine groups within the gelatin and the negatively charged sulfate groups within the kappa-carrageenan (Antonov and Gonçalves, 1999). This leads to the formation of (bio)polyelectrolyte complexes, which affects the thermo-stability of the system, increasing the gelation rate (Derkach et al., 2015). The formulation of gelatin alone is a transparent mixture, but upon addition of kappa-carrageenan, the mixtures become turbid due to associative phase separation of the two polymers (Antonov and Gonçalves, 1999).

Researchers from Murmansk State Technical University (Murmansk, Russia) have found that the addition of kappa-carrageenan accelerated the gelation and increased the melting temperature (Derkach et al., 2015). It was also found that a gelatin/kappa-carrageenan mixture at the ratio of 10/1 led to a storage modulus of approximately double that of just a pure gelatin solution (Derkach et al., 2015).

2.3.3 Gellan gum

Gellan gum is a linear extracellular polysaccharide which is composed of repeating tetrasaccharide units (1,3-β-d-glucose, 1,4-β-d-glucuronic acid, 1,4-β-d-glucose, 1,4-α-l-rhamnose) (Figure 2.18) and synthesized from the bacteria *Sphingomonas elodea* (Fasolin et al., 2013). The native polymer is known as high acyl gellan and contains two ester groups, an acetyl and a glyceryl group on the (1→3)-linked glucose residue. When this is exposed to alkali at high temperatures, both of the acyl groups are hydrolysed and the deacylated form of low

acyl gellan gum is obtained (Mao et al., 2000). High acyl gellan forms weak gels due to the bulky acetyl and glyceryl group which prevent close association between the gellan polymer chains in the double-helix formation and also hinder compact packing of the cross-linked double helix (Mao et al., 2000). With the removal of these acyl groups, closer bonds are able to be formed, resulting in low acyl gellan forming firm, brittle, non-elastic gels even at very low concentration (0.05 % gum and 99.55 % water) (Damodaran and Parkin, 2017).

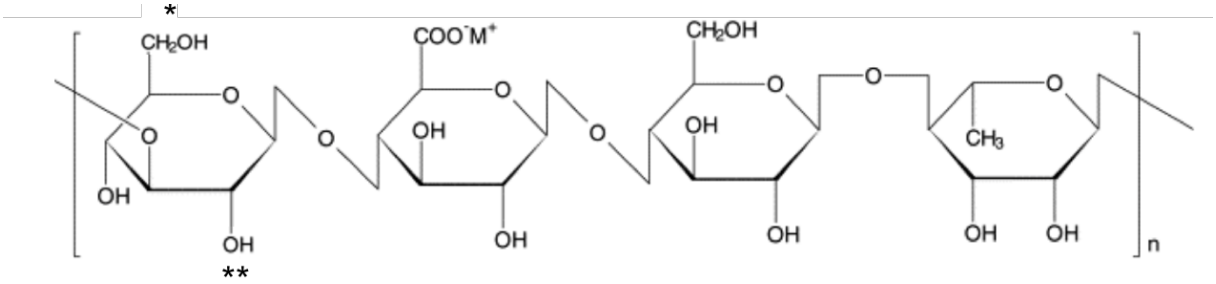

Figure 2.18. Tetrasaccharide repeating unit of deacylated gellan. The sites of attachment of acetyl (*) and glyceryl (**) substituents, found in native gellan (also known as high acyl gellan) have been indicated. Figure adapted from Mao et al. (2000).

Gellan appears as a white or off white powder or soft flakes (Smith and Hong-Shum, 2011). Gellan gels are prepared by dispersion of the powder into water heated to at least 75 ˚C, in order to dissolve the gum (Arendt and Dal Bello, 2008). Similar to kappa-carrageenan, gelation of gellan is based on the 'domain' model and therefore occurs due to the association of double helices (Ahmed et al., 2017). Gelation of gellan can be promoted by the presence of both monovalent and divalent cations, but monovalent cations (e.g. potassium ions) cause gelation at a lower temperature than divalent ions (e.g. calcium ions) (Grasdalen and Smidsrød, 1987). The gelation temperature for low acyl gellan is between 40 to 50 ˚C, whereas for high acyl gellan the gels typically set between 70 to 80 ˚C (Phillips and Williams, 2009b).

Blends of the two forms of gellan have the ability to form a large range of textures, however, no evidence of the formation of double helices involving both high and low acyl gellan have thus far been found (Phillips and Williams, 2009b).

Gellans are currently used within the food industry as thickening agents, gelling agents and for coating of foods in contact with surfaces (Smith and Hong-Shum, 2011).

Upon the addition of gellan to gelatin, the gellan may form coupled networks with the gelatin molecule wherein the anionic domains of the gellan forms new heterolytic junction zones with cationic domain of the gelatin molecules leading to increases in gelation temperature, gelation rate and gel strength (Fonkwe, Narsimhan, & Cha, 2003). The addition of low acyl gellan to gelatin gels has been found to increase the gelation rate constant (Pranoto et al., 2007).

A group from Washington State University (Washington, USA) have investigated the textural properties and turbidity of various mixtures of gellan and gelatin. They discovered that a broad range of textures could be achieved by altering the ratio of gellan to gelatin and that a formulation of 0.6 % gellan to 1 % gelatin has a fat-like softness and opacity, meaning this combination could potentially be used a fat replacer (Lau et al., 2000).

2.3.4 Agar

Agar, first discovered in Japan in 1658, is a hydrocolloid which is extracted from certain marine algae of the class Rhodophyceae (Flick, 1990). Its structure comprises of 1,3-linked, D-galactose and 1,4-linked, 3,6-anhydrogalactose (Feiner, 2006). Commercial agar is a mixture of agaropectin and agarose fractions in variable proportions which depends on the raw material and the manufacturing process (Phillips and Williams, 2009b). It is the agarose component of the agar which causes gelation of agar. A schematic of the basic chemical structure of agarose can be seen in Figure 2.19 (Hotta et al., 2016).

Agar is tasteless, colourless and not soluble in cold water (Pandey et al., 2015). Agar gels are prepared by dispersing agar powder in boiling water and then cooling to room temperature or lower (Labropoulos et al., 2001). At high temperatures, agar sols are transparent, however, upon cooling below the gelation temperature turbidity of the solutions increases, due to the aggregation of helices into bundles and the resulting gel appears opaque (Aymard et al., 2001).

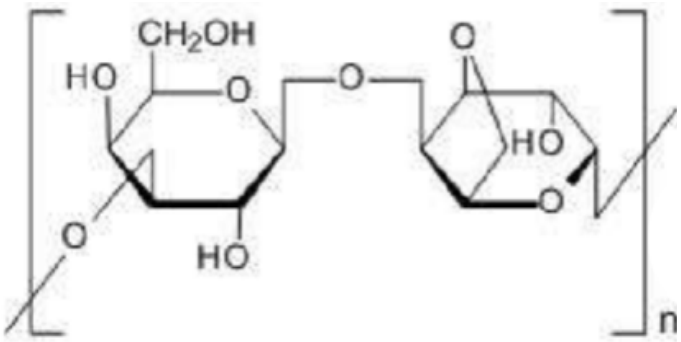

Figure 2.19. Basic chemical structure of agarose (Hotta et al., 2016).

Similar to gelatin and kappa-carrageenan, agar gelation has been attributed to the double helix formation upon cooling from the sol state (Schafer and Stevens, 1995). The structure of agar gels is formed by the molecules uniting solely by hydrogen bonds (Phillips and Williams, 2009b). It is due to this type of structuring, which enables an important property of agar gels: their reversibility, forming gels upon cooling and melting upon heating. This transformation could be repeated indefinitely, as long as the gel is not exposed to aggressive substances which could hydrolyse the agarose molecules (Phillips and Williams, 2009b). Unlike most other gelling agents, agar gels exhibit a high gelling hysteresis, where the gels gel at a temperature much lower than their melting temperatures (Armisén and Galatas, 2000). Gelation temperature of agar varies with concentration, but is commonly around 38 ˚C, while melting temperatures of at least 80 ˚C are necessary in order to re-melt the structures (Shahidi and Simpson, 2004).

Agar gives brittle gels, and is the preferred gelling agent if this is a desirable feature (confectionary products, jellies etc.) (Phillips and Williams, 2009a).

Gelatin and agar mixtures have received a great deal of attention due to their inherent biocompatible natures (Wakhet et al., 2015). When mixed together, the two liquid phases are immiscible, but coexist in thermodynamic equilibrium (Singh et al., 2007b). Therefore, these two materials form a complex coacervate sample which is a heterogeneous viscous material (Singh et al., 2007a). Micrographs taken by Clark et al. (1983) provide evidence of the microstructure of a 1 % agar and 5 % gelatin gels, shown in Figure 2.20, the light areas indicate agar and the dark areas indicate gelatin.

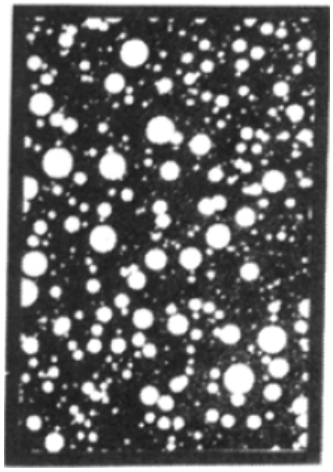

Figure 2.20. Micrograph of a 1 % agar and 5 % gelatin mixture (Clark et al., 1983).

For this concentration, the gelatin is the continuous phase, with the agar being the dispersed phase. When the concentration of agar was increased to 2 %, the inversion point was estimated to lie between 5 and 6 % gelatin (Clark et al., 1983). With agar in the dispersed phase, as the mixture was reduced in temperatures from 80 ˚C, initially the agar began to gel in the continuous medium of the gelatin, which did not gel at that temperature. Watase and Nishinari (1980) determined that the presence of the gelatin may hinder the gelation of agar due to their incompatibility.

In the mixed gel of gelatin and agar, the network formation of one of the components is hindered in part by the other component (Shiinoki and Yano, 1986). Two individual networks are formed from the two gelling agents due to the dependence of the gelation temperature on the proportion on the gelatin present (Horiuchi and Sugiyama, 1987). Somboon et al. (2014) found that the value of G' was lower at higher temperatures when 1 % agar was mixed with gelatin than when it was by itself. This could be due to the fact that the gelatin had melted while the dispersed agar was still a gel, but could not form a continuous network connecting the shear surfaces.

A team at Unilever (Bedford, UK), investigated the properties of mixtures of agar and gelatin and discovered that using a concentration of 5 % gelatin, as the concentration of agar was increased to 1 %, the magnitude of G' approximately doubled (Clark et al., 1983). There was a further smaller increase of G' as the concentration of agar was increased to 2 %.

Researchers at Yamagata University (Yamagata, Japan) combined agar and gelatin in order to try and take advantage of the key properties of each of the two components (the melt-in the-mouth gelatin property and the easy handling of the agar) (Fujii et al., 2000). They found that it was possible to achieved a range of textures by controlling which of the components was continuous and which was dispersed.

2.3.5 Potential functionality

There is a significant potential towards functionality in all of the previously described systems, containing both gelatin and secondary biopolymers, however, there is still a need to study and design such systems specifically for AM purposes. This way it is possible to actualise their potential and function over their current, existing, applications. In order to ensure that these mixtures will be printable, it is necessary to examine how they will behave under high strains, similar to being printed and then how they will recover, so a cohesive shape can be obtained.

CHAPTER 3. MATERIALS AND METHODS

3.1 Introduction

This chapter provides detailed information on the materials used and their preparation, as well as the methods utilised for sample analysis. Some theory behind the different analytical techniques has also been included.

3.2 Materials

Porcine gelatin (250 bloom), kappa-carrageenan, low-acyl gellan and agar were purchased from Sigma-Aldrich (UK). Deionised water was used, which had been purified using a Millipore purifier. The materials were used without any further purification or modifications.

3.2.1 Preparation of a 5 % (w/w) gelatin solution

The 5 % (w/w) gelatin solution was prepared by dispersing the required amount of gelatin into reverse osmosis water at a temperature of 60 ˚C, while under agitation and left to fully hydrate for at least 30 minutes in accordance with Takayanagi et al. (2000).

3.2.2 Preparation of gelatin and kappa-carrageenan solutions

Three different formulations of gelatin and kappa-carrageenan were investigated for this research, 5 % (w/w) gelatin with 1, 2 and 3 % (w/w) kappa-carrageenan. The samples were prepared by dispersing the required amount of kappa-carrageenan into the reverse osmosis water at a temperature of 70 ˚C on a heated bed, under agitation using a magnetic stirrer bar for 30 minutes. Subsequently, the gelatin was added to the solution, at a temperature of 60 ˚C, and left to fully hydrate for 30 minutes.

In order to gauge an estimate of how much kappa-carrageenan needed to be added to a 5 % (w/w) gelatin solution to create a bi-continuous system (where both phases are characterised as

being the continuous phase (Norton and Frith, 2003)), a phase diagram (shown in Figure 3.1) was consulted from Antonov and Gonçalves (1999). This revealed that at a temperature of 40 ˚C, 1.5 % (w/w) kappa-carrageenan was required to create a bi-continuous system. Therefore, it was decided to investigate two mixtures which were gelatin continuous (5 % (w/w) gelatin and 5 % (w/w) gelatin with 1 % (w/w) kappa-carrageenan), and two which were assumed to be kappa-carrageenan continuous, even though they were off the diagram (5 % (w/w) gelatin with 2 and 3 % (w/w) kappa-carrageenan). The maximum concentration of kappa-carrageenan was chosen as 3% as this was a "high" concentration of polymers within a food system and preliminary results showed that any higher would likely be unpalatable in a food product.

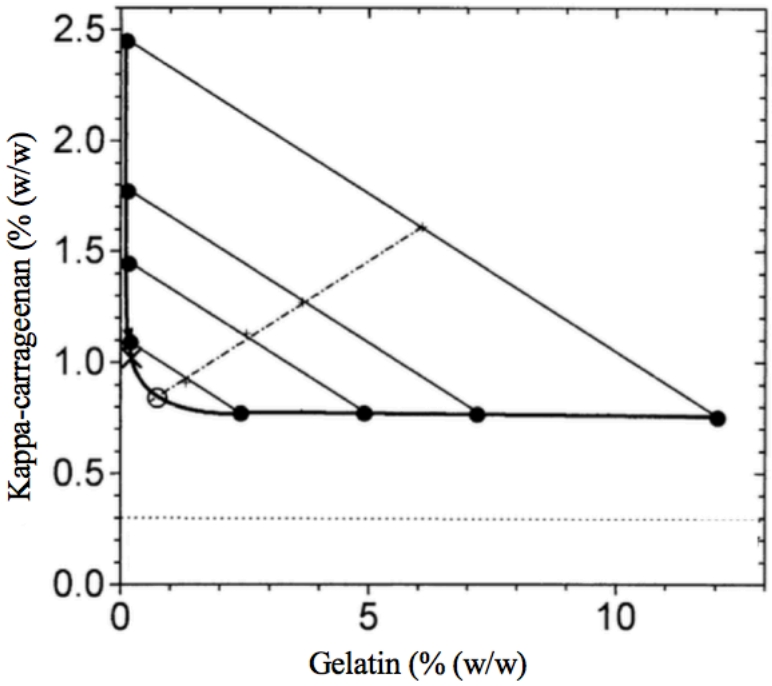

Figure 3.1. Phase diagram of gelatin and kappa-carrageenan at 40 ˚C. Adapted from Antonov and Gonçalves (1999).

No salts were added (which would strengthen the gel), so as to avoid introducing a further variable into the systems, and potentially affecting the chemical and mechanical properties by affecting the interaction of the solvent on the gel network (Phillips and Williams, 2009b).

Macroscopic phase separation was observed with the formulations of 5 % (w/w) gelatin with 1 % (w/w) kappa-carrageenan, due to their thermodynamic incompatibility (Fang et al., 2006). This behaviour was not observed with the formulations with 2 and 3 % (w/w), potentially due to the increased viscosity of these formulations reducing the rate of macroscopic phase separation (Michon et al., 2000).

3.2.3 Preparation of gelatin and gellan solutions

In order to compare the results from the gelatin and kappa-carrageenan to the gelatin and gellan solutions, the same concentrations were used for the gelatin and gellan samples. The three samples of 5 % (w/w) gelatin with 1, 2, and 3 % (w/w) gellan were prepared by dispersing the required amount of gellan into the reverse osmosis water at a temperature of 85 ˚C on a heated bed, under agitation using a magnetic stirrer bar for 30 minutes. Subsequently, the gelatin was added to the solution, at a temperature of 60 ˚C, and left to fully hydrate for 30 minutes.

3.2.4 Preparation of gelatin and agar solution

Typical concentrations of agar in applications vary between 0.5 and 2 % (Armisén and Galatas, 2000). Therefore, the concentration of the agar within the gelatin mixtures was also maintained at the same concentrations of 1, 2 and 3 % (w/w). The three samples of 5 % (w/w) gelatin with 1, 2, and 3 % (w/w) agar were prepared by dispersing the required amount of agar into the reverse osmosis water at a temperature of 90 ˚C on a heated bed, under agitation using a magnetic stirrer bar for 30 minutes. Subsequently, the gelatin was added to the solution, at a temperature of 60 ˚C, and left to fully hydrate for 30 minutes.

3.3 Methods

3.3.1 Differential Scanning Calorimetry (DSC)

Differential Scanning Calorimetry (DSC) is a thermo-analytical technique used in a range of different industries including automotive, pharmaceuticals and food (Tunick et al., 1989, Kurtz, 2016, Šimon et al., 2006). A DSC measures the difference in the heat flow rate (in mW or $mJ.s^{-1}$) between a sample and a reference as a function of time and temperature (Davies, 2017). This is achieved by loading a sample of the test material into the cell and also creating a reference cell with the desired reference material (the reference is typically equivalent to the test sample minus the component with thermal transitional interest). These cells are then loaded into a DSC machine and then both the sample and reference cells are subjected to the same controlled temperature programme. The difference in energy input necessary to maintain identical temperatures in the test material and the reference material is recorded. When the sample undergoes a transition involving a change in enthalpy that change is indicated by a departure from the base line of the heat flow record (OECD, 1981)

These departures can appear as a peak, in the case of a first order transition, such as melting or gelling, or as a step, for a second order transition, such as the glass transition (T_g). When heat is removed from the system, an exothermic event occurs, whereas when addition heat is required, an endothermic event occurs. An example thermograph displaying three different peaks is shown in Figure 3.2.

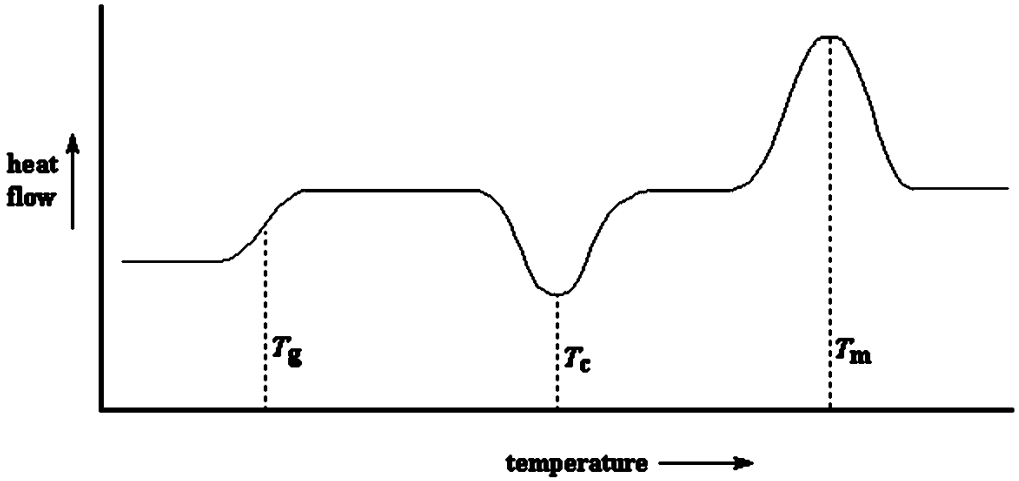

Figure 3.2. An example thermograph of a DSC scan, where Tg is the glass transition, Tc is the crystallisation temperature and Tm is the melting temperature (PSLC, 2018).

There are two main categories of DSC which are in current use. For both, the signal is proportional to the heat flow, but they differ in their design and measuring principle:

- Power compensated - the temperature of the sample and reference are maintained independently using separate furnaces. The temperatures of the sample and reference are kept the same by varying the power input to the furnaces and the energy require to do this is a measure of the enthalpy change of the sample relative to the reference sample (Bhadeshia, 2018).

- Heat flux - the sample and reference are connected together by a low resistance heat flow path (generally a metal disc) and the assembly is contained within a single furnace. The enthalpy change in the sample cause a difference in its temperature relative to the reference and this temperature difference is recorded and then related to the change in enthalpy in the sample using calibration experiments (Bhadeshia, 2018).

Within this work, a power-compensated micro-DSC (μDSC) was utilised and an outline is given below.

3.3.1.1 Micro-Differential Scanning Calorimetry (μDSC)

Micro differential scanning calorimetry (μDSC) uses larger samples sizes, compared to conventional DSCs, they are extremely sensitive and capable of measuring small changes in the thermal properties of materials (MacNaughtan and Farhat, 2008). Due to the larger sample size, the μDSC typically uses a slower heating range (between 0.001 – 2 ˚C.min^{-1}) to ensure that there is thermal equilibrium within the whole of the sample mass (Gabbott and Mann, 2016).

3.3.1.2 Sample analysis (Chapters 4 and 6)

A Seteram MicroDSC 3 evo (Seteram, France) was used in order to analyse the thermal transitions of the formulations. Around 0.7 g of the sample was packed into a stainless-steel cell and the reference cell was filled with an equivalent amount of reverse osmosis water. Samples were then analysed using the following profile: initially the sample was cooled to a temperature of 0 ˚C and then held there for 60 minutes. A heating ramp was applied at a scanning rate of 1.2 ˚C.min^{-1} up to 60 ˚C (apart from the samples with agar, which were heated to 80 ˚C) and then cooled at the same rate back to 0 ˚C, where it was held for another 60 minutes. This cycle was repeated twice, so that 3 heating and 3 cooling curves were obtained in total. Gelling and melting temperatures were determined as the onset of their respective peaks.

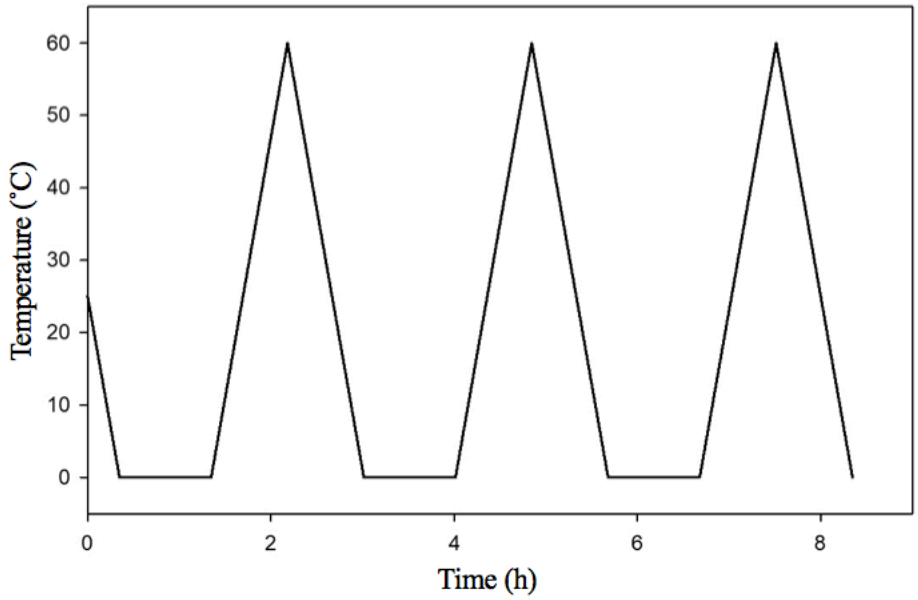

Figure 3.3. Schematic representation of the μDSC temperate profile used for samples of gelatin with kappa-carrageenan and gelatin with gellan. Samples of gelatin with agar were heated to a temperature of 80 ˚C. Temperature ramps were conducted at 1.2 ˚C.min^{-1}.

Three cycles were conducted in order to see if there was any hysteresis effect on the material as it was heated and cooled repeatedly. Each material was tested three times and the results presented are the average ± one standard deviation.

3.3.2 Rheology

Rheology has been defined as the study of the flow and deformation of a materials (Barnes, 2000). When investigating the flow of a material, the viscosity is considered, which is the resistance of the material to movement (Schramn, 2000). Deformation investigates the viscous and elastic behaviour of the material when sheared. Modern rheometers can be used for shear testing and torsional testing by operating with either continuous rotation or rotational oscillations, as shown in Figure 3.4 (Paar, 2018).

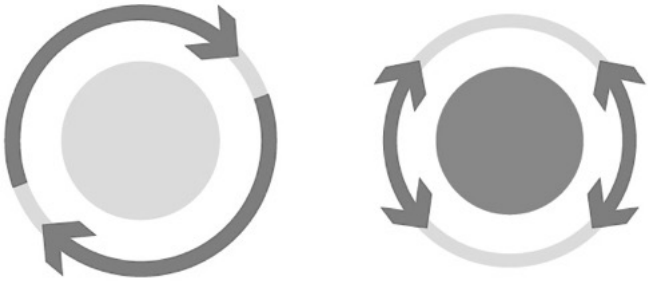

Figure 3.4. The two measuring principles of a modern rheometer: continuous rotation (left) and rotational oscillation (right) (Paar, 2018).

The different types of tests and results achieved using these two measuring principles are discussed below.

3.3.2.1 Rotational testing and viscosity

Viscosity is a measure of the flow behaviour of a fluid under a shear stress and describes how certain materials flow easily, such as water, while others do not, such as tar (Schaschke, 2014). Viscosity in terms of shear rate and shear stress can be defined as:

$$\eta = \frac{\tau}{\dot{\gamma}}$$

Equation 3.1. Definition of viscosity in terms of shear stress (τ) and shear rate ($\dot{\gamma}$).

The definition of the shear stress and the shear rate have been expressed in Equation 3.2 and Equation 3.3 respectively.

$$\tau = \frac{Force\ (N)}{Area\ (m^2)} = \frac{F}{A}$$

Equation 3.2. Definition of shear stress in terms of force and area.

$$\dot{\gamma} = \frac{v}{h}$$

Equation 3.3. Definition of the shear rate in terms of velocity (v) and height (h).

Equation 3.1 is a rearrangement of Newton's Law of viscosity ($\tau = \eta.\dot{\gamma}$). This law applies to materials that are ideally viscous materials, where the viscosity is independent of the shear rate applied (Schaschke, 2014). Typical examples of Newtonian materials include water, silicone oil and solvents such as acetone (Paar, 2018).

'Non-Newtonian' fluids are materials that exhibit behaviour where the viscosity is dependent upon the shear rate applied. Typical non-Newtonian behaviours include shear thinning and shear thickening. With materials that exhibit shear thinning, as the shear rate increases, the viscosity decreases, with examples including shampoos, coating and glues. Materials that exhibit shear thickening behaviour display an increase in viscosity with an increase in shear rates with examples including dental filling masses and ceramic suspensions.

Rotational testing can be undertaken in two different operation modes, either by defining the rotational speed or the shear rate in order to achieve the torque and shear stress or vice versa. Within the rheological testing of this study, the shear rate was set within the printer, therefore the shear rate was controlled rather than the shear stress or torque.

In order to depict the material's flow behaviour, flow curves are generally constructed by plotting τ vs $\dot{\gamma}$, or alternatively a viscosity curve is plotted by replacing τ with η. A typical viscosity curve is shown in Figure 3.5 which displays materials that are Newtonian (1), shear thinning (2) and shear thickening (3) (Paar, 2018).

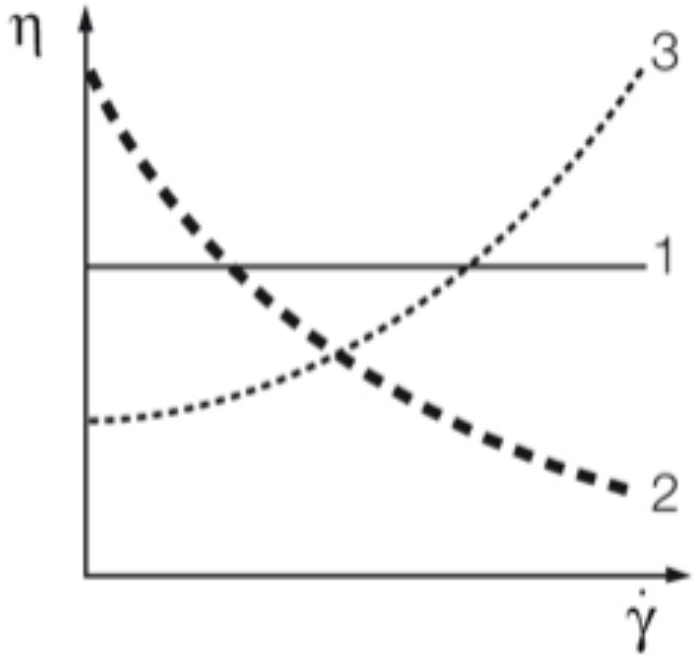

Figure 3.5. Typical viscosity curve depicting materials which are Newtonian (1), shear thinning (2) and shear thickening (3) (Paar, 2018).

The minimum shear-stress value required in order to breakdown a sample's structure is known as the yield point. At stresses above this value, the material will exhibit fluid-like behaviour. Different tests can be undertaken in order to investigate the viscosity of the material. These include investigating the time-dependent flow behaviour, where the shearing is kept constant throughout the experiment or a temperature-dependent flow behaviour, where the shear is constant and the test is undergone over a temperature gradient.

3.3.2.2 Oscillation testing and viscoelasticity

An ideal solid deforms elastically, and the energy required for deformation is fully recovered when the stress is removed. An ideal fluid deforms irreversibly, the energy that is required for their deformation is dissipated within the fluid in the form of heat energy and cannot be recovered by the removal of the stresses (Schramn, 2000). In reality, most liquids are somewhere between these two extremes with varying amounts of solid and liquid behaviour, and are classified as 'visco-elastic'. When materials are sheared, they can display a mixture of

elastic and viscous behaviour, also known as viscoelastic behaviour i.e. the energy spent for their deformation will be partly recovered. Oscillation testing works by having a sample placed between two plates, one of which is stationary and one rotating at a constant rotational speed, corresponding to a constant oscillating frequency and imposing a time dependent strain on the sample. Generally the strain plotted against time results in a sine curve. The force that is required as a counter force in order to keep the stationary plate in position is also measured. This signal is rheologically evaluated as the shear stress, τ. The two sine curves achieved (the pre-set curve as well as the response curve) oscillate at the same frequency. If the samples displayed completely elastic behaviour, then there would be no time lag between the pre-set curve and the measured curve. If the samples displayed completely liquid behaviour, there would be a difference of 90 ˚ between the two curves. However, most samples exhibit some viscoelastic behaviour, therefore there is generally a time lag between the two curves. This time lag is known as the phase shift (δ) and is always between 0 ˚ and 90 ˚. If the phase shift of the material is between 0 and 45 ˚, the material is dominated by solid-like behaviour, whereas if the phase shift is between 45 and 90 ˚, the material is dominated by fluid-like behaviour. The complex shear modulus, G*, describes the entire viscoelastic behaviour of the material and is defined as:

$$G^* = \frac{\tau_A}{\gamma_A}$$

Equation 3.4. Definition of the complex modulus, G, in terms of the shear-stress amplitude (τ_A) and the strain amplitude (γ_A).*

The complex modulus can be broken down into two parts, the storage modulus, G', which represents the elastic portion of the viscoelastic behaviour, and the loss modulus, G", which represents the viscous portion of the viscoelastic behaviour. These two moduli can be calculated using the equations below:

$$G'(Pa) = G^*.\sin(\delta)$$

Equation 3.5. Definition of the loss (viscous) modulus.

$$G''(Pa) = G^*.\cos(\delta)$$

Equation 3.6. Definition of the storage (elastic) modulus.

Sometimes tanδ is plotted in addition to the curves for the G' and G". Tanδ describes the ratio of the two moduli of the viscoelastic behaviour, and is defined as:

$$tan\delta = \frac{G''}{G'}$$

Equation 3.7. Definition of tan delta in terms of the loss and storage moduli.

The two main tests undertaken as oscillations are amplitude and frequency sweeps. Amplitude sweeps describe the deformation of a material in a non-destructive deformation range, known as the LVR (linear viscoelastic region). Within this region, a material will return to its original state when the strain is removed. At strains above the LVR, the material experiences large deformations and may be irreversibly deformed. Any subsequent testing of the material should be undertaken within the LVR. A frequency sweep generally describes the time-dependent behaviour of a material in the non-destructive deformation range. Both the amplitude sweep and frequency sweep can classify a material into two general behaviours: visco-elastic solid or visco-elastic liquid (Malvern, 2010).

A rheometer has a finite range of torque, therefore different geometries are used for different materials. Materials that are highly viscous generate a high amount of torque, therefore a geometry with a small surface area is used, in order to ensure that the measured force is within the measurement limits of the machine. Low viscosity materials generate less torque, therefore the surface area of the geometry is increased, to spread the force, to maximise torque, to be

within range of the equipment (Malvern, 2010). There are a variety of different geometries which can be attached to the rheometer, the most common are highlighted below:

3.3.2.3 Cone and plate

Within the cone and plate, the liquid is confined between a bottom flat plate and a coned top plate, as shown in Figure 3.6. An important advantage of using the cone and plate geometry is the constant shear rate across the gap. The velocity of the cone is given by:

$$V = \omega . r$$

Equation 3.8. Definition of the velocity of the liquid. ω is angular frequency and r is the radius.

The distance between the cone and plate can be found from:

$$y = r . tan\vartheta$$

Equation 3.9. Definition of the gap distance. ϑ is the angle of the cone.

Finally, the shear rate can then be determined as:

$$\gamma = \frac{V}{y} = \frac{\omega . r}{r . tan\vartheta} = \frac{\omega}{tan\vartheta} = \frac{\omega}{\vartheta}$$

Equation 3.10. Definition of the shear rate in the cone and plate as a function of the angular velocity (ω) and angle of the cone (ϑ).

Since the angle of the cone is small (generally < 4 °), the $tan\vartheta \approx \vartheta$. This indicates that the shear rate is independent of the radius and is only a function of the angle of the cone (Braun and Rosen, 2000). Due to the changing radius, a differential balance between the torque (Γ) and shear stress (τ) at a radius of dr needs to be undertaken in order to find the value for the shear stress.

$$d\Gamma = 2.\pi.r^2.\tau dr$$

Equation 3.11. Differential balance between the torque (Γ) and the shear stress (τ) at a set radius (r).

Integrating this equation leads to an equation for the shear stress:

$$\tau = \frac{3.\Gamma}{2.\pi.R^3}$$

Equation 3.12. Shear stress (τ) in terms of the torque (Γ) and radius (R).

Therefore, by measuring the torque and the rotational speed, the shear stress and the shear rate can be measured respectively.

In addition to the constant shear rate across the geometry, the key advantages of the cone and plate are that it is easy to clean and less quantity is required compared to other geometries. However, this geometry cannot be used with samples that have particles in, as the particles can jam in the gap and due to the small gap size (Malvern, 2010).

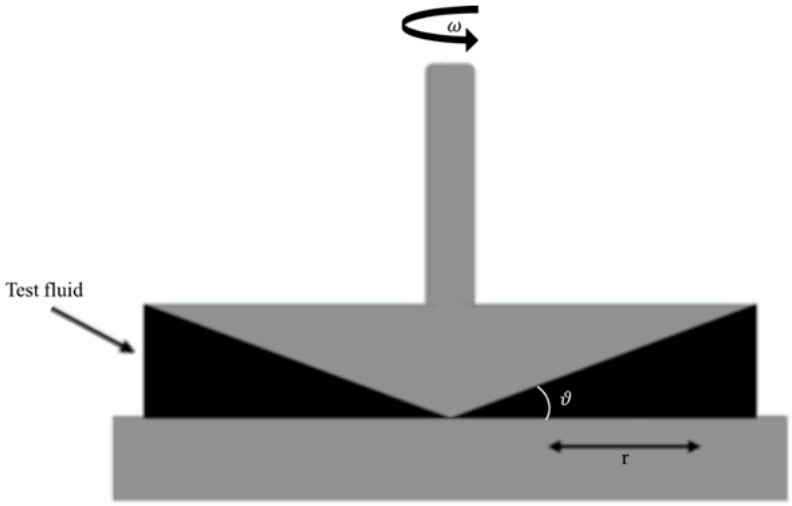

Figure 3.6. Schematic of cone and plate, where ω is angular frequency, ϑ is the angle of the cone and r is the radius.

3.3.2.4 Parallel plate

The parallel plate geometry works in a similar way as the cone and plate geometry, but the rotations of two parallel plates, (one fixed plate, and the other rotating) instead of a cone as shown in Figure 3.7 (Malkin and Isayev, 2006). However, this geometry suffers the problem that the shear rate is not constant between the two plates as the linear velocity changes with the radius. This leads to the equation for shear rate as (Gunasekaran and Mehmet Ak, 2002):

$$\dot{\gamma} = \frac{\omega . r}{h}$$

Equation 3.13. Definition of shear rate ($\dot{\gamma}$) in a parallel plate. ω is the angular frequency, r is the radius and h is the height.

This indicates that the shear rate can not only be varied by changing the rotational speed (ω), as for the cone and plat geometry, but also by changing the gap size (h) (Gunasekaran and Mehmet Ak, 2002).

The shear stress will also vary in the radial direction, therefore the stress which corresponds to a specific shear rate cannot be calculated from a single measurement. The equation for the shear stress at the edge of the geometry (r = R) is given by (Mewis and Wagner, 2012):

$$\tau = \frac{\Gamma}{2.\pi.R^3}\left(3 + \frac{d \ln \Gamma}{d \ln \dot{\gamma}\,(R)}\right)$$

Equation 3.14. Definition of the shear stress (τ) at the edge of a parallel plate geometry. Γ is the torque, R is the radius at the edge of the geometry and $\dot{\gamma}$ is the shear rate.

This equation requires torque measurements at different rotational speeds in order to make a plot of Γ vs γ (R). These equations in this study were computed using the Kinexus software, rSpace. The parallel plate has the advantage that the gap height can be adapted, even when reloading the sample. This geometry is also suitable for samples that are very viscous (Mewis and Wagner, 2012).

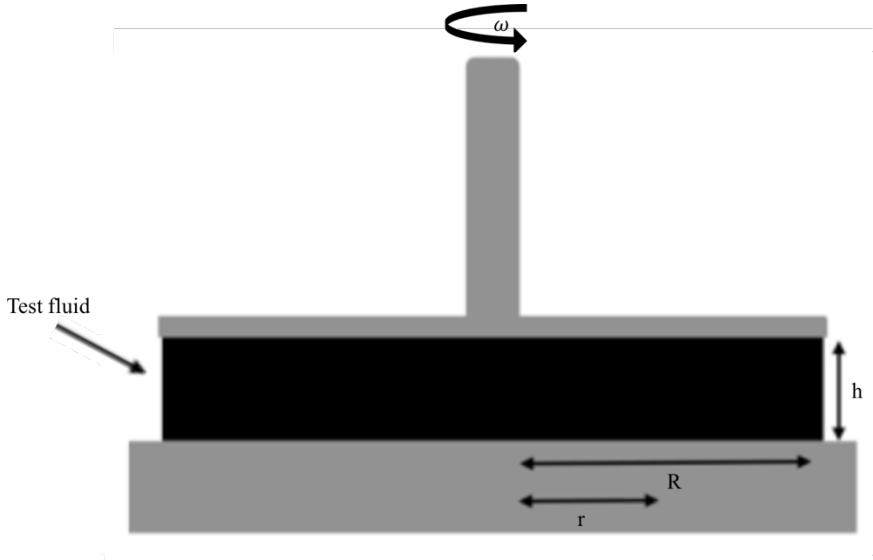

Figure 3.7. Schematic of a parallel plate where ω is angular frequency, h is the height, r is the radius and R is the radius to the edge.

The parallel plate is also easy to clean, and the gap size can be varied, however, the main disadvantage is the variable shear rate across the gap (Malvern, 2010).

3.3.2.5 Concentric cylinder (Couette)

The concentric cylinder geometry consists of a rotating cylindrical spindle and a stationary cup, with a radius only slightly larger than that of the spindle ($r_1/r_2 > 0.96$), as shown in Figure 3.8. Both the shear stress and the shear rate at this geometry are calculated at the surface of the spindle (Braun and Rosen, 2000). The flow between the two cylinders can be considered as the shear flow between two flat plates, which are wrapped around in order to form a continuous cylinder (Chhabra and Richardson, 2011). In this way, the shear rate is approximately uniform, and can therefore be calculated using the equation:

$$\dot{\gamma} \approx \frac{v}{R_2 - R_1} = \frac{R_2.\omega}{R_2 - R_1}$$

Equation 3.15. Definition of the shear rate ($\dot{\gamma}$) in a concentric cylinder. v is velocity, R_1 and R_2 are radii and ω is angular frequency.

At a given radius, r, the shear stress can be calculated by a balance between the shear stress acting on the sample within the cylinder and the torque on the motor shaft:

$$\frac{\Gamma}{r} = \tau . 2 . \pi . r$$

Equation 3.16. Balance between the torque (Γ) on the motor shaft and the shear stress (τ) acting within the cylinder.

Rearranging this in terms of the shear stress gives:

$$\tau = \frac{\Gamma}{2 . \pi . r^2 . L}$$

Equation 3.17. Definition of the shear stress (τ) acting on the sample within the cylinder in terms of the torque (Γ), radius (r) and length (L).

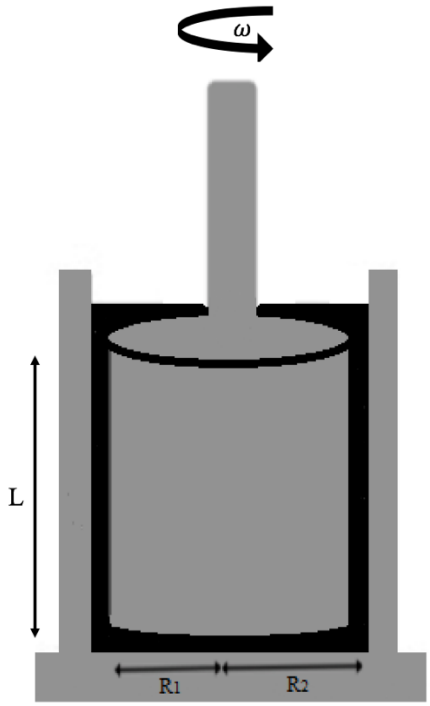

Figure 3.8. Schematic of concentric cylinder geometry where ω is angular frequency R_1 is the radius of the cylinder, R_2 is the radius of the cup and L is the length of the cylinder.

Due to the availability of geometries, two different rheometers were used within this study. The majority of the experiments were undertaken on a Kinexus pro rheometer (Malvern, UK).

However, when determining the gelling rates of the materials a Bohlin Gemini Nano Rheometer (Malvern, UK) was used.

The high surface area of this geometry allows for greater sensitivity for low viscosity samples. However, this geometry can be hard to clean and only a limited frequency range can be tested due to high inertia (Malvern, 2010).

The different tests which have been used within this study have been outlined below.

3.3.2.6 Oscillation test at a single frequency (Chapters 4 and 6)

An oscillation test undertaken at a single frequency was conducted at a frequency of 1 Hz and a strain of 1 %. The sample was loaded at 60 ˚C and cooled at a rate of 1 ˚C.min^{-1} to 20 ˚C, during which the evolution of the storage (G') and the loss modulus (G") were recorded. A serrated 60 mm diameter parallel plate geometry was used (as shown in Figure 3.9), with a gap of 1 mm for the formulations with a secondary biopolymer, and a gap of 0.35 mm for the formulation of gelatin only. This geometry was used in order to avoid slip and a small amount of silicon oil was spread around the lip of the geometry, to act as an oil trap to prevent evaporation of the mixture.

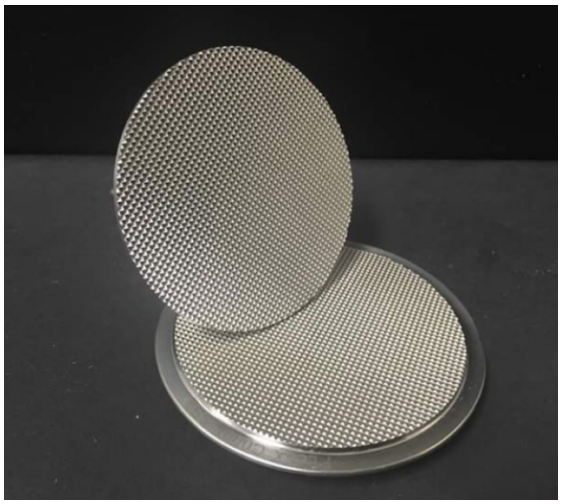

Figure 3.9. Image of the 60 mm diameter serrated plates used within the experiments.

3.3.2.7 Amplitude sweeps (Chapters 4 and 6)

Using the same serrated plate geometry as shown in Figure 3.9, oscillatory tests were conducted in order to determine the LVR of each of the formulations. These tests were undertaken using a strain controlled amplitude sweep from 0.1 to 100 % strain at a temperature of 20 ˚C and the values of G' and G" were recorded.

3.3.2.8 Frequency sweep (Chapters 4 and 6)

Frequency sweeps were obtained for all the samples measuring the G' and G" through a range of applied frequency (0.1 - 10 Hz), the strain was maintained at 1 %. This range was within the LVR of all of the materials, as determined by amplitude sweeps. For the formulations of gelatin and gelatin with kappa-carrageenan, tests were undertaken at 20, 30, 40 and 50 ˚C, apart from the 5 % (w/w) gelatin formulation, which was only tested up to 40 ˚C, due to the sensitivity of the rheometer. The formulations of gelatin with gellan and gelatin with agar were only tested at 20 ˚C. A serrated plate (as shown in Figure 3.9) was used with a gap of 0.35 mm at temperatures above the gelling temperatures of each of the materials and a gap of 1 mm at temperatures below the gelling temperatures. The only exception was the 5 % (w/w) gelatin, where a gap of 0.35 mm was used for all measurements, due to its low viscosity.

3.3.2.9 Printing simulation with set shear rate (Chapter 4)

A custom-made extrusion sequence was run in order to simulate how the material would behave as it passed through the nozzle and post-extrusion. When the material passes through the nozzle, it will experience a shearing force and a temperature drop. Both of these variables will affect how the material will flow, therefore it was important to investigate how they affected the material's behaviour. Once the material was extruded, it needed to have a fast recovery rate, in order for it not to spread and also be able to support the weight of any subsequent layers. A

two-part sequence was created; the first part investigated how the viscosity of the material was affected through a range of temperatures. The temperature range was reduced from 40 to 20 ˚C for the 5 % (w/w) gelatin only and from 50 to 20 ˚C for the gelatin with kappa-carrageenan mixtures at a constant shear rate. A lower temperature range was used for the formulation with just gelatin, as the properties of this mixture at higher temperatures were outside the sensitivity of the rheometer used. The average shear rate within the nozzle was determined using Equation 3.18.

$$\dot{\gamma} = \frac{4.Q}{\pi.R^3}$$

Equation 3.18. Definition of shear rate through a die. Q is the flow rate and R is the radius.

Initially, the flow rate was found by printing a shape of known volume (10.26 ml) and recording the time taken to print. The printed shape was a cuboid with holes, the CAD drawing for which can be seen in Figure 6.18 D. The volumetric flow rate was then determined using Equation 3.19.

$$Q = \frac{V}{t}$$

Equation 3.19. Definition of volumetric flow rate. V is the volume and t is time.

The shear rate applied to the material during extrusion through the syringe barrel (needle of diameter 0.6 mm) was calculated to be of the order of 100 s^{-1} at a printing speed of 10 $mm.s^{-1}$, closely corresponding to previous data presented by Li et al. (2016). The second part of the sequence measured the G' and G" over 10 minutes at a frequency of 1Hz and strain of 0.1 %. A serrated plate geometry was used for all these tests, with a gap of 1 mm. Figure 3.10 depicts a graphical representation of this printing simulation.

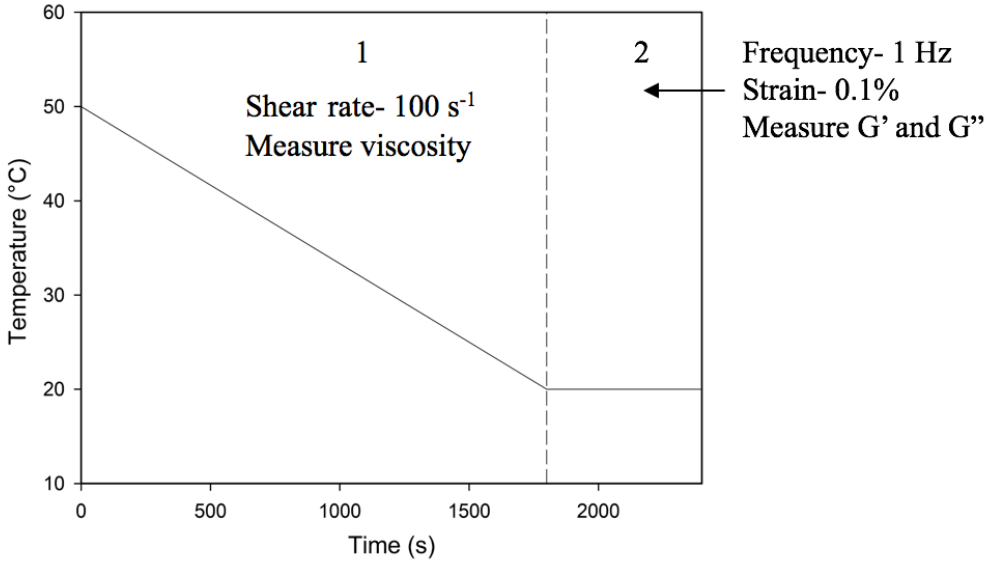

Figure 3.10. Graphical representation of the two-part printing simulation. Measuring the viscosity at a shear rate of 100 s^{-1} from a temperature of 50 to 20 ˚C (1) and then measuring G' and G" over a 10 minute period at a frequency of 1 Hz and strain of 0.1 %.

3.3.2.10 Printing simulation with various shear rates and temperatures (Chapter 5)

The previous printing simulation investigated how the material would act assuming that the material would reduce in temperature as it was extruded from the nozzle and then be at the temperature of the plate, as soon as the material had been extruded. However, ideally the nozzle would be completely insulated, meaning that the material would leave the nozzle at the printing temperature and the cooling down would occur when the material was on the plate. Therefore, a secondary printing simulation was created in order to investigate the behaviour of the material assuming a fully insulated nozzle. Similar to the previous simulation, this simulation consisted of two parts: a viscosity curve followed by small deformation oscillation. The viscosity measurement was undertaken at a constant temperature, as well as a constant shear rate for a specific period of time, which was dependent on the speed of the printing, in order to mimic the conditions, the material would experience within the nozzle. Five different printing temperatures were investigated: 40, 45, 50, 55 and 60 ˚C (apart from the formulations with 3 %

(w/w) kappa-carrageenan, where the minimum temperature was 45 ˚C). The shear rate and time for the viscosity curve was dictated by the printing speed of the experiment (10, 25 and 50 $mm.s^{-1}$). The average residence time that the material would experience a shear within the nozzle at each of the printing speeds was determined as 12.7, 5 and 2.5 seconds for the printing speeds of 10, 25 and 50 $mm.s^{-1}$ respectively. The average residence time was taken as during material extrusion, the material at the walls will experience the highest shear rate, and will be approximately stationary, whereas the material in the middle of the die will have a very low shear rate, and have a high velocity. These facts suggest that different parts of the fluid remain inside the nozzle for the same amount of time, but for practical purposes it was useful to calculate an average residence time. As these times were so short, the time for the viscosity curve was multiplied by 10, in order to allow the rheometer time to reach equilibrium. Therefore, the time taken for each of the viscosity curves was 127, 50 and 25 seconds for a printing speed of 10, 25 and 50 $mm.s^{-1}$ respectively. In accordance with section 3.3.2.9, the shear rate within the nozzle was evaluated using Equation 3.18, with the flow rate through the nozzle determined using Equation 3.19. However, it was noted that the printing time recorded also included the time of the non-print moves, where the nozzle was moving, but not extruding, therefore not placing any shear on the formulation. Therefore, in order to determine a more accurate shear rate through the nozzle, the time taken to complete just the printing moves was established. Initially the total printing time (t_{tot}) was defined as the time taken for printing moves (t_p) and the time taken for non-print moves (t_{np}), as defined within Equation 3.20.

$$t_{tot} = t_p + t_{np}$$

Equation 3.20. Definition of the total print time (t_{tot}).

The time taken for print moves can be rewritten as the total distance for the print moves (d_p) over the speed of the print moves (S_p), as seen in Equation 3.21. This can be repeated for the total non-print moves (Equation 3.22).

$$t_p = \frac{d_p}{S_p}$$

Equation 3.21. Definition of the printing time in terms of distance and speed.

$$t_{np} = \frac{d_{np}}{S_{np}}$$

Equation 3.22. Definition of the time for non-print moves in terms of distance and speed.

By rearranging the above three equations, a new definition of the total time was established:

$$t_{tot} = \frac{d_p}{S_p} + \frac{d_{np}}{S_{np}}$$

Equation 3.23. Rearranged definition of the total print time using the speed of printing and distance of the print and non-print moves.

This equation could then be plotted as a linear function of the total time against $1/S_p$, with the intercept giving the time of the non-print moves. The time taken to print a 22 mm diameter cylinder, with a height of 20 mm at several different printing speeds, and a constant non-print move speed of 100 mm.s^{-1}, was recorded and then plotted against the reciprocal of the printing speed, the results of which can be seen in Figure 3.11.

From these results, it was found that the time taken for non-print moves with a non-print move speed of 100 mm.s^{-1} was 18.6 s. This non-print time was then deducted from the total printing time, in order to determine the time for print moves only. This new time, was then used to determine the flow rate at various speeds, using Equation 3.19. Once found, it was then possible

to use these flow rates to determine the corrected shear rates using different nozzle sizes. An example, using a nozzle size of 1.1 mm at various printing speeds, can be seen in Table 3.1.

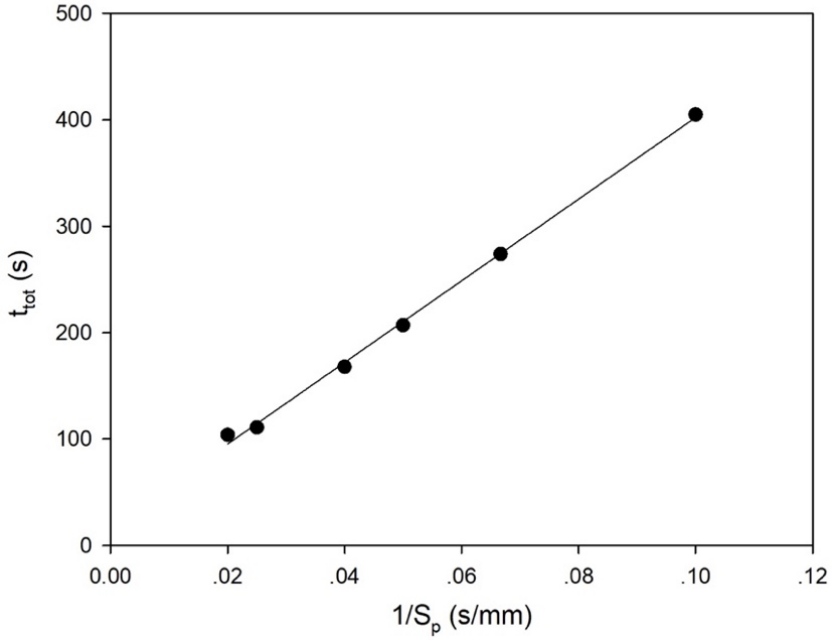

Figure 3.11. Determination of the non-print movement time.

Table 3.1. Determination of the shear rate using a nozzle of diameter 1.1 mm and non-print move speed of 100 mm.s^{-1}.

	Print Speed (mm.s^{-1})		
	10	**25**	**50**
Total print time (t_{tot}) (s)	405	168	104
Time for print-moves only (t_p) (s)	386	150	85
Flow Rate (Q) (mm^3.s^{-1})	1.37 x 10^{-8}	3.55 x 10^{-8}	6.21 x 10^{-8}
Uncorrected Shear Rate (s^{-1})	108	260	420
Corrected Shear Rate (s^{-1})	113	293	513

At the slowest printing speed (10 $mm.s^{-1}$), the time taken for non-print moves did not significantly affect the shear rate within the system, due to the long total printing time. At the higher printing speeds (50 $mm.s^{-1}$), there was a substantial difference between the corrected and uncorrected shear rates.

The second part of the simulation was a small deformation oscillation section, which was conducted from the temperature used during the viscosity, to a temperature of 20 ˚C, using a scanning rate of 3 ˚$C.min^{-1}$, frequency of 1 Hz and a strain of 0.1 %. In reality, the material would cool significantly faster and also experience a temperature gradient after extrusion. Due to the nature of the rheometer and the temperature being controlled by the plates, this temperature gradient could not be replicated, therefore the fastest cooling rate that the rheometer could control was used.

For each of the formulations, 15 different experiments were undertaken, at the 5 different temperatures and 3 different printing speeds (apart from the formulation with 3 % (w/w) kappa-carrageenan, where the minimum temperature tested was 45 ˚C). As an example of an experiment, when considering a printing speed of 10 $mm.s^{-1}$ at a temperature of 50 ˚C, the large deformation part would be undertaken at a shear rate of 113 s^{-1} for 127 seconds at a temperature of 50 ˚C, immediately afterwards a small deformation oscillation section would be undertaken from 50 to 20 ˚C at a rate of 3 ˚$C.min^{-1}$ and a frequency of 1 Hz and a strain of 0.1 %. A graphical representation of this printing simulation can be seen in Figure 3.12.

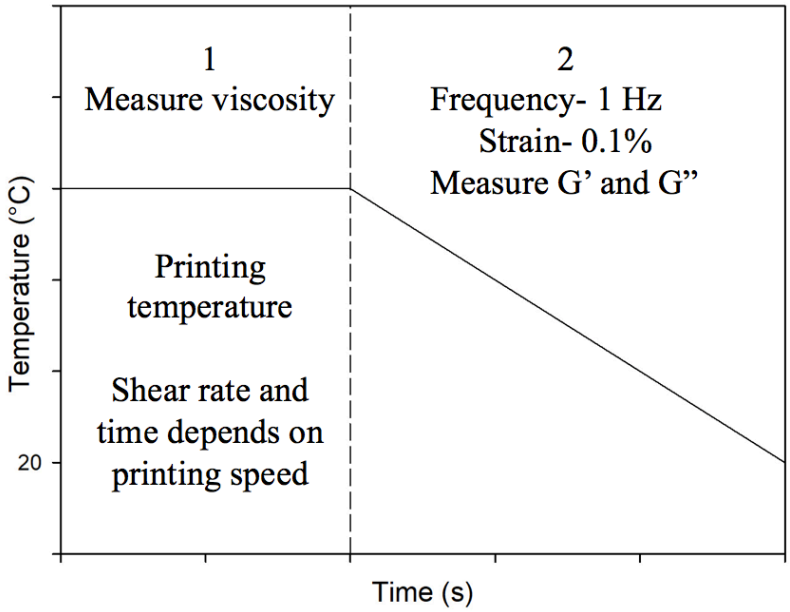

Figure 3.12. Graphical schematic of the print simulation with various printing temperatures and speeds. At the desired temperature and for a set time and shear rate (relating to the printing speed) the viscosity is measured (1). Then the magnitude of G' and G" are recorded as the temperature is decreased to 20 ˚C at a frequency of 1 Hz and strain of 0.1 %.

3.3.2.11 Viscosity (Chapters 5 and 6)

The viscosity of all of the formulations was determined via a shear rate sweep on the rheometer. The viscosity sweep recorded the viscosity of the material across a range of shear rates from 1 - 1000 s^{-1} and this test was undertaken at each of the printing temperatures the formulation was subjected to (45, 50, 55 and 60 ˚C for all of the formulations and 40 ˚C for the formulations of 5 % (w/w) gelatin and 5 % (w/w) gelatin with 1 and 2 % (w/w) kappa-carrageenan). The same serrated plate, of diameter 60 mm (as shown in Figure 3.9) was used for all of the formulations and each temperature was tested in triplicate.

3.3.2.12 Gelling Rates (Chapters 5 and 6)

A gel is an intermediate phase between a solid and a liquid and gelation generally occurs when the material is cooled forming stable noncovalent bonds among exposed functional groups of the various molecules (Damodaran and Parkin, 2017). Due to the nature of the rheometers used

within this work, it was not possible to measure the gelation rate. In order to get an idea of how quickly the materials were structuring, the rate of increase of G' from a high temperature to low temperature of the materials were characterised on a Bohlin rheometer. A 20 mm serrated parallel plate was loaded onto the machine and the gap set to 1 mm. An oscillation sequence was initiated at 20 ˚C and then molten sample was added. The molten samples were heated to 90 ˚C before addition to the rheometer, in order to allow a large temperature gradient between the loading temperature and the material's gelling temperatures. The results were plotted with G' as a function of time and a typical curve obtained can be seen in Figure 3.13. The initial values, shown in the shaded box were erratic, as this is where the sample was added. When analysing the data these initial values were discarded and the beginning point taken from where the curve was flat. The beginning of gelation was taken as the value of G' began to increase from the initial values, and the end of gelation was taken when the value of G' began to plateau and the percentage difference between two points was less than 5 % over 3 consecutive points. A line was drawn between the point of initial increase of G' and the point where the G' value began to plateau. The gradient of this line was taken as the rate of increase of G'.

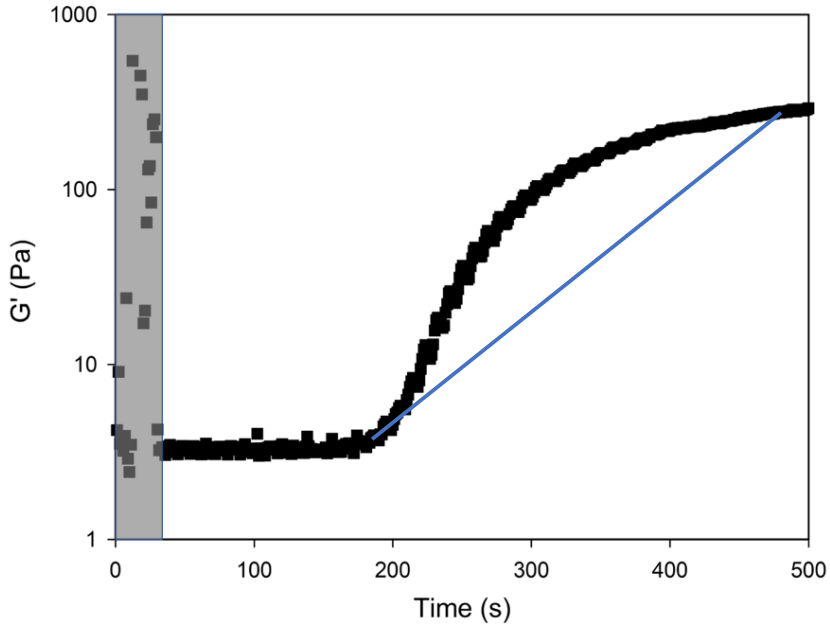

Figure 3.13. Typical gelling rate curve. The shaded area indicates the initial values obtained while putting the sample into the rheometer, therefore, these values have been removed. The blue line indicates the line draw, of which the gradient was then taken as the rate of increase of G'.

3.3.3 Fused Deposition Modelling (FDM) Printer Set-Up and Alterations

Considering the type of materials to be printed within this work, it was determined that an FDM printer would be the most suitable choice, due to the ease of printing and the wide availability of this type of printer, which could be adapted to print the required materials. There are several different types of FDM printers available, which all work in the same way of extruding the material, but move the print head in different ways to produce the printed objects. Most extrusion based food printers currently in use are modified plastic material machines. As the edible material generally needs a syringe to hold the material, it results in an increase in the weight of the print head, which can affect the quality of the print. It is important to keep the weight of the print head to a minimum. Some of the different types of FDM machines available and several of their key advantages and disadvantages have been outlined in Table 3.2.

Table 3.2. Outline of the different types of types of FDM machines (Sun et al., 2017).

Type	Outline of process	Pros/ Cons	Schematic
Cartesian	Has x-, y- and z- axes for left to right, front to back and up and down motion, respectively. Stage which moves along the z-axis, with the print head moving in the x- and y- directions, or the stage moves along y-axis and the print head moves in the x- and z-directions.	Large amount of software and hardware is readily available; Easy to maintain and calibrate. Requires a large space for printing operation; The moving print head compromises the printing speed and printing quality due to jerking motion when changing directions.	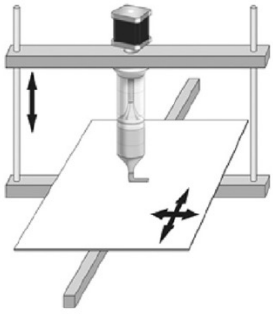
Delta	Fixed circular print bed. Print head suspended by three arms above the bed in a triangular configuration. Arms move up and down their channels in order to move the print head.	Fewer components, reducing maintenance and machine costs; Cheaper and faster. Not precise in position control; Hard to calibrate; Fast moving print head with the rapid acceleration/deceleration can lead to liquid vibration in the printing process.	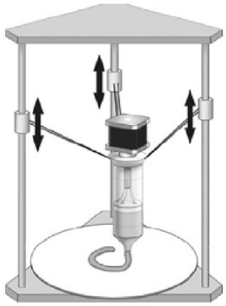
Polar	Uses polar coordinated to describe the points on a circular grid. Usually has a spinning stage, a print head which can move up and down to cover the z- direction and left and right to cover the x- and y- axis.	Can achieve a perfect circle; Minimum calibration. Still primarily in the conceptual stage, moving towards engineering designs.	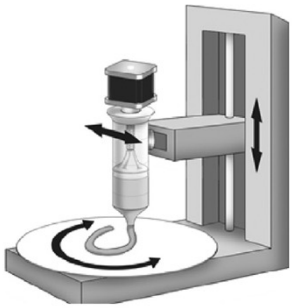

In order to minimise the functional variables relating to the movement of the print head, a Cartesian machine was utilised, with the bed which moved in the y-axis direction. Although the delta machine would have printed out shapes faster, the calibration of these types of printers are difficult, due to the nature of machines movement.

The custom-made FDM printer was created by modifying a commercially available Hictop Prusa i3 printer, the original printer is shown in Figure 3.14. This FDM machine achieved printer objects by having the printer nozzle mounted on a gantry which can moved in the x-direction. The whole gantry was affixed onto screws on either side of the bed, so that the nozzle could be lifted up and down, in order to achieve movement in the z-axis and build the object up. Under the bed was a pulley system, which moved the bed back and forth in order to achieve movement in the y-direction.

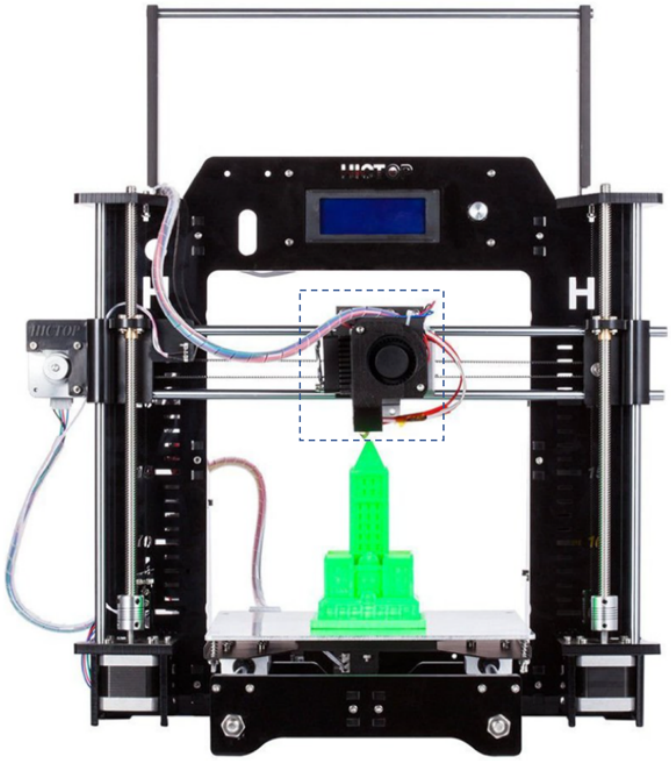

Figure 3.14. Hictop i3 Prusa with plastic print head. The dashed box indicates the plastic nozzle head which was removed. Image from Hictop (2018).

In order to modify the printer to enable syringe-based printing, the whole plastic nozzle head was removed, shown in the dashed box in Figure 3.14. This was replaced with a custom designed metal syringe based extrusion configuration, which consisted of a back plate, a syringe bottom holder and top holder and a guide rod aligner, shown in Figure 3.15. The bottom holder fitted into the bottom of the back plate, while the guide rod holder and top holder fit together, in order to hold the syringe in place and keep it steady while printing. All of the parts were printed using polylactic acid (PLA), and the back plate was reinforced with steel plates in order to strengthen the plate and ensure that it did not bend during extrusion.

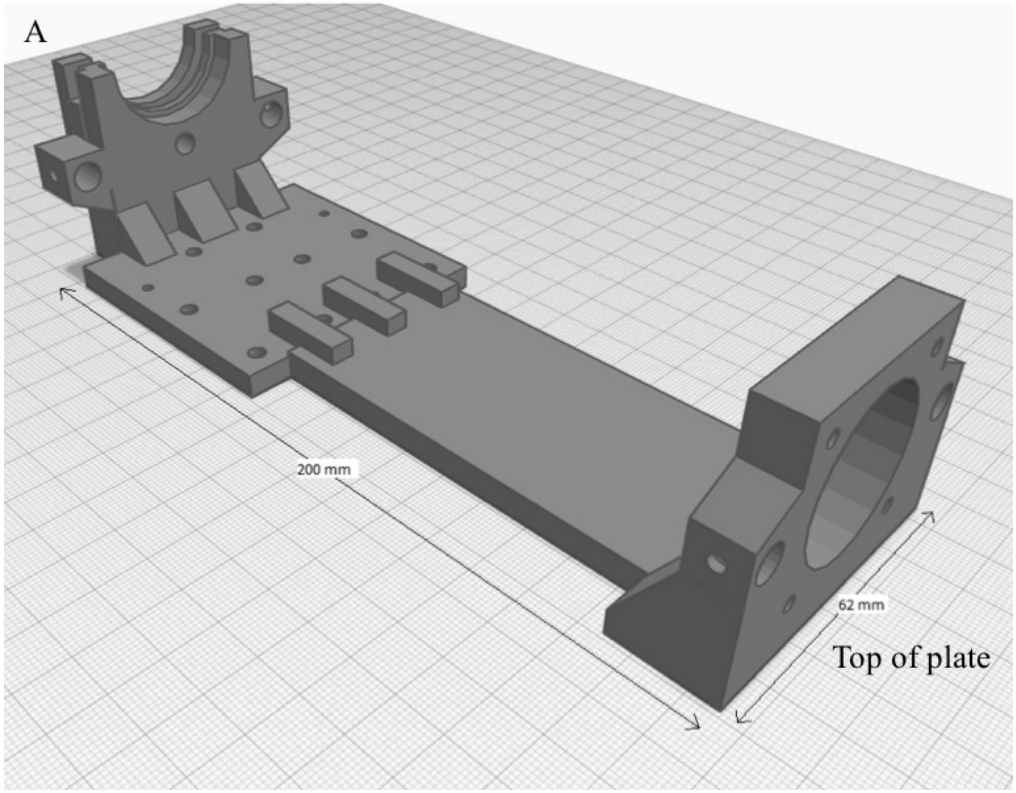

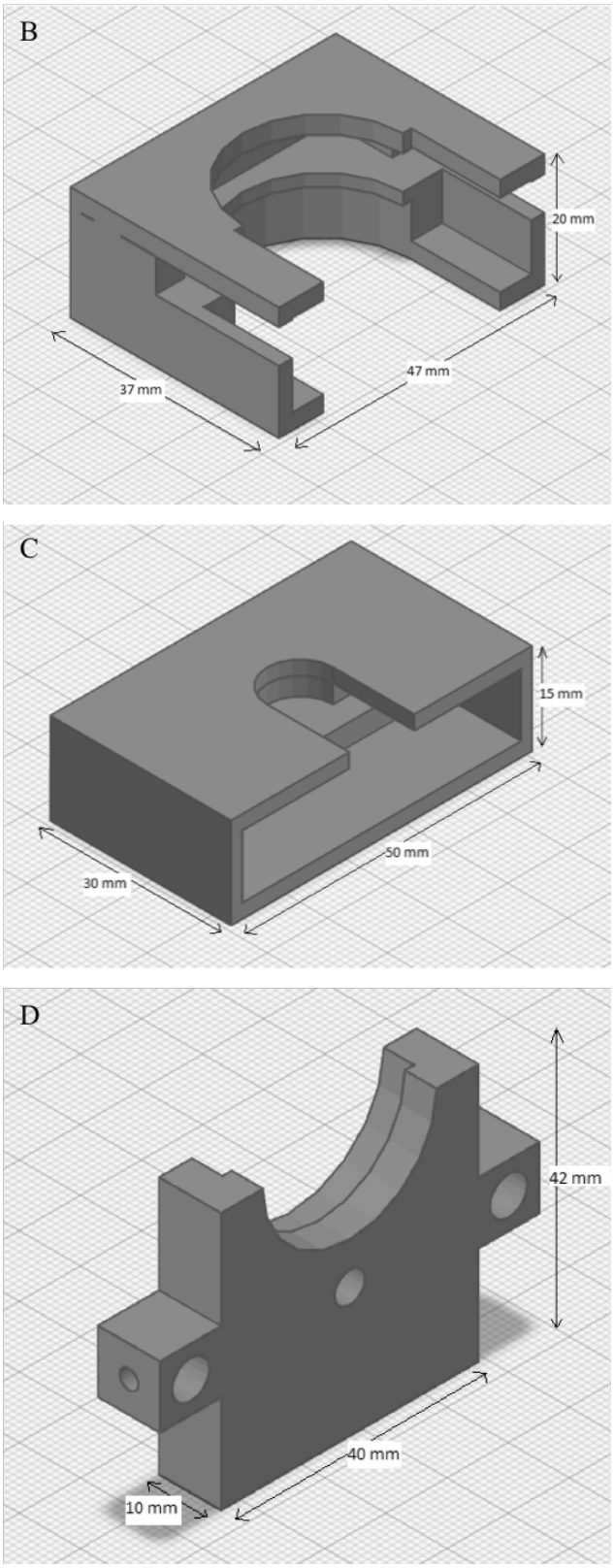

Figure 3.15. Technical drawings of the back plate (A), syringe bottom (B) and top holder (C) and a guide rod aligner (D). All of these parts were printed in PLA and when joined together, created the syringe extruder.

Ideally in order to increase the rigidity of the back plate, it would have been made entirely from metal. However, due to the nature of this type of FDM machine, the nozzle moved in the x- and y-directions, therefore it was important to try and keep the head as light as possible as any addition mass in this area led to reduction in the movement precision (Anzalone, 2015).

The printer was also modified in several other ways, in order to try and enable the highest quality print. Belt tensioners were designed and printed in PLA for the two axes which use a belt system (x- and y-axis) as shown in Figure 3.16. The belt tensioners aided the tightening of the belts, reducing the risk of the belts slipping a tooth, which could then lead to a missed step when printing, resulting in the object not be printing in the desired way. Both of the tensioners created worked in the same way, using screws to increase the length of the belt. Due to the positioning of belt of the x-axis, the tensioner had to be created through the gantry chamber. Three different pieces were printed, the belt screw holder, the end holder and the tightening cog. The belt screw holder (the part printed in yellow in Figure 3.16 A), had a square end on one side to hold the screw holding the belt, whereas the other end was long, with a hole for a screw at the other end. This screw is the one that can be seen protruding the other side of the image and when the cog was turned in a certain direction pulled the belt screw holder closer, and increased the tautness of the belt. The y-axis tensioner was a relatively simple design with the tensioner printed with holes for the large screw to hold the belt and small screws which protruded through the base of the printer. When these smaller screws were tightened, the belt was pulled further apart, increasing the tautness.

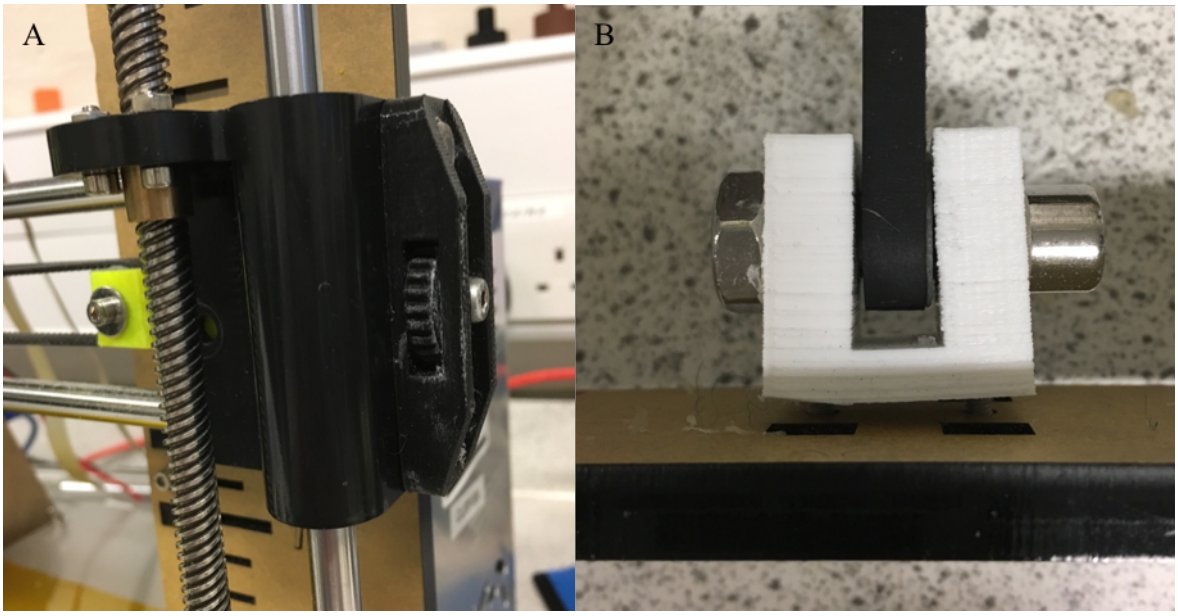

Figure 3.16. Belt tensioners for the x-axis (A) and y-axis (B).

The final modification changed the z-endstop. An endstop is a switch which is located at the extreme of each of the axis directions. When the printer reaches a limit from one of the directions, the endstop is activated, and will immediately stop the movement in the printer, to ensure that the printer does not try and print outside of the bed area. An image of an endstop switch can be seen in the insert of Figure 3.17. Within the original design of the printer, the z-endstop was located on a slider, which allowed the user to move it up and down, to change where the machine hit the endstop. The plastic nozzle head was relatively small compared to the syringe print head, and was only a few centimetres lower than the bars that held it in place. However, the syringe base system was a lot larger, and protruded further from the parallel bars. Therefore, a device was created in order to allow the end stop to be hit, when the syringe nozzle had reached the plate. Figure 3.17 displays the device created in order to manipulate where the z-endstop was hit. The screws, clearly visible on the left, allowed this device to be increased or decreased in height, to allow the user more control of where the end stop was hit.

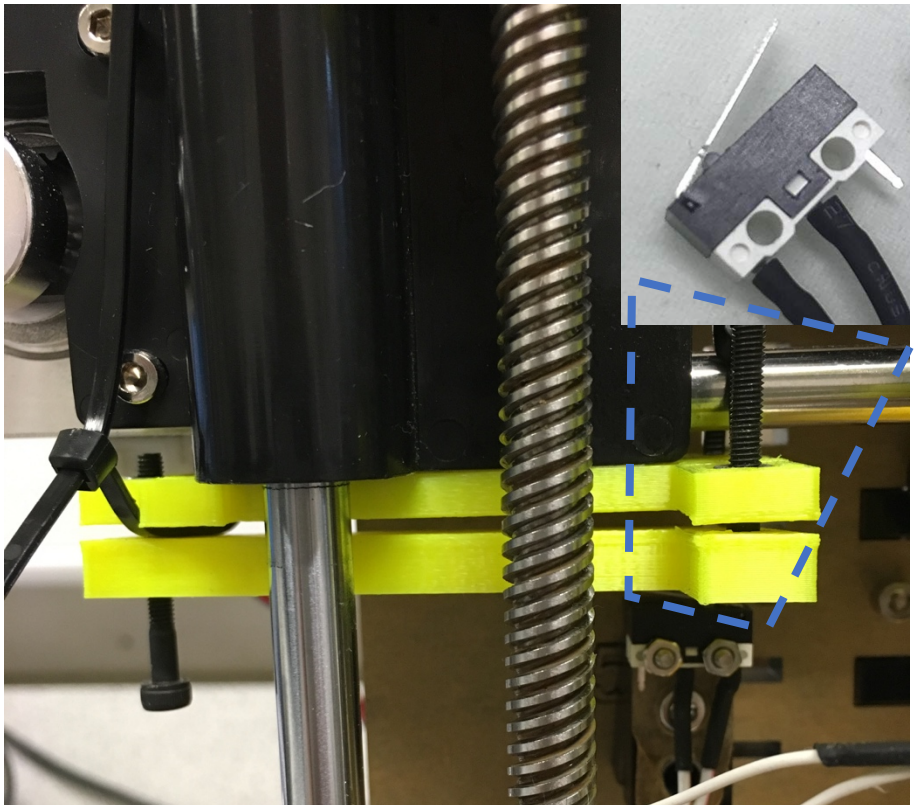

Figure 3.17. z-axis end stop modifier. Insert shows an image of the endstop and indicates where it goes for this axis.

The syringe employed within this study was a 30 ml metal syringe and was encased in a silicone heater pad purchased from RS Components (Northamptonshire, UK), as shown in Figure 3.18, and extrusion was controlled using a stepper motor connected to a screw plunger.

Figure 3.18. Syringe (left) and silicone heater pad (right).

Four metal needles of gauges 16, 17, 18 and 20 (relating to an internal diameter of 1.2, 1.1, 0.8 and 0.6 mm respectively) were purchased from TECHCON (Hampshire, UK), shown in Figure 3.19.

Figure 3.19. Photograph of the four different nozzles used, with gauges from left to right of 16 (1.2 mm), 17 (1.1 mm), 18 (0.8 mm) and 20 (0.6 mm).

The needle used while printing was attached to the syringe and insulated using aluminium foil in order to prevent heat loss.

The metal bed of the printer was covered in Kapton tape (which is a polyimide film (Naftulin et al., 2015)) in order to provide a smooth surface for the printed object (Hawatmeh et al., 2016). The Kapton tape also made it easy to remove the printed objects and on occasion if the nozzle was too close to the bed and scratched the tape, the tape was easy to remove and replace.

Figure 3.20 shows a labelled picture of the fully set up syringe printer, with the insert showing a close-up of the insulated needle.

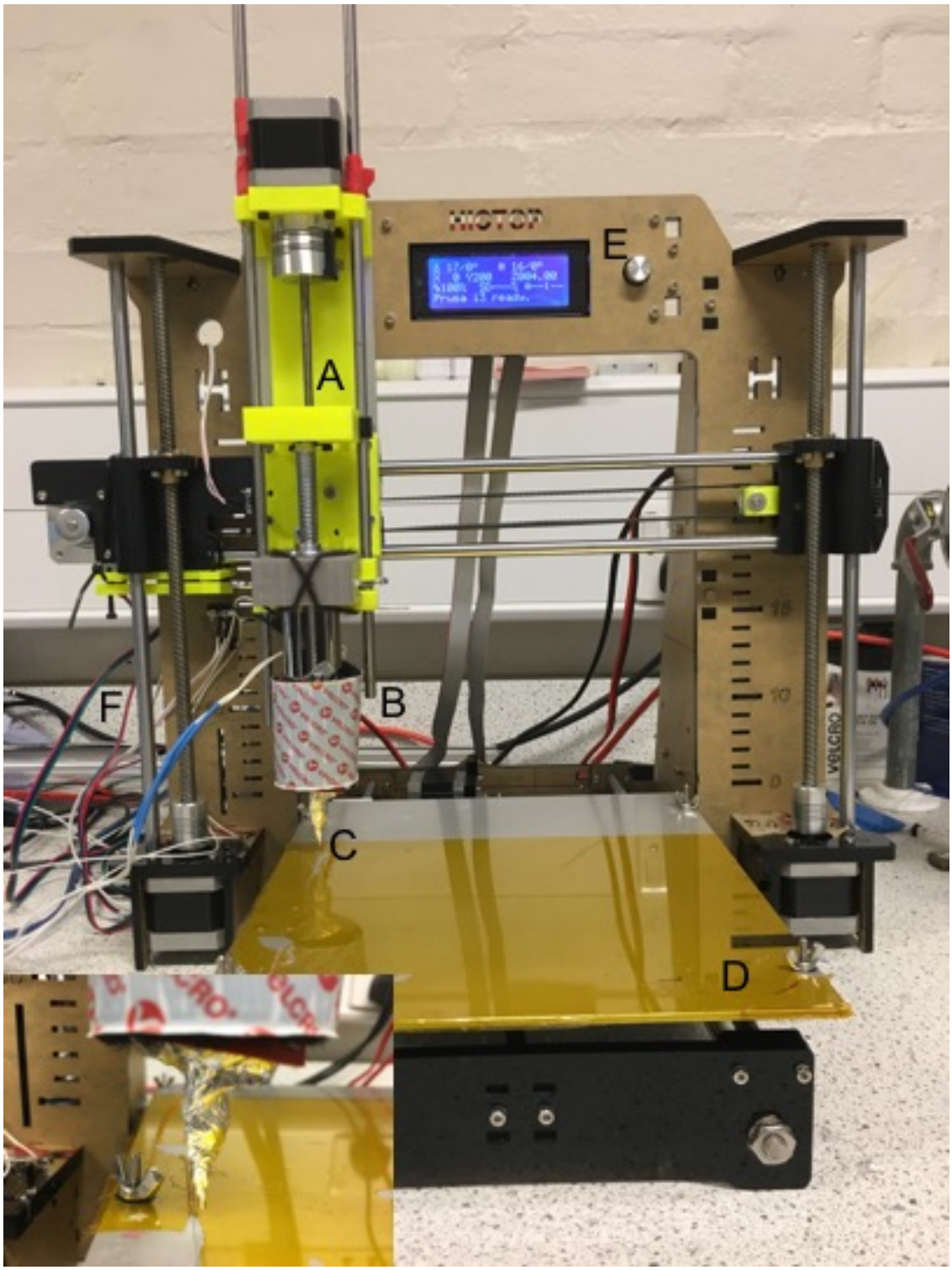

Figure 3.20. Labelled photograph of the modified Hictop Prusa i3 printed, with the custom syringe pump (A. Custom built back plate, B. Metal syringe encased in a silicone heating pad, C. Metal needle insulted with tin foil, D. Printing bed, E. Control display, F. Circuit board that connects to the printer and controls the motors). Insert shows a close-up of the insulated needle.

Before each print the bed-level was levelled manually, by manually moving the nozzle to each of the four corners and measuring a 100 micron gap with a gauge between the bed and nozzle by tightening or loosening the screws located in the corners, shown in Figure 3.21.

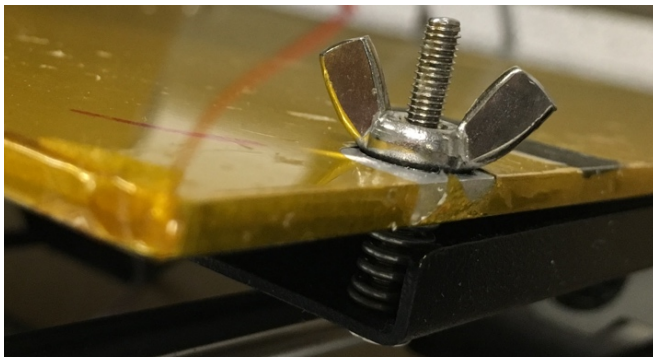

Figure 3.21. Screw with spring at each of the corners helped to calibrate the bed level.

All of the printed samples were printed at ambient temperatures (approximately 20 ˚C) without the aid of an external cooling apparatus. During the printing process, the syringe was loaded with approximately 15 ml of material (due to the height of the heater pad only covering this much of the syringe) and then the needle was attached and insulated using aluminium foil. The syringe was then attached to the back plate and held using the holders.

The software used within this work in order to control the printer was ‘Repetier’. Once the machine had been set up, the first action was to calibrate the syringe pump by printing a known volume of material, weighing the printed material and then modifying the extrusion multiplier factor within the software. This was repeated until the weight of the printed material was within 5 % of the desired weight. After this was completed, it was possible to commence printing of the formulations.

In order to create an object to be printed, a computer-aided design (CAD) model of the object was input into the software (Wong and Hernandez, 2012). The software then ‘sliced’ the object into a pre-determined number of layers and calculated a path which is then used for the creation

of the object. During the printing process, the syringe followed this path and extruded material where necessary, in order to create the shape. Some of the properties of the printer are outline in Table 3.3.

Table 3.3. Example of a few different printing properties, their definition and description.

Property	**Definition**	**Description**
Layer/ nozzle height	The height of the printed layers.	Decreasing the layer height gives a higher resolution of the printed part, but increases print time.
Nozzle/ printing temperature	Temperature that the nozzle is set to.	If the printing temperature is too high then the material could flow out, but too low and the material will not be molten enough and will block the nozzle.
Bed temperature	Temperature that the bed is set to.	When printing plastic, if the bed temperature is set too high the material may not stick down. If the bed temperature is set too low the material will solidify too quickly, so the layers may not stick together.
Nozzle height	The height the nozzle is above the bed when printing the part.	The closer it is to the bed the more it squashes the material down, forcing the layers to stick, too close and the object will be squashed when printed. If the nozzle is too far away, the layers will not stick together.
Extrusion multiplier factor (EMF)	A setting in the software which determines how much material is extruded.	Increasing the EMF increases the amount extruded, too high can lead to over extrusion. If the EMF is too low, not enough material is extruded which could lead to gaps within the shapes.
Retraction Speed	Speed the motor retracts material once the layer has been completed.	Increasing the retraction speed results in more material being pulled up by the motor after the layer has finished, in order to reduce the pool of material which can be created once the layer has finished.

3.3.4 Microscopy (Chapter 5)

Microscopes are instruments which are designed to magnify small objects in order to make them visible to the human eye or camera (Abramowitz and Davidson, 2018). There are a variety of different microscopy techniques which are able to capture different sizes of specimen. A diagram depicting some of the different samples able to be imaged using different types of microscope can be seen in Figure 3.22, adapted from Findlay (2018).

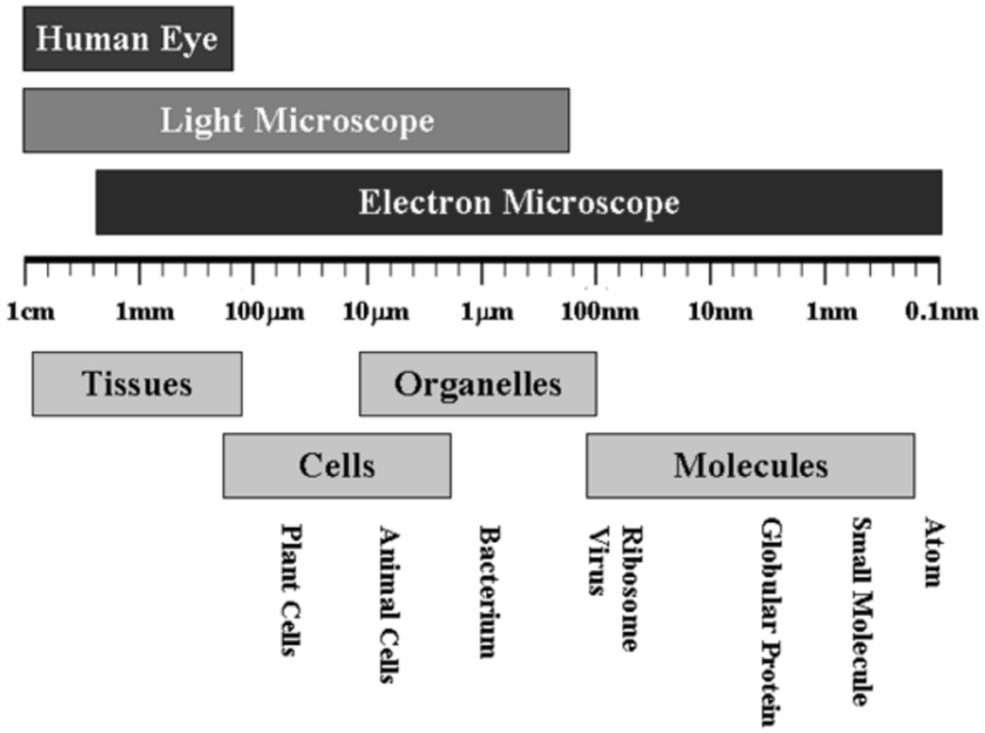

Figure 3.22. Diagram depicting the different types of microscope techniques across different length scales. Adapted from Findlay (2018).

A light (optical) microscope possesses a number of lenses, which are curved pieces of glass or plastic, which bend rays of light in order to magnify the object. Light from a lamp source is either passed through (transmission) or reflected off (reflection) the samples and then passed through the lenses, magnifying the sample, making it visible to the human eye. The electron

microscope uses a beam of electrons in order to image the sample, and is capable of much higher magnification compared to a light microscope.

Due to the size of the samples within this work, an optical microscope (Leica, Microsystems, UK) was used in order to image a cross-sectional area of the printed lines, using an objective lens of 4x magnification. The printed lines were cut with a scalpel blade and placed on a microscope slide in order to image them. The microscope was used on the reflective light microscopy setting, which allows imaging of samples even though they are opaque. Because the light is unable to pass through the sample, the light is directed at the surface of the object and returned to microscope objective by either specular or diffused reflection (Abramowitz and Davidson, 2018).

3.3.5 Texture Analyser (TA) (Chapters 5 and 6)

Texture analysis (TA) is a mechanical testing method used in order to evaluate the textural parameters of a wide range of materials including food, cosmetics, pharmaceuticals and other consumer products (Peleg, 1976). This technique measures the compression (or tension) force (in Newtons) over time produced by the TA when deforming some material (de Huidobro et al., 2005). There are a variety of parameters which can be measured using different tests and geometries. An outline of some of these tests, taken from Stable Micro Systems (2018):

- Compression - the sample is deformed using a compression probe and the extent of the deformation offered by the sample is recorded and used an index of the texture of the material;
- Puncture/penetration - a probe penetrates the sample to a defined depth and the force necessary to achieve this depth or the time taken to reach the depth is measured and used as an index for firmness, toughness or hardness;

- Cutting/shearing - a blade is cut/ sheared through the sample and the force needed to achieve this is measured and taken as an index of toughness or firmness;
- Tension - a force normal to the surface, is applied to the sample and the amount of force required to fracture the sample in a plane approximately perpendicular to the plane of applied tension is recorded and used an index of tensile strength of the food.

Compression testing of food is a commonly used technique in order to measure the mechanical properties of a material as it gives an idea of how the material will feel within the mouth (Pascua et al., 2013). Within this study, a compression test was conducted on the materials in order to easily compare the peak force of the printed cylinders printed at different printing temperatures and speeds. The peak force was the force required to fracture the objects.

The peak forces of cast samples of the formulations were also determined for comparison purposes. The cast cylinders were created by pouring molten material into a mould and allowing the material to set or re structure in the fridge at a temperature of 3 ˚C for one hour. The printed cylinders were created by printing the material, at a set temperature and speed. All of the printed samples were also place in the fridge at 3 ˚C for an hour before testing. Both of the cast and printed samples were placed in the fridge before testing in order to allow the materials time to gel, in accordance with Fonkwe et al. (2003) who determined the rate of increase of G' for gelatin and polysaccharide samples began to plateau after approximately 1 hour. Both the cast and printed samples were created with a diameter of 22 mm, and a length of approximately 20 mm. The texture analyser used was a TA.XT.plus (Stable Micro Systems LTD., UK), fitted with a 40 mm diameter cylindrical aluminium probe. For the majority of the experiments, a 5 kg cell was used, apart from the cast samples of the 5 % (w/w) gelatin with 2 and 3 % (w/w) kappa-carrageenan and 5 % (w/w) gelatin with 2 and 3 % (w/w) gellan, where a 30 kg cell was used. The compression rate was set to 2 $mm.s^{-1}$ and the measurements were made to a strain

compression of 50 %, using a trigger force of 10 g. A thin layer of silicone oil was applied to the plates before the measurements, in order to reduce the friction during compression. The data shown is a mean of at least 5 replicates with ± one standard deviation.

3.3.6 Statistical analysis (Chapter 4)

All of the μDSC and rheological experiments have been repeated in triplicate, while the printed squares have been repeated 6 times. All of the data has been presented as the mean of the results ± 1 standard deviation. Data analysis of the width and the heights of the printed squares was processed with SigmaPlot software, with differences of $p < 0.05$ considered to be significant.

CHAPTER 4. RELATING THE VISCOELASTIC PROPERTIES OF GELATIN AND KAPPA-CARRAGEENAN MIXTURES WITH THEIR PRINTABILITY

4.1 Introduction

Recent interest in personalisation of food through AM has identified a need for more information on the formulation and printability of potential ingredients. Research undertaken to date has concentrated on exploring the rheological properties and printability of hydrogels using materials which maintain their shape due to a yield stress. The total amount of literature available for additive manufacturing of food is still relatively limited. Whilst this technique is satisfactory, a greater variety of foods and finishes could be provided with the benefit of an enhanced understanding of the material properties necessary in order to print food that transitions from a liquid to a solid.

The main objectives of this chapter were to investigate the viscoelastic properties of a temperature dependent gelatin-based solution and then correlate these properties with the printability of the material. Four different formulations were explored, 5 % (w/w) gelatin with 0, 1, 2 and 3 % (w/w) kappa-carrageenan. Initially the gelling temperatures of the systems and the rheological characteristics including: flow profiles, evolution of elastically dominated structures and frequency dependent behaviour were established. The mixtures were subsequently printed at two temperatures, just above and much greater than, their gelling temperatures. Finally, design rules were established in order to determine the properties necessary to achieve a print within 10 % of the desired shape.

Initially, within this research, mixtures of just gelatin were investigated for the extrusion process, because of their high gel strength (Gómez-Guillén et al., 2011). However, conversion of the coils to helices in gelatin is a slow process (Harrington and Morris, 2009), which resulted in the printed objects not retaining their shape after printing. Kappa-carrageenan was added in order to accelerate the gelation of the system enabling better shape retention.

4.2 Results and Discussion

4.2.1 Thermal properties of the gelatin and kappa-carrageenan mixtures

The behaviour of the material within the nozzle will be affected by its thermal properties. Such properties of the various printing materials (5 % (w/w) gelatin with 0, 1, 2 and 3 % (w/w) kappa-carrageenan) were investigated using a μDSC and rheological techniques.

The μDSC was used in order to determine the melting and gelling temperatures of the formulations of 5 % (w/w) gelatin with additions of 0, 1, 2 and 3 % (w/w) kappa-carrageenan. Figure 4.1 A shows the heating endotherms while Figure 4.1 B shows the cooling exotherms obtained from the first cycle for all of the formulations.

The 5 % (w/w) gelatin exhibits a single endothermic peak and a single exothermic peak. As the temperature of the mixture was increased, the gelatin immediately starts to melt, therefore a base line before the peak was not attained (Michon et al., 1997). The endothermic heat ends at around 36 ˚C, which corresponds to the temperature at the end of the helix-to-coil transformation, a similar value was found by Ninan et al. (2014), who ran a comparative study on the functional properties of carp skin and mammalian gelatins.

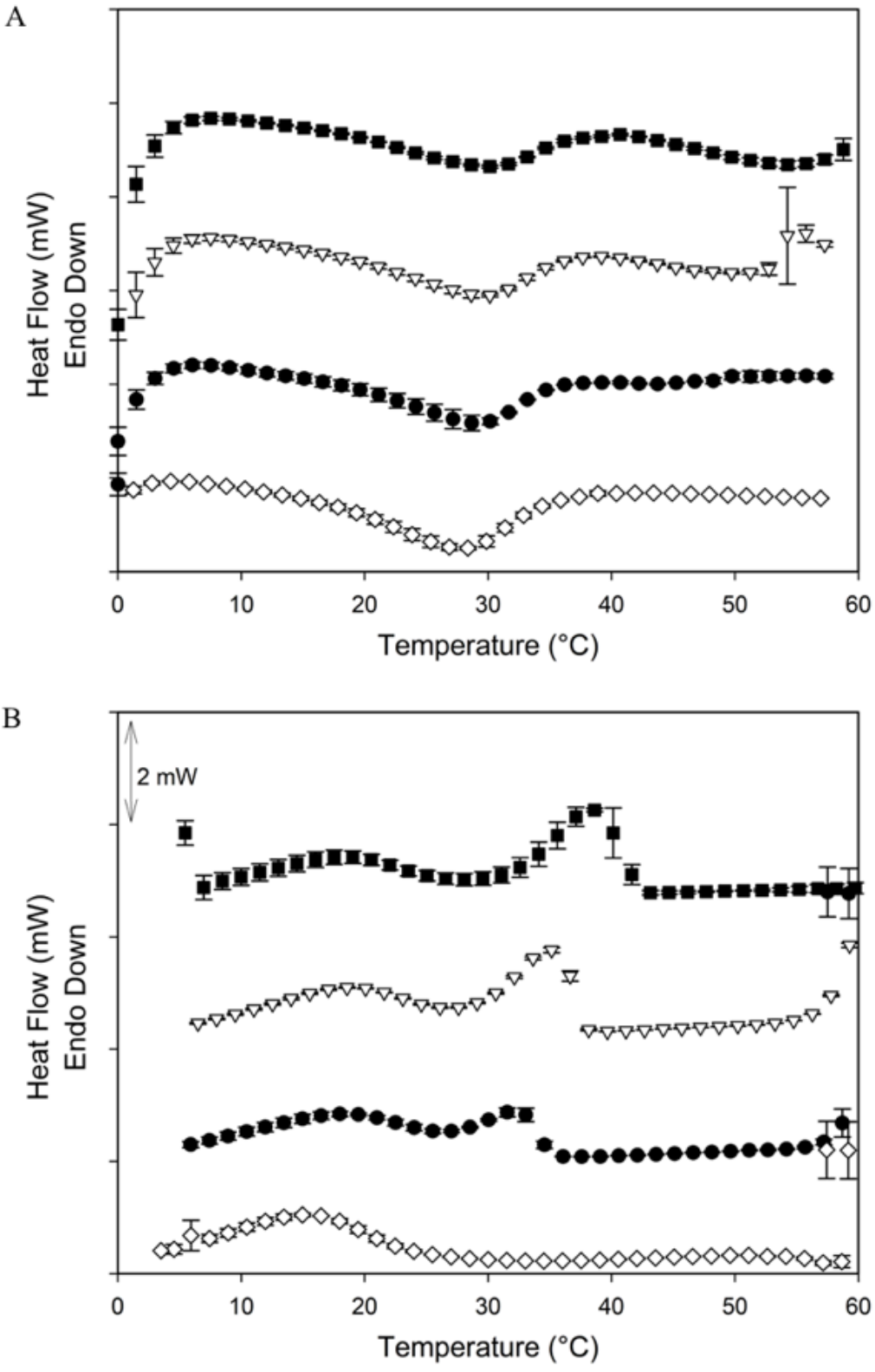

Figure 4.1. The first heating (A) and cooling (B) µDSC profiles of 5 % (w/w) gelatin with 0 (◇), 1 (●), 2 (▽), and 3% (w/w) (■) kappa-carrageenan over a temperature range from 0 to 60 ˚C, using a cooling rate of 1.2 ˚C.min^{-1}. (n = 3 ± SD).

The exothermic peak was attributable to the coil-helix transformation of the gelatin (Michon et al., 1997), with the result determined comparable to the result found by Bohidar and Jena (1993). Following the addition of the various concentrations of the secondary bio-polymer, kappa-carrageenan, two exothermic peaks and two endothermic peaks were observed on each of their respective μDSC curves. For the melting curves, the peak spanning from the initial rise in temperature to around 36 ˚C was attributed to the gelatin. The second peak, at higher temperatures, which was clearer in the curves with the higher concentration of kappa-carrageenan, has been attributed to the gel-sol transition of the kappa-carrageenan. These peaks were similar to those found from the heating of different concentrations of kappa-carrageenan by Iijima et al. (2007). For the gelation curves, a similar phenomenon has occurred, with two peaks occurring for each of the formulations. The broad peak spanning 10 to 20 ˚C was attributed to the gelation of the gelatin. The second peak at much higher temperatures, ca. 30 ˚C, was attributable to the gelation of the kappa-carrageenan as also observed by Wang et al. (2015). These cooling results obtained for the kappa-carrageenan were also found to be similar to results obtained by Iijima et al. (2007).

The gelation of the two bio-polymers was further explored using a rotational rheometer. The oscillation test at a single frequency sweep was run from a temperature of 60 to 20 ˚C and the results for the G' and G" for 5 % (w/w) gelatin mixtures with the addition of 0, 1, 2 and 3 % (w/w) kappa-carrageenan have been shown in Figure 4.2 A, B, C and D respectively.

G" was greater than G', at high temperatures for all of the formulations, with the exception of 5 % (w/w) gelatin with 3 % (w/w) kappa-carrageenan. This result indicated that at high temperatures the systems behaved as a viscoelastic liquid. At 24, 36 and 44 ˚C for the formulations of 5 % (w/w) gelatin with 0, 1 and 2 % (w/w) kappa-carrageenan respectively,

there was a rapid increase in both G' and G". This increase would appear to be due to the random coils (initially of the kappa-carrageenan, and then the gelatin) within the mixture transitioning to ordered helices through hydrogen bonding (Parker and Povey, 2012).

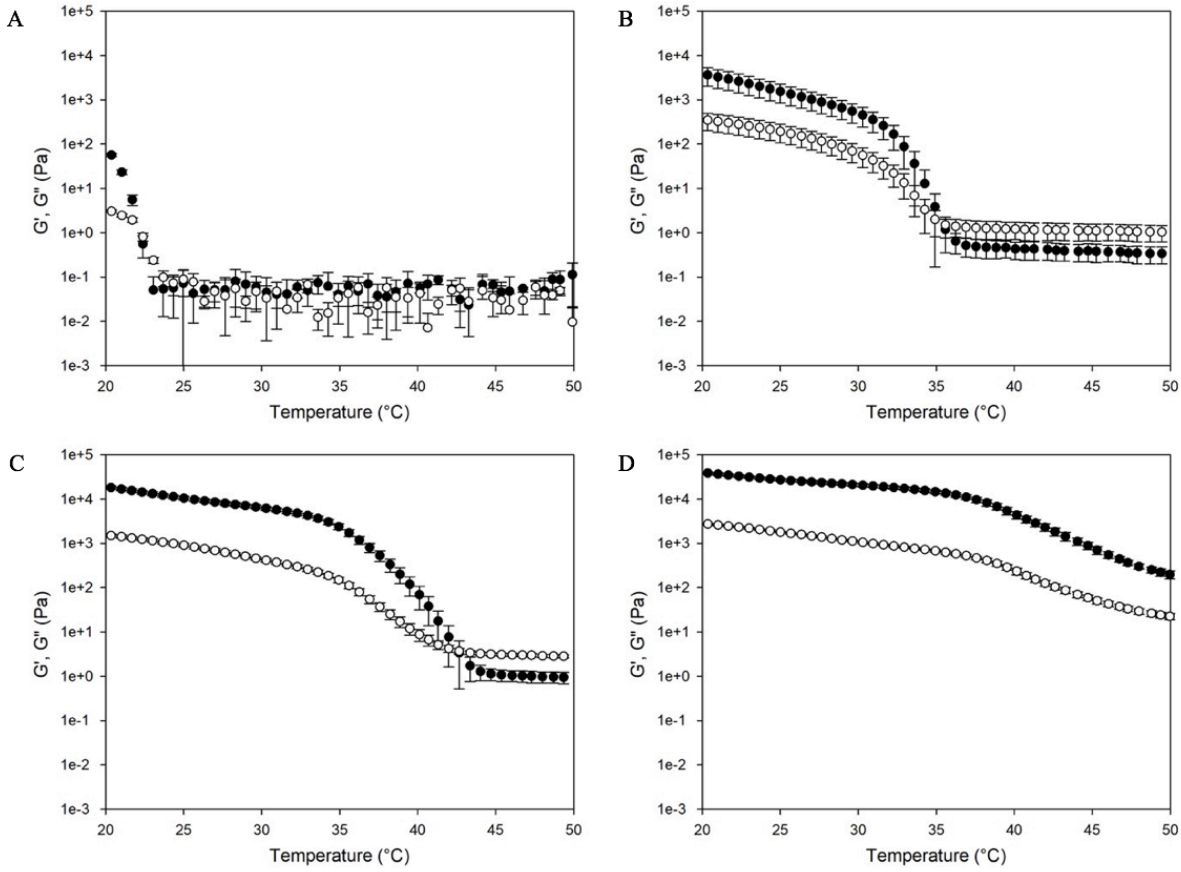

Figure 4.2. Storage (●) and loss modulus (○) of 5 % (w/w) gelatin with 0 (A), 1 (B), 2 (C) and 3 % (w/w) (D) kappa-carrageenan from a temperature of 50 to 20 ˚C at a cooling/ heating rate of 1 ˚C.min^{-1}, using a frequency of 1 Hz and a strain of 1 %. (n=3 ± SD).

A cross-over point occurred between G' and G" shortly after the increase and the temperature this occurred was taken as the gelling temperature in accordance with Djabourov et al. (1988). The result obtained for the 5 % (w/w) gelatin solution, using this method, was similar to that obtained by Tosh and Marangoni (2004), who determined the gelling temperature to be 24.5 ˚C. The slightly higher temperature found by Tosh and Marangoni could be attributed to the slower rate and higher frequency that was within their experiments. At temperatures which were

lower than the gelling temperature, the G' was greater than the G". This indicated that the mixture behaved as a viscoelastic solid, likely owing to the rheologically significant sample-spanning network of polymeric helices.

The formulation with 3 % (w/w) kappa-carrageenan displayed a higher G' across the whole range of temperatures tested, indicating that, even at high temperatures, such a high concentration of polymer within the solution resulted in the material being elastically dominated.

Table 4.1indicates the results from both the μDSC and the rheological data and showed that the addition of kappa-carrageenan resulted in a higher gelation temperature. As the temperature was reduced below the gelling point of the kappa-carrageenan, gelation of the kappa-carrageenan commenced, forming an elastic self-supporting structure which acted as a scaffold for the gelatin. When the temperature was subsequently reduced to the gelling point of the gelatin, gelation of the gelatin commenced leading to further solidification and strengthening of the hydrogel. The control of the printability of the material and the resultant resolution of the product could be enhanced by this two-step mechanism as it would prevent the primary polymer (gelatin) from spreading during the cooling process.

The gelling temperatures obtained from both the μDSC and the rheometer were found to be very similar. The small difference observed may have been due to the different rates used for each of the pieces of equipment. The results found from the onset of the μDSC were taken forward as the gelling temperature.

Table 4.1: Gelling temperatures of 5 % (w/w) gelatin with various amounts of kappa-carrageenan (κC) as determined using rheology and μDSC. (n=3 ± SD).

	Gelling temperature (˚C)	
Composition (% (w/w))	**Onset of exotherm**	**Cross-over temperature**
5 % gelatin	24 ± 0.4	22 ± 0.2
5 % gelatin and 1 % κC	36 ± 0.4	36 ± 1.3
5 % gelatin and 2 % κC	39 ± 0.01	42 ± 0.9
5 % gelatin and 3 % κC	42 ± 0.01	-

4.2.2 Rheological characterisation of the gelatin mixtures

It is important to understand the rheological properties of the materials to be printed because the resultant product must not only be edible but it must also be desirable (Van Vliet, 2013). The linear viscoelastic region (LVR) of each of the formulations of gelatin and kappa-carrageenan was determined by an amplitude sweep, shown in Figure 4.3. It can clearly be seen that for all the formulations, G' is independent of strain, until a strain of about 7 %, where G' begins to decrease for the formulation of 5 % (w/w) gelatin with 3 % (w/w) kappa-carrageenan, showing the material was beginning to break up and no longer within the LVR region. Therefore, continuing with a strain of 1 % ensured that all of these formulations were within their LVR region.

Frequency sweeps were performed on all of the materials at different temperatures, both above and below their gelling temperature. The G' and G" determined from the frequency curves obtained from a mixture of 5 % (w/w) gelatin with 2 % (w/w) kappa-carrageenan at 20, 30, 40 and 50 ˚C can be seen in Figure 4.4. The shape of the curves obtained were typical for all of the other formulations.

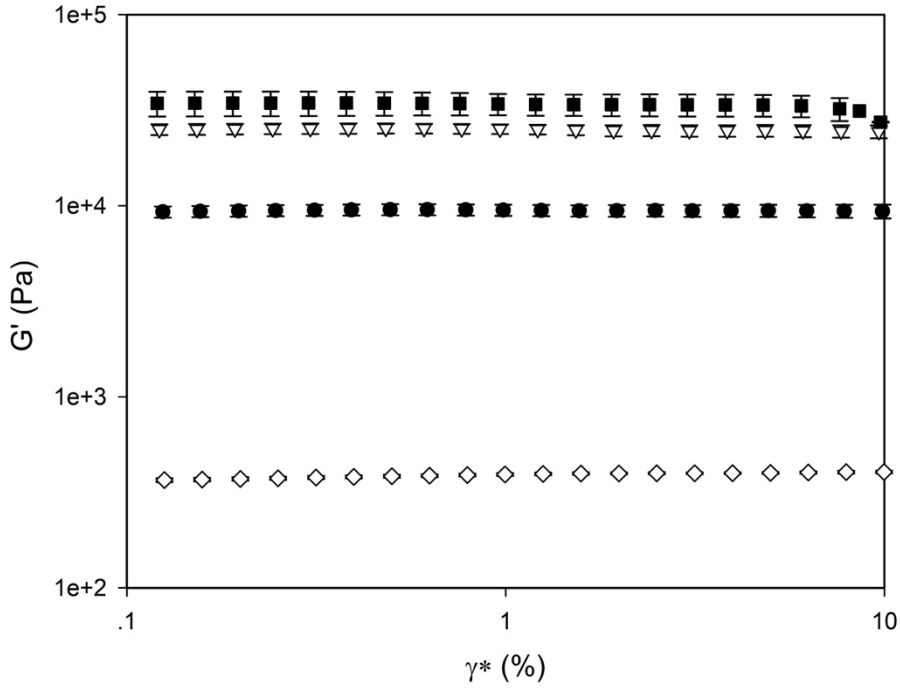

Figure 4.3. Amplitude sweeps of 5 % (w/w) gelatin with 0 (◇), 1 (●), 2 (▽) and 3 % (w/w) (■) kappa-carrageenan at a temperature of 20 ˚C over a range of strains from 0.1 to 100 %. (n=3 ± SD).

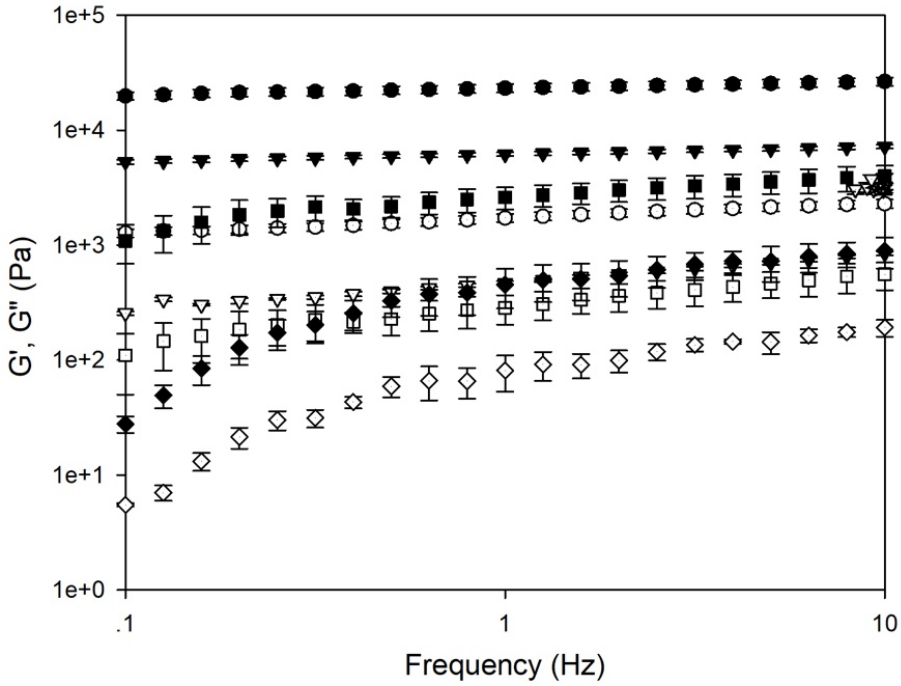

Figure 4.4. Frequency sweeps over a range frequencies from 0.1 to 10 Hz, of 5 % (w/w) gelatin with 2 % (w/w) kappa-carrageenan at 20 (○), 30 (▽), 40 (□) and 50 ˚C (◇), open symbols are the G", while closed symbols are the G'. (n=3 ± SD).

For each of the different materials tested, when the testing temperature was greater than the gelling temperature, both G' and G" were dependent on frequency; this demonstrated that the materials were liquid-like. It was observed that at temperatures greater than the gelling temperatures, the storage and loss moduli of each formulation exhibited similar values, with a difference of 4, 8, 10 and 3 % for formulations of 5 % (w/w) gelatin with 0, 1, 2 and 3 % (w/w) kappa-carrageenan, respectively. As a result of the finding that the viscoelastic properties were no longer dependent on the temperature when the gelling point was exceeded, it was likely there would likely be no material benefit to printing at a higher temperature.

When the testing temperature was reduced below the gelling temperatures of each of the four formulations, G' and G" became independent of frequency, indicating confirmation of the solid-like state of the material (Derkach et al., 2015). This result was also observed by del Carmen Núñez-Santiago and Tecante (2007) who investigated the evolution of moduli of 1 % kappa-carrageenan.

Figure 4.5 depicts the value of G' and G" for all the four formulations taken from the frequency sweeps, at a value of 1 Hz and at temperatures of 20 and 50 ˚C. At all temperatures tested, as the concentration of kappa-carrageenan was increased, the magnitude of G' increased. This was the result of the synergistic effects of the gelatin and kappa-carrageenan (Derkach et al., 2015). The hydrogen bonds formed with kappa-carrageenan were stronger than those formed with just gelatin molecules. Costakis et al. (2016) determined that an increase in G' would allow better shape retention post printing. The greater the value of the G' indicated higher gel strength, which would enable the material to retain its shape following extrusion. Due to the nature of the system it was not possible to load the samples at the temperatures below their gelling temperature, so it was necessary to load at a higher temperature and then give the formulations time to equilibrate at the required testing temperature for 5 minutes. During the time elapsed

between 0.1 – 1 Hz frequency the structural recovery that occurred within the equilibration period may have continued. This may have contributed to the G' value at 1 Hz, in addition to the increase caused by increasing frequency, resulting in an over estimation of G' at 1 Hz. However, the contribution due to the structural recovery during the elapsed time between 0.1 – 1 Hz cannot be resolved quantitatively.

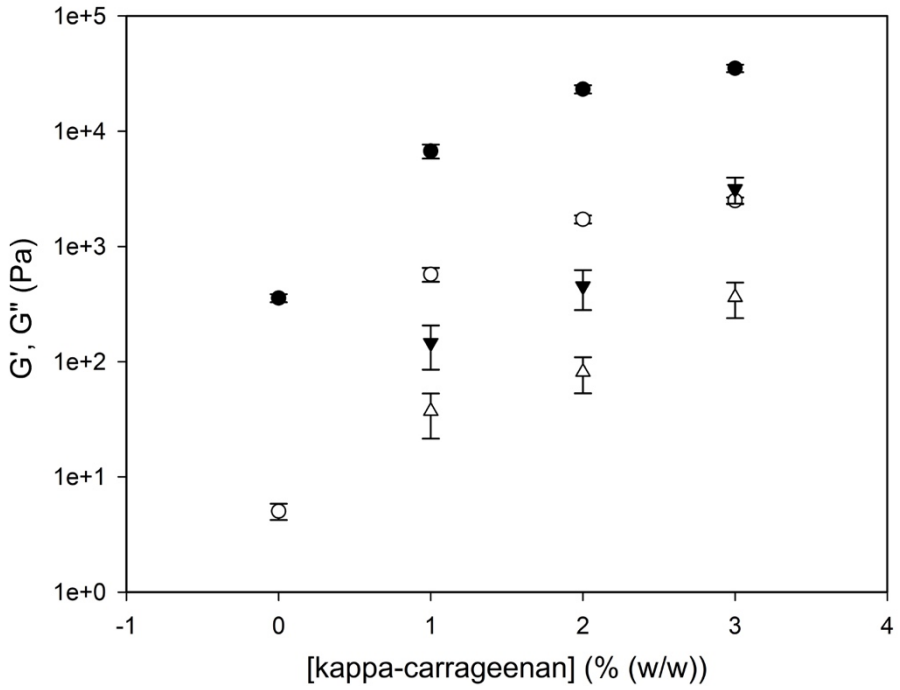

Figure 4.5. Frequency at 1 Hz of 5 % (w/w) gelatin and different concentrations of kappa-carrageenan at 20 (○) and 50 ˚C (▽), open symbols are the G", while closed symbols are the G'. (n=3 ± SD).

In order to have an idea of how the magnitude of G' evolved over time, for each of the different formulations gelling rates experiments were investigated, from a high temperature, to 20 ˚C and the results can be seen in Figure 4.6. Although the numerical values have been shown, due to the way in which the test was conducted, the values were not accurate, rather they have been used for comparative purposes between each of the formulations. The beginning of gelation was taken when the value of G' began to increase from the initial values, and the end of gelation was taken when the value of G' began to plateau and the percentage difference between two

consecutive points was less than 5 % over 3 consecutive points. A line was then drawn between the point of initial increase of G' and the point where the G' value began to plateau and the gradient of this line was taken as the rate of increase of G'.

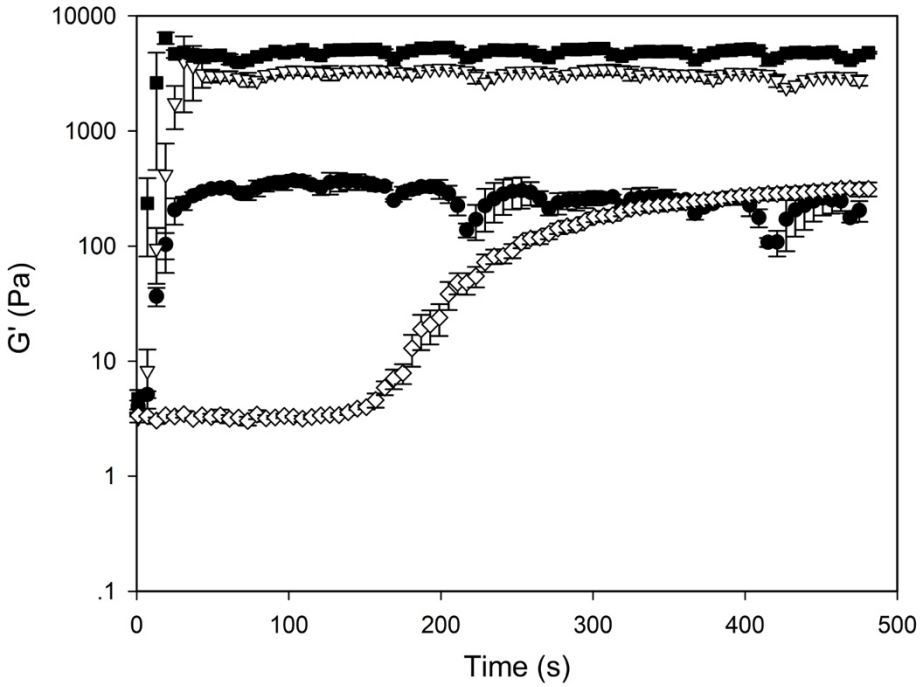

Figure 4.6. Gelling rate curve of 5 % (w/w) gelatin and 0 (◇), 1 (●), 2 (▽) and 3 % (■) (w/w) kappa-carrageenan. (n=3 ± SD).

It can clearly be seen that for the formulation of 5 % (w/w) gelatin, the beginning of gelation occurred a long time after the formulations with kappa-carrageenan. Once the magnitude of G' began to increase, it then took a long time to reach its maximum G' value, as opposed to the formulations with kappa-carrageenan. As previously mentioned, this was likely due to the slow conversion of the coils to helices within the gelatin (Harrington and Morris, 2009). In comparison, the values of G' for all of the formulations with the addition of kappa-carrageenan immediately increase after they have been loaded and it was possible to see that they all reach their maximum values of G' in around 28 seconds. Although the formulations reached their maximum G' values at similar times, the maximum value of G' for the formulation of 5 %

(w/w) gelatin with 1 % (w/w) kappa-carrageenan was approximately 95 % lower than the formulation with 2 or 3 % (w/w) kappa-carrageenan.

With regards to printing, this meant that it would take double the amount of time for the formulations of 5 % (w/w) gelatin with 1 % (w/w) kappa-carrageenan to gel and even longer for the formulation of 5 % (w/w) gelatin, compared to the formulations with 2 and 3 % (w/w) kappa-carrageenan. During this longer gelation time, it was likely that these two formulations (5 % (w/w) gelatin and 5 % (w/w) gelatin with 1 % (w/w) kappa-carrageenan) could experience spreading of the material after extrusion, leading to large deviations from the desired printed shape to the final printed object.

A simple simulation of the extrusion process was developed using a rotational rheometer in order to determine the behaviour of the material during extrusion. The simulation consisted of two parts: firstly, a viscosity curve was undertaken to mimic the extrusion of the material using the average shear rate established in section 3.3.2.9; secondly, small deformation rheology was employed to monitor the structuring of the material on the plate post-printing.

The viscosity curves, at a shear rate of 100 s^{-1} from a temperature of 60 to 20 ˚C, of all four formulations is shown in Figure 4.7. A rapid increase in viscosity was observed at temperatures of 22, 34, 37 and 42 ˚C for 5 % (w/w) gelatin with 0, 1, 2 and 3 % (w/w) kappa-carrageenan respectively. These values were very similar to the gelling temperatures found previously using both the μDSC and the rheometer, this increase in viscosity was therefore attributed to the gelling of the material. The results obtained for the 5 % (w/w) gelatin were in agreement with those obtained by Madhamuthanalli and Bangalore (2014), who determined that at 25 ˚C the viscosity was 0.032 Pa.s, while the results for the 1 % (w/w) kappa-carrageenan were similar to those obtained by Gabriele et al. (2009).

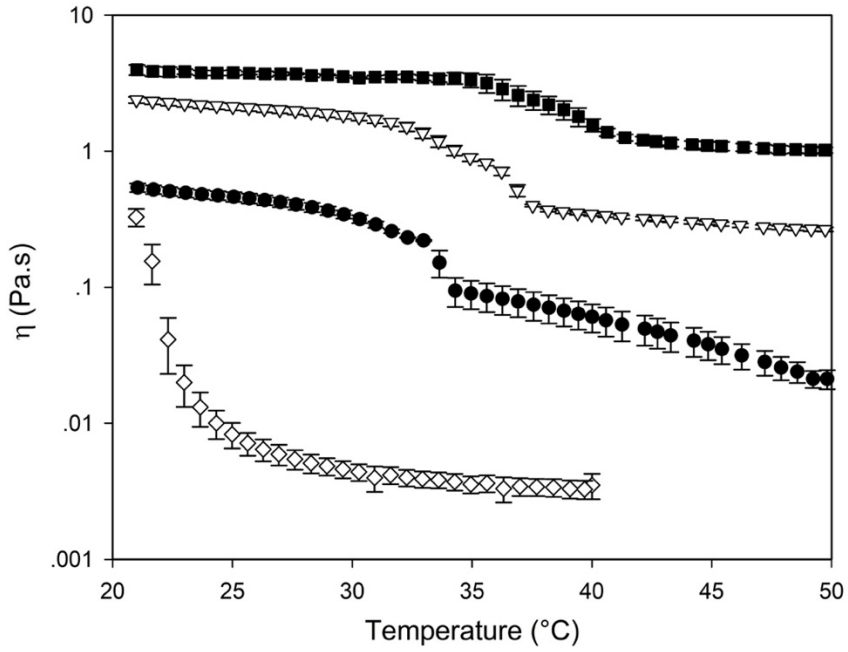

Figure 4.7. Viscosity curves on cooling 5 % (w/w) gelatin with 0 (◇), 1 (●), 2 (▽) and 3 % (w/w) (■) kappa-carrageenan at a shear rate of 100 s^{-1}. For the formulations with kappa-carrageenan, the temperature was reduced from 50 to 20 ˚C, while the formulation with just gelatin was reduced from 40 to 20 ˚C, all of the experiments were conducted at a cooling rate of 1 ˚C.min^{-1}. (n=3 ± SD).

Chang et al. (2011) determined previously that the minimum material viscosity required to successfully print was 0.03 Pa.s, using nozzles with diameters between 0.9 and 0.3 mm. Only the formulations with 2 and 3 % (w/w) kappa-carrageenan were above this minimum viscosity throughout the range of temperatures tested. The viscosities of the formulations with 0 and 1 % (w/w) kappa-carrageenan were below this minimum value of viscosity, until the temperatures exceed their gelling temperatures and the materials started to gel. If these formulations were extruded at a temperature too far above their gelling temperatures, the viscosity might be too low, resulting in material which just flowed out of the nozzle (He et al., 2015).

Analysis of the recovery of the material was important in order to determine whether the material would spread after extrusion and whether subsequent layers could be printed onto it. The recovery graphs exhibit how both the G' (Figure 4.8 A) and G" (Figure 4.8 B) behaved

following removal of the shear whilst at a constant temperature of 20 ˚C. The graph only records results up to 200s as, within this timeframe, any additional layers would be printed.

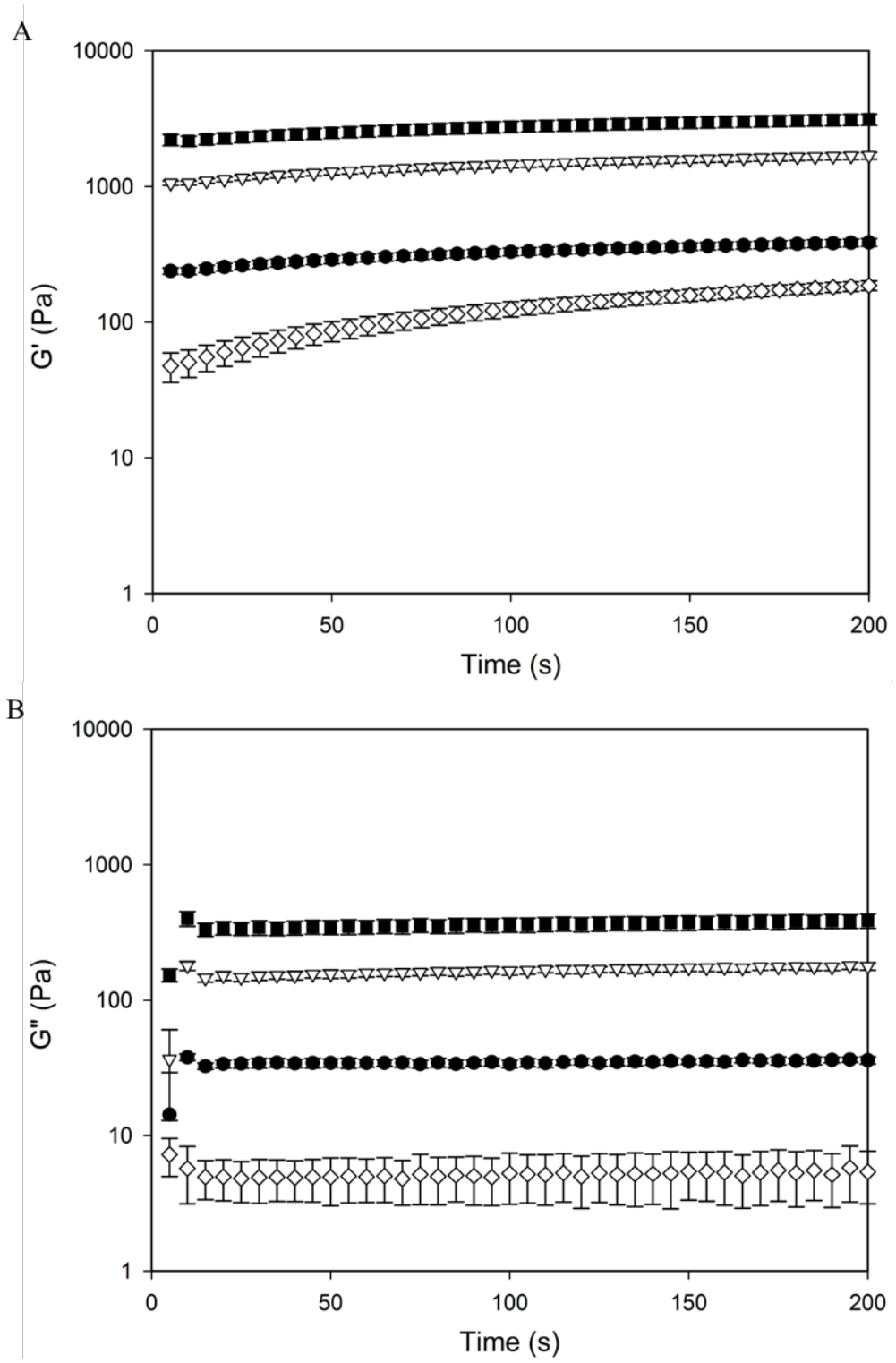

Figure 4.8. G' (A) and G" (B) of 5 %(w/w) gelatin with 0 (◇), 1 (●), 2 (▽) and 3 % (w/w) (■) kappa-carrageenan), at a frequency of 1 Hz and a strain of 0.1 %. (n=3 ± SD).

As soon as the shear was removed all of the formulations displayed an elastically dominant system. The time taken for the system to reach an equilibrium, which meant that the system was a solid gel, was a function of kappa-carrageenan concentration. The curves were fit to an exponential growth equation, shown in Equation 4.1.

$$y = y_0 + a(1 - e^{-bt})$$

Equation 4.1. Exponential growth equation, describing the evolution of G' (y) as a function of the initial G' (y_0) and a growth factor. Where a is the final growth, b is the rate of growth and t is time.

Once these values had been obtained from each of the individual curves, the recovery of the formulations with 1, 2 and 3 % (w/w) kappa-carrageenan at 2 minutes was found to be 67, 73 and 75 % of their maximum G' values respectively. The formulation without the kappa-carrageenan only recovered to 45 % of its maximum G' value, indicating that the recovery occurred a lot faster for the formulation with kappa-carrageenan compared to the formulation without, as a result of the strong interactions between the two different molecules.

4.2.3 Determination of printability using the rheological data

Printability was evaluated by assessing the uniformity of the extrusion during the printing process along with the accuracy and stability of the printed part (Lille et al., 2017). The temperature control within the printing process was of utmost importance due to the temperature dependence sol-gel transition of the gelatin and kappa-carrageenan (Billiet et al., 2014). It was found previously that at temperatures higher than the gelling temperature the viscoelastic properties of the material were similar. However, there was a change in the properties when the gelling temperature was reached. In order to determine how much the viscoelastic properties affected the printability, 2D and 3D squares were printed out in each of the formulations, at their respective gelling temperature and at a higher temperature.

Each of the printed squares were intended to measure 20 mm x 20 mm with a width of 1 mm and the extrusion commenced in the bottom left corner. The 2D squares were printed with 1 layer (height of 0.3 mm) and the 3D squares were printed using 4 layers (height of 1.2 mm). By printing both 2D (Figure 4.9) and 3D (Figure 4.10) structures it was possible to determine whether the materials were gelling fast enough to allow layers to be built up.

The other printing parameters used when printing the squares included using a nozzle of diameter 0.6 mm, similar to that used for plastic printing a printing movement speed of 10 $mm.s^{-1}$ and a non-print move speed of 100 $mm.s^{-1}$.

In order to determine the accuracy of the resultant printed squares, the width and the height of each square were measured. This analysis process was similar to that of Derossi et al. (2018) who measured the heights and width of a fruit-based formulation to determine if their printed snacks matched the design structure. The width of the printed square was measured at the bottom right corner, after the first corner using calipers, whilst the height was measured at the four corners using the FDM machine and averaged. The level of spreading was determined by the deviation from the intended values. Table 4.2 shows the results of the measurement of the width of the 2D and 3D squares printed at both the formulation's gelling temperature ($T=T_{gel}$) and at the higher temperature ($T > T_{gel}$) for all of the systems tested with the addition of kappa-carrageenan. Deviation was calculated as the percentage difference between the desired value of 1mm and the experimental widths found. Neither the 2D nor the 3D squares extruded with 'gelatin only' formulation exhibited a uniform width, therefore these results were not presented. The 2D and 3D squares, obtained by the printing of the formulation with no kappa-carrageenan, displayed poor resolution, broken lines and a large amount of spreading. Costakis et al. (2016) determined that materials with a higher G' resulted in better shape retention. The G' for the formulation without any kappa-carrageenan was 0.7 kPa, which resulted in pools of material

being formed rather than a solid line. The spreading occurred as the gelation process was not rapid enough to prevent the material from spreading (Wei et al., 2015). Etxabide et al. (2019) observed similar results when printing a 5 % gelatin simulation, to be used as a scaffold for drug delivery, that slow solidification of this formulation resulted in spreading of the printed structure.

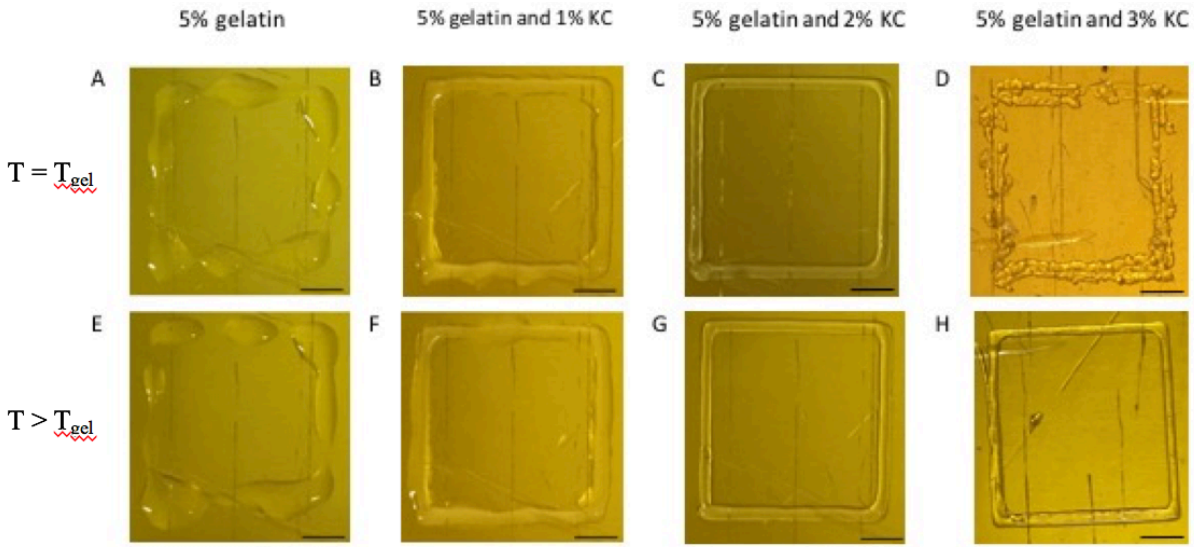

Figure 4.9. Top view images of 2D printed squares (1 layer) printed from the bottom left corner at a printing temperature of 24 (A), 36 (B), 39 (C), 42 (D), 40 (E), 50 (F), 50 (G), and 50 ˚C (H). Scale bar = 5mm.

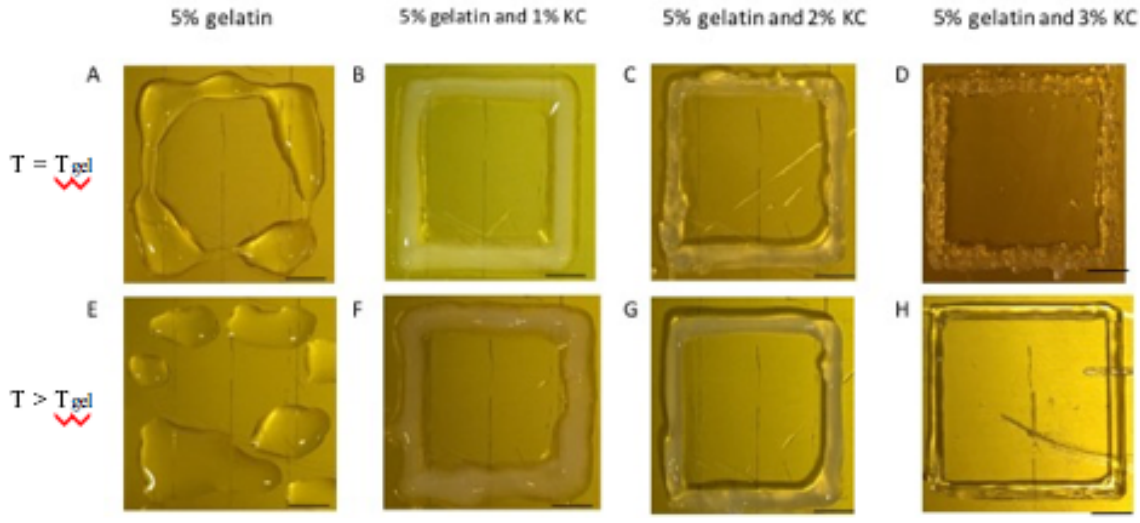

Figure 4.10. Top view images of 3D printed squares (4 layers) printed from the bottom left corner at a printing temperature of 24 (A), 36 (B), 39 (C), 42 (D), 40 (E), 50 (F), 50 (G), and 50 ˚C (H). Scale bar = 5mm.

Table 4.2. Widths of 2D and 3D printed squares of 5 % (w/w) gelatin with 1, 2 and 3 % (w/w) kappa-carrageenan (κC) printed at their gelling temperature ($T=T_{gel}$) (36, 39 and 42 ˚C respectively), and a higher temperature ($T>_{gel}$) (50 ˚C). The desired width was 1 mm. Values with the same letters across the row show significant difference ($p < 0.05$). ($n = 6 \pm SD$).

		Concentration of κC added (% (w/w))					
		1		**2**		**3**	
	No. of layers	**Width (mm)**	**Deviation (%)**	**Width (mm)**	**Deviation (%)**	**Width (mm)**	**Deviation (%)**
$T=T_{Gel}$	**1**	1.6 ± 0.1^{a}	60	1.1 ± 0.1^{ab}	10	1.6 ± 0.5^{b}	60
	4	2.5 ± 0.4^{a}	150	1.8 ± 0.2	80	1.7 ± 0.7^{a}	70
$T>T_{Gel}$	**1**	1.4 ± 0.2^{ab}	40	1.1 ± 0.05^{a}	10	1.1 ± 0.1^{b}	10
	4	3.4 ± 0.6^{ab}	240	1.7 ± 0.2^{a}	70	1.4 ± 0.2^{b}	40

Spreading of the extruded material also occurred when the formulation with 1 % (w/w) kappa-carrageenan was printed. The width of the 2D squares were at least 40 % larger than desired at both temperatures printed. The spreading was not only due to the long gelation time of this material and the low G' (ca. 4.5 kPa), but also due to the macroscopic material phase separating due to their thermodynamic incompatibility (Fang et al., 2006). When subsequent layers were added, more spreading occurred, with a large difference of width observed between the two temperatures used for printing. The squares printed at a higher temperature showed greater levels of spreading (240 %) compared to the squares printed at the gelling temperature (150 %). The squares printed at a lower temperature reached their gelation temperature faster, which reduced the spreading of the material.

The width of the 2D squares printed with the addition of 2 % (w/w) kappa-carrageenan were observed to be within 10 % of the standard value at both temperatures tested. In this instance over 73 % of the material's structuring was recovered within 200 seconds and that, combined with the high G' (ca. 23 kPa), ensured that spreading was inhibited due to the strong elastic network within the system being created quickly as a result of the fast recovery time. When the 4 layers high, 3D square was printed using the 2 % (w/w) kappa-carrageenan formulation, the width of the square spread ca. 70 %. This outcome was the result of insufficient adhesion between the subsequent layers, the material did not bond quickly enough as further layers were added, resulting in the newly deposited layer sliding off the lower layer. The width of this formulation was similar at both of the temperatures tested for this formulation.

The width of the 2D square printed with the mixture containing 3 % (w/w) kappa-carrageenan was within 10 %, when printed at a temperature higher than its gelling temperature. When this formulation was printed at its gelling temperature, the width was found to be a lot wider. In Figure 8D, it can be seen that the square printed at the gelling temperature (42 ˚C) did not produce a shape with solid lines. This was likely to be due to the material gelling within the nozzle itself resulting in extrusion of a solid material. The same broken lines could also be seen when a 3D square was printed at this temperature (Figure 4.10 D). The 2D shape obtained when printing at a higher temperature was within 10 % of the printed width, due to the fast gelation time and high G' of this material. The 4 layers high 3D shapes, printed using the formulation of 3 % (w/w) kappa-carrageenan displayed a well printed square, close to the desired width.

Table 4.3 documents the results of the measurements of the heights of the 2D and 3D squares printed at both the formulations gelling temperature ($T=T_{gel}$) and at the higher temperature ($T > T_{gel}$) for all of the formulations tested. The deviation was calculated as the percentage difference

between the desired values of 0.3 mm for 1 layer and 1.2 mm for 4 layers and the determined experimental heights.

Table 4.3. Heights of 2D and 3D printed squares of 5 % (w/w) gelatin with 0, 1, 2 and 3 % (w/w) kappa-carrageenan (κC) printed at their gelling temperature ($T=T_{gel}$) (36, 39 and 42 ˚C respectively), and a higher temperature ($T>_{gel}$) (50 ˚C). The desired height was 0.3 mm for 1 layer and 1.2 mm for 4 layers. Values with the same letters across the row show significant difference ($p < 0.05$). ($n = 6 \pm SD$).

		Concentration of κC added (% (w/w))							
		0		**1**		**2**		**3**	
	No. of Layers	**Height (mm)**	**Deviation (%)**	**Height (mm)**	**Deviation (%)**	**Height (mm)**	**Deviation (%)**	**Height (mm)**	**Deviation (%)**
$T=T_{Gel}$	**1**	0.5 ± 0.08^{abc}	67	0.3 ± 0.09^{ad}	0	0.2 ± 0.08^{b}	- 33	0.2 ± 0.06^{cd}	- 33
	4	1.6 ± 0.1^{abc}	33	1.0 ± 0.2^{ad}	- 17	1.3 ± 0.2^{bde}	8	0.9 ± 0.05^{ce}	- 25
$T>T_{Gel}$	**1**	0.2 ± 0.1	- 33	0.2 ± 0.07	- 33	0.2 ± 0.07	- 33	0.2 ± 0.04	- 33
	4	$0.5 \pm 0.1_{abc}$	- 58	0.9 ± 0.2^{ade}	- 25	1.4 ± 0.1^{bdf}	17	1.3 ± 0.1^{cef}	8

For the formulation without kappa-carrageenan, both the 2D and 3D squares achieved a greater than desired height at the lower temperature tested. During printing of these squares, it was observed that the material was dragged along, leading to excess material forming pools rather than lines and resulting in the higher than expected heights. It would appear that some structuring was occurring within this system, but not fast enough to prevent the pools from forming. The height of the 2D printed square, printed at the higher temperature (40 ˚C) was lower than was desired due to the material not structuring in time, therefore not able to hold the shape together. The height of the 3D printed square at the higher temperature was observed to

be over 50 % less than the desired height. The higher printing temperature and slow elastic network formation led to the gelatin acting like a viscoelastic liquid. A 3D network of polymers was not able to form, resulting in spreading of the material as the lower structure was unable to support the subsequent layers and therefore the desired height was not achieved.

The table illustrated that, despite the fact both spread beyond the desired width, there was a height difference between the 5 % (w/w) gelatin with 1 % (w/w) kappa-carrageenan 2D squares printed at the gelling temperature and the higher temperatures. For the formulation with 5 % (w/w) gelatin and 1 % (w/w) kappa-carrageenan, an elastic network began to form at 35 ˚C. Printing at a slightly higher temperature caused a minimal delay in the formation of the network. This delay in time prior to network development increased when the printing temperature was increased to 50 ˚C. The result of this time differential led to the square printed at the lower temperature achieving a greater height as a result of the quicker formation of the network. Using the same formulation, the printed height of the 3D shapes achieved was about 80 % less than the desired height. Despite the fact that the width was affected by spreading of the printed material some height was achieved. This indicated that the observed large width discovered was likely due to the phase separation of the material.

For the formulation with 5 % (w/w) gelatin with 2 % (w/w) kappa-carrageenan, the same printed height was achieved for the 2D squares when extruding at both temperatures. The fast gelation time of this material ensured that the temperatures did not affect the mixture. However, at both temperatures, when the 3D squares were printed the height and width were greater than desired. This was caused by the lack of bonding between the layers leading to material slipping off the previous layers resulting in the greater width and pooling in certain areas, resulting in the higher than desired height.

The squares obtained from printing the 5 % (w/w) gelatin with 3 % (w/w) kappa-carrageenan mixture at its gelling temperature were broken and ill defined. The height of the 2D shapes was similar to the squares printed with the mixture printed with 5 % (w/w) gelatin with 2 % (w/w) kappa-carrageenan. However, the squares themselves were dissimilar with the uneven printing of the former giving a false impression of height. When printed at the higher temperature, the height of the 2D and 3D squares were identical to the heights achieved with the formulation of 5 % (w/w) gelatin with 2 % (w/w) kappa-carrageenan. The fast gelation time of this material enabled the printed object to retain the desired shape.

As the concentration of the kappa-carrageenan within the system was increased, the printability of the system improved, with printed squares of the formulation of 5 % (w/w) gelatin with 3 % (w/w) kappa-carrageenan producing squares closest to the desired shape when printing at the higher temperature.

4.3 Conclusions

This chapter presented an assessment of the printability of 5 % (w/w) gelatin solutions with additions of kappa-carrageenan in order to establish design rules for the printing of thermally gelling hydrocolloids. It was found that in order to print well defined structures, the magnitude of the G' needed to be greater than 2 kPa at the printing temperature and greater than 23 kPa at the temperature of the environment in which the object was being printed (during these experiments the temperature of the room was set to 20 ˚C). It was also necessary for the formulation to recover at least 73 % of its maximum G' within 200 seconds which facilitated the rapid formation of an elastic network necessary to prevent spreading and achieve shape retention.

It was established that the printing temperature affected the printability of the different formulations. The addition of kappa-carrageenan resulted in an increase in the gelling temperature which enabled greater control of the printing, due to a larger gradient between the printing temperature and gelling temperature, when compared to the formulation of just gelatin alone, which gelled just above room temperature. The increased gelling temperature provided a greater temperature differential when printing at room temperature, allowing the material to solidify faster and create the desired shape. In general, the objects printed with the different formulations at their gelling temperatures achieved a more defined structure with less spreading of the material. The exception was of the formulation of 5 % (w/w) gelatin with 3 % (w/w) kappa-carrageenan printed at room temperature, which displayed poor printed shapes. This was due to the magnitude of the G' being too great at this temperature, ca. 6 kPa which led to structuring within the nozzle, resulting in the formulation being extruded as solid-like and leading to broken lines. When this formulation was printed at an increased temperature, good printability was achieved.

The influence of rheological and thermal transitions on the printability of thermoreversible materials outlined above could be applied to 3D printing of various other materials undergoing the same thermal gelation process which will be the focus of subsequent studies.

CHAPTER 5. INVESTIGATION OF THE PRINTING PARAMETERS FOR FORMULATIONS OF GELATIN AND KAPPA-CARRAGENAN

5.1 Introduction

During the extrusion printing process, a material will undergo two distinct phases: 1. Extrusion through the nozzle, and 2. Solidifying on the printing plate. Within the extrusion section, the material undergoes a shearing force, which can affect the viscosity of the material as it is extruded, whereas after extrusion, as the material gels on the printer bed, it is the evolution of G' which will determine final quality of the printed object.

Within the previous chapter, design rules for the printability of formulations of 5 % (w/w) gelatin with 0, 1, 2 and 3 % (w/w) kappa-carrageenan were established. It was found that the formulation needed to possess a sufficiently high G' value after printing and recover quickly in order to print an object with a maximum deviation of 10 % compared to the intended basic shape. Although the behaviour of the material during extrusion was touched upon, the majority of Chapter 4 focused on the behaviour after extrusion. This current chapter concentrates on the behaviour of the material during the extrusion through the nozzle, focusing on the viscosity of the material and how varying different printing parameters affected the behaviour and altered the printability.

During the extrusion of a material, a suitable viscosity, within an optimal range is critically important (He et al., 2016, Hong et al., 2015). As the material is extruded through the nozzle it will experience high shear rates and will need to be able to flow, however, the material needs to be able to quickly regain a high viscosity at rest in order to support the structure after

deposition (Lille et al., 2018). The viscosity can be significantly affected by variables such as shear rate, temperature, pressure and the time of shearing (Marcotte et al., 2001).

$$\eta = f(\dot{\gamma}, T, p, t)$$

Equation 5.1. Viscosity (η) is a function of the shear rate ($\dot{\gamma}$), temperature (T), pressure (p) and time of shearing (t).

During the printing process, the average shear rate could be determined using the printing speed and the nozzle diameter.

$$\dot{\gamma} = f(S_p, d_n)$$

Equation 5.2. Shear rate is a function of the printing speed (S_p) and nozzle diameter (d_n).

Which leads to

$$\eta = f(S_p, d_n, T, p, t)$$

Equation 5.3. Viscosity (η) is a function of the printing speed (S_p), nozzle diameter (d_n), temperature (T), pressure (p) and time of shearing (t).

Within this chapter, these different printing parameters, nozzle diameter, printing speed, time and printing temperature were investigated in order to see how the printability was affected as the viscosity changed. The pressure was not calculated separately, rather was considered as the shear stress, and therefore included within the shear rate data. The time the material undergoes a certain shear depends on the average residence time within the needle. The same materials (5 % (w/w) gelatin with 1, 2 and 3 % (w/w) kappa-carrageenan), were investigated, following from the previous chapter. Due to the complete lack of printability of the formulation of 5 % (w/w) gelatin, this formulation was not carried forward. The formulation of 5 % (w/w) gelatin with 1 % (w/w) kappa-carrageenan displayed poor signs of printability, but this formulation

was continued to be investigated in order to confirm that the previous design rules stand even after changing certain printing parameters.

5.2 Results and Discussion

5.2.1 Varying different printing parameters

5.2.1.1 Investigation of nozzle diameter

The nozzle diameter directly affects the resolution and accuracy of the printed objects (Hao et al., 2010). Periard et al. (2007) determined that a safe rule of thumb was to select the smallest nozzle tip which allowed for easy extrusion, as this would enable production of printed objects with the finest resolution and smoothest surface. However, the smaller nozzle size leads to an increased pressure, which can then lead to poor quality printed objects with inconsistent diameters of the printed lines (Wang et al., 2017). Therefore, a compromise between the smallest nozzle diameter and the pressure within the nozzle needs to be obtained in order to determine the optimum printing nozzle.

A range of different nozzle diameters were investigated in order to see how they affected the printability of the formulation of gelatin and kappa-carrageenan. Four different nozzle diameters were investigated with internal diameters of 1.2, 1.1, 0.8 and 0.6 mm. In order to assess each of the nozzles, 1 and 5 layer lines were printed using all 3 of the formulations of gelatin and kappa-carrageenan. The widths, heights and lengths of the lines were recorded in order to determine how close they were to their intended values.

Wang and Shaw (2005) determined the critical nozzle height, the height between the tip of the nozzle and the substrate could be established from Equation 5.4 for formulations of dental slurries.

$$h_c = \frac{V_d}{v_n D_n}$$

Equation 5.4. Estimation of the critical nozzle height Wang and Shaw (2005). Where h_c is the critical nozzle height, V_d is the volume of material extruded per unit time, v_n is the nozzle movement speed and D_n is the diameter of the nozzle.

This led to a critical nozzle height of approximately 0.08 mm when using the smallest nozzle, which, for these formulations was too close to the bed to be able to print anything, indicating that this equation was not suitable for the materials chosen within this work. Hao et al. (2010), who investigated the printing of chocolate also determined that this equation did not give a suitable indication of the optimal nozzle height, suggesting that such differences in materials from chocolate to dental slurries dictated a significantly different extrusion height. In order to maintain continuity across the different nozzle diameters, it was determined that the width and height of each of the printed lines be kept to the same value as the diameter of the nozzle, which was in accordance with work done by Yang et al. (2018). The intended length of the printed line was set to 100 mm, and the printing speed was maintained at 10 $mm.s^{-1}$.

Figure 5.1 depicts the micrographs of the cross-sectional area and pictures of the printed lines of the 5 % (w/w) gelatin with 2 % (w/w) kappa-carrageenan using a nozzle of diameter 1.2 (A), 1.1 (B), 0.8 (C) and 0.6 mm (D). These images are consistent with the other formulations tested.

The widths, heights and lengths of each of the formulations for the one layer line have been shown in Figure 5.2 A, B and C respectively. The width of the formulation with 5 % (w/w) with 1 % (w/w) kappa-carrageenan were greater than desired for all of the nozzles used. This was likely due to the material possessing a low G' value, below 23 kPa at room temperature, as has been discussed previously, leading to the material deviating from the desired width. Due to the spreading of the material, the height of all of the materials printed with 5 % (w/w) gelatin with

1 % (w/w) kappa-carrageenan was considerably lower than was expected, as can be seen from Figure 5.2 B.

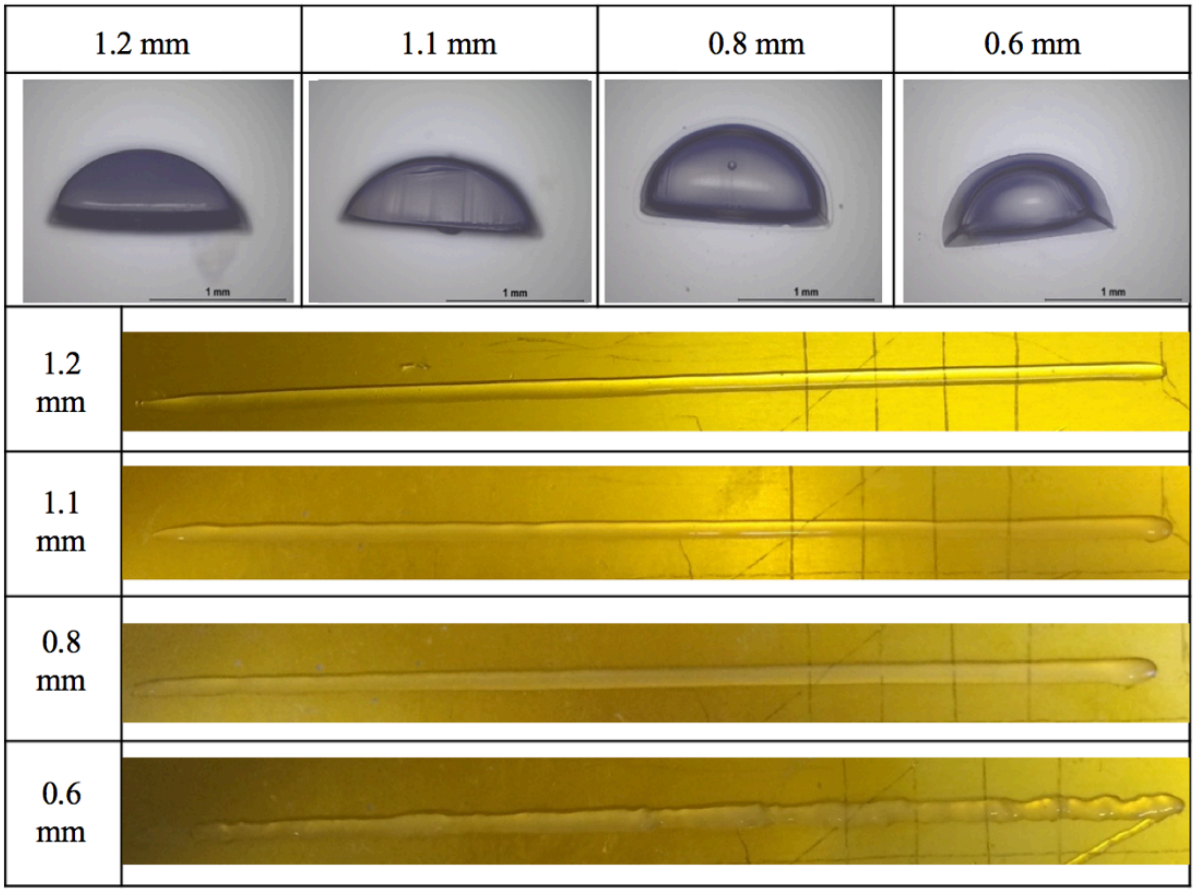

Figure 5.1. Micrographs of the cross-sectional profile (top images) and images of the top view of 5 % (w/w) gelatin and 2 % (w/w) kappa-carrageenan printed 1 layer lines using nozzle diameter 1.2, 1.1, 0.8 and 0.6 mm (lower images). The heights and widths were maintained as the nozzle diameter, the length of the line was 100 mm and the printing speed was 10 mm.s^{-1}. The lines were printer right to left.

The width of the formulations of 5 % (w/w) gelatin with 2 and 3 % (w/w) kappa-carrageenan using the two smaller nozzle diameters were all at least 50 % greater than the desired width. There are several reasons why the material exhibited higher than desired width, including extrudate swelling, 'squeezing' effect or a mixture of both. Extrudate swelling occurs when a polymer melt is extruded from a restrained edge. The observed cross-sectional area of the extrudate material is larger than that of the die due to the high shear rate within the nozzle

(Ariffin et al., 2011). ‘Squeezing’ of the extruded material generally occurs when the nozzle height is too close to the print bed, or too small and the material is forced to take up space beyond the defined volume (Wang and Shaw, 2005). The lines which have been printed using the smallest nozzle (shown in Figure 5.1 D) clearly showed an extreme extrudate swelling effect, which is commonly referred to as ‘sharkskin’ instabilities, where the shear rate in the material leads to short wavelengths of deformations on the interface, a problem commonly seen in polymer extrusion (van Saarloos, 2003). It is commonly proposed that the sharkskin defect occurs around the die exit, as the molten material is leaving the die the change in velocity profile induces elongational stresses within the skin of the extrudate, leading to fracturing of the surface (Allal et al., 2006). This defect can be mitigated by reducing the flow rate within the die (Agassant et al., 2006), however printing at any slower speed would result in a very long printing time when printing any larger shape. As the nozzle was close to the bed, it was also possible that the material has also exhibited a ‘squeezing’ effect, with both of these effects leading to the larger than expected width. Increasing the layer height of objects printed with this diameter nozzle may result in the ability to print more accurate parts. However, the effect of the layer height was not tested within the scope of this work, and may be something interesting to consider in the future.

The results of the heights for the formulations of 5 % (w/w) gelatin with 2 and 3 % (w/w) kappa-carrageenan using the 0.6 mm diameter nozzle show heights approximately 30 % greater than the intended height. As is clear from the image in Figure 5.1 D, the printed line was non-uniform, showing ‘sharkskin’ instabilities which had undulations, which may have led to the increased height.

The lines printed with a nozzle diameter of 0.8 mm display a smoother line compared to the smaller nozzle. As the shear rate was lower, due to the large nozzle diameter the extrudate

swelling effect was less dominant, however, is likely that it was still a mixture of this effect and the ‘squeezing’ effect which led to the large width. Although both of the formulations of 5 % (w/w) gelatin with 2 and 3 % (w/w) kappa-carrageenan showed spreading with the 0.8 mm nozzle, the heights achieved were a maximum of 4 % deviation from their intended values.

The width of the formulations of 5 % (w/w) gelatin with 2 and 3 % (w/w) kappa-carrageenan using a nozzle of diameter 1.1 and 1.2 mm were around 20 % larger than the desired width indicating less deviation compared to the smaller nozzles. The larger diameters meant that the shear rates were lower, leading to even less of an extrudate swelling effect and the material also did not experience as great a ‘squeezing’ effect leading to widths close to the desired width.

The height of the printed line using a nozzle of diameter 1.1 mm using a formulation of 5 % (w/w) gelatin with 2 % (w/w) kappa-carrageenan was approximately 6 % lower than desired, while for the formulation of 5 % (w/w) gelatin with 3 % (w/w) kappa-carrageenan, the height was approximately 1 % greater than desired. These values were extremely close to the intended values, indicating that this nozzle was suitable to print these formulations.

The height of the printed lines established for the formulations of 5 % (w/w) gelatin with 2 and 3 % (w/w) kappa-carrageenan using a nozzle of diameter 1.2 mm were approximately 8 and 18 % lower than desired respectively. It can be seen from the micrographs in Figure 5.1 A that the cross-sectional area of the line of 5 % (w/w) gelatin with 2 % (w/w) kappa-carrageenan was relatively wide and short, which was similar to that observed with the formulation of 5 % (w/w) gelatin with 3 % (w/w) kappa-carrageenan. This indicates that with this large nozzle diameter, the material is flowing out under gravity, resulting in over extrusion, as seen from the greater than intended width, therefore this nozzle diameter was not suitable for this material.

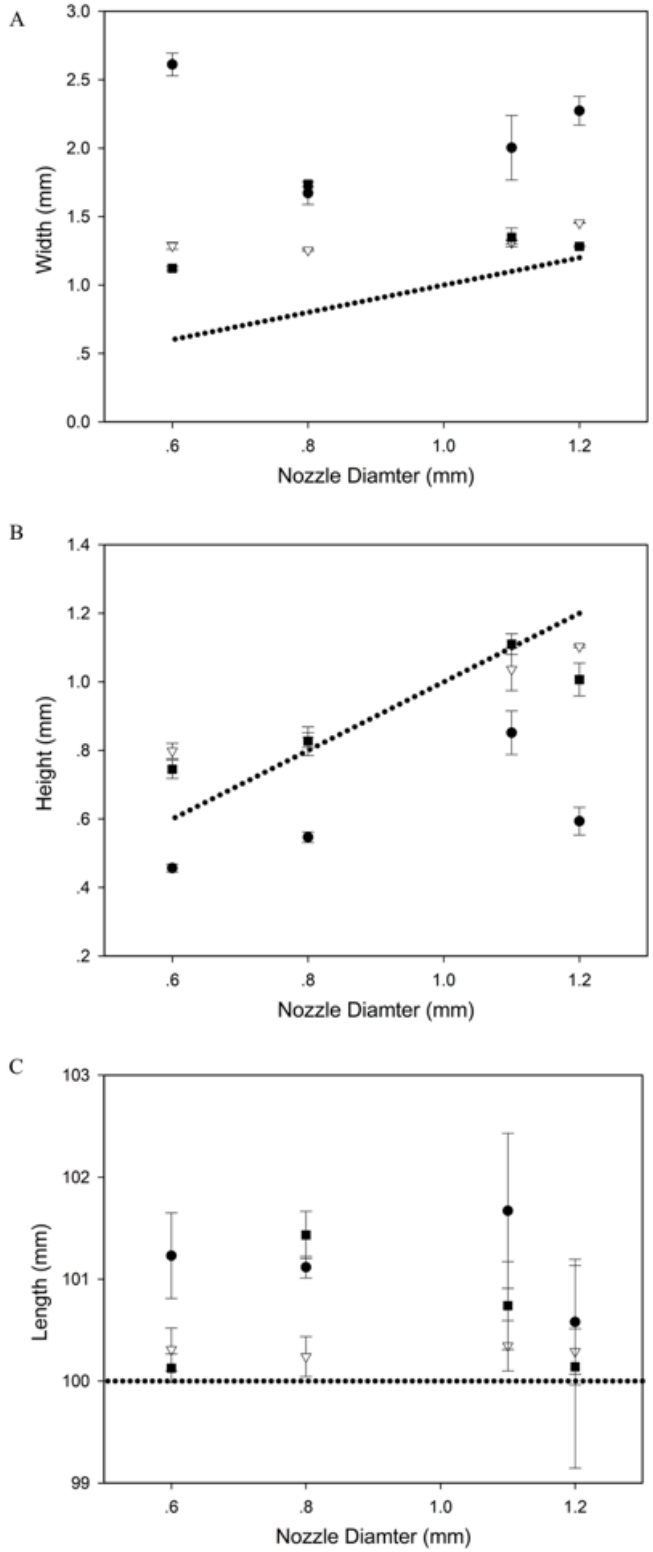

Figure 5.2. Width (A), height (B) and length (C) of 1 layer printed lines printed using 5 % (w/w) gelatin with 1 (●), 2 (▽) and 3 % (w/w) (■) kappa-carrageenan using different diameter nozzles. The dotted line indicates the desired value for each of the different nozzles. (n=3 ± SD).

The length for all of the formulations using all of the nozzle diameters, were within 1.5 % of the desired length. The slight increased length may be due to some excess material being extruded once the line had finished printing, which could be altered with a change in retraction speed of the material, which was a hardware issue. However, the results were close to the desired values, therefore this parameter of the printer was not altered.

In order to further explore the effect of the nozzle diameter, lines with 5 layers were printed and the results have been investigated. The intended widths and heights of each layer were maintained as the nozzle diameter, meaning that the expected heights of each of the lines for all of the formulations should have been 6, 5.5, 4 and 2.4 mm for the nozzles of diameter 1.2, 1.1, 0.8 and 0.6 mm respectively. Figure 5.3 shows the micrographs, as well as the top and side pictures of the 5 layer lines printed with each of the different nozzles using a formulation of 5 % (w/w) gelatin with 2 % (w/w) kappa-carrageenan, which was typical of the other formulations. Figure 5.4 shows the width, height and length of the 5 layers printed line for all of the different formulations of gelatin and kappa-carrageenan.

The formulation of 5 % (w/w) gelatin with 1 % (w/w) kappa-carrageenan again indicates width which are at least 55 % larger than the desired width, using all of the nozzle diameters.

The smallest nozzle (0.6 mm) once again led to inconsistent lines, which had a larger width than desired, due to the ‘sharksin’ instabilities and a greater height due to the undulations.

The results from the nozzle of 0.8 mm indicate a larger than desired width as well as a larger than desired height. The micrograph in Figure 5.3 C indicated how the initial layer was wide, and then the material thinned in subsequent layers. This initial wide layer, was due to a mixture of extrudate swell and ‘squeezing’ affect, as seen when printing with one layer. When subsequent layers were added, the resulting layers were thinner than intended. This thinning of

subsequent layers could be caused by the contact angle of the different surfaces. Kapton Tape, which covered the bed, may have a low contact angle, which caused the material to spread, but the material may have a high contact angle, which allowed the material extruded onto previous material to retain its shape. The contact angle of all of the formulations with gelatin and kappa-carrageenan were investigated during the course of this work, however due to limitations in machinery, definitive numbers could not be achieved.

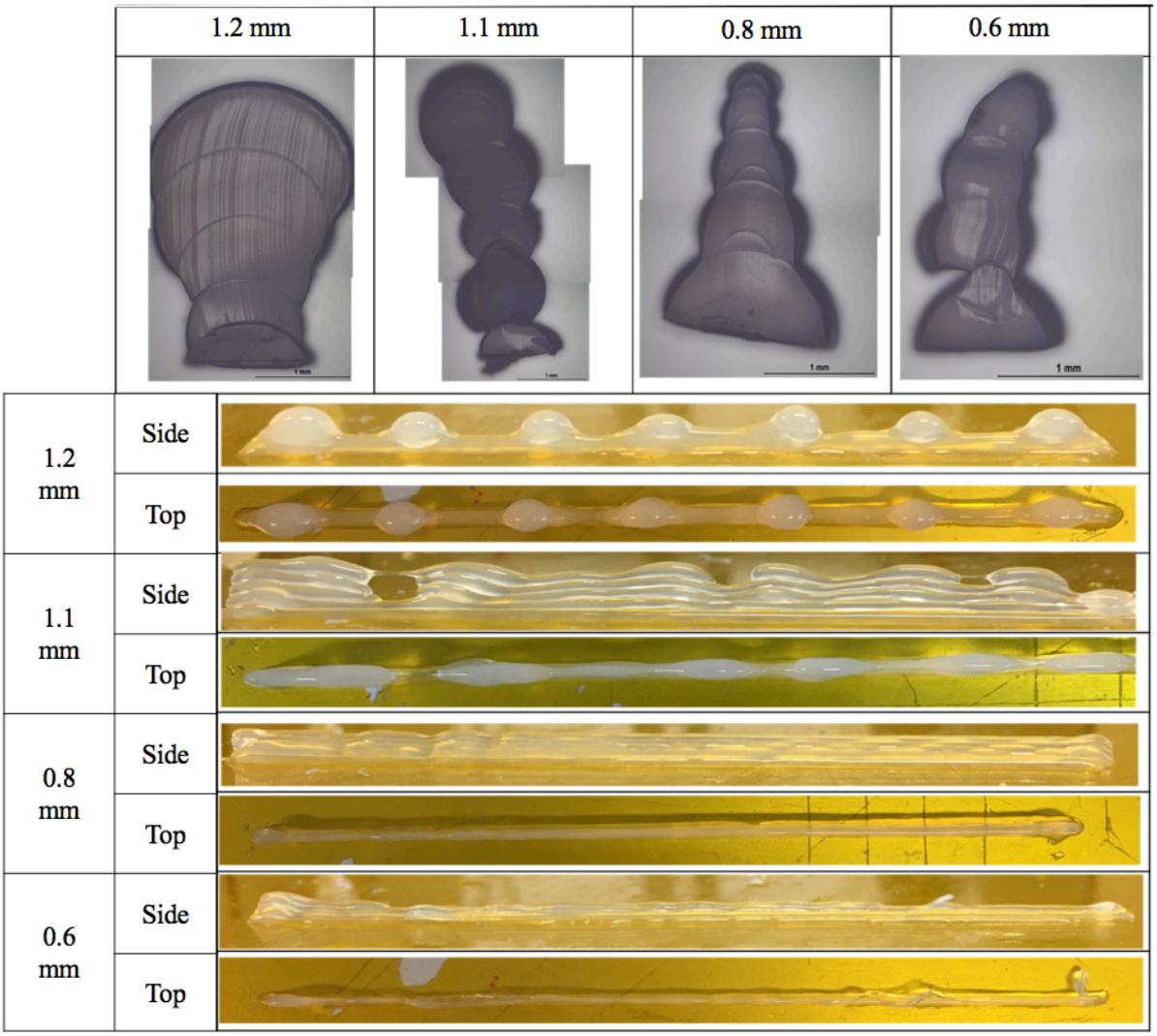

Figure 5.3. Micrographs of the cross-sectional profiles (top images) and images of the top and side views of the formulation of 5 % (w/w) gelatin with 2 % (w/w) kappa-carrageenan printed 5 layer lines using nozzle diameter 1.2, 1.1, 0.8 and 0.6 mm (lower images). The heights and widths of each layer were maintained as the nozzle diameter, the length of the line was 100 mm and the printing speed was 10 mm.s^{-1}. All of the layers were printed right to left.

When printing with the 1.1 mm diameter nozzle, all of the layers in the micrograph were a similar size, apart from the first layer which had slumped slightly under gravity, due to the material not setting in time. The heights and width achieved with the formulations of 5 % (w/w) gelatin with 2 and 3 % (w/w) kappa-carrageenan were within 7 % deviation.

The line printed using the largest diameter nozzle (1.2 mm) displayed a discontinuous line, where build-up of material had occurred at certain intervals. From the micrograph, the first two layers were relatively uniform, however, above this the excess material led to a greater width. This build-up of material in certain areas could be due to the material not achieving the desired height, so when the new layer of material was added, there was no contact, so the material was not extruded onto it, rather was dragged along until it reaches somewhere where it could be deposited, leading to these areas of excess material.

Although the images give an idea of how well the 5 layer lines printed using each of the different nozzles, in order to compare the results quantitatively, the deviation from the ideal value was calculated using Equation 5.5.

$$D = \frac{W_m - W_d}{W_d}$$

Equation 5.5. Calculation of the deviation (D). W_d is the measured width, and W_d is the desired width.

This was repeated for the measured and desired heights and lengths, in order to find their deviations. Each of the deviations from the intended values for all of the different formulations and nozzle diameters were calculated and the results can be seen in Table 5.1.

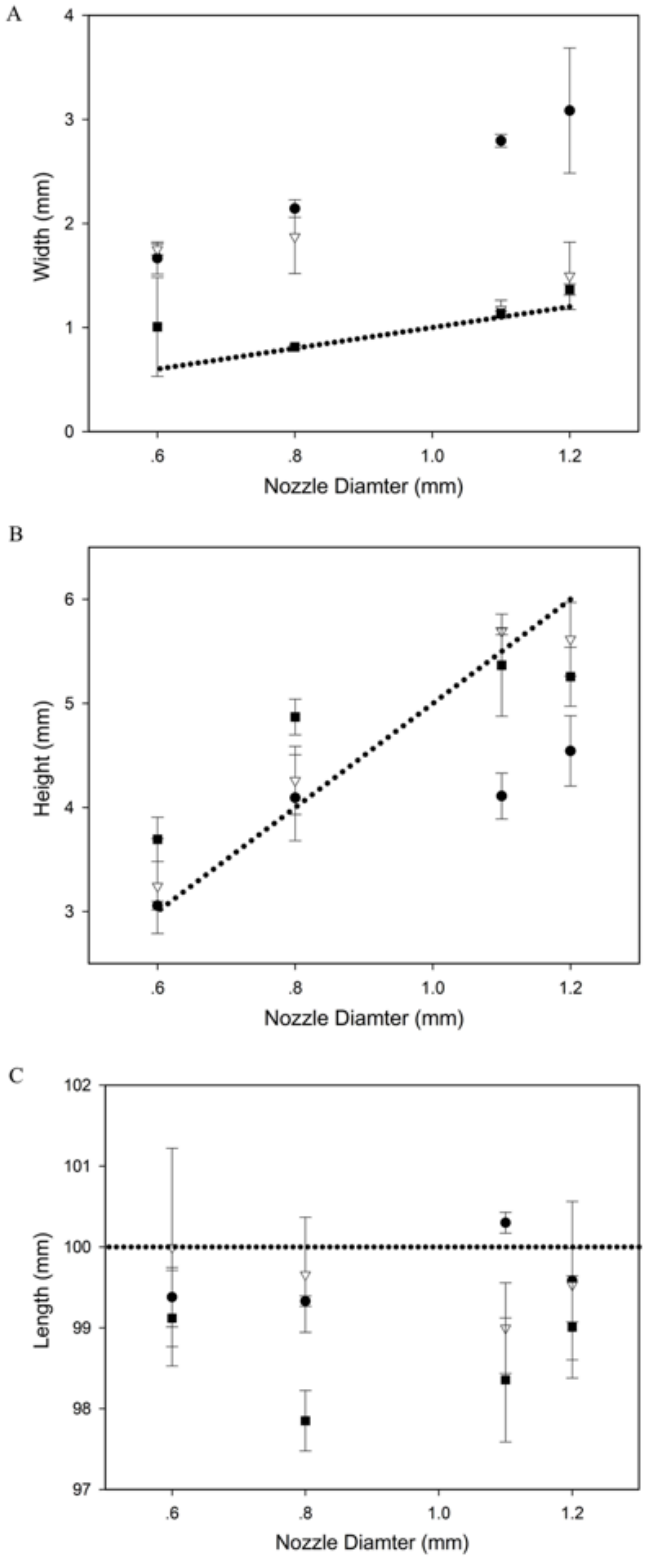

Figure 5.4. Width (A), height (B) and length (C) of 5 layer printed lines printed using 5 % (w/w) gelatin with 1 (●), 2 (▽) and 3 % (w/w) (■) kappa-carrageenan using different diameter nozzles. The dotted line indicates the desired value for each of the different nozzles. (n=3 ± SD).

Table 5.1. Deviations from the intended value for each of the different formulations of gelatin and kappa-carrageenan (κC) of the 5 layer printed lines using each of the different nozzle diameters.

		Deviations (%) for various concentration of κC added (% (w/w))		
	Nozzle Diameter (mm)	**1**	**2**	**3**
Width	**1.2**	157	25	3
	1.1	154	7	1
	0.8	168	134	0
	0.6	178	192	14
Height	**1.2**	-24	-6	-12
	1.1	-25	4	-2
	0.8	2	7	22
	0.6	2	8	23
Length	**1.2**	0	0	-1
	1.1	0	0	-1
	0.8	-1	0	-2
	0.6	-1	0	-1

When comparing the results obtained from the printed shapes when using the nozzles of different diameters, it was clear to see that the nozzle which displayed the results consistently closest to the desired values was the nozzle of diameter 1.1 mm. Due to the pre-determined set up of the printer, the smaller nozzles resulted in a 'squeezing' effect of the materials, as the nozzles were too close to the bed. Although in the future this effect could possibly be mitigated by increasing the layer height, this was not investigated within this work. The nozzle of

diameter 1.2 mm displayed similar deviations to that of 1.1 mm, however a rule of thumb when printing is to pick the smallest tip which allows easy material extrusion as this will afford the user the finest resolution when printing an object (Periard et al., 2007).

5.2.1.2 Investigating of the printing temperature

As previously established in Chapter 4, the printing temperature is an important parameter to be considered when printing temperature dependent materials. However, within this chapter, considering the material as it is being extruded, the printing temperature is vital as the viscosity of food material is directly correlated with the temperature (Liu et al., 2017) and this will affect how the material behaves. Kirchmajer et al. (2015) determined that a compromise needed to be made with respect to the magnitude of the temperature drop: too small and the material would have a high viscosity and require high pressure to expel, but too large would result in the material taking a long time to cool down and gel, likely resulting in the material spreading.

Previously, a high and a low temperature were investigated for each of the formulations in order to determine which temperature produced a better printed square. It was found that printing at a temperature closer to the gelling temperature produced more defined printed objects. A variety of temperatures have been investigated within this work in order to determine a range of temperatures over which a material can be printed.

It was determined that the object to be printed would be a cylinder, in order to allow subsequent compression testing of these objects, in accordance with previous literature (Culioli and Sherman, 1976, Cassanelli et al., 2018).

Figure 5.5 displays the printed cylinders for a formulation of 5 % (w/w) gelatin with 2 % (w/w) kappa-carrageenan at printing temperatures between 40 to 60 ˚C, the trend seen in the printed shapes is typical for the other formulations.

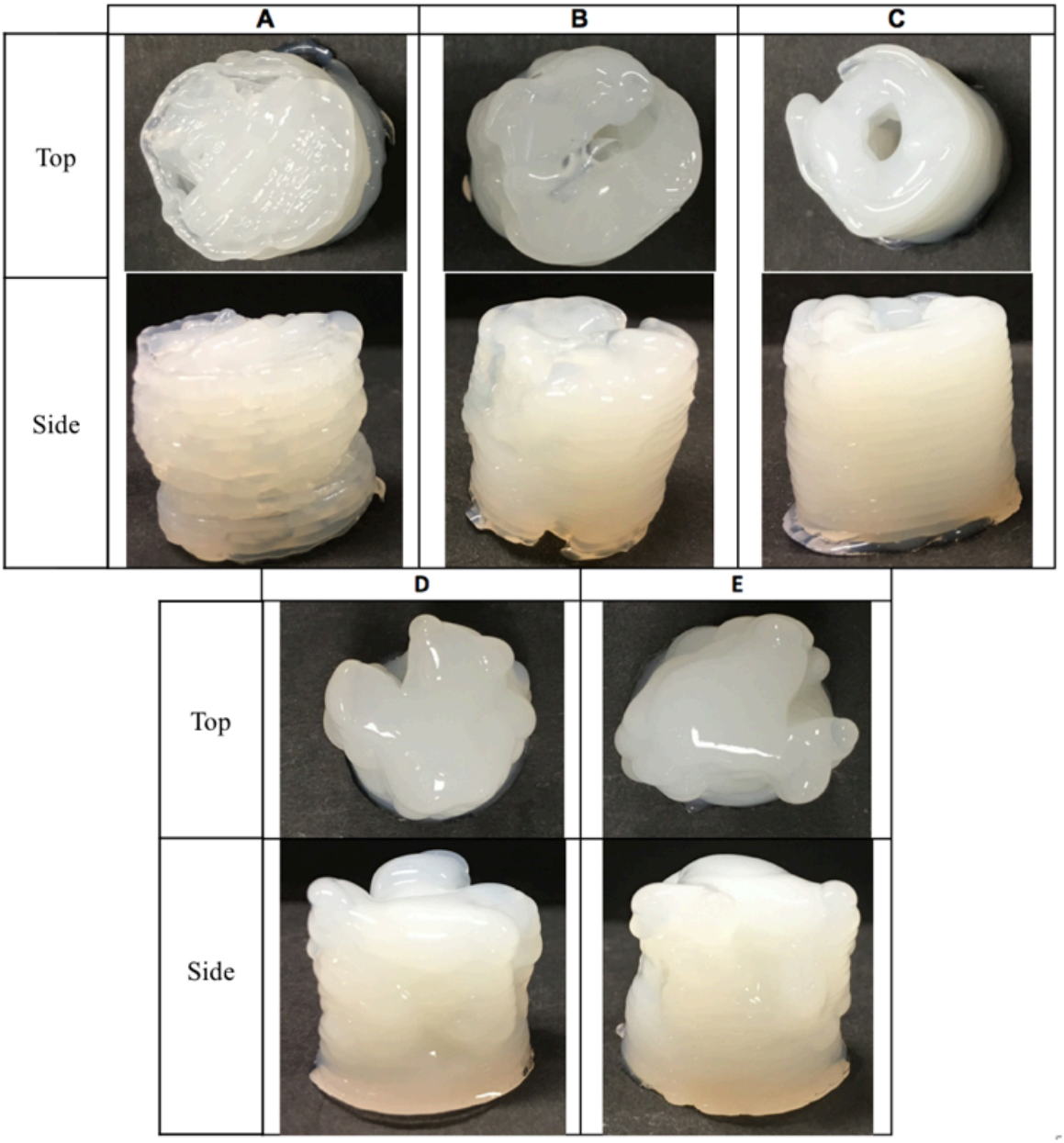

Figure 5.5. Top and side images of 5 % (w/w) gelatin with 2 % (w/w) kappa-carrageenan printed at a temperature of 40 ˚C (A), 45 ˚C (B), 50 ˚C (C), 55 ˚C (D) and 60 ˚C (E). Other extrusion parameters are nozzle diameter 1.1 mm, printing speed 10 mm.s^{-1} and non-printing speed 100 mm.s^{-1}.

It has been found that the minimum printing temperature should be at least approximately 4 ˚C above the material gelling temperature. When printing the formulations of 5 % (w/w) gelatin with 2 and 3 % (w/w) kappa-carrageenan at temperatures closer than 4 ˚C to their gelling temperatures, it was possible to see that the printed shapes consisted of delaminated layers,

rather than a bonded, cohesive shape. Delamination is a large drawback of using the FDM technique, however, the issue of printing too close to the material's gelling temperature exacerbates the problem (Sun et al., 2015b).

When printing at temperature above the minimum printing temperatures, well-defined cylinders were created and even though it was still possible to see the different layers, they were fused together in order to form a cohesive shape.

5.2.1.3 Investigation of the printing speed

The printing speed affects the printability as it changes the amount of extrusion per unit length per unit time (Yang et al., 2018). The printing speed also affects the shear rate that the material will experience within the nozzle, therefore will alter the behaviour of the material as it is extruded. Previous studies have investigated the production of anisotropic micogel particles within phase separated biopolymer mixtures as it is cooled under shear (Stokes et al., 2001). Wolf et al. (2000) demonstrated how the influence of shear whilst cooling formulations of gelatin and gellan resulted in microstructures that ranged from spherical particles, at the lower shear rates (up to around 0.2 Pa) to long extended particles at the high shear rate (between 0.5 – 10 Pa). The ability to control and predict the resulting microstructure could result in the production of novel microstructure designs for the control of the material properties, including textural characteristics (Stokes et al., 2001). Through the use of additive manufacturing, these novel microstructures could be created just by altering the printing speed of the formulation. In order to explore the variety of microstructures created when printing at various speeds, a more in-depth investigation needs to be undertaken, which due to time limitations was not conducted within this research.

The effect of the printing speed on the printing of the cylinders was investigated using 3 different printing speeds: 10, 25 and 50 $mm.s^{-1}$. The results obtained from printing a formulation of 5 % (w/w) gelatin with 2 % (w/w) kappa-carrageenan at each of these different speeds, at a temperature of 45 ˚C has been shown in Figure 5.6.

With this type of extrusion mechanism, the nozzle head is attached to a moving part. At the fast printing speed (50 $mm.s^{-1}$), the rapid acceleration can cause vibration within the printing process, leading to an unstable extrusion process (Sun et al., 2017). This led to almost all of the formulations failing to print cohesive cylinders at this printing speed. When the printing speed was set too high, it caused dragging of the extruding filaments of the product, which caused a breaking of the extruded slurry filament (Yang et al., 2018). Rao and Rai (2016) determined that dragging was caused when the nozzle movement speed was greater than the velocity at which the material was extruded through the nozzle, resulting in thinning of the extruded material, and the material not bonding with the lower layer, which led to fabrication failure. Due to the nature of the machine, there was a maximum extrusion rate at which the motors could extrude the material, therefore, increasing the speed further resulted in a decrease in the extrusion efficiency (Kuznetsov et al., 2018). This resulted in the material being unevenly spread around the object, and led to the material not forming a coherent shape and forming overhanging parts as can be seen in Figure 5.6 C. As well as this, at this printing speed, there was insufficient time for the material to gel before the subsequent layer was printed, with each layer only taking 6 s to complete. In literature, it has been shown that the inter-layer cooling time, the time interval between the start of two consecutive layers, has a significant influence on the printed object (Faes et al., 2015). When the inter-layer cooling time is too fast, the material does not have enough time to cool down, resulting in the material being unable to form

connections with the previous layers, ultimately leading to weaker printed objects (Faes et al., 2016).

The only formulation which was able to produce a defined printed shape at the highest printing speed, was the formulation of 5 % (w/w) gelatin with 3 % (w/w) kappa-carrageenan, when printed at the two lowest printing temperatures (45 and 50 ˚C). This was likely due to the extremely high magnitude of G' (35 kPa) of this formulation, meaning that even though the nozzle was moving faster than it was extruding, the material was still able to hold itself together in order to retain the printed object shape.

When the printing speed was decreased to 10 and 25 $mm.s^{-1}$, the formulations had more time to gel while printing (each layer took 27 and 11 seconds to print, respectively) and the vibrations in the printing process were reduced. This meant that the materials had sufficient strength to be able to have the next layer loaded onto it. Therefore, when printing at the slower speeds, a uniform cylinder was created with the formulations of 5 % (w/w) gelatin with 2 and 3 % (w/w) kappa-carrageenan as was intended. The printing speed dictated the time that the material was in the nozzle, thus how long the material was subjected to a shear rate, affecting the viscosity of the material. The average time for the material to be within the nozzle, experiencing a shear rate was calculated as 12.7, 5 and 2.5 seconds for the printing speeds of 10, 25 and 50 $mm.s^{-1}$ respectively. The effect of this upon the material will be discussed in more detail in section 5.2.2.

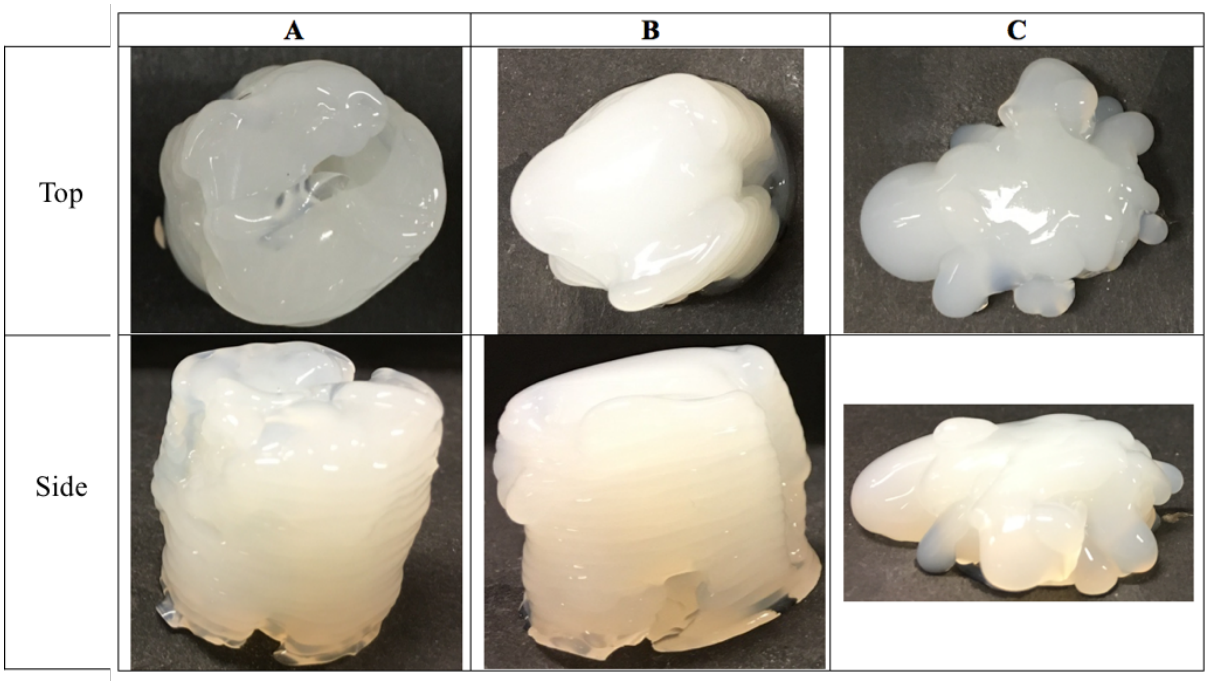

Figure 5.6. Top and side images of 5 % (w/w) gelatin with 2 % (w/w) kappa-carrageenan printed at a speed of 10 (A), 25 (B) and 50 mm.s^{-1} (C). Other extrusion parameters are nozzle diameter 1.1 mm, printing temperature 45 ˚C and non-printing speed 100 mm.s^{-1}.

Images of the printed cylinders with all of the formulations of gelatin and kappa-carrageenan at all of the printing temperatures and speeds can been seen in the appendix.

A major consideration when creating objects through the use of AM, is the time taken to create the objects, as one of the ways that AM will become commonplace is whether there is a significant time benefit over current food manufacturing techniques (Wegrzyn et al., 2012). The total printing time for each of the cylinders, using the different printing speeds can be seen in Figure 5.7. Although objects created at the slower speeds produced more aesthetically pleasing shapes, as the printing speed was increasing, the total printing time dropped significantly. In the future, a compromise may need to be found between how close to the intended shape the printed object needs to be and how quickly the object needs printed.

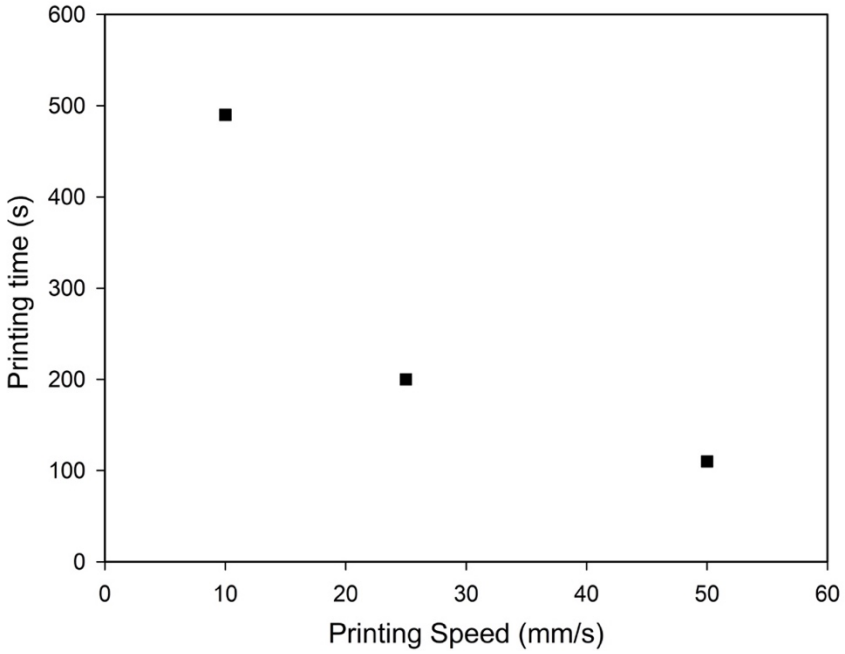

Figure 5.7. Total printing time for the cylinder as a function of the printing speed.

5.2.1.4 Investigation of the printability of the printed cylinders

Analysis of all of the printed cylinders using all the different formulations was undertaken in order to determine the printability at each temperature and speed. The infill of the cylinders was set to 50 %, to allow slight spreading of the materials. The diameter of the printed cylinder was set to 22 mm. The height of the cylinder was set in AutoCAD to 20 mm, however, when the cylinder was sliced for printing, the software sliced it into 18 layers, with each layer having a height of 1.1 mm, resulting in the ideal print height for the printed cylinders as 19.8 mm.

The heights of the cylinders were acquired from the TA measurements in order to achieve a consistent method of measuring the heights. When creating shapes through an AM technique, two common types of surface defect are usually encountered, these are: chordal error and staircase error (Masood et al., 2000). The .STL representation of the CAD model consists of triangles representing the surface, therefore, any curved surfaces will have an error involved, which is known as the chordal error (Jamieson and Hacker, 1995). The staircase error is caused

by the layer by layer nature of the AM technique and is predominantly seen on inclined and curved surfaces. Although this error can be mitigated by the reduction of layer thickness, it can never be fully eliminated (Yasa et al., 2016). Dimensional tolerances for printed parts have been evaluated in several different studies (Lieneke et al., 2016, Masood et al., 2000). When considering the shapes within this study, from visual inspection, it was determined that samples within 98 % of the intended height did not show any major visual difference, therefore these shapes were considered as well printed, and have been indicated in green within Figure 5.9. The cylinders that had printed with a height between 98 – 95 % of the intended height, a clear visual difference could be seen compared with those that had printed well (above 98 % of the height), however, these cylinders still produced a defined shape, therefore were classified as almost printed, and these cylinders have been indicated with orange, within Figure 5.9. It could be seen that cylinders printed below this threshold of 95 % had not produced a defined shape, therefore these have been classified as not reaching the criteria for the minimum height and have been indicated in red within Figure 5.9.

The weights of the printed samples were also investigated in order to establish whether the machine was over- or under- extruding. The desired weight of the printed cylinders was calculated as 4.8 g. The weight of all of the printed cylinders for all of the formulations was about 5.3 ± 0.2 g. This indicated that the machine may be over extruding slightly, but was repeatedly extruding the same amount, even with different formulations, showing that it was consistent. This over extrusion could have been reduced by reducing the EMF, however this weight was considered close enough to the desired value for this work.

There were three main reasons why some of the cylinders did not pass the criteria of being printable. These were:

I. Complete collapse - never any definition within the printed object;

II. Partial collapse - a cylinder structure could be seen printed from the first few layers, however after several layers the structure collapsed;

III. Partial solidification - the material was printed out solid-like meaning that the layers did not bond together. Some cylinders printed with this issue still managed to achieve the desired height, so were considered printed.

Images of different cylinders which did not meet the requirement in order to be defined as printable can be seen in Figure 5.8. The reasons for not meeting the criteria have also been highlighted within Figure 5.9.

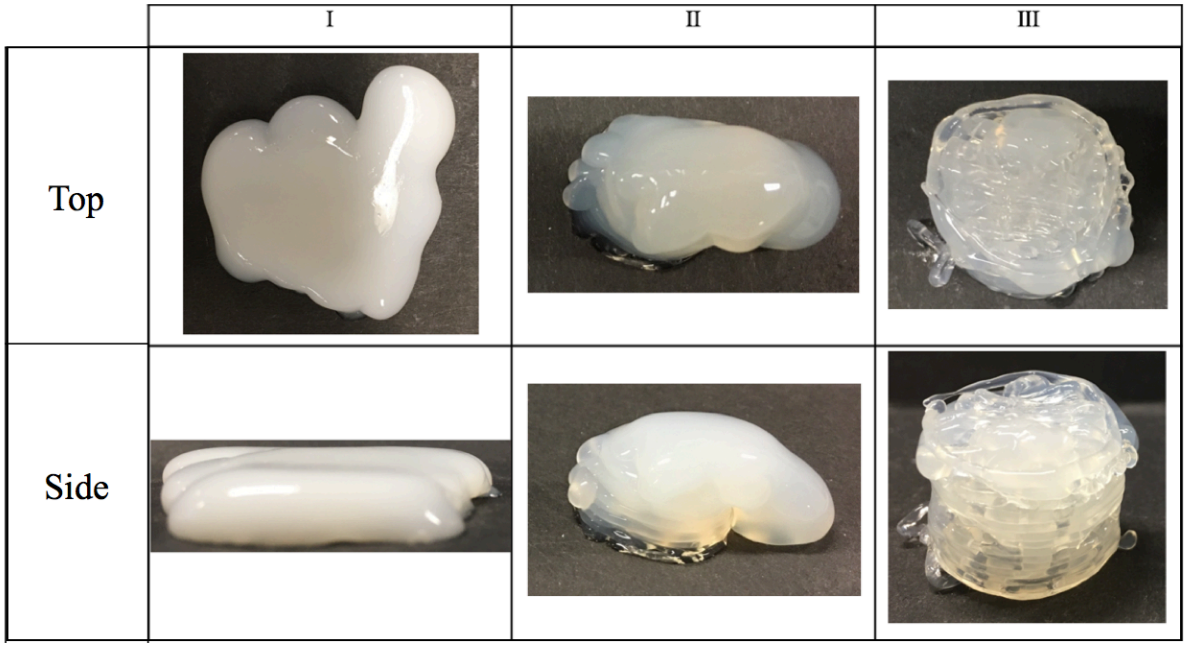

Figure 5.8. Top and side views of different types of failures for the cylinders that did not pass the criteria in order to be defined as 'printed'. I- complete collapse, II- partial collapse and III- partial solidification.

A

Speed (mm/s)	Temperature (˚C) 40	45	50	55	60
10	II	II	II	II	I
25	II	I	I	I	I
50	I	I	I	I	I

B

Speed (mm/s)	Temperature (˚C) 40	45	50	55	60
10	III				II
25	III		II	II	I
50	II	I	I	I	I

C

Speed (mm/s)	Temperature (˚C) 40	45	50	55	60
10		III			
25		III		II	II
50		III		II	II

Figure 5.9. Traffic light table of printability at different temperatures and speeds of 5 % (w/w) gelatin with 1 (A), 2(B) and 3 % (C) (w/w) kappa-carrageenan. Green indicating that it had printed well, orange indicating that it had printed ok and red indicating that it had not printed well. The roman numerals signify the print quality: complete collapse (I), partial collapse (II) and partial solidification (III).

When looking at the printability of the cylinders using all of the formulations, print temperatures and speeds, a clear pattern was seen regarding why the cylinders did not meet the required criteria to be defined as printable.

For the formulation of 5 % (w/w) gelatin with 1 and 2 % (w/w) kappa-carrageenan when printing at higher temperatures and speeds, the reason for the printed shape to not be deemed as printable was due to complete collapse. As the printing temperature and speed was decreased for these formulations, the reason for failure became partial collapse, indicating that these materials were almost printable, but did not quite possess the exact properties necessary in order to print a well-defined shape.

For the formulation of 5 % (w/w) gelatin with 2 % (w/w) kappa-carrageenan, once the printing temperature and speed had been reduced sufficiently, objects were able to be printed. However, when the temperature became too low, the printed objects exhibited signs of the materials beginning to gel within the nozzle.

A similar pattern was seen with the formulation of 5 % (w/w) gelatin with 3 % (w/w) kappa-carrageenan, although none of the objects printed with this formulation indicated complete failure. At the high temperatures and speeds, partial failures occurred, where the shape had initially begun to form, but after several layers the shape had collapsed. Below 50 ˚C and at the slowest speed of 10 $mm.s^{-1}$, all of the objects printed in a well-defined way. At the lowest temperature tested with this formulation, although the objects were categorised as well-defined, having met the requirements, the printed objects displayed results that the material had gelled within the nozzle and not formed a cohesive shape.

5.2.2 Rheological characterisation of the formulations

The viscosity is a critical parameter of the material to be printed, as it needs to be low enough to be extruded through the fine nozzle (Godoi et al., 2016). Previously, the viscosities of the materials were investigated at a constant shear rate, whilst undergoing a temperature ramp between 60 to 20 ˚C. This work focuses on how the viscosity was affected at different shear rates at a set temperature. Therefore, it was possible to see which viscosities enabled printing of defined objects at each of the printing temperatures and speeds.

Figure 5.10 illustrates the viscosity of 5 % (w/w) gelatin with 3 % (w/w) kappa-carrageenan at different temperatures, between a shear rate of 1 and 1000 s^{-1}, which was typical of all the different formulations of 5 % (w/w) gelatin with kappa-carrageenan. All systems showed an increase in the viscosity, as the shear rate was decreased, indicating shear-thinning behaviour (Yang et al., 2018). It was also clear that as the temperature of the experiment was increased, the viscosity decreased, which is in line with the results found earlier under the temperature ramp. The time dependent effects at the lower shear rates at the lowest tested temperature (45 ˚C) results in the sample not getting to steady state, thus the increase in viscosity is likely to be an over representation of the actual viscosity of the system (Wilkes, 1981).

The shear rate that the material will experience within the nozzle at printing speeds of 10, 25 and 50 $mm.s^{-1}$ have previously been determined as 113, 293 and 513 s^{-1} respectively. The viscosity at each of these different shear rates for each of the different formulations have been plotted in Figure 5.11 A, B and C. These values were determined by fitting each of the individual viscosity curves to the Cross Model using Kinexus software, shown in Equation 5.6.

$$\eta = \eta_\infty + \frac{\eta_0 - \eta_\infty}{1 + (k\dot{\gamma})^n}$$

Equation 5.6. Cross model equation. η_∞ is infinite shear viscosity, η_0 is the zero-shear viscosity, k is the cross time constant and n is the rate constant.

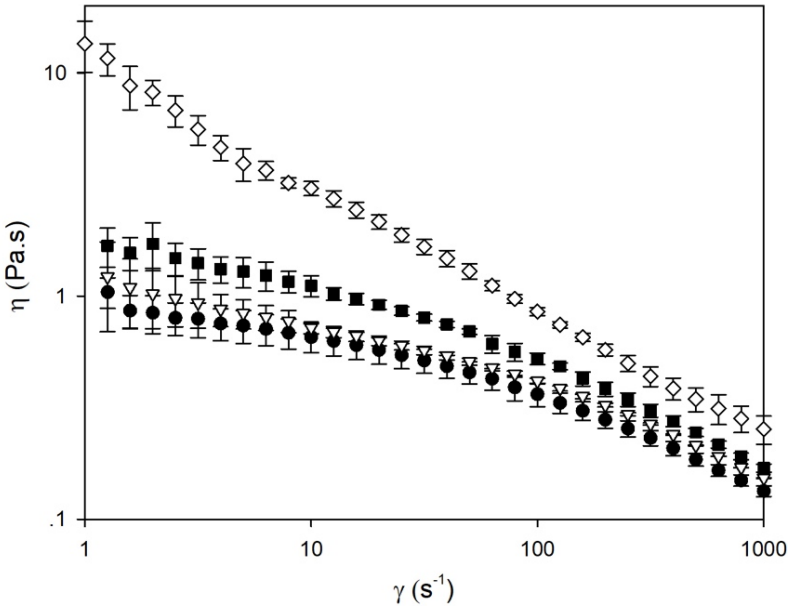

Figure 5.10. Viscosity curves from a shear rate of 1 – 1000 s^{-1} of 5 % (w/w) gelatin with 3 % (w/w) kappa-carrageenan at temperatures of 60 (●), 55 (▽), 50 (■) and 45 ˚C (◇). (n=3 ± SD).

Within each of the graphs, the shaded regions indicate the cylinders which did not meet the criteria of being defined as well printed.

From all the curves, there was a minimum viscosity of 0.21 Pa.s, which needed to be overcome in order for the material to achieve a good print. This was slightly lower than was suggested by He et al. (2016), who determined that the minimum viscosity to be printed was 0.3 Pa.s. However, He et al. (2016) was investigating printing organ structures, therefore needed to be extremely precise, which could explain the reason the limit for the minimum viscosity was slightly higher.

Some of the cylinders achieved this minimum viscosity, but still did not manage to meet the criteria in order to be defined as printed. In order for the whole object to be printed, it was necessary for the material of a certain layer to have gelled together enough immediately after printing to be strong enough to support subsequent layers, but not so much that it did not then gel with the subsequent layer when it was added. For these printed cylinders, a single layer took

6, 11 and 27 seconds for a printing speed of 50, 25 and 10 $mm.s^{-1}$. Therefore, if the $T_p > T_g + 13$ ˚C, then the material needed more than 11 seconds in order to be able to be printed, otherwise the printed structure collapsed.

The two results at a lower temperature and high viscosity that did not print were likely to have not printed due to the material gelling within the nozzle and therefore did not fail because of the viscosity.

During extrusion the material will experience a high shear rate, however immediately after extrusion, the material will experience a shear rate close to zero (Cesarano et al., 1998). In order to try and understand the behaviour of the material during printing, a print simulation was established which investigated the viscosity at a given temperature, shear rate and duration in order to mimic the material as it was extruded through the nozzle, assuming the nozzle was fully insulated. This step was immediately followed by small deformation rheology section under a temperature ramp down to 20 ˚C at a rate of 3 $˚C.min^{-1}$, in order to imitate the material once it had been extruded onto the bed. Using the corrected shear rates found in section 3.3.2.10, a printing simulation was undertaken on the rheometer in order to simulate the different speeds printed. The test was undertaken at each of the different printing temperatures (40, 45, 50, 55 and 60 ˚C) and each of the different printing speeds (with the shear rates and duration for each speed given in Table 5.2).

Table 5.2. Different shear rates and shearing times dependent on the printing speed.

Printing speed	Shear Rate (s^{-1})	Time undergone shearing (s)
10	113	127
25	293	50
50	513	25

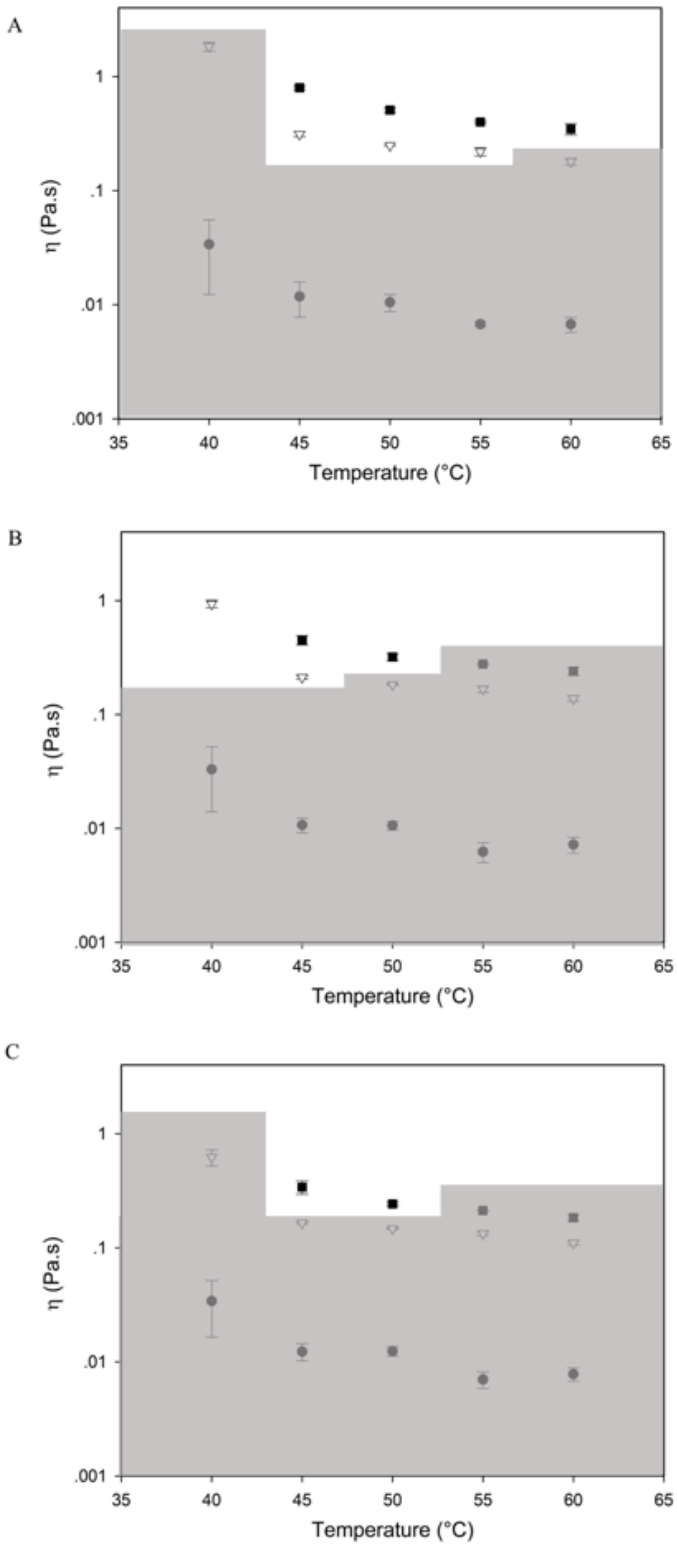

Figure 5.11. Viscosity of 5 % (w/w) gelatin with 1 (●), 2 (▽) and 3 % (w/w) (■) kappa-carrageenan at a shear rate of 113 (A), 293 (B) and 513 s^{-1} (C). The shaded area incidcates the cylinders that did not print, while the lighter area shows the cylinders that were defined as printed. (n=3 ± SD).

The viscosity for each of the formulations (5 % (w/w) gelatin with 1, 2 and 3 % (w/w) kappa-carrageenan) undertaken with the printing simulation at a printing speed of 10 $mm.s^{-1}$ can be seen in Figure 5.12. For the formulations with 2 and 3 % (w/w) kappa-carrageenan, as the temperature was reduced, the viscosity reduced. The viscosity results found for these formulations from the printing simulation were very similar to the viscosities determined from the viscosity curves. However, for the formulation with 1 % (w/w) kappa-carrageenan, only the viscosities at temperatures of 40 and 45 ˚C were consistent with the values found from the viscosity curves. Due to this formulation having such low viscosity at higher temperatures, it was likely that the results were out of range of the rheometer, resulting in the values not reaching steady flow equilibrium. When a double gap geometry was used, which was more suitable to this low viscosity system, the same issues occurred, therefore it was likely that these results at the higher temperatures for this formulation were inaccurate. Therefore, the results determined at the higher temperature for the formulation of 5 % (w/w) gelatin with 1 % (w/w) kappa-carrageenan which indicate that the viscosity increased with temperature should be disregarded.

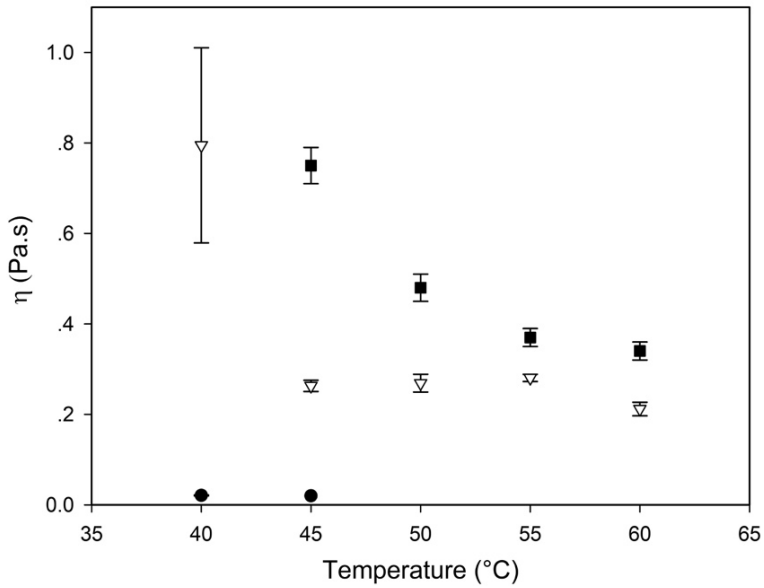

Figure 5.12. Viscosity from the printing simulation at various temperatures of formulation of 5 % (w/w) gelatin with 1 (●), 2 (▽) and 3 % (w/w) (■) kappa-carrageenan at a printing speed of 10 $mm.s^{-1}$ (shear rate of 113 s^{-1}). (n=3 ± SD).

Analysis of the small deformation rheology was important in order to determine the behaviour of the material as the temperature was reduced and how it would behave as it was cooling on the bed. The small deformation rheology section undertaken in order to see how at the different printing temperatures and speeds affected the material's behaviour and if it would maintain its shape post extrusion. Due to the fact that the value of G' was extremely similar for each of the formulations at a temperature of 20 ˚C, tanδ (G"/G') was plotted against temperature in order to see how the ratio between the two moduli changed. The two extreme temperatures, 45 and 60 ˚C for the formulation of 5 % (w/w) gelatin with 3 % (w/w) kappa-carrageenan have been plotted against each of the simulated printing speeds in Figure 5.13 A and B respectively.

The cylinders printed at a temperature of 45 ˚C fulfilled the criteria of printing the correct height and width, however, when trying to move the cylinders, it became clear that the layers had not gelled together properly. This could be explained by the low tanδ value of approximately 1.4, at all of the printing speeds. This was indication that the material was behaving solid-like almost immediately as soon as the shear was removed, therefore, was extruding like a filament, and not bonding with subsequent layers. In comparison, when considering the materials that did not print at all, such as the cylinders printed at the higher temperatures, initial spreading was seen and their tanδ values were much higher, closer to 5. This indicated that with such a high tanδ value, the materials were less elastic and prone to deform continuously under gravitational stress. This showed that although a high G' value was important, it was also important that there was a large difference between G' and G", otherwise the materials were still likely to slump.

Therefore, in order for the material to be initially printable, the value for tanδ needs to be higher than 1.4, but lower than 5 when the shear was removed and the material needed to start printing.

Although this data from the second part of the new print simulation indicated whether the material would spread after extrusion, the error bars for the data were extremely large (not

shown), therefore it was not possible to correlate the results across different speeds. Therefore, no data could be stipulated from these results across different speeds or formulations.

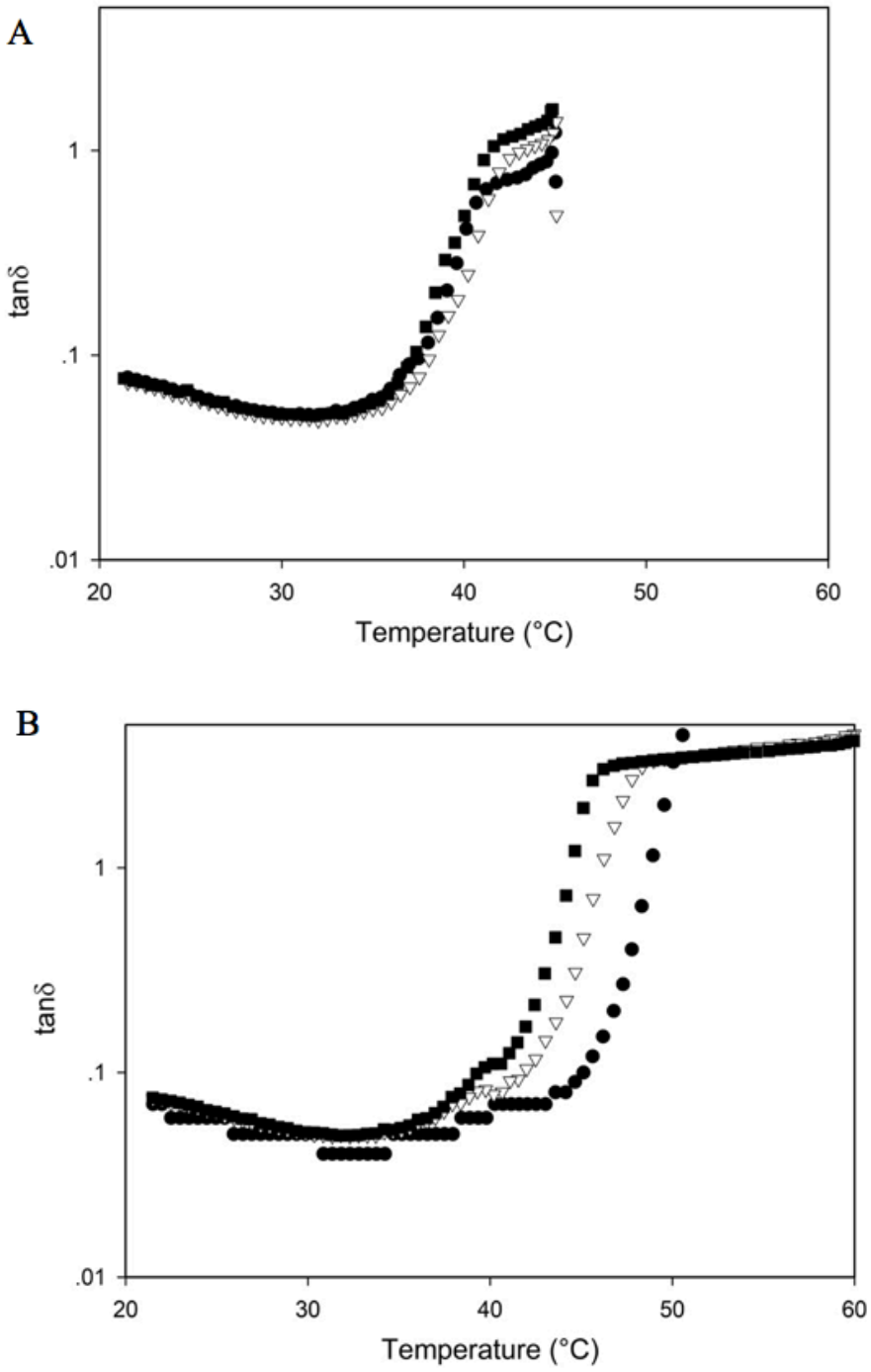

Figure 5.13. Tanδ from the printing simulation of 5 % (w/w) gelatin with 3 % (w/w) kappa-carrageenan conducted at simulated printing speeds of 10 (●), 25 (▽) and 50 mm.s^{-1} (■) and simulated printing temperatures of 45 (A) and 60 ˚C (B). Frequency was set to 1 Hz with a strain of 0.1 %.

5.2.3 Mechanical properties of printed vs cast cylinders

The bonding quality along the deposited material in the FDM process determines the integrity and the mechanical properties of the resultant printed object (Sun et al., 2003). In order to understand the influence of the printing process on the mechanical properties of the formulations, the cylinders were subjected to a compression test on a texture analyser. These tests were conducted in a similar way to Le Tohic et al. (2018) who investigated the effects of AM on the textural properties of cheese. Initially cast samples were prepared by pouring molten samples of the formulations into a sample pot and allowing to cool for an hour. Due to the macroscopic phase separation observed with the formulation of 5 % (w/w) gelatin with 1 % (w/w) kappa-carrageenan, due to their thermodynamic incompatibility (Fang et al., 2006), it was not possible to acquire measurements with this formulation. This phase separation was not observed within the formulations of 5 % (w/w) gelatin with 2 and 3 % (w/w) kappa-carrageenan potentially due to the increased viscosity of these formulations reducing the rate of macroscopic phase separation (Michon et al., 2000), therefore the peak force of these samples determined from the compression test have been presented in Table 5.3.

Table 5.3. Peak force of cast samples of formulations of 5 % (w/w) gelatin with various concentrations of kappa-carrageenan (κC). Formulations of 5 % (w/w) gelatin and 1 % (w/w) were not tested due to phase separation. (n=5 ± SD).

Concentration κC (% (w/w))	Peak force (N)
1	-
2	102 ± 1.2
3	125.6 ± 8.6

The peak force was higher for the formulation with 3 % (w/w) kappa-carrageenan than with 2 % (w/w) kappa-carrageenan. As mentioned in section 4.2.2, this was due to the synergist

effects of the gelatin and kappa-carrageenan and more bonds with more biopolymer making the gel stronger (Derkach et al., 2015).

The results of the gel strength of the printed cylinders, which met the criteria to be called 'printed' can be seen in Figure 5.15. The results for the printed cylinders were considerably lower than for the cast samples of both of the formulations. This was due to the fracturing of the samples, as can be seen in Figure 5.14.

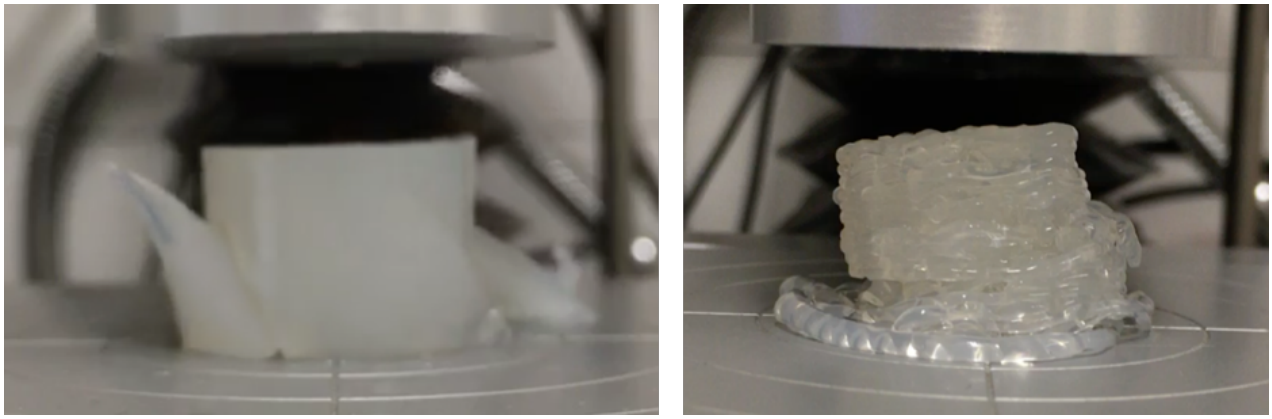

Figure 5.14. Images of cast (left) and printed (right) images of 5 % (w/w) gelatin with 3 % (w/w) kappa-carrageenan, post compression test.

In the cast samples (shown on the left), the peak force was due to the breaking of the material. However, in the printed sample (shown on the right), delamination occurred as the layers were not bonded together sufficiently, therefore this was the point of weakness of the printed samples. This bonding between layers will need to be addressed in order for printing to find a place in commercial usage. For both of the formulations, as the temperature was increased, the peak force also increased. This indicated that even though the cylinders printed at a slower speed and temperature looked visually better, the stronger cylinders were printed at higher printing temperatures and faster printing speeds. The higher melt temperature led to better adhesion between successive layers, resulting in a greater mechanical strength of the printed part (Turner et al., 2014). Therefore, when considering materials for printing, the material needs

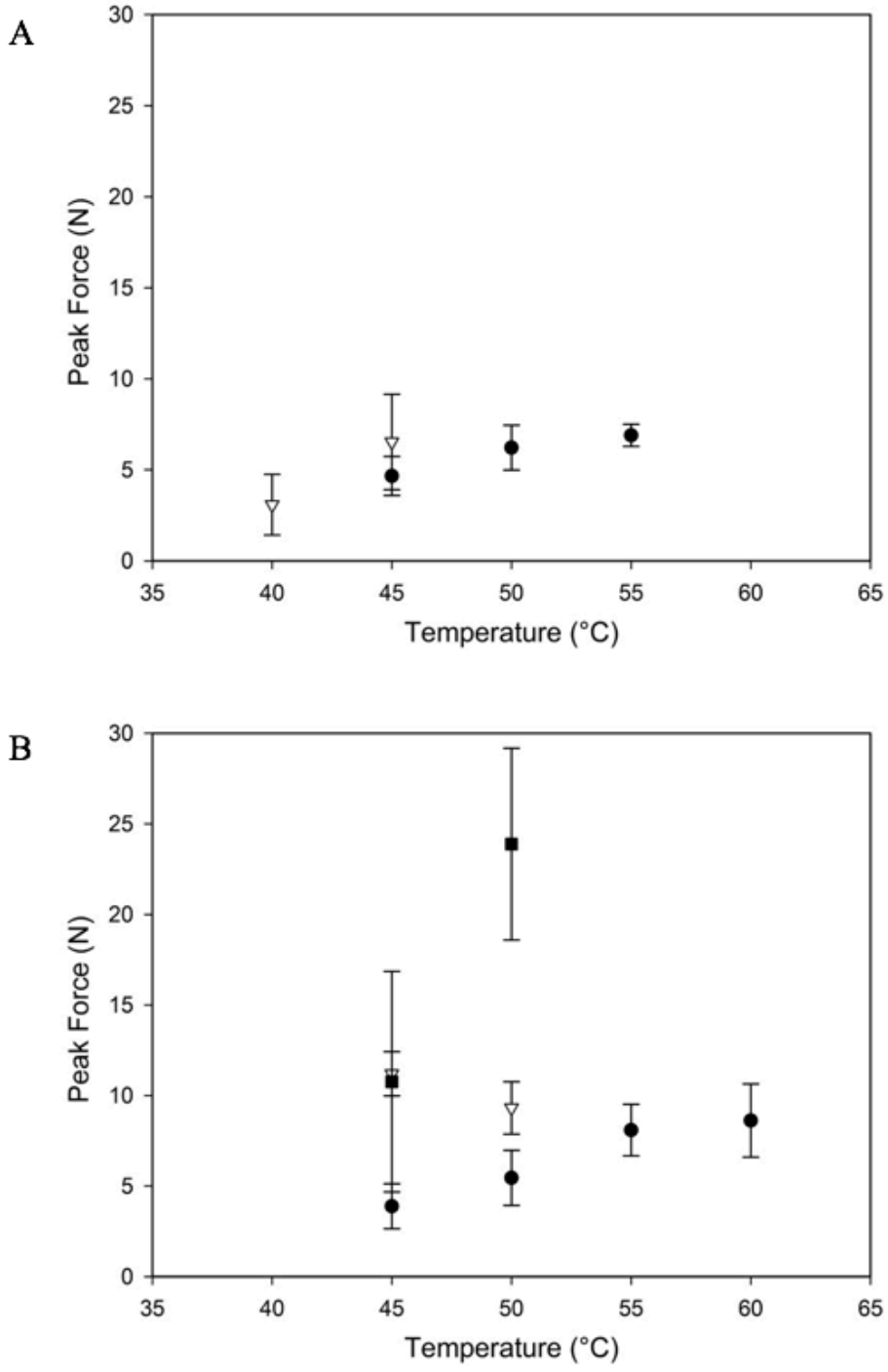

Figure 5.15. Peak force of the formulations of 5 % (w/w) gelatin with 2 (A) and 3 % (w/w) (B) kappa-carrageenan at different printing speeds of 10 (●), 25 (▽) and 50 mm.s^{-1} (■). The results for the cast values were 102 and 126 N for the formulations of 5 % gelatin and 2 and 3 % kappa-carrageenan respectively. (n=3 ± SD).

to have a high enough G' and low tanδ in order to stop the initial spreading, but the higher the printing temperatures results in more time for bonding to occur between layers, creating a stronger printed object.

As the printing speed was increased, the peak force also increased. This increase in strength with an increase in printing speed was also observed by Le Tohic et al. (2018) who compared printing cheese at different printing speeds. This was due to the material having sufficient initial G', to stop the material from spreading and the new layer of material being added rapidly in order to allow diffusion whilst the material was in the cooling state enabling layer adhesion once helices form on cooling.

5.3 Conclusions

The nozzle diameter, printing temperature and printing speed have been assessed for the printing of formulations of 5 % (w/w) gelatin with the addition of various amounts of kappa-carrageenan.

In the previous chapter the design rules which were established determined that the formulations of 5 % (w/w) gelatin and 5 % (w/w) gelatin with 1 % (w/w) kappa-carrageenan did not possess the correct characteristics in order to allow them to print defined shapes. Due to the macroscopic phase separation, it was unlikely that this formulation will be able to print defined printed shapes using this technique.

When changing the diameter of the nozzle it was found that the two smaller nozzles exhibited a high extrudate swelling effect as well as a 'squeezing' effect of the formulations, resulting in diameters greater than was expected. The largest diameter nozzle resulted in inconsistent lines, therefore the optimal nozzle diameter was chosen as 1.1 mm.

It has been established that the minimum viscosity of a material to enable printing of defined shapes was 0.2 Pa.s, using a nozzle with diameter 1.1 mm. When materials possessed lower viscosity than this, the printed objects did not create uniform cylinders.

A balance needs to be found when printing thermally dependent materials as it is important the material gels together enough after extrusion so that the material does not spread, but not so much that the material does not gel with the subsequent layer. From analysis of the results, the minimum printing temperature was determined to be approximately 4 ˚C above the gelling temperature of the formulation, otherwise the material gelled within the nozzle and created a cylinder where the layers had barely bonded together. Although the objects printed at the lowest temperatures and speeds seemed visually finest, it was determined that the optimal printing temperature was approximately 9 ˚C above the gelling temperature of the formulation, as this allowed the materials to print at all of the printing speeds. Printing at this temperature yielded the strongest printed cylinders, indicating that the layers had bonded together.

Between the minimum printing temperature and the optimal, the cylinders were only able to print at the slower printing speeds (10 and 25 $mm.s^{-1}$). This was likely due to the materials gelling fast, therefore collapsing if the printing speed was too fast. These cylinders yielded the weakest results, as the materials were not bonding sufficiently with the subsequent layers, therefore when tested, the layers were quickly delaminating and not holding the structure together.

Above the optimal printing temperature, defined printed cylinders were only established at the slowest printing speed. With such a large difference to the gelling temperature, the formulations needed a long time between successive layers to be allowed to gel, otherwise the materials collapsed. However, as the materials were taking a long time to gel together, this allowed good adhesion between layers, resulting in cylinders that were relatively strong.

This section of the work focused on printing objects with the layer height set to the same magnitude as the nozzle diameter. In the future, it may be of interest to change the layer height in order to determine whether the ‘squeezing’ effect can be mitigated, resulting in the formulations being printable using smaller nozzles, allowing printing of more defined shapes. Further to this, it could then be possible to establish whether the minimum viscosity was consistent when printing with other diameter nozzles.

CHAPTER 6. PRINTABILITY OF OTHER BIOPOLYMER MIXTURES

6.1 Introduction

The design rules for thermo setting gels found in the previous chapters determined that there was a minimum magnitude of G' and viscosity, which a material must overcome, as well as the necessity for the material to possess a "fast" gelation rate and have shear thinning behaviour in order to be printable. These established design rules will be tested by printing formulations of 5 % (w/w) gelatin with different secondary biopolymers in order to determine whether the rules can be used predictively with other materials. Two secondary polymers were chosen, gellan and agar, as they gel in a similar way to that of kappa-carrageenan, a coil-helix transformation (Chandrasekaran and Radha, 1995, Schafer and Stevens, 1995). However, gellan and agar form different mixed structures with gelatin, with the gellan forming coupled networks with the gelatin (Fonkwe et al., 2003) and the agar forming two liquid phases which are immiscible, but coexist in thermodynamic equilibrium (Singh et al., 2007b).

As established in the literature review, upon the addition of gellan to gelatin, the gellan may form coupled networks with the gelatin molecule wherein the anionic domains of the gellan forms new heterolytic junction zones with cationic domain of the gelatin molecules leading to increases in gelation temperature, gelation rate and gel strength (Fonkwe et al., 2003, Pranoto et al., 2007). This effect was also observed by Shim (1985) who determined that the synergistic effects between gelatin and gellan produced gels with greatly increased gel strength. This should result with mixtures which have a high G' value and fast gelation rate, enabling the extruded material to retain its shape and produce a well-defined object. However, there may be

a risk that the layers will not adhere together if the gelation is too fast, so a compromise must be found. As well as this, Lee et al. (2003) investigated the physico-chemical properties of a range of concentrations of gelatin/gellan blends and determined that they all exhibited shear thinning behaviour. This characteristic will allow the materials to go through the extrusion process and not block the nozzle. Therefore, it is hypothesised that the mixtures of gelatin and gellan will be able to meet the minimum threshold requirements in order to be printable.

Mixtures of gelatin and agar are incompatible and immiscible but coexist in a thermodynamic equilibrium (Singh et al., 2007b). In the mixture gel of gelatin and agar, the network formation of one of the components is hindered in part by the other component (Shiinoki and Yano, 1986). Singh et al. (2009) has determined that as the temperature is reduced, the agar initially forms double helix structures through specific interactions, resulting in the formation of agar-rich gel phase and an ungelled complex network of gelatin and agar. These ungelled domains undergo osmotic swelling, due to the abundance of solvent, resulting in a bi-continuous topology that is thermally stable, but structurally not (Singh et al., 2009). The gel strength contributed by agar in the mixture is accepted to be less than would be expected on the basis of the concentration of agar present (Clark et al., 1983). With a low gel strength, this may result in the magnitude of G' not achieving its threshold value, resulting in the printed object failing to meet the criteria to be defined as printable.

Following on from the investigations detailed in previous chapters, initially the gelling temperatures of all of the systems were determined, followed by establishing the rheological characteristics including: flow profiles, evolution of elastically dominated structures, frequency dependent behaviour and rate of increase of G'. The mixtures were then printed at various printing temperatures and speeds in order to produce a "traffic-light" graph of printability. This

printability was then compared to the design rules in order to determine whether they were accurate and the findings have been discussed.

6.2 Results and Discussion

6.2.1 Thermal properties of the formulations of gelatin with gellan and agar

The thermal properties of the formulations of gelatin with gellan and agar were investigated using the same techniques as gelatin and kappa-carrageenan, through the use of a μDSC and rheological techniques of a temperature sweep, maintaining the frequency and strain at constant values.

The first heating and cooling cycle for the formulations of 5 % (w/w) gelatin with 0, 1, 2 and 3 % (w/w) gellan can be observed in Figure 6.1 A and B respectively. The reason the diagram appears to show a single endothermic peak for the heating curves of the formulations with the addition of gellan, was due to the endotherms for helix-coil transition of both the gelatin and gellan overlapping. Compared to the endothermic peak for just the gelatin alone, the formulations with the addition of gellan displayed a larger shoulder on the right of the peak, indicating the transition of the gellan, similar to those found by Miyoshi et al. (1995). Two distinct exothermic peaks could be observed for each of the formulations with the addition of gellan on their respective μDSC curves. Similar to the formulations of gelatin and kappa-carrageenan, the broad peak, spanning 10 to 20˚C was attributed to the gelation of the gelatin. The secondary peak, occurring at a temperature around 37 ˚C, was attributed to the helix-coil transition of the gellan molecules, which was in accordance with Miyoshi et al. (1995).

The second and third heating cycles of the gelatin and gellan solutions were extremely similar to the curves shown, indicting there were no major changes upon cooling and heating.

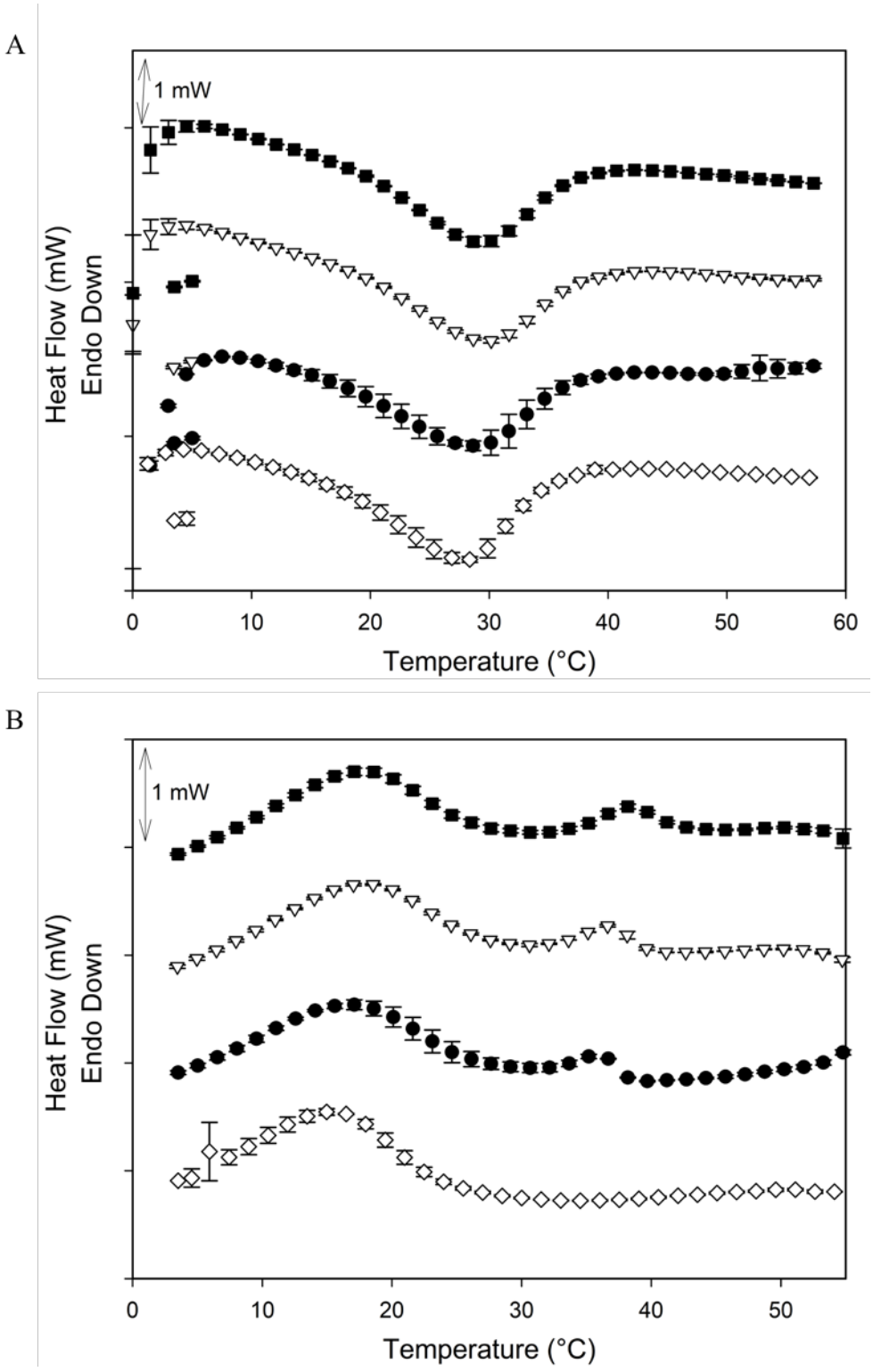

Figure 6.1. µDSC heating (A) and cooling (B) profiles of the first scan of 5 % (w/w) gelatin with 0 (◇), 1 (●), 2 (▽) and 3 % (w/w) (■) gellan, over a temperature range of 0 to 60 ˚C using a cooling/heating rate of 1.2 ˚C.min^{-1}. (n=3 ± SD).

The first heating and cooling cycles for the formulations of 5 % (w/w) gelatin with 0, 1, 2 and 3 % (w/w) agar have been shown in Figure 6.2 A and B respectively. Two endothermic and two exothermic peaks can be seen for all of the formulations with the addition of agar. Similar to the formulations with kappa-carrageenan and gellan, the broader peak for both the endotherm and exotherm was attributed to the gelation of the gelatin within the formulation, these results were comparable to those found by Singh et al. (2007a), who also investigated the thermal properties of gelatin and agar mixtures. The second peak (at approximately 80 ˚C on the endotherm and 40 ˚C on the exotherm), was attributed to the melting and setting of the agar, via the helix-coil transitions, which were similar to results found by Watase and Nishinari (1988). The sharp peak of gelation for the agar emphasizes the cooperative conformational transition as compared to the ongoing structural development of the gelatin network, which was the broader peak (Shrinivas et al., 2009). It is clear to see the significant temperature hysteresis of agar, with melting occurring around 80 ˚C, while gelation occurs closer to around 40 ˚C. These were similar to the typical melting and gelling temperature of agar (Baines and Seal, 2012). As anticipated, the size of the peak attributed to the agar for both heating and cooling, increased with increasing concentration of agar. With increasing concentration, there was a slight rise in the observed gelation temperature, which was also observed by Somboon et al. (2014).

The second and third heating cycles for all of these formulations of gelatin and agar were extremely similar to the curves shown, indicating that there were no major changes upon heating and cooling.

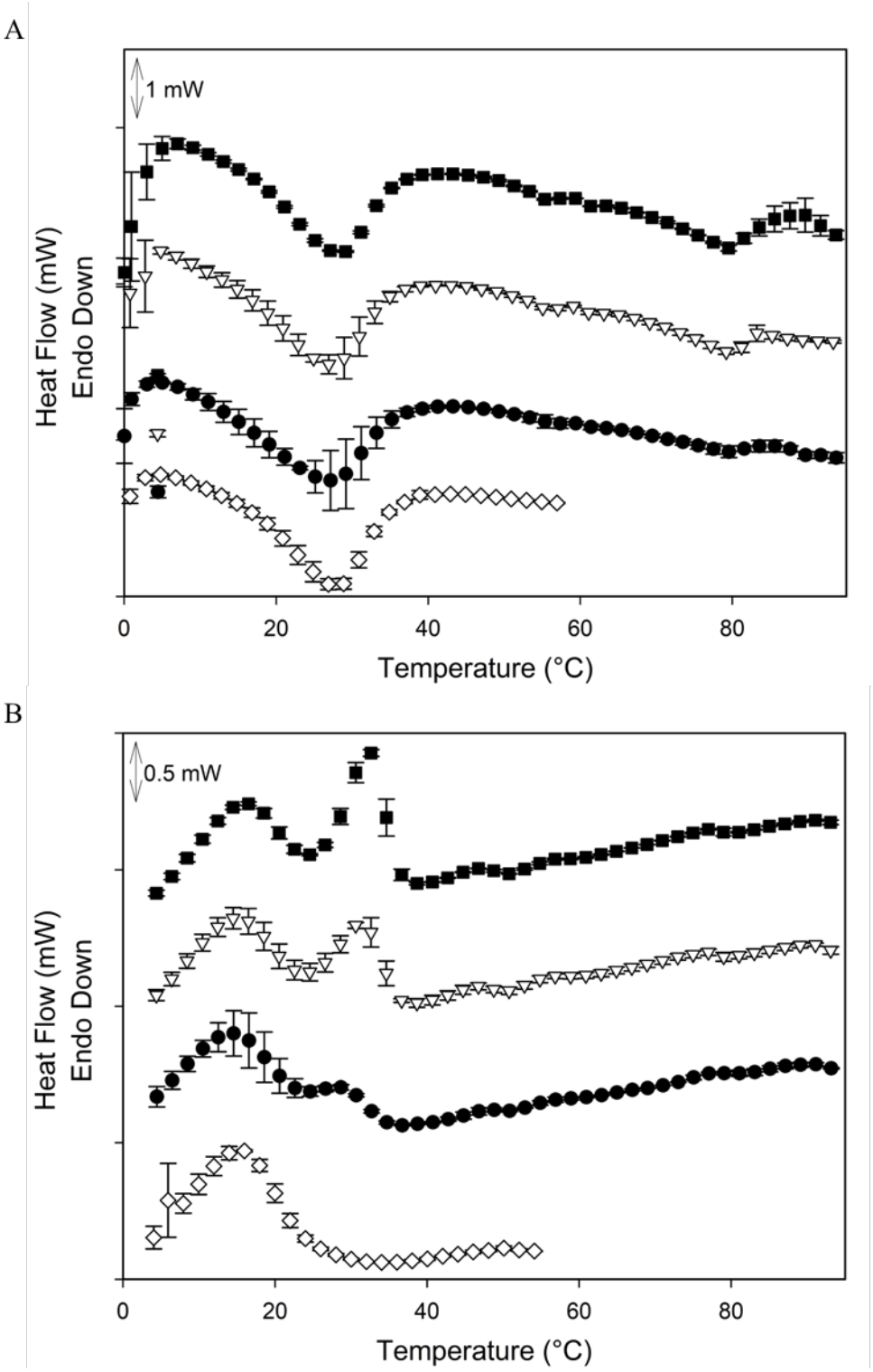

Figure 6.2. µDSC heating (A) and cooling (B) profiles of the first scan of 5 % (w/w) gelatin with 0 (◇), 1 (●), 2 (▽) and 3 % (w/w) (■) agar, over a temperature range of 0 to 60 ˚C using a cooling/heating rate of 1.2 ˚C.min^{-1}. (n=3 ± SD).

The thermal properties of these materials were further explored by performing temperature sweeps using a rotational rheometer, in accordance with Wei et al. (2015). The oscillation tests were conducted from a temperature of 60 to 20 ˚C, and the evolution of G' and G" for the formulation with gelatin and gellan is illustrated in Figure 6.3, whilst Figure 6.4 depicts the results for the formulations of gelatin and agar.

From Figure 6.3, it can be seen that the throughout the range of temperatures tested for all of the formulations with gellan, G' is always larger than G", indicating that the gellan is altering the gelling process of the gelatin. This suggested the intermolecular complex formation between the gelatin and gellan forms a physical cross-linked network which was distinct from the network of gelatin alone (Zheng et al., 2018). This indicated that across the whole range of temperatures tested, the formulations with gelatin and gellan were elastically dominated. It was observed within these systems that there was no cross-over point of the two moduli; Nakamura et al. (1993) observed a similar trend when investigating the effect of the concentration of gellan on its viscoelastic properties and therefore used the inflection point of the G' as the gelling temperature. There was a clear inflection point for the formulation of 5 % (w/w) gelatin with 1 % (w/w) gellan at a temperature of approximately 38 ˚C. The other two formulations have slightly less pronounced inflections at temperatures of approximately 41 and 42 ˚C for the formulations of 5 % (w/w) gelatin with 2 and 3 % (w/w) gellan respectively. These smaller inflections may be due to the high concentration of polymer within the system, meaning the system is permanently acting like a visco-elastic solid at all tested temperatures, resulting in only a small increase in G' at the gelling temperature.

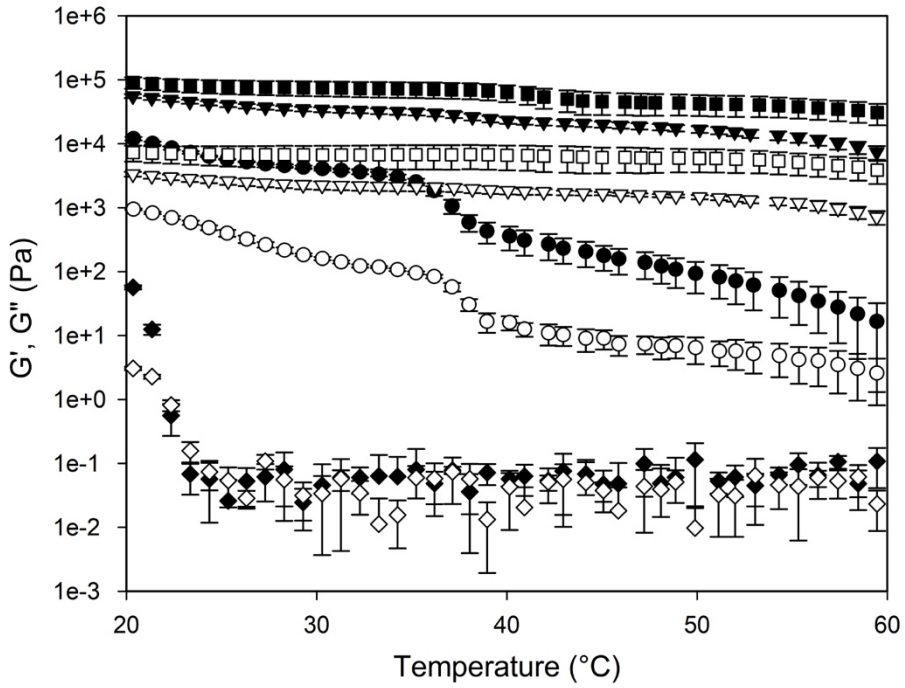

Figure 6.3. Single frequency of 5 % (w/w) gelatin with 0 (◆), 1 (●), 2 (▼) and 3 % (■) (w/w) gellan, closed symbols are G', open symbols are G". The frequency was maintained at 1 Hz and a strain of 1 %. (n=3 ± SD).

A similar phenomenon was observed with the formulations of gelatin and agar in that G' was greater than G" at all of the temperatures tested as shown in Figure 6.4 indicating that the material was behaving as a viscoelastic solid over all of the temperatures tested. As the temperature was reduced, the magnitude of G' continuously gradually increased. At a temperature of approximately 36 ˚C, there was a change in the rate of increasing G', which began to increase at a faster rate than previously. This inflection point was similar to the gelation temperature determined from the μDSC. This increase in G' was also observed by Somboon et al. (2014) who investigated the sol-gel transition of fish gelatin and agar using a rheometer.

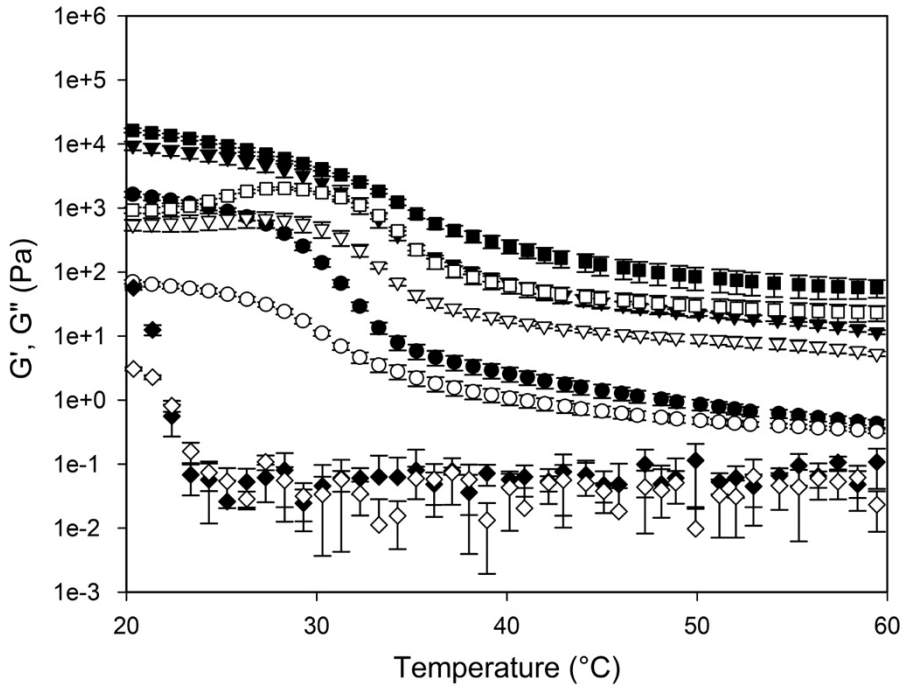

Figure 6.4. Single frequency of 5 % (w/w) gelatin with 0 (◆), 1 (●), 2 (▼) and 3 % (w/w) (■) agar, closed symbols are G', open symbols are G". The frequency was maintained at 1 Hz and a strain of 1 %. (n=3 ± SD).

As there was no cross-over temperature from the temperature sweep and the inflection point was not always clear, the gelling temperatures were determined as the onset of the curve from the μDSC, and the results can be seen in Table 6.1.

Table 6.1. Gelling temperatures of the formulations of gelatin with gellan and agar using the μDSC. (n=3 ± SD).

	Gelling temperature from onset of exotherm (˚C)	
Concentration of secondary biopolymer (% (w/w))	**Gellan**	**Agar**
1	39 ± 0.005	36 ± 0.005
2	40 ± 0.01	37 ± 0.02
3	42 ± 0.01	38 ± 0.01

For ease of comparison, the same data from Table 6.1, plus for the formulations of gelatin and kappa-carrageenan has been plotted in Figure 6.5.

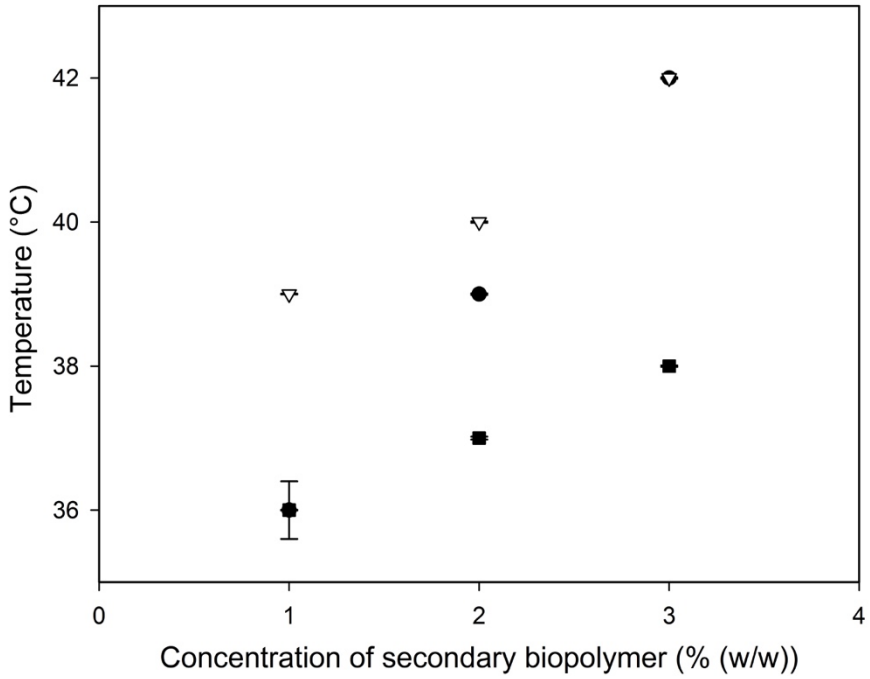

Figure 6.5. Gelling temperatures for the formulations of 5 % (w/w) gelatin with kappa-carrageenan (●), gellan (▽) and agar (■) from the μDSC. (n=3 ± SD).

The design rules established for the mixtures of gelatin and kappa-carrageenan determined that there was a minimum and maximum printing temperature of the mixture in order for the material to be printable. Below the minimum printing temperature, the mixture would gel within the nozzle, resulting in distinctive, non-cohesive layers, while above the maximum printing temperature, the mixture would flow uncontrollably out of the nozzle due to gravity. Considering that the gelling temperatures of the formulations with gellan and agar were within a similar range to the formulation with kappa-carrageenan, the printing temperatures established to print the new formulations were maintained to the range of temperatures used when printing the formulations of gelatin and kappa-carrageenan. Therefore, printing

temperatures of 45, 50, 55 and 60 ˚C were used in order to determine the range of printing temperatures for the formulations of gelatin with gellan and agar.

6.2.2 Rheological characterisation of the formulations of gelatin with gellan and agar

Initially, in order to investigate the interactions between the different formulations (Franck, 2017), amplitude sweeps were conducted in order to determine the LVR of each of the different formulations (data shown in the appendix). It was determined that all of the formulations were within their LVR at a strain of 1 % and therefore this value was used when undertaking the frequency sweep.

Frequency sweeps were conducted on all of the formulations of gelatin with gellan and agar, at a temperature of 20 ˚C (data not shown). At this temperature, both of the moduli for all of the formulations were frequency independent, indicating that the materials were in a visco-elastic solid-like state (Derkach et al., 2015). It could also be seen from the frequency sweeps that as the concentration of the secondary polymer increased, the magnitude of G' increased, due to the higher concentration of the secondary polymer providing more network bonds, resulting in stronger mixtures. This trend of increasing moduli with increasing biopolymer concentration was in agreement with reported literature for mixtures of gelatin with gellan (Fonkwe et al., 2003) and agar (Clark et al., 1983) as its secondary biopolymer.

In order to compare all of the different formulations (gelatin with kappa-carrageenan, gellan and agar), a representative value of G' was taken at 1 Hz for each of the formulations and has been plotted as a function of the secondary biopolymer concentration, shown in Figure 6.6. The determined frequency dependence of G", exhibited similar values to that of G', however, the values of G" were approximately one order of magnitude lower than that of G'.

At each of the concentrations of the secondary biopolymer, the magnitude of G' was largest for the formulations with gellan followed by kappa-carrageenan and then agar. For each of the different formulations a positive trend was observed, with increasing secondary biopolymer resulting in an increase in the magnitude of G'. It was important for the materials to possess a sufficiently high G' in order to maintain fidelity in the printed shape (Compton and Lewis, 2014). The design rules established in Chapter 4 for the formulations of gelatin and kappa-carrageenan stated that the minimum value of G' at the temperature the material was being printed into (room temperature, approximately 20 ˚C) needed to be 23 kPa. When the magnitude was below this value, the material did not maintain its intended shape when printed. The required critical values for the formulations with gellan and agar will be established once these formulations have been printed.

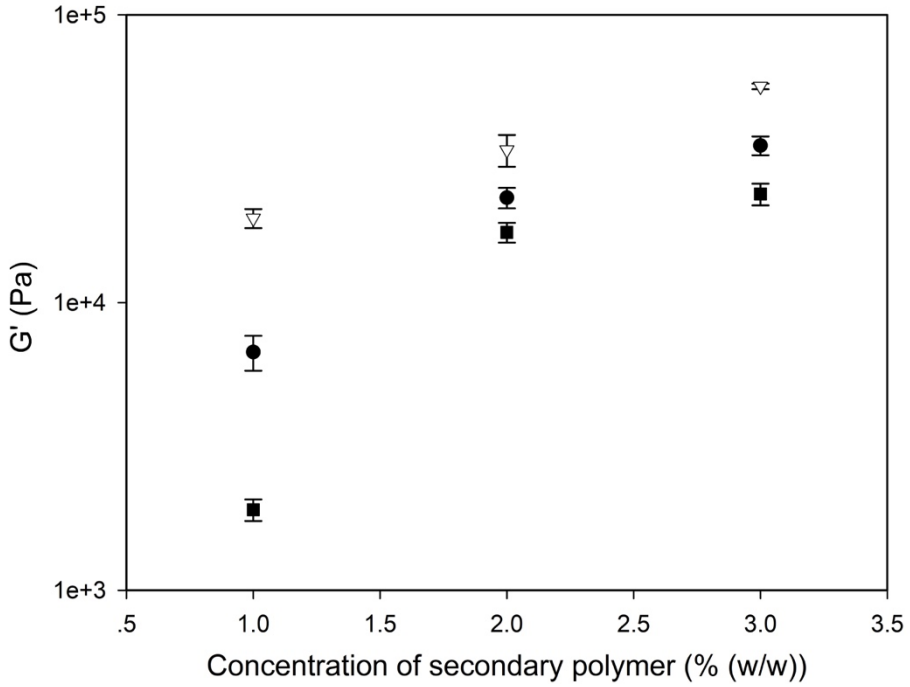

Figure 6.6. Frequency at 1Hz and 20 ˚C of 5 % (w/w) gelatin with various amounts of kappa-carrageenan (●), gellan (▽) and agar (■). (n=3 ± SD).

The flow properties of all of the materials were probed in order to determine how they would behave during the extrusion process. It was critically important that the materials had a viscosity which enabled extrusion of the material, but stopped the material from extruding from the nozzle under gravity (Godoi et al., 2016). The viscosities of each of the formulations of gelatin with gellan and agar were measured over a shear rate range of 1 - 1000 s^{-1} at each of the different printing temperatures (45, 50, 55 and 60 ˚C). All of the different formulations exhibited shear thinning behaviour across the range of shear rates tested and they also displayed an increase in viscosity as the testing temperature was decreased. This shear thinning behaviour was observed by Lee et al. (2003) for formulations of gelatin and gellan, while Singh et al. (2009) observed this behaviour for formulations of gelatin and agar. It was also possible to see that as the concentration of the secondary biopolymer was increased, the viscosity increased, indicating that the materials were flowing less because the network of polymers within the gel were stronger.

The viscosity curves of all of the formulations with both gellan and agar, were fit to the Cross model (shown in Equation 5.6), in order to interpolate the viscosity values at a shear rate of 113, 293 and 512 s^{-1}, relating to printing speeds of 10, 25 and 50 $mm.s^{-1}$ respectively. The results of the viscosity for the formulations of 5 % (w/w) gelatin with 1, 2 and 3 % (w/w) gellan have been presented in Figure 6.7 A, B and C respectively, while the results of the viscosity for the formulations of 5 % (w/w) gelatin with 1, 2 and 3 % (w/w) agar have been presented in Figure 6.8 A, B and C. The formulation of 5 % (w/w) gelatin with 3 % (w/w) gellan have not been reported at a temperature of 45 ˚C as such a high viscosity was outside of the limit of the rheometer.

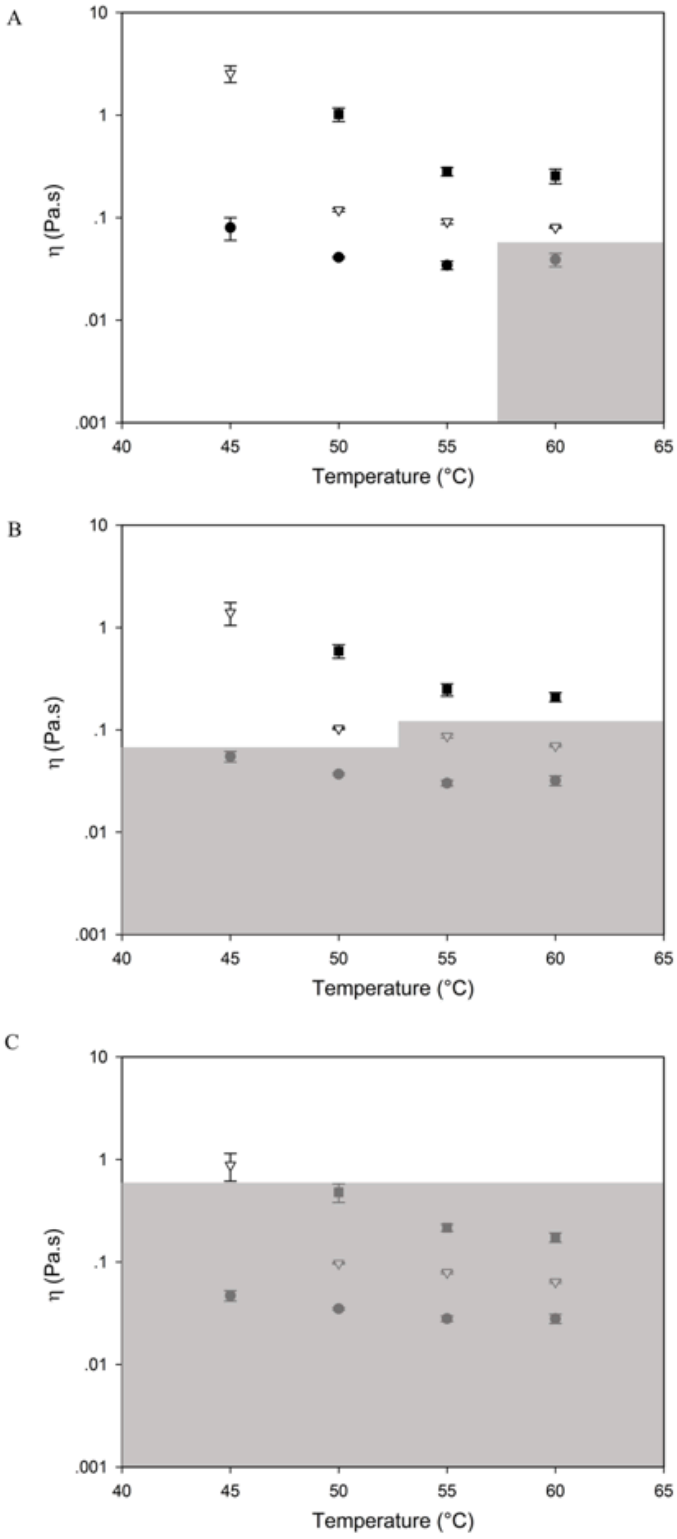

Figure 6.7. Viscosity of 5 % (w/w) gelatin with 1 (●), 2 (▽) and 3 % (w/w) (■) gellan at a shear rate of 113 (A), 293 (B) and 513 s^{-1} (C). The shaded area incidcates the cylinders that did not print, while the lighter area shows the cylinders that were defined as printed. (n=3 ± SD).

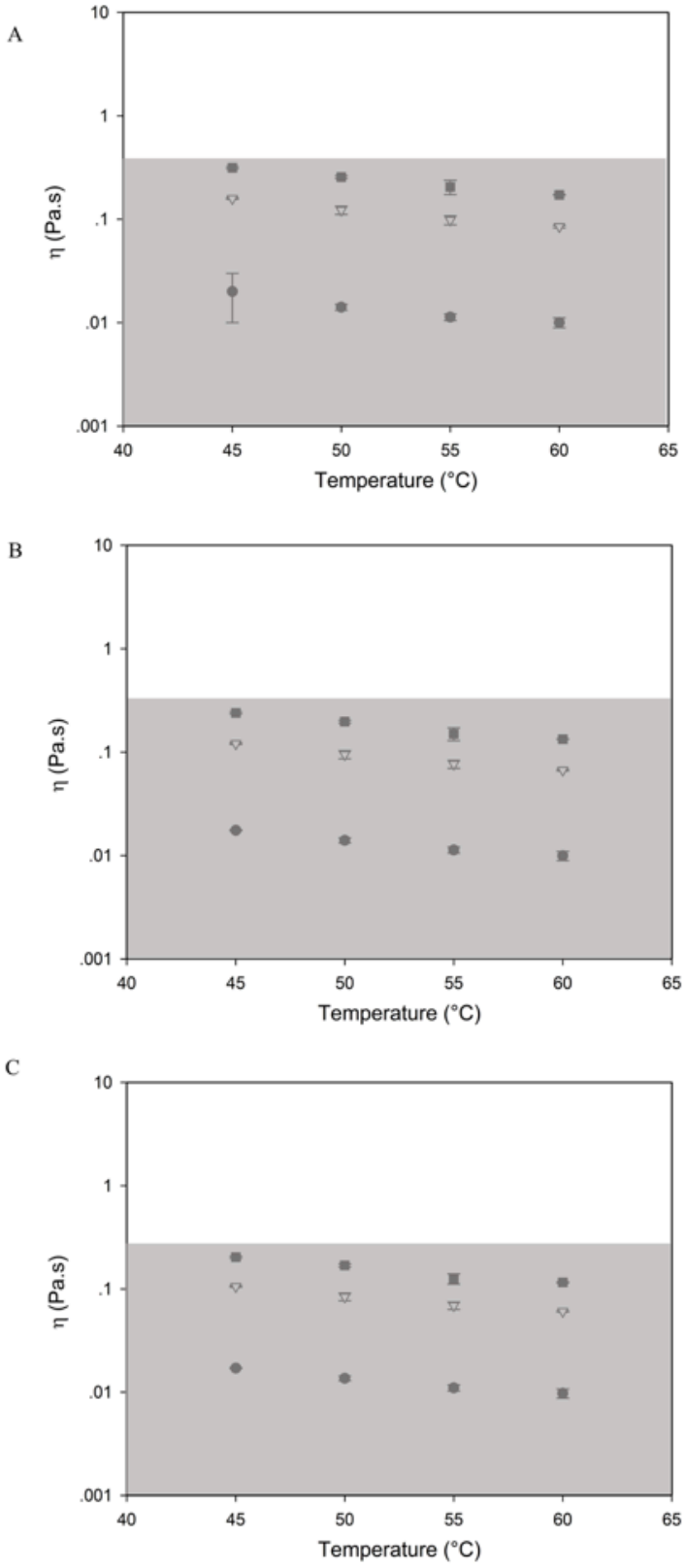

Figure 6.8. Viscosity 5 % (w/w) gelatin with 1 (●), 2 (▽) and 3 % (w/w) (■) agar at a shear rate of 113 (A), 293 (B) and 513 s^{-1} (C). The shaded area incidcates the cylinders that did not print, while the lighter area shows the cylinders that were defined as printed. (n=3 ± SD).

The shaded regions within the graph indicated the cylinders which did not meet the minimum requirement in order to produce a defined shaped when printed. These results will be discussed further in section 6.2.3.

Once the material had been extruded onto the print bed, it was important to establish how it would behave and whether the material will spread. Therefore, the evolution of G' from a high temperature to a low temperature of the formulations with gellan and agar have been investigated. As previously mentioned in section 4.2.2, due to the way this test was conducted the numerical values are for comparison purposes only, rather than absolute values. The values where the magnitude of G' began to plateau (see section 3.3.2.12), have been plotted in Figure 6.9 with the different colours indicating the secondary polymer which had been added to the formulation (kappa-carrageenan, gellan or agar) and the different symbols indicate the concentration of the secondary polymer.

The time taken for the formulations with kappa-carrageenan and gellan were very similar, with a difference of only a few seconds for each of the formulations. The formulations with agar took considerably longer to reach the plateau of G', although the plateau still occurred faster than for the formulation of just 5 % (w/w) gelatin, which took approximately 320 seconds. Similar to the formulations of kappa-carrageenan, the formulations also indicated an increasing G' with increasing concentration of secondary biopolymer.

With the knowledge of the printability of the formulations of gelatin and kappa-carrageenan and the similarities to the gelation with gelatin and agar, it can be assumed from this graph that it was likely that the formulations with gellan would be able to gel sufficiently quickly in order to retain its shape post extrusion and produce defined printed objects. However, it also indicated that it took the formulations of agar a long time to gel, suggesting the material may be prone to spreading after extrusion, which could result in the shapes not printing in a defined manner.

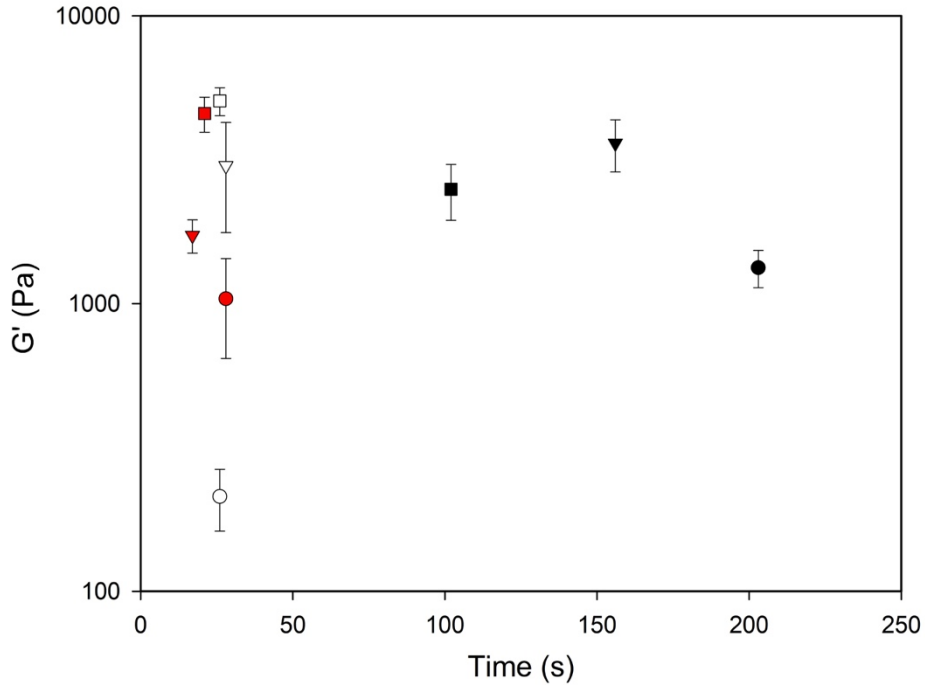

Figure 6.9. Gelling times of 5 % (w/w) gelatin with the addition of 1 (○), 2 (▽) and 3 % (w/w) (□) of kappa-carrageenan (white), gellan (red) and agar (black). (n=3 ± SD).

The characterisation of the formulations of gelatin with gellan and agar assessed above were compared to the results of the design rules created within the previous two chapters. The data thus produced indicated that it was likely that the formulations of gelatin and gellan would be able to produce well-defined shapes due to their high G' and viscosity values and rapid rate of increase of G'. In turn, the formulations with gelatin and agar would likely lead to printed shapes which were not well defined as a result of their low G', viscosity and long gelation time, which was likely to lead to in spreading of the material post extrusion.

For each of the formulations, at all of the printing speeds, the recovery percentage was calculated, by taking the value of G' at the layer time at the determined printing speed and then taking this value as a percentage of the plateau value of G'. The formulations of gelatin and kappa-carrageenan indicated similar percentage recovery at each of the printing speeds, with the percentage recovery almost 100 % when printing at the slowest printing speed (10 $mm.s^{-1}$,

with a layer time of 27 seconds) and a very low recovery of approximately 5 % at the highest printing speed (50 $mm.s^{-1}$, with a layer time of 6 seconds). The formulations of gelatin and agar indicated low percentage recoveries of around 3 % at all of the printing speeds.

6.2.3 Printability of gellan and agar

In order to determine the printability of 5 % (w/w) gelatin with various concentrations of gellan or agar, cylinders were printed at different printing temperatures (45, 50, 55 and 60 ˚C) and speeds (10, 25 and 50 $mm.s^{-1}$). The formulations with agar were printed at a maximum temperature of 55 ˚C as the cylinders displayed a large amount of spreading at this temperature, so were not be printed at higher temperatures.

Images of the printed cylinders, printed from the formulation of 5 % (w/w) gelatin with 1 (column 1), 2 (column 2) and 3 % (w/w) gellan (column 3) at the two extreme printing parameters 45 ˚C and 10 $mm.s^{-1}$ (top row) and 60 ˚C and 50 $mm.s^{-1}$ (bottom row) have been displayed in Figure 6.10. Images of the printed cylinders with all of the formulations of gelatin and gellan at all of the printing temperatures and speeds can been seen in the appendix.

Partial solidification of all of these formulations occurred when the cylinders were printed at the lowest printing temperature and speed. This was an indication that the formulations were gelling within the nozzle and therefore extruding in a semi-solid state, giving the rough looking, delaminated layers. Landers et al. (2002) also noted this problem, and determined that early gelation during extrusion prior to contact with the subsequent layer must be prevented in order to produce a well-defined shape. This phenomenon of delamination also occurred when printing in plastic the printing temperature was too low, the layers would not bond together, resulting in a weak shape (Simplify3D, 2019). Therefore, this indicated that this temperature was too low to be able to print cohesive shapes with these formulations.

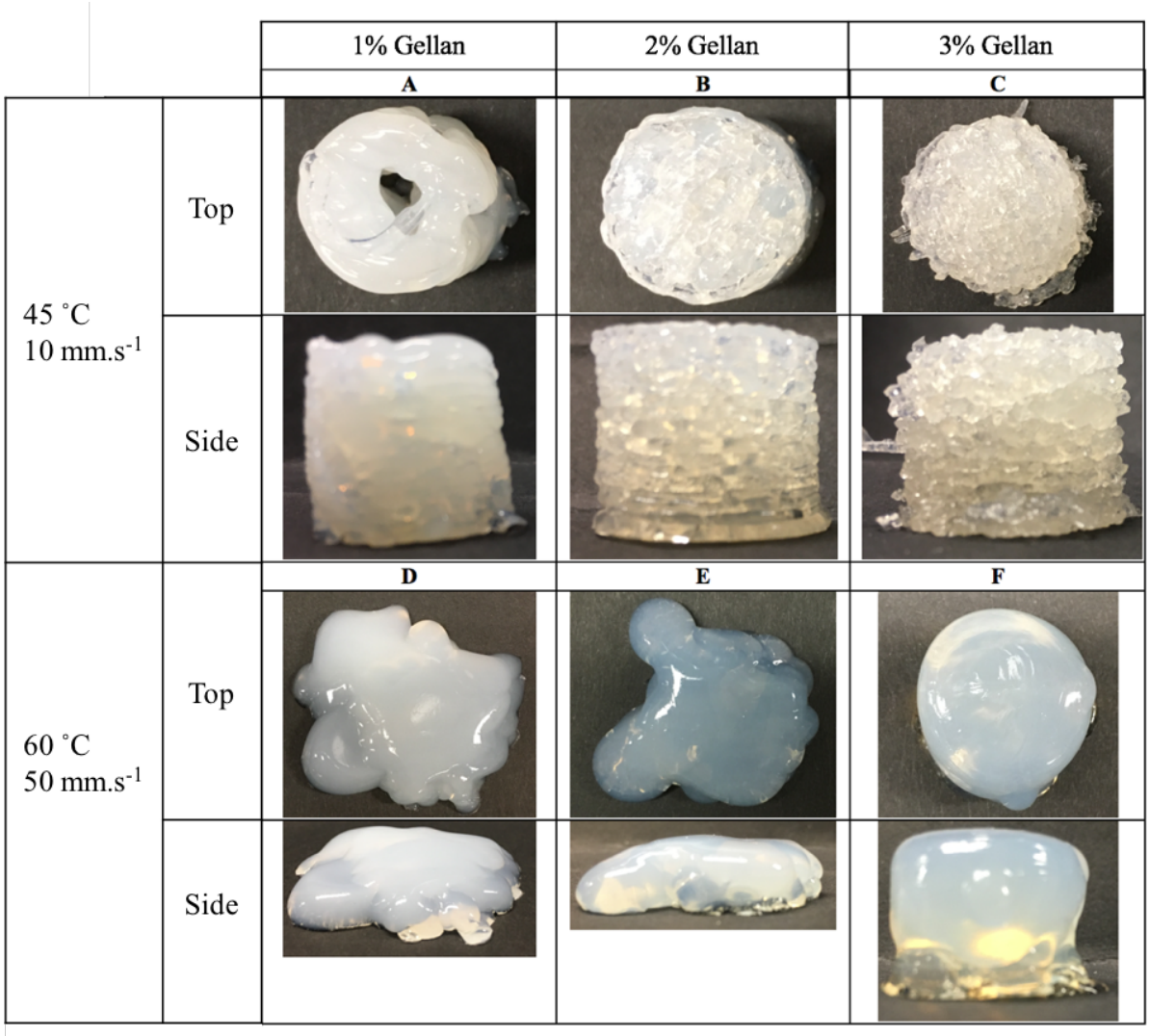

Figure 6.10. Top and side view images of printed cylinders of 5 % (w/w) gelatin and 1 (A, D), 2 (B, E) and 3 % (w/w) (C, F) gellan. Printed at 45 ˚C and 10 mm.s^{-1} (top row) and at 60 ˚C and 50 mm.s^{-1} (bottom row).

At the very highest printing temperature and speed, it was seen that the formulations of 5 % (w/w) gelatin with 1 and 2 % (w/w) gellan resulted in complete collapse, due to their low magnitudes G'. The formulation of 5 % (w/w) gelatin with 3 % (w/w) gellan managed to maintain a cylindrical shape due to its stronger rheological properties. As mentioned in section 5.2.1.3 the microstructure of the gel will be altered by the shear rate applied during gelation, which will affect the properties of the gel. In future, it would be interesting to investigate the morphology of the microstructure and tailor this to create defined properties.

The cylinders printed with the formulations of gelatin and gellan at the range of other printing temperatures and speeds displayed a similar trend to the formulations of gelatin and kappa-carrageenan, with the cylinders printed at the lower temperatures and speeds producing a well printed cylinder, while increasing the printing temperature and speed led to prints that resulted in spreading of the material. The results will be discussed in greater detail further within the next few paragraphs.

Figure 6.11 displays the cylinders printed with 5 % (w/w) gelatin and various concentrations of agar (1 (w/w)- column one, 2 (w/w)- column two and 3 % (w/w)- column 3), at the two extreme printing parameters: 45 ˚C and 10 $mm.s^{-1}$ (top row) and 55 ˚C and 50 $mm.s^{-1}$ (bottom row). Images of the printed cylinders with all of the formulations of gelatin and agar at all of the printing temperatures and speeds can been seen in the appendix.

It was observed that none of the formulations of gelatin and agar printed at the higher printing temperature and speed displayed signs of being able to retain the printed shape, rather, once the material was extruded from the nozzle, it created pools rather than a cohesive shape. This lack of ability to retain its shape was likely due to the low G' and long gelling time of these formulations at this temperature.

At the lowest printing temperature and speed, the formulation of 5 % (w/w) gelatin with 1 % (w/w) agar displayed poorly printed cylinders, which had pooled a large amount, rather than creating a cohesive shape. The formulation of 5 % (w/w) gelatin with 2 % (w/w) agar displayed more cylinder-like printed shapes as the printing speed and temperature were reduced. However, with relatively low values of G', the material still spread significantly and the heights of the cylinders did not reach the minimum requirement in order to be classed as printable. A greater height was achieved from the formulation of 5 % (w/w) gelatin with 3 % (w/w) agar at these printing parameters. The cylinders printed with this formulation had an improved

aesthetic appearance as the printing temperature and speed was reduced. Even though the magnitude of G' was relatively large for this formulation ensuring that the shape was retained when printing, the long gelation time resulted in the cylinders failing to achieve the desired height as the material spread to a larger diameter than was intended.

The results for the printed cylinders printed at the other printing temperatures and speeds will be discussed in the subsequent paragraphs.

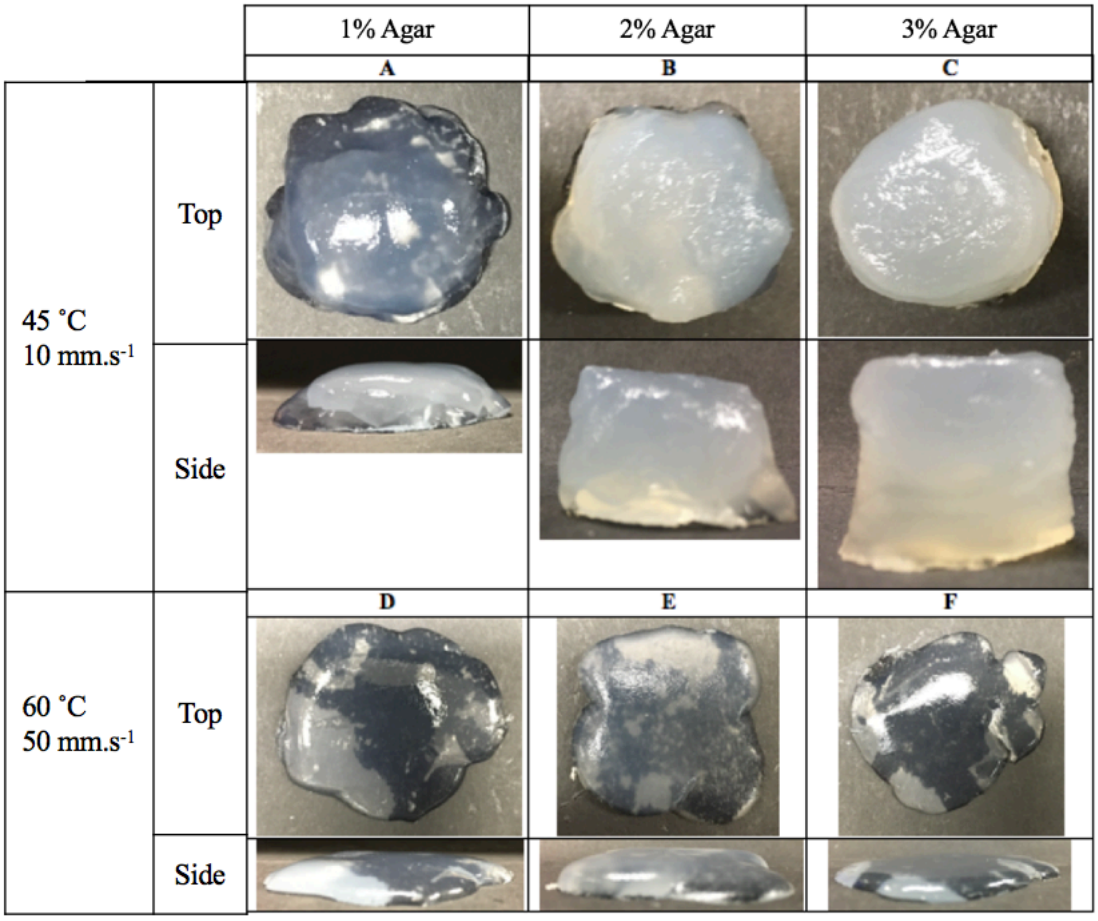

Figure 6.11. Top and side views of printed cylinders of 5 % (w/w) gelatin and 1 (A, D), 2 (B, E) and 3 % (w/w) (C, F) agar. Printed at 45 °C and 10 mm.s^{-1} (top row) and at 55 °C and 50 mm.s^{-1} (bottom row).

The traffic-light graph of printability for all of the cylinders printed at each of the different printing temperatures and speeds, using all of the different formulations of gelatin and gellan,

and gelatin and agar can be seen in Figure 6.12 and Figure 6.13 respectively. When examining the visual definition of the formulations with gelatin and gellan and gelatin and agar, the same criteria was determined for the tolerances of geometrical accuracy, as determined in section 5.2.1.4. Printed cylinders with a height over 98 % of the intended value were defined as well printed (highlighted in green). The cylinders which had printed with a height between 98 – 95 % of the intended height were classified as almost printed (highlighted in orange) and the printed cylinders whose heights were below 95 % of the intended value, were considered as not meeting the printing requirement (highlighted in red).

The formulations with gelatin and gellan displayed similar printability trends as the formulations of gelatin and kappa-carrageenan, with the cylinders printed at the highest temperatures and speeds resulting in cylinders which did not meet the required minimum height. This was due to the low viscosity of the materials resulting in the material which was flowing too quickly out of the nozzle, as well as the low G' magnitudes, meaning that the material did not retain its shape once it had been extruded. When the printing temperature and speed were reduced, the cylinders produced indicated printed cylinders which did meet the requirement and were considered printable, indicating that the magnitudes of G' and viscosity had reached a threshold value to allow defined printed objects to be created.

It was determined that the minimum viscosity necessary for the formulations of gelatin and gellan, in order to achieve a defined printed shape, was 0.88 Pa.s (this was the viscosity which allowed the formulations to print at all of the printing speeds tested). Due to the high magnitude of G', the formulation of 5 % (w/w) gelatin with 3 % (w/w) gellan was able to maintain its shape at the two slower printing speeds even though the magnitude of viscosity was below this value. At the slowest printing speed, the formulations of 5 % gelatin with 1 and 2 % (w/w)

gellan were also able to maintain defined printed shapes, due to their respective high G' values and the printing speed being slow enough to allow the extruded material time to gel together.

As previously mentioned, it was shown that none of the formulations of gelatin and agar managed to print a defined cylinder. When extruding with the formulation of 5 % (w/w) gelatin with 1 % (w/w) agar, all of the printed shapes exhibited large amounts of pooling of the material, indicating that the material was not strong enough to retain its shape after printing. With the low magnitudes of viscosity and G' for this formulation at all of the printing temperatures, it was little surprise that this formulation did not successfully print.

The outline of cylindrical shapes could be determined when printing at the lowest temperature and the two lowest speeds of the formulation of 5 % (w/w) gelatin with 2 % (w/w) agar. However, with such low values of G' and viscosity, the material was not able to maintain its shape, resulting in a small amount of spreading and the material not reaching the necessary height.

A similar issue was seen with the formulation of 5 % (w/w) gelatin with 3 % (w/w) agar which, although had larger magnitudes of G' and viscosity, were still not large enough to maintain the printed shape. As well as this, the long gelation time of this material would also have resulted in spreading, meaning that the material could not reach the intended height.

A

Speed (mm/s)	Temperature (˚C) 45	50	55	60
10	III			II
25	II	II	I	I
50	I	I	I	I

B

Speed (mm/s)	Temperature (˚C) 45	50	55	60
10	III			II
25	III		II	II
50	III	II	II	I

C

Speed (mm/s)	Temperature (˚C) 45	50	55	60
10	III	III		
25	III			II
50	III	II	II	II

Figure 6.12. Traffic-light graph of printability at different temperatures and speeds of 5 % (w/w) gelatin and 1(A), 2 (B) and 3 % (w/w) (C) gellan. Green indicating that it had printed well, orange indicating that it had printed ok and red indicating that it had not printed well. The roman numerals signify the print quality: complete collapse (I), partial collapse (II) and partial solidification (III).

A

Speed (mm/s)	Temperature (˚C) 45	50	55	60
10	I	I	I	
25	I	I	I	
50	I	I	I	

B

Speed (mm/s)	Temperature (˚C) 45	50	55	60
10	II	I	I	
25	II	I	I	
50	I	I	I	

C

Speed (mm/s)	Temperature (˚C) 45	50	55	60
10	II	I	I	
25	II	I	I	
50	I	I	I	

Figure 6.13. Traffic-light graph of printability at different temperatures and speeds of 5 % (w/w) gelatin and 1(A), 2 (B) and 3 % (w/w) (C) agar. Green indicating that it had printed well, orange indicating that it had printed ok and red indicating that it had not printed well. The roman numerals signify the print quality: complete collapse (I), partial collapse (II) and partial solidification (III).

In order to generalise the conditions necessary for these hydrocolloid materials to be printable, a generic printability diagram has been proposed, in Figure 6.14. This indicated how the optimal printing conditions for any formulation were within a certain printing temperature and speed range. This diagram was formulation specific, with the exact range of printing temperature and speeds necessary to form well defined printed shapes dependent on the materials used. This diagram gives an indication of the issues which occurred when printing and in future can be used as a guide by other researchers in order for them to determine optimum printing properties with various formulations.

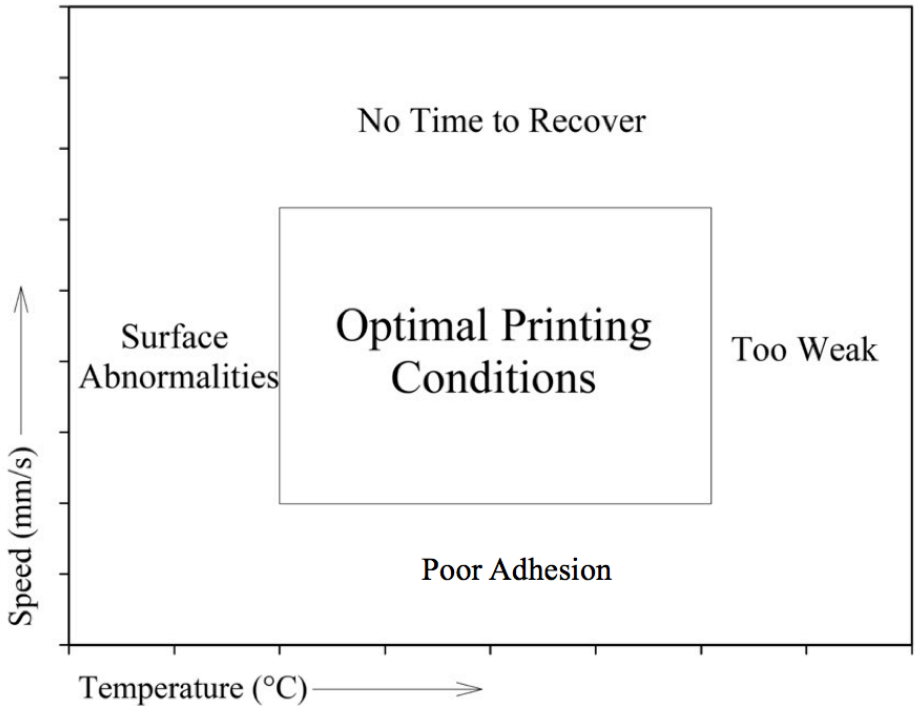

Figure 6.14. Generic printability diagram.

6.2.4 Mechanical properties of the printed cylinders

In order to determine how well the printed cylinders gelled together, their mechanical properties were investigated using a compression test via a texture analyser. Initially the mechanical properties of cast cylindrical samples of all of the formulations were investigated in order to

evaluate how strong the formulations were when created via casting through pouring into a mould, resulting in no defined layers. Figure 6.15 shows the peak force of the cast cylinders of gelatin with various concentrations of secondary biopolymer, gellan and agar; the results for the peak force of gelatin and kappa-carrageenan have also been included. As the concentration of the secondary biopolymer increased for all of the formulations, the peak force increased. This phenomena was also observed by Lau et al. (2000) who investigated mixtures of gelatin and gellan and Banerjee and Bhattacharya (2011) who investigated blends of gelatin and agar. The peak force of the formulations with gelatin and agar were considerably lower than those with gellan and kappa-carrageenan, likely due to a mixed system not forming a combined network structure (Moritaka et al., 1980).

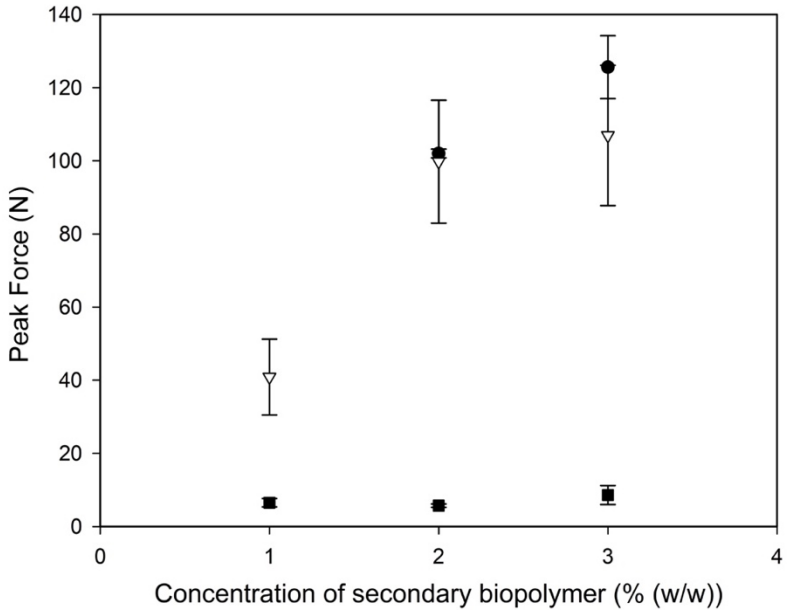

Figure 6.15. Peak force of cast cylinders of 5 % (w/w) gelatin with various concentration of kappa-carrageenan (●), gellan (▽) and agar (■). (n=5 ± SD).

The mechanical properties of the printed cylinders which were deemed as printable have also been investigated via textural analysis. The difference between the cast samples and the printed samples were the way in which the cylinders were created. Therefore, when comparing the cast to the printed samples the main point of investigation was determining how well the layers

adhered together, with stronger samples indicating that the layers had held together, while weaker samples indicating that the layers had not adhered well with each other.

As none of the formulations with agar were regarded as printable, none of their results have been presented. The results of the peak force at different printing speeds for the formulations of 5 % (w/w) gelatin with 1, 2 and 3 % (w/w) gellan are shown in Figure 6.17 A, B and C respectively.

For the formulation of 5 % (w/w) gelatin with 1 % (w/w) gellan, as the printing temperature was increased, the peak force also increased. As mentioned in section 5.2.3, the higher melt temperature led to better adhesion between the successive layers, resulting in stronger parts (Turner et al., 2014). Similar to the results for the kappa-carrageenan, this indicated that the greater printing temperature enabled better adhesion between the layers.

When printing at the lowest temperature (45 ˚C) the formulations of 5 % (w/w) gelatin with 2 and 3 % (w/w) gellan successfully printed at all three printing speeds tested, with the strongest cylinder printed at the fastest speed (50 $mm.s^{-1}$) and weakest cylinder printed at the slowest speed (10 $mm.s^{-1}$). This trend was also observed with the formulations of gelatin and kappa-carrageenan and was due to the formulations having less time to gel when the material was added faster, meaning the material gelled with the next layer making the printed shape stronger (Le Tohic et al., 2018). As the material was strong enough to maintain its shape and not spread, the faster the material was added on top, which resulted in greater bonding between the layers as they were extruded. As mentioned in section 5.2.1.3, the time between the joining of two consecutive layers had a big influence on the printed object (Faes et al., 2015).

Similar trends could be seen with these formulations of gelatin and gellan as was seen with the formulations of gelatin and kappa-carrageenan, which demonstrates that an increase in printing

temperature resulted in an increase in the interlayer adhesion, leading to increased strength of the printed object. This increased interlayer adhesion was due to the high temperature gradient produced from printing at the high printing temperatures, as also observed by Sood et al. (2010).

When printing, the formation of bonds with FDM parts is driven by the thermal energy of the extruded material (Sun et al., 2008). The quality of bonding depends on the growth of the neck which is formed between two adjacent printed lines, shown in Figure 6.16 (Sun et al., 2003). A large temperature gradient from the printing temperature to the gelling temperature allowed more time for the materials to interact with the surrounding material, resulting in the material forming greater contact with the adjacent material, which in turn led to a stronger object.

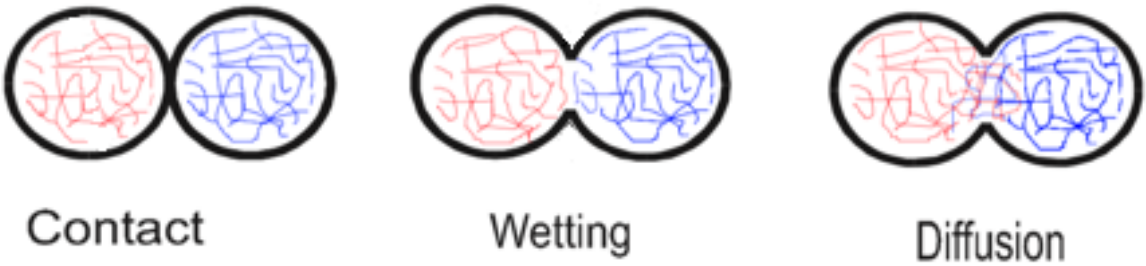

Figure 6.16. The bond formation process between two adjacent filaments (Sun et al., 2003).

The peak force values for the printed cylinders were considerably lower than the peak force of the cast cylinders of the same formulation. Due to the nature of layer by layer manufacturing, the printed shape will intrinsically have weaker points at each of the layers, which did not occur in the cast samples. A single layer, as was for the cast sample, would result in an increased peak force, however, with many layers used for AM, resulted in a weaker shape. When printing with ABS, Kim et al. (2016) determined that the strength of the printed object was approximately 26 % of the strength of the injection molded part, indicating how much the layers affected the strength of printed objects. The results for the printed formulations of gelatin and secondary biopolymer are between 13 – 23 % of the strength of the cast samples.

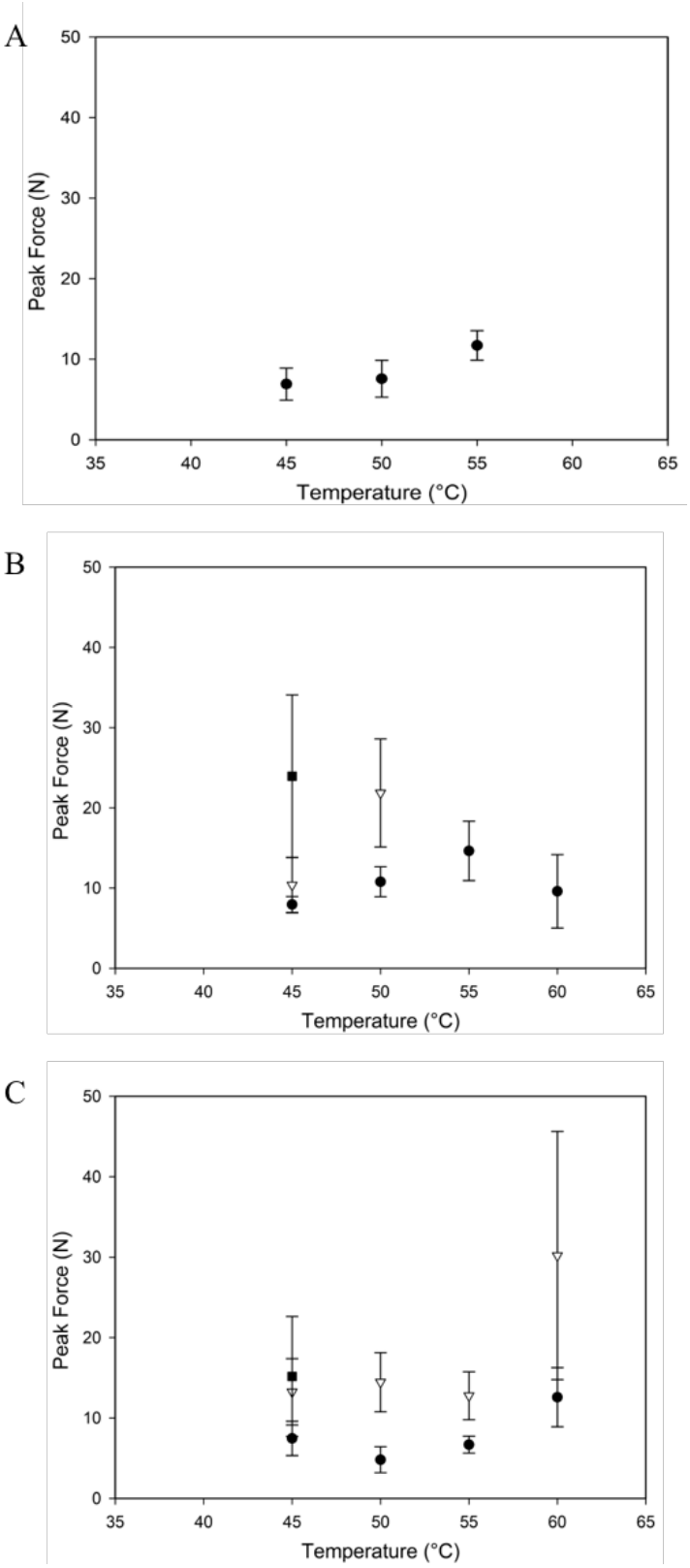

Figure 6.17. Peak force of the formulations of 5 % (w/w) gelatin with 1 (A), 2 (B) and 3 % (w/w) (C) gellan at different printing speeds of 10 (●), 25 (▽) and 50 mm.s^{-1} (■). The results for the cast values were 41, 100 and 106 N for the formulations of 5 % (w/w) gelatin and 1, 2 and 3 % (w/w) gellan respectively. (n=5 ± SD).

6.2.5 Printing intricate shapes

In order to further assess the printability of the various formulations, complex shapes were printed, including a ring, star, pyramid and a cuboid with square cavities, shown in Figure 6.18 A, B, C and D respectively. The dimensions of each of the shapes have been included in the images. Not only did the printing of these intricate shapes test the formulations being printed, to establish whether they spread and that they extruded in the right place, but the shapes also tested the custom syringe plated FDM machine. Previously the shapes printed were either simple lines or cylinders where the platform and nozzle only had a little distance to move. With these new shapes, cavities, sharp corners and pointed layers were introduced which tested the machine's ability to move in such a way in order to achieve these angles.

Three different formulations, one of each of the tested secondary biopolymers, were investigated in order ascertain whether the intricate shapes could be produced; these were 5 % (w/w) gelatin with 3 % (w/w) kappa-carrageenan, 2 % (w/w) gellan, and 3 % (w/w) agar. Although previous work demonstrated that it was likely that the formulation of 5 % (w/w) gelatin and 3 % (w/w) agar would fail to produce well defined shapes, it was interesting to print this formulation in order to see how the shapes turned out. Due to their high G' values and sufficiently high viscosity, it was considered likely that the formulations of 5 % (w/w) gelatin with 3 % (w/w) kappa-carrageenan and 2 % (w/w) gellan would be able to produce well defined shapes. An attempt was made to print using the formulation of 5 % (w/w) gelatin with 3 % (w/w) gellan. However, the force necessary to print was too great, resulting in bending of the back-plate of the machine and therefore, those tests were not completed. This outcome was likely due to the high magnitude of the G' for this formulation, meaning that it was too strong.

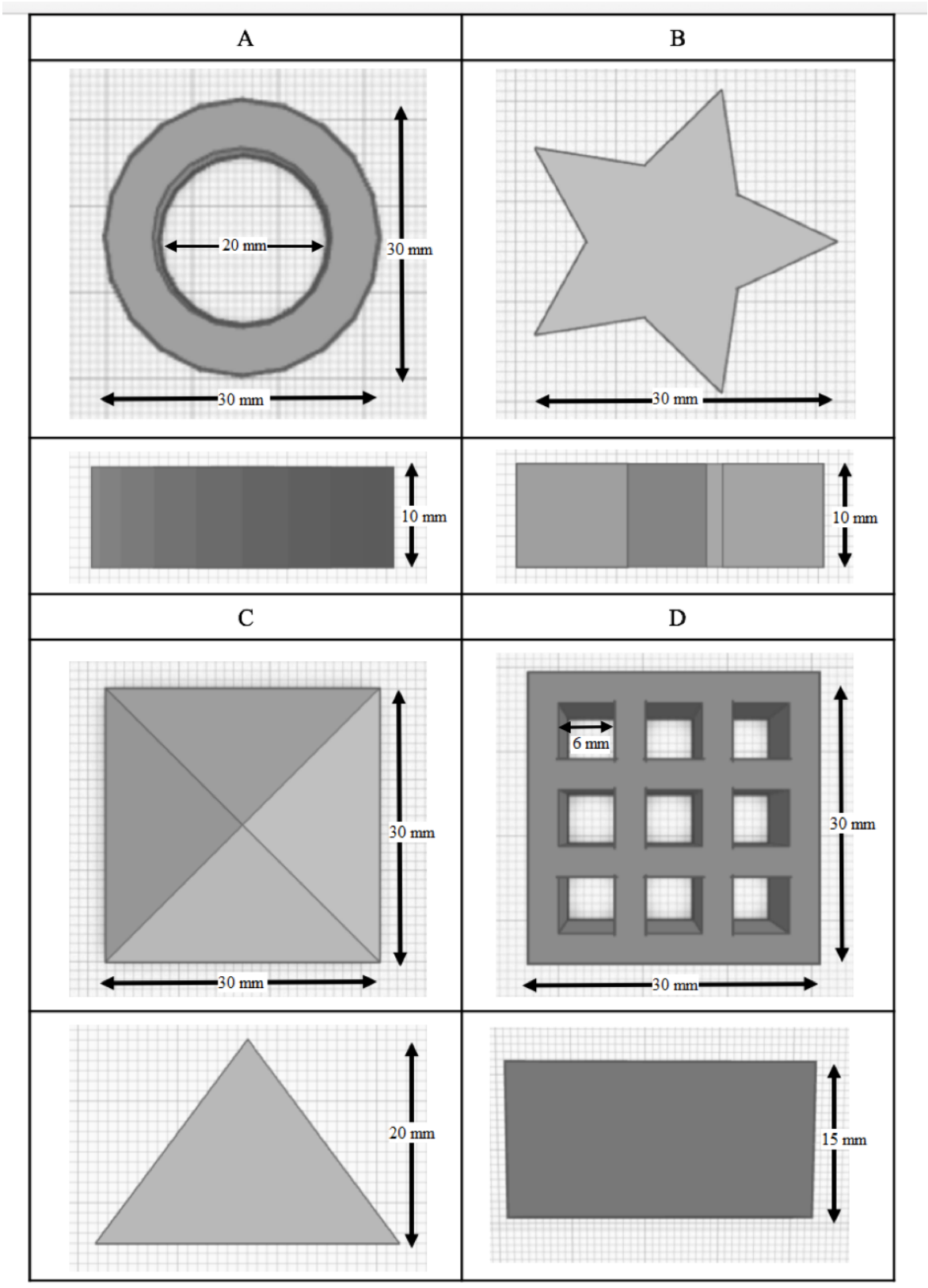

Figure 6.18. Top and side views of AutoCAD drawings of the complex shapes and their dimensions printed out using various formulations: Ring (A), Star (B), Pyramid (C), and Cuboid with cavities (D).

The printing temperature for all of the formulations was maintained at 50 ˚C, as this was close to the optimal printing temperature of all of the formulations. As the aim of this printing was to achieve highly aesthetic looking pieces, rather than stronger pieces, the slowest printing speed of 10 $mm.s^{-1}$ was used. The nozzle diameter utilised was 1.1 mm and the layer height was maintained at the same magnitude. Figure 6.19 shows the images of the printed intricate shapes for each of the different formulations.

The shapes printed using the formulation of 5 % (w/w) gelatin with 3 % (w/w) kappa-carrageenan and 2 % (w/w) gellan printed defined shapes which were all within approximately 10 % of the desired object. However, both of these formulations struggled to achieve the cavities within the cuboid shape. This may not be helped by the path created in the .STL file, which although created the shortest path in order to complete the layer, sometimes resulted in the nozzle crossing the path it had just printed, resulting in the material being dragged around. Recoding of this path may, in future, result in the ability to print a defined version of this shape, which could be achieved by creating specific software designed for food printing applications of this type.

As expected, none of the shapes printed using the formulation of 5 % (w/w) gelatin with 3 % (w/w) agar achieved a defined shape. The ring was printed in the correct shape, but the material lacked the required strength when layers were added, which led to the material spreading and resulting in an uneven ring. The printed cuboid showed good definition in the cuboid shape, but similar to the other formulations had over extruded, therefore the cavities have been filled in.

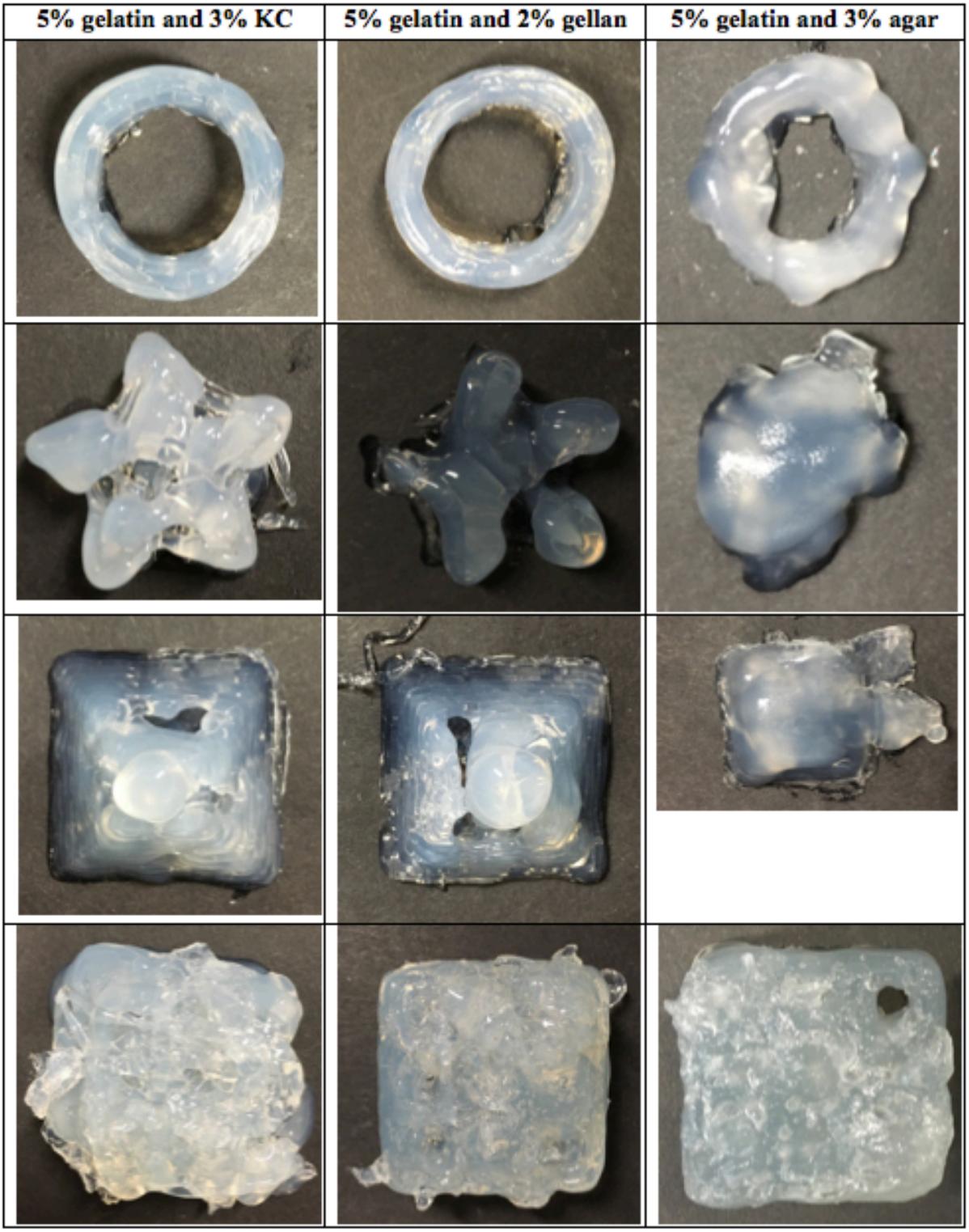

Figure 6.19. Top view images of intricate printed shapes printed from 5 % (w/w) gelatin with 3 % (w/w) kappa-carrageenan (KC), 2 % (w/w) gellan and 2 % (w/w) agar.

6.3 Conclusion

The design rules focusing on finding a critical value for G' and viscosity have been probed in order to check their validity using formulations of gelatin with other secondary biopolymers, specifically gellan and agar. It was determined that for the formulations of gelatin and gellan, the minimum magnitude for G' was 19 kPa and for viscosity was 0.88 Pa.s. Printing formulations which had values of G' and viscosity below these values resulted in poor quality prints, which did not meet the standard in order to be defined as printable. The upper limit of the magnitude of G' was determined as approximately 56 kPa as the formulation of 5 % (w/w) gelatin with 3 % (w/w) gellan exhibited a large amount of gelling within the nozzle, meaning it was difficult to extrude this material. None of the formulations of gelatin and agar were printable. Even formulations printed with the highest G' value of 24 kPa and a viscosity of 0.24 Pa.s, resulted in printed shapes below the required criteria, which was likely due to the formulations having too long a gelation time. Fast gelation was key to the printability, as the formulations of gelatin and agar, which took a long time to gel, did not manage to cohesively print any objects, as the material pools when extruded rather than retaining a shape. From the gelation curve, the maximum percentage recovery for the formulations with agar was approximately 30 %, which was not fast enough for the formulations to retain their printed shape. The formulations of gelatin and gellan, whose rate of increase of G' were similar to those of gelatin and kappa-carrageenan managed to print well defined cylinders. The recovery rates from the rate of increase of G' for the formulations which printed well-defined cylinders were greater than 80 %, indicating that the material was recovering its structure fast enough to retain its shape.

The minimum printing temperatures established for the formulations of gelatin and gellan determined that the printing temperature needed to be at least 5 ˚C above the gelling temperature

of the material, otherwise the material would gel within the nozzle, producing printed shapes with clearly defined layers which had not gelled with the previous or subsequent.

The optimal printing range in order to produce the most aesthetically pleasing printed shapes was determined to be 8 to 13˚C above the gelling temperature of the formulations.

Above the optimal printing temperature, defined cylinders were established at the slowest printing speed, when G' was large, leading to the material being able to retain its shape.

The peak force of the cylinders which printed increased with increasing printing temperature and speed. The greater printing temperature and speed resulted in the formulation having less time to gel as a filament, therefore allowing the formation of a stronger gel with the subsequent and previous layers. An exciting prospect of AM was to be able to create new textures, which has been achieved by merely altering the printing parameters. As long as the printed object was in the desired shape, this technique could open up a range of textures that would have been very hard to achieve by manufacturing in any other way.

Finally, complex shapes were printed using one formulation of gelatin and each of the various secondary biopolymers which had produced the most aesthetically pleasing shapes. The formulations with kappa-carrageenan and gellan were able to produce relatively well-defined shapes, showing that it was possible to produce additively manufactured shapes to a high standard although further optimisation of printing parameters could further enhance this.

This methodology of probing the printability could be utilised for other formulations which also involve a sol-gel transition. Through determination of the gelling temperature, G' and evolution of G' and the viscosity of a material, it was possible to determine if a certain material would be able to produce defined shapes. This work will allow others to determine which printing parameters might need adjusting in order to produce a well-defined shape.

CHAPTER 7. CONCLUSIONS AND FUTURE WORK

Detailed conclusions were presented at the end of each of the chapters within this work. This chapter details the overall outcomes of this work and proposes ideas for future work.

7.1 Conclusions

The research reported literature for the printability of edible materials has predominantly been investigated at single temperatures, with materials that maintain their shape due to a yield stress, such as cheese and icing sugar. This limits the amount of materials which can be used. Whilst there has been a significant amount of research into AM of non-edible materials, such as plastics and metals, the current focus of AM of edible products has mainly been concentrated on producing aesthetically pleasing objects from paste-like food or fused powder food. In order to expand the available feedstock of printable materials to materials with thermal transitions, the aim of this work was to develop novel edible material feedstock which could be used in a thermal extrusion AM process. This thesis also aimed to determine a set of design rules in order to allow the quick assessment of other edible materials in order to determine whether they would be suitable for creating defined objects using this process.

The following sections detail specific conclusions determined during this work.

7.1.1 Development of a thermal extrusion printer

It was determined that a thermal FDM printer would be the optimal printer to be used for this work. The machine was created by altering an off-the-shelf plastic FDM printer with a custom-built syringe pump extruder. Due to the nature of this type of printer, the design of the syringe pump was created to try and minimise its weight, in order to limit the amount of work the motors needed to do to move the new head. Also by keeping the weight of the print head to a

minimum, the adverse effect on the printed object was reduced by allowing smoother movement of the nozzle. When the back-plate of the syringe pump was created from only plastic, the force required to bend the plastic was less than the force to push the syringe, resulting in bending of the back plate. Therefore, metal plates were bolted onto the syringe plate in order to prevent this event from occurring. After several alterations, the final syringe plate designed enabled printing of all of the chosen formulations and was able to create the desired printed shapes.

7.1.2 Development of novel feedstocks

Due to the type of machine chosen for this work, the selected materials for this work were limited to materials which underwent a thermal transition. Known for its strength, high viscosity, prevalence in a large variety of foods and desirability to the consumer, gelatin was chosen as the key material for this work. Initial printing of formulations of gelatin displayed poor signs of shape retention, therefore, a secondary biopolymer was introduced to the system in order to increase the evolution of G' of the formulation. The addition of the secondary biopolymers (kappa-carrageenan, gellan and agar) increased the evolution of G', and the magnitude of the formulation's G'. Various concentrations of the secondary biopolymers were added in order to modulate these viscoelastic properties to determine the optimal range of thermal and mechanical properties in order to enable printing of defined objects.

7.1.3 Understanding of thermal extrusion printing using edible materials

To date, the majority of research into extrusion printing for edible materials has investigated food materials which maintain their shape after extrusion due to a yield stress. This project has investigated the way in which a thermal extrusion process works and has produced a model of

design rules for which future researchers will be able to use as a guideline in order to print edible materials.

7.1.4 Design rules for printing

By investigating the thermal and mechanical properties of thermally dependent gel systems, the following design rules have been determined in order to produce a well-defined printed object from thermal reversible biopolymer formulations:

- There is a minimum magnitude of G' which a material must overcome in order for the printed object to retain its shape;
- There is also a minimum viscosity value, below which the material will flow out of the nozzle, resulting in spreading of the material and a failed print;
- The gelation of the material needs to be rapid, in order to avoid slumping of the material (but slow enough to allow annealing between layers).
- The minimum printing temperature must be overcome in order for a material to print smoothly from the nozzle and not gel within the nozzle;
- A lower printing temperature, above the minimum printing temperature achieved aesthetic, well-defined printed shapes;
- Printing at a higher temperature or the longer the time between initiation of gelation to completion will allow stronger bonds to form between layers and within layers, resulting in stronger shapes.

By following these design rules, it was possible to tailor novel formulations to allow printing of well-defined shapes. When the materials fit the design rules, a range of different textures could be achieved, by manipulating the printing parameters, such as the printing temperature

and speed. In the future, this could enable the consumer to choose the exact texture of food, which they prefer, while still eating the food that they need.

This research has built on the library of edible materials which are available for the use in AM processes. With this preliminary work carried out, it should be possible to quickly determine if a material is suitable for this type of AM process.

7.2 Future Work

Having determined the design rules, based on mixtures of biopolymers which all undergo the same reversible thermal transition, it would be interesting to observe if the rules apply for biopolymers and mixtures of biopolymers which undergo other types of reversible thermal transition, such as alginates. This would increase the library of printable materials and help future researchers have a knowledge of which hydrocolloid materials are and are not printable. As well as this, the addition of salts to formulations, either during or after printing, could increase the range of mechanical properties of the printed object.

One of the main issues faced within this work, was the reliability of the printer. By adapting this machine with a heavy print head, in order to allow the extrusion of heated edible materials, the increased weight led to a reduce in accuracy and consistency of the machine. Creation of a stronger FDM machine, with larger motors to move the heavier print head could help to relieve this issue and increase the repeatability of the printed objects.

Whilst some good printed structures were produced, there is still some optimisation of print parameters to be explored such as retraction, printing path/ slicing and minimum layer time, if the formulations were to be taken forwards for application.

Using similar formulations of phase separated biopolymer mixtures, it would be interesting to study the internal microstructure of the final product as it is printed and examine the microgel

particles formed, which may lead to the ability to produce novel microstructures using this technique.

The maximum size of the printed object was defined by the amount of material within the syringe. For future work, it would be interesting to try and adapt the printer to either hold a larger syringe, or devise a similar method to how printing plastic works, with a reservoir of material by the side of the printer and heated tubing to transport the material to the nozzle. This would allow larger materials to be printed and reduce the time spent changing the syringe, due to the material running out.

Having determined the range of parameters which enable a material to print on a Cartesian printer, it may be interesting to see the effect of the print on a delta printer. This would allow an increase of the printing speed, which could then produce an even greater range of different mechanical properties of the printed object.

REFERENCES

ABRAMOWITZ, M. & DAVIDSON, M. 2018. *Anatomy of the Microscope: Intoduction* [Online]. Olympus. Available: https://www.olympus-lifescience.com/en/microscope-resource/primer/anatomy/introduction/ [Accessed 13/11 2018].

AGASSANT, J.-F., ARDA, D. R., COMBEAUD, C., MERTEN, A., MUENSTEDT, H., MACKLEY, M. R., ROBERT, L. & VERGNES, B. 2006. Polymer processing extrusion instabilities and methods for their elimination or minimisation. *International Polymer Processing,* 21**,** 239-255.

AHMED, J., PTASZEK, P. & BASU, S. 2017. *Advances in Food Rheology its Application,* UK, Woodhead publications.

ALLAL, A., LAVERNHE, A., VERGNES, B. & MARIN, G. 2006. Relationships between molecular structure and sharkskin defect for linear polymers. *Journal of Non-Newtonian Fluid Mechanics,* 134**,** 127-135.

AMRG. 2018. *The 7 Categories of Additive Manufacturing* [Online]. Loughborough University. Available: https://www.lboro.ac.uk/research/amrg/about/the7categoriesofadditivemanufacturing/ [Accessed 20/11 2018].

ANON. 2006. *Bloom* [Online]. Available: sizes.com/units/bloom.htm [Accessed 26/04 2016].

ANTONOV, Y. A. & GONÇALVES, M. 1999. Phase separation in aqueous gelatin–κ-carrageenan systems. *Food Hydrocolloids,* 13**,** 517-524.

ANZALONE, W., PEARCE 2015. Multi-material additive and subtractive prosumer digital fabrication with a free and open-source convertible delta RepRap 3-D printer. *Rapid Prototyping Journal,* 21**,** 506-519.

ARENDT, E. & DAL BELLO, F. 2008. *Gluten-Free Cereal Products and Beverages* USA, Elsevier.

ARIFFIN, A., ARIFF, Z. & JIKAN, S. 2011. Evaluation on extrudate swell and melt fracture of polypropylene/kaolin composites at high shear stress. *Journal of Reinforced Plastics and Composites,* 30**,** 609-619.

ARMISÉN, R. & GALATAS, F. 2000. Agar. *In:* PHILLIPS, G. O. & WILLIAMS, P. A. (eds.) *Handbook of hydrocolloids.* UK: Woodhouse Publishing Limited.

ASTM 2012. Standard Terminology for Additive Manufacturing Technologies. *ASTM F2792-12a.* West Conshohocken, PA.

ASTM_STANDARD 2012. ISO/ASTM 52900: 2015 Additive manufacturing-General principles-terminology. *ASTM F2792-10e1*.

AYMARD, P., MARTIN, D. R., PLUCKNETT, K., FOSTER, T. J., CLARK, A. H. & NORTON, I. T. 2001. Influence of thermal history on the structural and mechanical properties of agarose gels. *Biopolymers: Original Research on Biomolecules,* 59**,** 131-144.

BAINES, D. & SEAL, R. 2012. *Natural Food Additives, Ingredients and Flavourings,* UK, Woodhead Publishing.

BANERJEE, S. & BHATTACHARYA, S. 2011. Compressive textural attributes, opacity and syneresis of gels prepared from gellan, agar and their mixtures. *Journal of Food Engineering,* 102**,** 287-292.

BANOVIĆ, L. & VIHAR, B. 2018. Development of an Extruder for Open Source 3D Bioprinting. *Journal of Open Hardware,* 2.

BARNES, H. A. 2000. *A handbook of elementary rheology,* UK, Cambrian Printers

BERG, J., TYMOCZKO, J., STRYER, L. & STRYER, L. 2002. Biochemistry, Ed 5th. WH Freeman, New York.

BHADESHIA, H. K. D. H. 2018. *Differential Scanning Calorimetry* [Online]. University of Cambridge, Materials Science & Metallurgy. Available: https://www.phase-trans.msm.cam.ac.uk/2002/Thermal2.pdf [Accessed 20/11 2018].

BILLIET, T., GEVAERT, E., DE SCHRYVER, T., CORNELISSEN, M. & DUBRUEL, P. 2014. The 3D printing of gelatin methacrylamide cell-laden tissue-engineered constructs with high cell viability. *Biomaterials,* 35**,** 49-62.

BOHIDAR, H. B. & JENA, S. S. 1993. Kinetics of sol–gel transition in thermoreversible gelation of gelatin. *The Journal of Chemical Physics,* 98**,** 8970-8977.

BOURRIOT, S., GARNIER, C. & DOUBLIER, J.-L. 1999. Phase separation, rheology and microstructure of micellar casein–guar gum mixtures. *Food Hydrocolloids,* 13**,** 43-49.

BRAUN, D. B. & ROSEN, M. R. 2000. *Rheology Modifiers Handbook - Practical Use and Application,* USA, William Andrew Publishing.

BUREY, P., BHANDARI, B. R., HOWES, T. & GIDLEY, M. J. 2008. Hydrocolloid Gel Particles: Formation, Characterization, and Application. *Critical Reviews in Food Science and Nutrition,* 48**,** 361-377.

CASSANELLI, M., PROSAPIO, V., NORTON, I. & MILLS, T. 2018. Acidified/basified gellan gum gels: The role of the structure in drying/rehydration mechanisms. *Food Hydrocolloids,* 82**,** 346-354.

CERNASOV, D., KOLMAN, B., GUERRERO, A., ATTLE, S. & MACCHIO, R. 2004. Highly viscous cosmetic product. Google Patents.

CESARANO, J., III., SEGALMAN., R. & CALVERT., P. 1998. *Robocasting provides moldless fabrication from slurry deposition. (dense ceramics freeform fabrication)* [Online]. High Beam Research. Available: https://www.highbeam.com/doc/1G1-20872588.html [Accessed 09/11 2018].

CHANDRASEKARAN, R. & RADHA, A. 1995. Molecular architectures and functional properties of gellan gum and related polysaccharides. *Trends in Food Science & Technology,* 6**,** 143-148.

CHANG, C. C., BOLAND, E. D., WILLIAMS, S. K. & HOYING, J. B. 2011. Direct-write bioprinting three-dimensional biohybrid systems for future regenerative therapies. *Journal of Biomedical Materials Research Part B: Applied Biomaterials,* 98**,** 160-170.

CHHABRA, R. P. & RICHARDSON, J. F. 2011. *Non-Newtonian flow and applied rheology: engineering applications*, Butterworth-Heinemann.

CLARK, A., RICHARDSON, R., ROSS-MURPHY, S. & STUBBS, J. 1983. Structural and mechanical properties of agar/gelatin co-gels. Small-deformation studies. *Macromolecules,* 16**,** 1367-1374.

CLARK, E. A., ALEXANDER, M. R., IRVINE, D. J., ROBERTS, C. J., WALLACE, M. J., SHARPE, S., YOO, J., HAGUE, R. J. M., TUCK, C. J. & WILDMAN, R. D. 2017. 3D printing of tablets using inkjet with UV photoinitiation. *International Journal of Pharmaceutics,* 529**,** 523-530.

COHEN, D. L., LIPTON, J. I., CUTLER, M., COULTER, D., VESCO, A. & LIPSON, H. Hydrocolloid printing: a novel platform for customized food production. Solid Freeform Fabrication Symposium (SFF'09), 2009.

COMPTON, B. G. & LEWIS, J. A. 2014. 3D-Printing of Lightweight Cellular Composites. *Advanced Materials,* 26**,** 5930-5935.

CONSIDINE, D. M. 2012. *Foods and Food Production Encyclopedia*, Springer US.

COSTAKIS, W. J., RUESCHHOFF, L. M., DIAZ-CANO, A. I., YOUNGBLOOD, J. P. & TRICE, R. W. 2016. Additive manufacturing of boron carbide via continuous filament direct ink writing of aqueous ceramic suspensions. *Journal of the European Ceramic Society,* 36**,** 3249-3256.

CROKER, J., KELLY, P. M. & BURR, R. D. 1998. *Printing inks*. US patent application.

CULIOLI, J. & SHERMAN, P. 1976. Evaluation of Gouda cheese firmness by compression tests. *Journal of texture Studies,* 7**,** 353-372.

DAKIA, P. A., BLECKER, C., ROBERT, C., WATHELET, B. & PAQUOT, M. 2008. Composition and physicochemical properties of locust bean gum extracted from whole seeds by acid or water dehulling pre-treatment. *Food Hydrocolloids,* 22**,** 807-818.

DAMODARAN, S. & PARKIN, K. L. 2017. *Fennema's food chemistry*, CRC press.

DAVIES, P. 2017. Differential Scanning Calorimetry (DSC). TA Instruments

DE CARVALHO, R. A. & GROSSO, C. R. F. 2004. Characterization of gelatin based films modified with transglutaminase, glyoxal and formaldehyde. *Food Hydrocolloids,* 18**,** 717-726.

DE HUIDOBRO, F. R., MIGUEL, E., BLÁZQUEZ, B. & ONEGA, E. 2005. A comparison between two methods (Warner–Bratzler and texture profile analysis) for testing either raw meat or cooked meat. *Meat Science,* 69**,** 527-536.

DEL CARMEN NÚÑEZ-SANTIAGO, M. & TECANTE, A. 2007. Rheological and calorimetric study of the sol–gel transition of κ-carrageenan. *Carbohydrate polymers,* 69**,** 763-773.

DERKACH, S. R., ILYIN, S. O., MAKLAKOVA, A. A., KULICHIKHIN, V. G. & MALKIN, A. Y. 2015. The rheology of gelatin hydrogels modified by κ-carrageenan. *LWT-Food Science and Technology,* 63**,** 612-619.

DEROSSI, A., CAPORIZZI, R., AZZOLLINI, D. & SEVERINI, C. 2018. Application of 3D printing for customized food. A case on the development of a fruit-based snack for children. *Journal of Food Engineering,* 220**,** 65-75.

DIAZ, J., V., VAN BOMMEL, K., J,C. , NOORT, M., W-J. & HENKET, J. B., P. 2014. *Method for the production of edible objects using sls and food products*. France patent application WO2014193226A1.

DICKINSON, E. 2003. Hydrocolloids at interfaces and the influence on the properties of dispersed systems. *Food Hydrocolloids,* 17**,** 25-39.

DJABOUROV, M., LEBLOND, J. & PAPON, P. 1988. Gelation of aqueous gelatin solutions. II. Rheology of the sol-gel transition. *Journal de Physique,* 49**,** 333-343.

DUL, M., PALUCH, K. J., KELLY, H., HEALY, A. M., SASSE, A. & TAJBER, L. 2015. Self-assembled carrageenan/protamine polyelectrolyte nanoplexes—Investigation of critical parameters governing their formation and characteristics. *Carbohydrate polymers,* 123**,** 339-349.

ETXABIDE, A., LONG, J., GUERRERO, P., DE LA CABA, K. & SEYFODDIN, A. 2019. 3D printed lactose-crosslinked gelatin scaffolds as a drug delivery system for dexamethasone. *European Polymer Journal,* 114**,** 90-97.

FAES, M., FERRARIS, E. & MOENS, D. 2016. Influence of Inter-layer Cooling time on the Quasi-static Properties of ABS Components Produced via Fused Deposition Modelling. *Procedia CIRP,* 42**,** 748-753.

FAES, M., VAN HOOREWEDER, B., WANG, Y., LAVA, P. & MOENS, D. 2015. Variability in Mechanical Properties of ABS parts produced by Fused Deposition Modelling. *Proc. 2015 NAFEMS World Congr., San Diego*.

FANG, Y., LI, L., INOUE, C., LUNDIN, L. & APPELQVIST, I. 2006. Associative and Segregative Phase Separations of Gelatin/κ-Carrageenan Aqueous Mixtures. *Langmuir,* 22**,** 9532-9537.

FASOLIN, L. H., PICONE, C. S. F., SANTANA, R. C. & CUNHA, R. L. 2013. Production of hybrid gels from polysorbate and gellan gum. *Food Research International,* 54**,** 501-507.

FEINER, G. 2006. *Meat products handbook: Practical science and technology*, Elsevier.

FINDLAY, K. 2018. *A sense of sclae* [Online]. John Innes Centre. Available: https://www.jic.ac.uk/microscopy/contact.html [Accessed 3/12 2018].

FLICK, E. W. 1990. Emulsifying Agents - An Industrial Guide - Guar Gum. William Andrew Publishing/Noyes.

FONKWE, L. G., NARSIMHAN, G. & CHA, A. S. 2003. Characterization of gelation time and texture of gelatin and gelatin–polysaccharide mixed gels. *Food Hydrocolloids,* 17**,** 871-883.

FRANCK, A. 2017. *Understanding Rheology of Structured Fluids* [Online]. Available: http://www.tainstruments.com/pdf/literature/AAN016_V1_U_StructFluids.pdf [Accessed 4/5 2017].

FUJII, K., KAJITA, R., KUROSAWA, M. & FUJII, T. 2000. Mechanical properties of two phase-disperse agar/gelatin mixed gels. *Journal of texture studies,* 31**,** 273-286.

GABBOTT, P. & MANN, T. 2016. Differential Scanning Calorimetry. *In:* GAISFORD, S., KETT, V. & HAINES, P. (eds.) *Principles of Thermal Analysis and Calorimetry.* UK: The Royal Society of Chemistry

GABRIELE, A., SPYROPOULOS, F. & NORTON, I. T. 2009. Kinetic study of fluid gel formation and viscoelastic response with kappa-carrageenan. *Food Hydrocolloids,* 23**,** 2054-2061.

GE. 2016. *3D Printing Creates New Parts for Aircraft Engines* [Online]. Available: geglobalresearch.com [Accessed 19/04 2016].

GIBSON, I., ROSEN, D. & STUCKER, B. 2015. Directed energy deposition processes. *Additive Manufacturing Technologies.* Springer.

GMIA. 2012. *Gelatin Handbook* [Online]. Available: http://www.gelatin-gmia.com/images/GMIA_Gelatin_Manual_2012.pdf [Accessed 04/11 2015].

GODOI, F. C., PRAKASH, S. & BHANDARI, B. R. 2016. 3d printing technologies applied for food design: Status and prospects. *Journal of Food Engineering,* 179**,** 44-54.

GÓMEZ-GUILLÉN, M. C., GIMÉNEZ, B., LÓPEZ-CABALLERO, M. E. & MONTERO, M. P. 2011. Functional and bioactive properties of collagen and gelatin from alternative sources: A review. *Food Hydrocolloids,* 25**,** 1813-1827.

GRASDALEN, H. & SMIDSRØD, O. 1987. Gelation of gellan gum. *Carbohydrate Polymers,* 7**,** 371-393.

GRAY, N. 2010. *Looking to the future: Creating novel foods using 3D printing* [Online]. Food navigator.com. Available: https://www.foodnavigator.com/Article/2010/12/23/Looking-to-the-future-Creating-novel-foods-using-3D-printing [Accessed 21/11 2018].

GUNASEKARAN, S. & MEHMET AK, M. 2002. *Cheese Rheology and Texture,* US, CRC Press.

GYTON, G. 2015. *Opinion split on 3D meat consumption* [Online]. Available: globalmeatnews.com [Accessed 26/04 2016].

HAO, L., MELLOR, S., SEAMAN, O., HENDERSON, J., SEWELL, N. & SLOAN, M. 2010. Material characterisation and process development for chocolate additive layer manufacturing. *Virtual and Physical Prototyping,* 5**,** 57-64.

HARDING, S. 1998. Dilute solution viscometry of food biopolymers. *Functional properties of food macromolecules,* 149.

HARRINGTON, J. C. & MORRIS, E. R. 2009. Conformational ordering and gelation of gelatin in mixtures with soluble polysaccharides. *Food Hydrocolloids,* 23**,** 327-336.

HAUG, I. J. & DRAGET, K. I. 2000. *Handbook of Hydrocolloids,* UK, Woodhead Publishing.

HAUG, I. J., DRAGET, K. I. & SMIDSRØD, O. 2004. Physical behaviour of fish gelatin-κ-carrageenan mixtures. *Carbohydrate Polymers,* 56**,** 11-19.

HAWATMEH, D., ROJAS-NASTRUCCI, E. & WELLER, T. A multi-material 3D printing approach for conformal microwave antennas. 2016 International Workshop on Antenna Technology (iWAT), 2016. IEEE, 7-10.

HE, Y., QIU, J., FU, J., ZHANG, J., REN, Y. & LIU, A. 2015. Printing 3D microfluidic chips with a 3D sugar printer. *Microfluidics and Nanofluidics,* 19**,** 447-456.

HE, Y., YANG, F., ZHAO, H., GAO, Q., XIA, B. & FU, J. 2016. Research on the printability of hydrogels in 3D bioprinting. *Scientific Reports,* 6**,** 29977.

HICTOP. 2018. *HICTOP Prusa I3 3D Desktop Printer* [Online]. Available: https://www.hic3dprinter.com/products/hictop-prusa-i3-3d-desktop-printer-diy-high-accuracy-cnc-self-assembly-tridimensional [Accessed 7/11 2018].

HOLLAND, S., TUCK, C. & FOSTER, T. 2018. Selective recrystallization of cellulose composite powders and microstructure creation through 3D binder jetting. *Carbohydrate Polymers,* 200**,** 229-238.

HONG, S., SYCKS, D., CHAN, H. F., LIN, S., LOPEZ, G. P., GUILAK, F., LEONG, K. W. & ZHAO, X. 2015. 3D printing of highly stretchable and tough hydrogels into complex, cellularized structures. *Advanced Materials,* 27**,** 4035-4040.

HORIUCHI, H. & SUGIYAMA, J. 1987. Mechanical and structural properties of agar-gelatin mixed gels. *Agricultural and Biological Chemistry,* 51**,** 2171-2176.

HOTTA, M., KENNEDY, J., HIGGINBOTHAM, C. & MORRIS, N. 2016. Durum Wheat Seed Germination Response to Hydrogel Coatings and Moisture under Drought Stress. *American Journal of Agricultural and Biological Sciences,* 11**,** 67-75.

HOY, M. B. 2013. 3D Printing: Making Things at the Library. *Medical Reference Services Quarterly,* 32**,** 93-99.

HU, W.-S. 2018. *Engineering Principles in Biotechnology*, Wiley & Sons.

HULL, C. W. 2015. The Birth of 3D Printing. *Research-Technology Management,* 58**,** 25-30.

IIJIMA, M., HATAKEYAMA, T., TAKAHASHI, M. & HATAKEYAMA, H. 2007. Effect of thermal history on kappa-carrageenan hydrogelation by differential scanning calorimetry. *Thermochimica Acta,* 452**,** 53-58.

IMESON, A. P. 2000. *Handbook of Hydrocolloids,* UK, Woodhead Publishing.

JAMIESON, R. & HACKER, H. 1995. Direct slicing of CAD models for rapid prototyping. *Rapid Prototyping Journal,* 1**,** 4-12.

KARIM, A. & BHAT, R. 2008. Gelatin alternatives for the food industry: recent developments, challenges and prospects. *Trends in food science & technology,* 19**,** 644-656.

KEMPKA, A. P., SOUZA, S. M. A. G. U. D., ULSON DE SOUZA, A. A., PRESTES, R. C. & OGLIARI, D. 2014. Influence of bloom number and plastifiers on gelatin matrices produced for enzyme immobilization. *Brazilian Journal of Chemical Engineering,* 31**,** 95-108.

KIETZMANN, J., PITT, L. & BERTHON, P. 2015. Disruptions, decisions, and destinations: Enter the age of 3-D printing and additive manufacturing. *Business Horizons,* 58**,** 209-215.

KIM, E., SHIN, Y.-J. & AHN, S.-H. 2016. The effects of moisture and temperature on the mechanical properties of additive manufacturing components: fused deposition modeling. *Rapid Prototyping Journal,* 22**,** 887-894.

KIRCHMAJER, D. M., GORKIN III, R. & IN HET PANHUIS, M. 2015. An overview of the suitability of hydrogel-forming polymers for extrusion-based 3D-printing. *Journal of Materials Chemistry B,* 3**,** 4105-4117.

KNUTSEN, S., MYSLABODSKI, D., LARSEN, B. & USOV, A. 1994. A modified system of nomenclature for red algal galactans. *Botanica marina,* 37**,** 163-170.

KOMMAREDDY, S., SHENOY, D. B. & AMIJI, M. M. 2007. Gelatin nanoparticles and their biofunctionalization. *Nanotechnologies for the Life Sciences: Online*.

KURTZ, S. M. 2016. *UHMWPE Biomaterials Handbook - Ultra-High Molecular Weight Polyethylene in Total Joint Replacement and Medical Devices,* UK, Elsevier.

KUZNETSOV, V. E., SOLONIN, A. N., TAVITOV, A. G., URZHUMTSEV, O. D. & VAKULIK, A. H. 2018. Increasing of Strength of FDM (FFF) 3D Printed Parts by Influencing on Temperature-Related Parameters of the Process.

LABROPOULOS, K. C., RANGARAJAN, S., NIESZ, D. E. & DANFORTH, S. C. 2001. Dynamic rheology of agar gel based aqueous binders. *Journal of the American Ceramic Society,* 84**,** 1217-1224.

LANDERS, R., HÜBNER, U., SCHMELZEISEN, R. & MÜLHAUPT, R. 2002. Rapid prototyping of scaffolds derived from thermoreversible hydrogels and tailored for applications in tissue engineering. *Biomaterials,* 23**,** 4437-4447.

LAU, M., TANG, J. & PAULSON, A. 2000. Texture profile and turbidity of gellan/gelatin mixed gels. *Food Research International,* 33**,** 665-671.

LE TOHIC, C., O'SULLIVAN, J. J., DRAPALA, K. P., CHARTRIN, V., CHAN, T., MORRISON, A. P., KERRY, J. P. & KELLY, A. L. 2018. Effect of 3D printing on the structure and textural properties of processed cheese. *Journal of Food Engineering,* 220**,** 56-64.

LEE, K. Y., SHIM, J., BAE, I. Y., CHA, J., PARK, C. S. & LEE, H. G. 2003. Characterization of gellan/gelatin mixed solutions and gels. *LWT - Food Science and Technology,* 36**,** 795-802.

LI, H., LIU, S. & LIN, L. 2016. Rheological study on 3D printability of alginate hydrogel and effect of graphene oxide. *2016,* 2.

LIENEKE, T., DENZER, V., ADAM, G. A. O. & ZIMMER, D. 2016. Dimensional Tolerances for Additive Manufacturing: Experimental Investigation for Fused Deposition Modeling. *Procedia CIRP,* 43**,** 286-291.

LIGON, S. C., LISKA, R., STAMPFL, J. R., GURR, M. & MÜLHAUPT, R. 2017. Polymers for 3D printing and customized additive manufacturing. *Chemical reviews,* 117**,** 10212-10290.

LILLE, M., NURMELA, A., NORDLUND, E., METSÄ-KORTELAINEN, S. & SOZER, N. 2017. Applicability of protein and fiber-rich food materials in extrusion-based 3D printing. *Journal of Food Engineering*.

LILLE, M., NURMELA, A., NORDLUND, E., METSÄ-KORTELAINEN, S. & SOZER, N. 2018. Applicability of protein and fiber-rich food materials in extrusion-based 3D printing. *Journal of Food Engineering,* 220**,** 20-27.

LIU, H., XU, X. M. & GUO, S. D. 2007. Rheological, texture and sensory properties of low-fat mayonnaise with different fat mimetics. *LWT - Food Science and Technology,* 40**,** 946-954.

LIU, Z., ZHANG, M., BHANDARI, B. & WANG, Y. 2017. 3D printing: Printing precision and application in food sector. *Trends in Food Science & Technology,* 69**,** 83-94.

LOZANO, R., STEVENS, L., THOMPSON, B. C., GILMORE, K. J., GORKIN, R., STEWART, E. M., IN HET PANHUIS, M., ROMERO-ORTEGA, M. & WALLACE, G. G. 2015. 3D printing of layered brain-like structures using peptide modified gellan gum substrates. *Biomaterials,* 67**,** 264-273.

MACNAUGHTAN, B. & FARHAT, I. A. 2008. Thermal methods in the study of foods and food ingredients. *Principles and Applications of Thermal Analysis***,** 330-409.

MADHAMUTHANALLI, C. V. & BANGALORE, S. A. 2014. Rheological and physico-chemical properties of gelatin extracted from the skin of a few species of freshwater carp. *International journal of food science & technology,* 49**,** 1758-1764.

MALKIN, A. Y. & ISAYEV, A. I. 2006. *Rheology - Concepts, Methods, & Applications,* Canada, ChemTec Publishing.

MALONE, E. & LIPSON, H. 2007. Fab@ Home: the personal desktop fabricator kit. *Rapid Prototyping Journal,* 13**,** 245-255.

MALVERN 2010. Kinexus Customer Training. *In:* MALVERN (ed.). UK.

MAO, R., TANG, J. & SWANSON, B. G. 2000. Texture properties of high and low acyl mixed gellan gels. *Carbohydrate Polymers,* 41**,** 331-338.

MARCOTTE, M., HOSHAHILI, A. R. T. & RAMASWAMY, H. 2001. Rheological properties of selected hydrocolloids as a function of concentration and temperature. *Food Research International,* 34**,** 695-703.

MASOOD, S. H., RATTANAWONG, W. & IOVENITTI, P. 2000. Part Build Orientations Based on Volumetric Error in Fused Deposition Modelling. *The International Journal of Advanced Manufacturing Technology,* 16**,** 162-168.

MCKENNA, B. 2003. *Texture in Food, Volume 1- Semi-Solid Foods,* UK, Woodhead Publishing.

MELCHELS, F. P. W., FEIJEN, J. & GRIJPMA, D. W. 2010. A review on stereolithography and its applications in biomedical engineering. *Biomaterials,* 31**,** 6121-6130.

MEWIS, J. & WAGNER, N. J. 2012. *Colloidal Suspension Rheology,* UK, Cambridge University Press.

MICHON, C., CUVELIER, G., RELKIN, P. & LAUNAY, B. 1997. Influence of thermal history on the stability of gelatin gels. *International Journal of Biological Macromolecules,* 20**,** 259-264.

MICHON, C., VIGOUROUX, F., BOULENGUER, P., CUVELIER, G. & LAUNAY, B. 2000. Gelatin/iota-carrageenan interactions in non-gelling conditions. *Food hydrocolloids,* 14**,** 203-208.

MILANI, J. & MALEKI, G. 2012. Hydrocolloids in Food Industry.

MIYOSHI, E., TAKAYA, T. & NISHINARI, K. 1995. Effects of salts on the gel-sol transition of gellan gum by differential scanning calorimetry and thermal scanning rheology. *Thermochimica Acta,* 267**,** 269-287.

MOLITCH-HOU, M. 2014. *11 Food 3D Printers to Feed the Future* [Online]. 3D Printing Industry Available: https://3dprintingindustry.com/news/11-food-3d-printers-36052/ [Accessed 10/04 2017].

MORITAKA, H., NISHINARI, K., HORIUCHI, H. & WATASE, M. 1980. Rheological properties of aqueous agarose-gelatin gels. *Journal of Texture Studies,* 11**,** 257-270.

MORRIS, V. J. & CHILVERS, G. R. 1983. Rheological studies of specific cation forms of kappa carrageenan gels. *Carbohydrate Polymers,* 3**,** 129-141.

MORRISON, N. A., CLARK, R. C., CHEN, Y. L., TALASHEK, T. & SWORN, G. 1999. Gelatin alternatives for the food industry. *In:* NISHINARI, K. (ed.) *Physical Chemistry and Industrial Application of Gellan Gum.* Berlin, Heidelberg: Springer Berlin Heidelberg.

NAFTULIN, J. S., KIMCHI, E. Y. & CASH, S. S. 2015. Streamlined, inexpensive 3D printing of the brain and skull. *PloS one,* 10**,** e0136198.

NAKAMURA, K., HARADA, K. & TANAKA, Y. 1993. Viscoelastic properties of aqueous gellan solutions: the effects of concentration on gelation. *Food Hydrocolloids,* 7**,** 435 - 447.

NICKERSON, M. T., PAULSON, A. T. & SPEERS, R. A. 2003. Rheological properties of gellan solutions: effect of calcium ions and temperature on pre-gel formation. *Food Hydrocolloids,* 17**,** 577-583.

NINAN, G., JOSEPH, J. & ALIYAMVEETTIL, Z. A. 2014. A comparative study on the physical, chemical and functional properties of carp skin and mammalian gelatins. *Journal of Food Science and Technology,* 51**,** 2085-2091.

NOORT, M., VAN BOMMEL, K. & RENZETTI, S. 2017. 3D-printed cereal foods. *Cereal Foods World,* 62**,** 272-277.

NORTON, I. & FOSTER, T. 2002. Hydrocolloids in real food systems. *Special Publication-Royal Society of Chemistry,* 278**,** 187-200.

NORTON, I. & FRITH, W. 2003. Phase separation in mixed biopolymer systems. *Food colloids, biopolymers and materials***,** 282-297.

OECD. 1981. *OECD Guidelines for the testing of chemicals* [Online]. Available: http://www.oecd.org/env/ehs/testing/oecdguidelinesforthetestingofchemicals.htm [Accessed 20/11 2018].

OSKAY, W. & EDMAN, L. 2014. *The CandyFab Project* [Online]. Evil Mad Scientist Laboratories. Available: https://candyfab.org/ [Accessed 21/11 2018].

PAAR, A. 2018. *Basics of rheology* [Online]. Available: https://wiki.anton-paar.com/en/basics-of-rheology/ [Accessed 20/11 2018].

PANDEY, A., HÖFER, R., TAHERZADEH, M., NAMPOOTHIRI, M. & LARROCHE, C. 2015. *Industrial biorefineries and white biotechnology*, Elsevier.

PAQUIN, P. 2009. *Functional and Speciality Beverage Technology,* UK, Woodhead Publishing.

PARKER, N. & POVEY, M. 2012. Ultrasonic study of the gelation of gelatin: phase diagram, hysteresis and kinetics. *Food Hydrocolloids,* 26**,** 99-107.

PASCUA, Y., KOÇ, H. & FOEGEDING, E. A. 2013. Food structure: Roles of mechanical properties and oral processing in determining sensory texture of soft materials. *Current Opinion in Colloid & Interface Science,* 18**,** 324-333.

PELEG, M. 1976. Texture profile analysis parameters obtained by an Instron universal testing machine. *Journal of Food Science,* 41**,** 721-722.

PERIARD, D., SCHAAL, N., SCHAAL, M., MALONE, E. & LIPSON, H. Printing food. Proceedings of the 18th Solid Freeform Fabrication Symposium, Austin TX, 2007. Citeseer, 564-574.

PETRIE, E. M. 2018. *What is Additive Manufacturing?* [Online]. SpecialChem. Available: https://omnexus.specialchem.com/selection-guide/3d-printing-and-additive-manufacturing-polymers-and-processes [Accessed 20/11 2018].

PHILLIPS, G. O. & WILLIAMS, P. A. 2009a. *Gums and Stabilisers for the Food Industry 12*, Royal Society of Chemistry.

PHILLIPS, G. O. & WILLIAMS, P. A. 2009b. *Handbook of Hydrocolloids (2nd Edition)*, Woodhead Publishing.

PRANOTO, Y., LEE, C. M. & PARK, H. J. 2007. Characterizations of fish gelatin films added with gellan and κ-carrageenan. *LWT-Food Science and Technology,* 40**,** 766-774.

PSLC. 2018. *Differential Scanning Calorimetry* [Online]. Polymer Science Learning Centre. Available: https://pslc.ws/macrog/dsc.htm [Accessed 21/11 2018].

RAO, R. V. & RAI, D. P. 2016. Optimization of fused deposition modeling process using teaching-learning-based optimization algorithm. *Engineering Science and Technology, an International Journal,* 19**,** 587-603.

RASLI, H. & SARBON, N. 2014. Effects of different drying methods on the rheological, functional and structural properties of chicken skin gelatin compared to bovine gelatin.

RAYNA, T. & STRIUKOVA, L. 2016. From rapid prototyping to home fabrication: How 3D printing is changing business model innovation. *Technological Forecasting and Social Change,* 102**,** 214-224.

REES, D. A. 1972. Polysaccharide gels. A molecular view *Chem. Ind.***,** 630.

ROBINSON, G., MORRIS, E. R. & REES, D. A. 1980. Role of double helices in carrageenan gelation: the domain model. *Journal of the Chemical Society, Chemical Communications***,** 152-153.

ROCHAS, C. & RINAUDO, M. 1984. Mechanism of gel formation in κ-carrageenan. *Biopolymers,* 23**,** 735-745.

SAHA, D. & BHATTACHARYA, S. 2010. Hydrocolloids as thickening and gelling agents in food: a critical review. *Journal of food science and technology,* 47**,** 587-597.

SCHAFER, S. E. & STEVENS, E. S. 1995. A reexamination of the double-helix model for agarose gels using optical rotation. *Biopolymers: Original Research on Biomolecules,* 36**,** 103-108.

SCHASCHKE, C. 2014. *Dictionary of Chemical Engineering,* USA, Oxford University Press.

SCHRAMN, G. 2000. *A Practical Approach to Rheolgy and Rheometry* Germany, ThermoHaake

SEGALL, L. 2014. *This 3D printer makes edible food* [Online]. CNN. Available: http://money.cnn.com/2011/01/24/technology/3D_food_printer/ [Accessed 10/04 2017].

SHAHIDI, F. & SIMPSON, B. K. 2004. *Seafood quality and safety: Advances in the new millennium*, DEStech Publications, Inc.

SHARON, N. 1975. Complex carbohydrates. *Their Chemistry, Biosynthesis, and Functions*, 258-281.

SHASTRY, A. V., COLLINS, T. M., SUTTLE, J. M., WILLCOCKS, N. A., BEN-YOSEPH, E. & WALTERS, M. 2009. *Edible inks for ink-jet printing on edible substrates*.

SHIINOKI, Y. & YANO, T. 1986. Viscoelastic behavior of an agar—gelatin mixture gel as a function of its composition. *Food Hydrocolloids,* 1**,** 153-161.

SHIM, J. L. 1985. *Gellan gum/gelatin blends*. U.S. patent application.

SHRINIVAS, P., KASAPIS, S. & TONGDANG, T. 2009. Morphology and mechanical properties of bicontinuous gels of agarose and gelatin and the effect of added lipid phase. *Langmuir,* 25**,** 8763-8773.

ŠIMON, P., FRATRIČOVÁ, M., SCHWARZER, P. & WILDE, H.-W. 2006. Evaluation of the residual stability of polyurethane automotive coatings by DSC: Equivalence of Xenotest and desert weathering tests and the synergism of stabilizers. *Journal of Thermal Analysis and Calorimetry,* 84**,** 679-692.

SIMPLIFY3D. 2019. *Print Quality Troubleshooting Guide* [Online]. Available: https://www.simplify3d.com/support/print-quality-troubleshooting/ - layer-separation-and-splitting [Accessed 13/02 2019].

SINGH, S. S., ASWAL, V. K. & BOHIDAR, H. B. 2007a. Structural studies of agar–gelatin complex coacervates by small angle neutron scattering, rheology and differential scanning calorimetry. *International Journal of Biological Macromolecules,* 41**,** 301-307.

SINGH, S. S., ASWAL, V. K. & BOHIDAR, H. B. 2009. Structural evolution of aging agar-gelatin co-hydrogels. *Polymer,* 50**,** 5589-5597.

SINGH, S. S., BOHIDAR, H. B. & BANDYOPADHYAY, S. 2007b. Study of gelatin–agar intermolecular aggregates in the supernatant of its coacervate. *Colloids and Surfaces B: Biointerfaces,* 57**,** 29-36.

SMITH, J. & HONG-SHUM, L. 2011. *Food Additive Data Book,* UK, John Wiley & Sons.

SOARES, S. 2011. *Insects au Gratin* [Online]. Available: susanasoares.com/index/php?id=82 [Accessed 05/04 2016].

SOMBOON, N., KARRILA, T., KAEWMANEE, T. & KARRILA, S. 2014. Properties of gels from mixed agar and fish gelatin. *International Food Research Journal,* 21.

SOOD, A. K., OHDAR, R. K. & MAHAPATRA, S. S. 2010. Parametric appraisal of mechanical property of fused deposition modelling processed parts. *Materials & Design,* 31**,** 287-295.

SRIAMORNSAK, P., THIRAWONG, N. & PUTTIPIPATKHACHORN, S. 2004. Morphology and buoyancy of oil-entrapped calcium pectinate gel beads. *The AAPS journal,* 6**,** e24-e24.

STABLE_MICRO_SYSTEMS. 2018. *Texture Analysis* [Online]. Available: https://www.stablemicrosystems.com/TextureAnalysis.html [Accessed 14/11 2018].

STOKES, J., WOLF, B. & FRITH, W. 2001. Phase-separated biopolymer mixture rheology: Prediction using a viscoelastic emulsion model. *Journal of Rheology,* 45**,** 1173-1191.

SUN, J., PENG, Z., ZHOU, W., FUH, J. Y. H., HONG, G. S. & CHIU, A. 2015a. A Review on 3D Printing for Customized Food Fabrication. *Procedia Manufacturing,* 1**,** 308-319.

SUN, J., ZHOU, W., HUANG, D., FUH, J. Y. H. & HONG, G. S. 2015b. An Overview of 3D Printing Technologies for Food Fabrication. *Food and Bioprocess Technology,* 8**,** 1605-1615.

SUN, J., ZHOU, W., YAN, L., HUANG, D. & LIN, L.-Y. 2017. Extrusion-based food printing for digitalized food design and nutrition control. *Journal of Food Engineering*.

SUN, Q., RIZVI, G., BELLEHUMEUR, C. & GU, P. Experimental study of the cooling characteristics of polymer filaments in FDM and impact on the mesostructures and properties of prototypes. 14th Solid Freeform Fabrication Symposium (SSF), Austin, TX, Aug, 2003. 4-6.

SUN, Q., RIZVI, G., BELLEHUMEUR, C. & GU, P. 2008. Effect of processing conditions on the bonding quality of FDM polymer filaments. *Rapid Prototyping Journal,* 14**,** 72-80.

SYSTEMS, D. 2018. *Culinary 3D Printing* [Online]. America. Available: https://www.3dsystems.com/culinary [Accessed 21/11 2018].

TAKAYANAGI, S., OHNO, T., OKAWA, Y., SHIBA, F., KOBAYASHI, H. & KAWAMURA, F. 2000. Sol-gel transition of a mixture of gelatin and κ-carrageenan. *The Imaging Science Journal,* 48**,** 193-198.

TOSH, S. M. & MARANGONI, A. G. 2004. Determination of the maximum gelation temperature in gelatin gels. *Applied Physics Letters,* 84**,** 4242-4244.

TUNICK, M. H., BASCH, J. J., MALEEFF, B. E., FLANAGAN, J. F. & HOLSINGER, V. H. 1989. Characterization of Natural and Imitation Mozzarella Cheeses by Differential Scanning Calorimetry. *Journal of Dairy Science,* 72**,** 1976-1980.

TURNER, B. N., STRONG, R. & GOLD, S. A. 2014. A review of melt extrusion additive manufacturing processes: I. Process design and modeling. *Rapid Prototyping Journal,* 20**,** 192-204.

VAN SAARLOOS, W. 2003. *"Melt fracture" in polymer extrusion: a visco-elastic instability* [Online]. Available: http://wwwhome.lorentz.leidenuniv.nl/~saarloos/Patternf/meltfracture.html [Accessed 17/12 2018].

VAN VLIET, T. 2013. *Rheology and fracture mechanics of foods*, CRC Press.

WAKHET, S., SINGH, V. K., SAHOO, S., SAGIRI, S. S., KULANTHAIVEL, S., BHATTACHARYA, M. K., KUMAR, N., BANERJEE, I. & PAL, K. 2015. Characterization of gelatin–agar based phase separated hydrogel, emulgel and bigel: a comparative study. *Journal of Materials Science: Materials in Medicine,* 26**,** 118.

WANG, J. & SHAW, L. L. 2005. Rheological and extrusion behavior of dental porcelain slurries for rapid prototyping applications. *Materials Science and Engineering: A,* 397**,** 314-321.

WANG, L., CAO, Y., ZHANG, K., FANG, Y., NISHINARI, K. & PHILLIPS, G. O. 2015. Hydrogen bonding enhances the electrostatic complex coacervation between κ-

carrageenan and gelatin. *Colloids and Surfaces A: Physicochemical and Engineering Aspects,* 482**,** 604-610.

WANG, L. & LIU, J. 2014. Liquid phase 3D printing for quickly manufacturing conductive metal objects with low melting point alloy ink. *Science China Technological Sciences,* 57**,** 1721-1728.

WANG, L., ZHANG, M., BHANDARI, B. & YANG, C. 2017. Investigation on fish surimi gel as promising food material for 3D printing. *Journal of Food Engineering*.

WARNER, E. L., NORTON, I. T. & MILLS, T. B. 2019. Comparing the viscoelastic properties of gelatin and different concentrations of kappa-carrageenan mixtures for additive manufacturing applications. *Journal of Food Engineering,* 246**,** 58-66.

WATASE, M. & NISHINARI, K. 1980. Rheological properties of agarose-gelatin gels. *Rheologica Acta,* 19**,** 220-225.

WATASE, M. & NISHINARI, K. 1988. Thermal and rheological properties of agarose-dimethyl sulfoxide-water gels. *Polymer journal,* 20**,** 1125.

WEGRZYN, T. F., GOLDING, M. & ARCHER, R. H. 2012. Food Layered Manufacture: A new process for constructing solid foods. *Trends in Food Science & Technology,* 27**,** 66-72.

WEI, J., WANG, J., SU, S., WANG, S., QIU, J., ZHANG, Z., CHRISTOPHER, G., NING, F. & CONG, W. 2015. 3D printing of an extremely tough hydrogel. *Rsc Advances,* 5**,** 81324-81329.

WILKES, G. 1981. An overview of the basic rheological behavior of polymer fluids with an emphasis on polymer melts. ACS Publications.

WOHLERS, T. & GORNET, T. 2012. History of additive manufacturing.

WOLF, B., SCIROCCO, R., FRITH, W. & NORTON, I. 2000. Shear-induced anisotropic microstructure in phase-separated biopolymer mixtures. *Food Hydrocolloids,* 14**,** 217-225.

WONG, K. V. & HERNANDEZ, A. 2012. A Review of Additive Manufacturing. *ISRN Mechanical Engineering,* 2012**,** 10.

WONG, T. W., LEE, H. Y., CHAN, L. W. & HENG, P. W. S. 2002. Drug release properties of pectinate microspheres prepared by emulsification method. *International Journal of Pharmaceutics,* 242**,** 233-237.

WÜSTENBERG, T. 2015. General overview of food hydrocolloids. *Cellulose and Cellulose Derivatives in the Food Industry: Fundamentals and Applications*.

YANG, F., ZHANG, M., BHANDARI, B. & LIU, Y. 2018. Investigation on lemon juice gel as food material for 3D printing and optimization of printing parameters. *LWT-Food Science and Technology,* 87**,** 67-76.

YASA, E., POYRAZ, O., SOLAKOGLU, E. U., AKBULUT, G. & OREN, S. 2016. A study on the stair stepping effect in direct metal laser sintering of a nickel-based superalloy. *Procedia CIRP,* 45**,** 175-178.

YERMAK, I. M., MISCHCHENKO, N. P., DAVYDOVA, V. N., GLAZUNOV, V. P., TARBEEVA, D. V., KRAVCHENKO, A. O., PIMENOVA, E. A. & SOROKINA, I.

V. 2017. Carrageenans-Sulfated Polysaccharides from Red Seaweeds as Matrices for the Inclusion of Echinochrome. *Marine drugs,* 15**,** 337.

ZHENG, Y., LIANG, Y., ZHANG, D., SUN, X., LIANG, L., LI, J. & LIU, Y.-N. 2018. Gelatin-Based Hydrogels Blended with Gellan as an Injectable Wound Dressing. *ACS Omega,* 3**,** 4766-4775.

APPENDICES

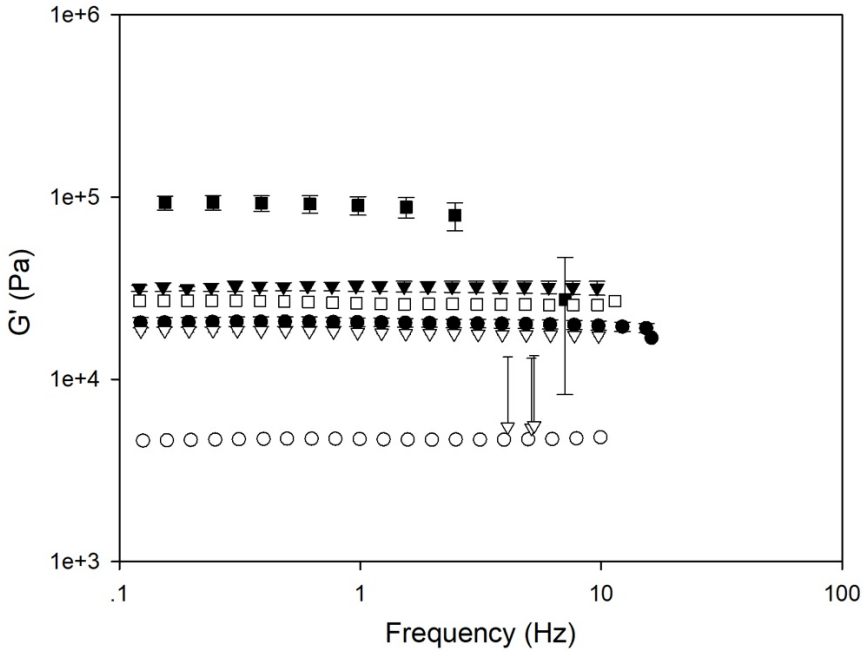

Amplitude sweep of 5 % (w/w) gelatin with 1 (●), 2 (▼) and 3 % (w/w) (■) gellan (closed symbols) and agar (open symbols)

		Temperature (˚C)				
		40	45	50	55	60
Speed (mm/s)	10		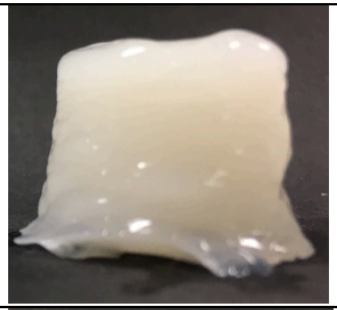	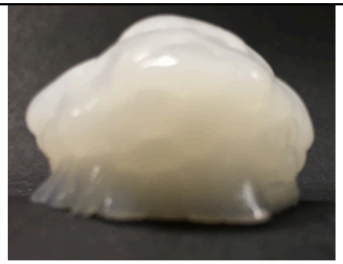	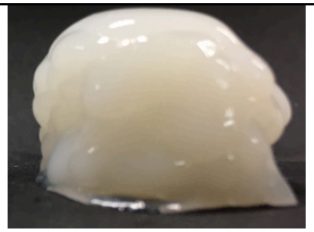	
	25	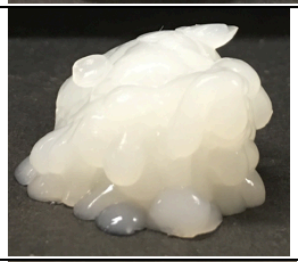				
	50					

Side view images of printed cylinders using a formulation of 5 % (w/w) gelatin with 1 % (w/w) kappa-carrageenan at various printing temperatures and speeds

		Temperature (˚C)				
		40	45	50	55	60
Speed (mm/s)	10			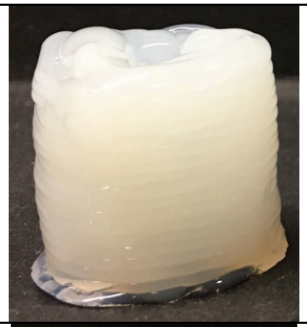	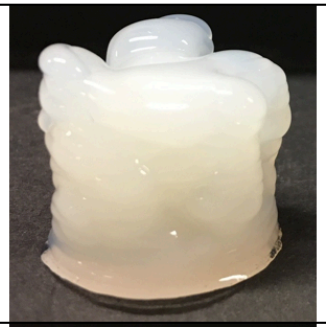	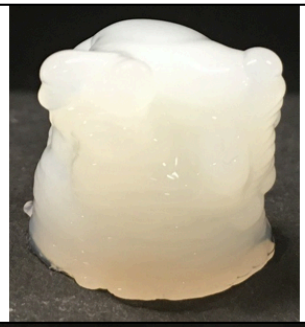
	25					
	50	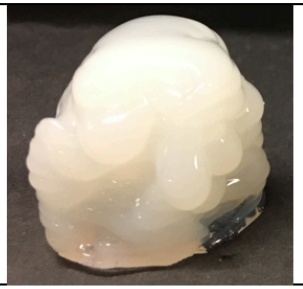		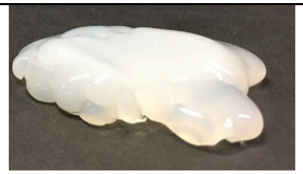		

Side view images of printed cylinders using a formulation of 5 % (w/w) gelatin with 2 % (w/w) kappa-carrageenan at various printing temperatures and speeds

		Temperature (°C)			
		45	50	55	60
Speed (mm/s)	10	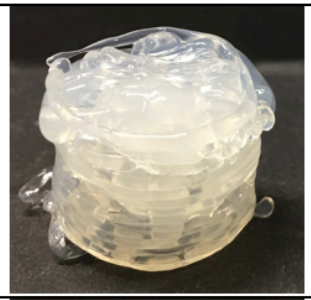	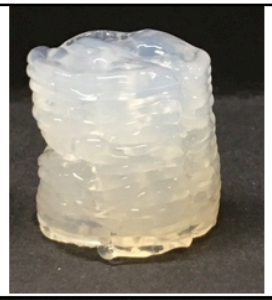	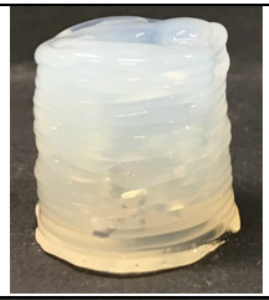	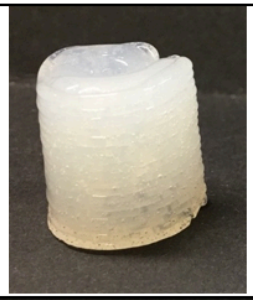
	25	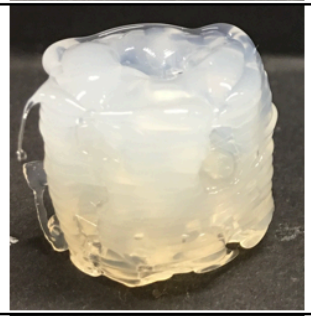	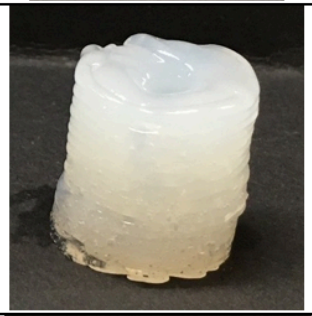	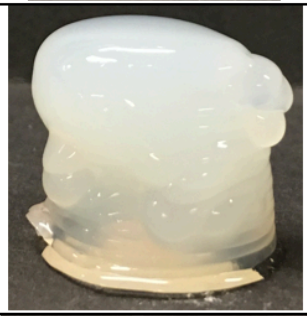	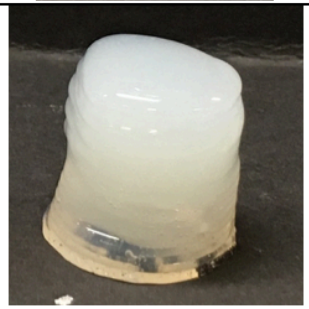
	50	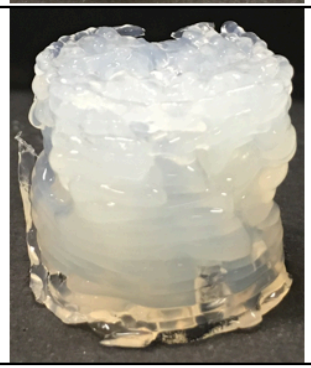			

Side view images of printed cylinders using a formulation of 5 % (w/w) gelatin with 3 % (w/w) kappa-carrageenan at various printing temperatures and speeds

		Temperature (˚C)			
		45	50	55	60
Speed (mm/s)	10	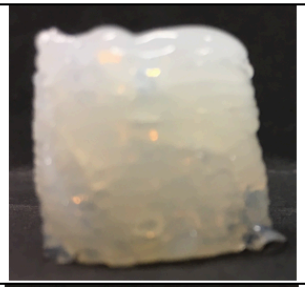		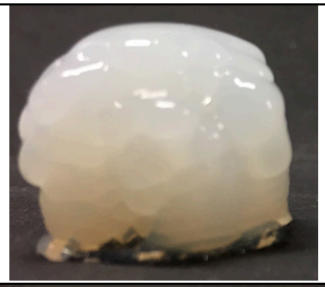	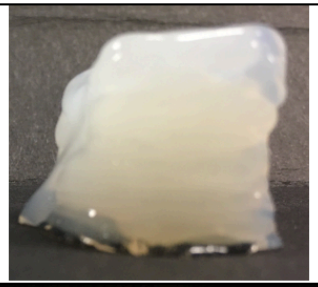
	25	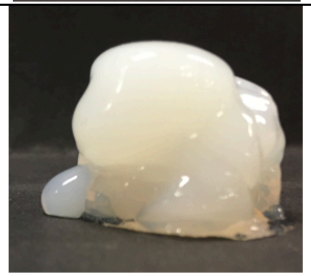	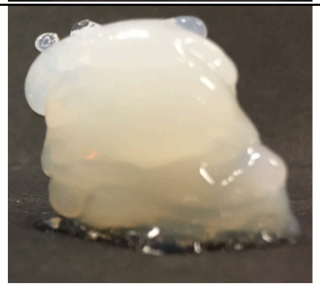		
	50	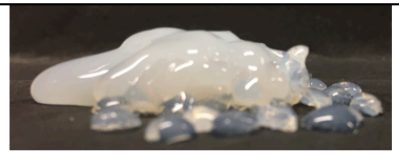		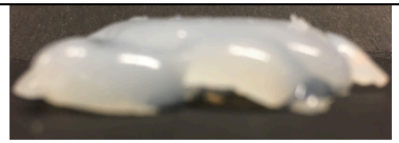	

Side view images of printed cylinders using a formulation of 5 % (w/w) gelatin with 1 % (w/w) gellan at various printing temperatures and speeds

		Temperature (˚C)			
		45	50	55	60
Speed (mm/s)	10	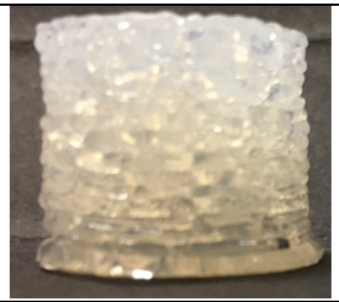	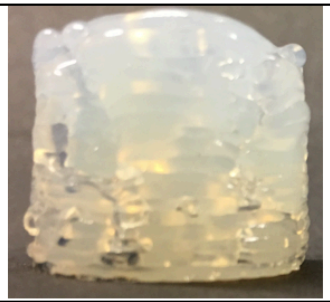	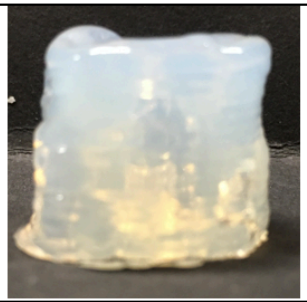	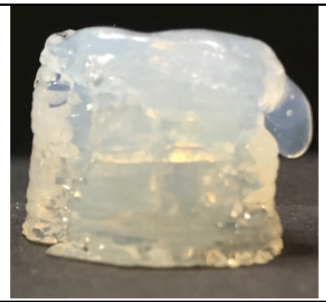
	25	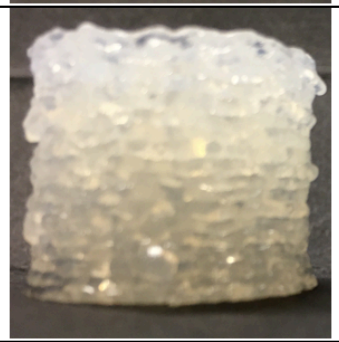		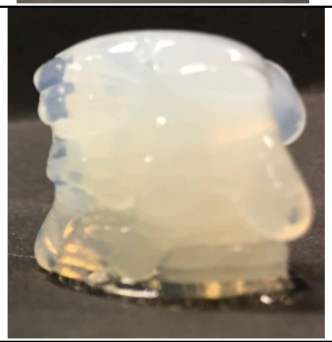	
	50	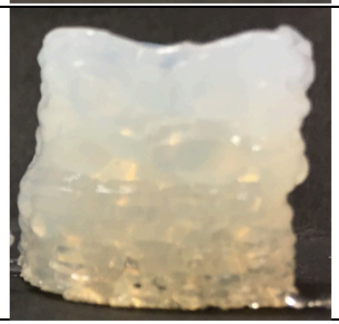		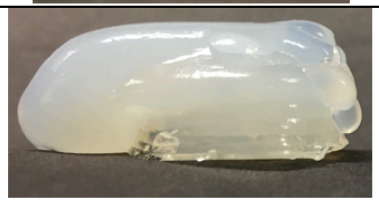	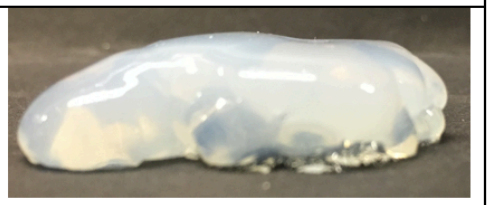

Side view images of printed cylinders using a formulation of 5 % (w/w) gelatin with 2 % (w/w) gellan at various printing temperatures and speeds

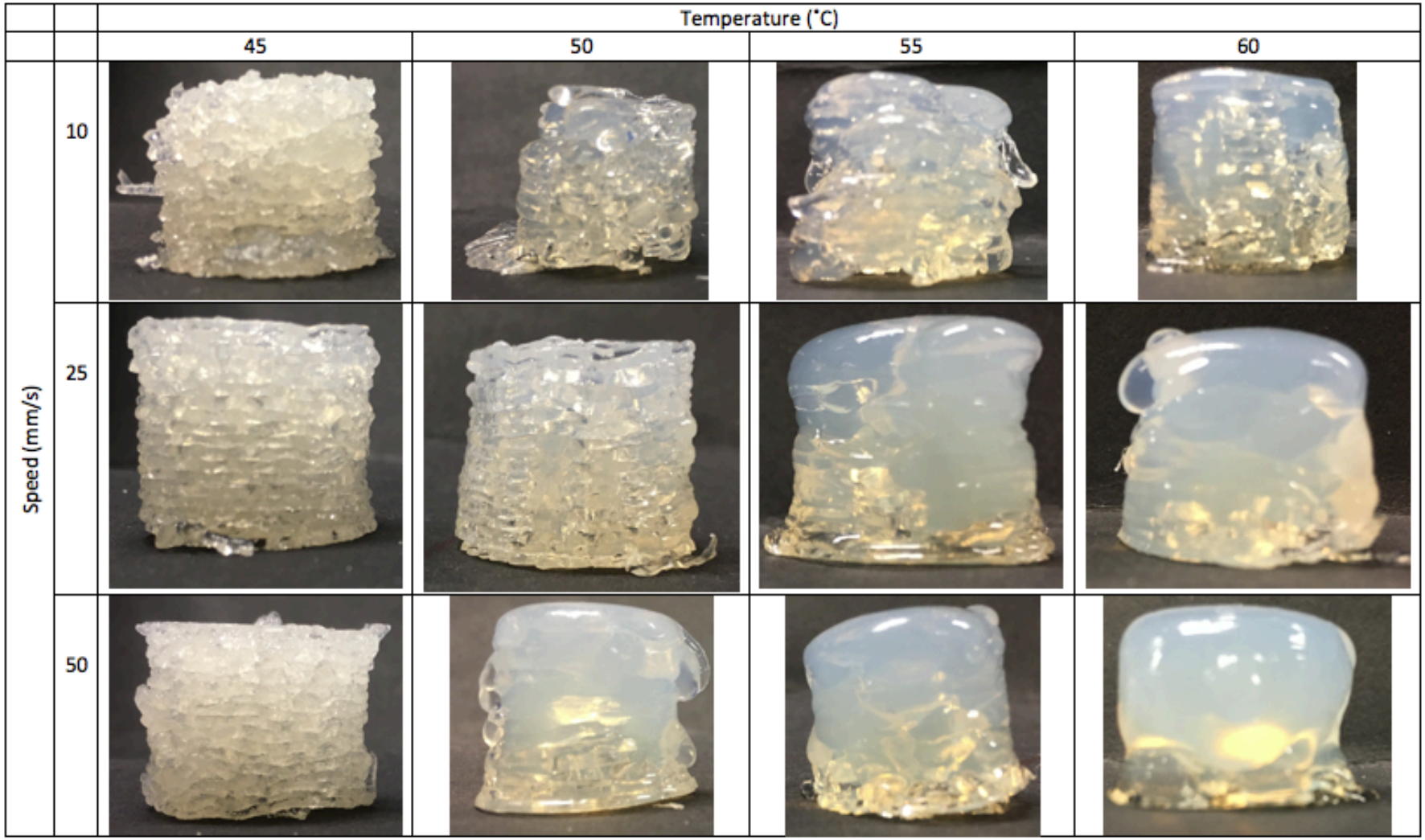

Side view images of printed cylinders using a formulation of 5 % (w/w) gelatin with 3 % (w/w) gellan at various printing temperatures and speeds

		Temperature (°C)		
		45	50	55
Speed (mm/s)	10	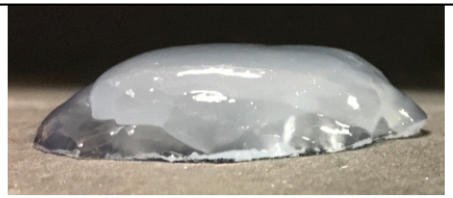	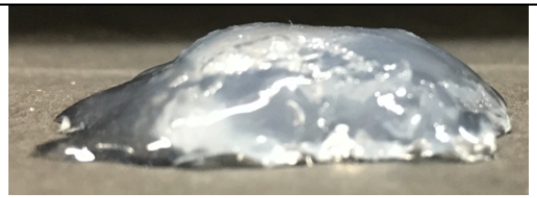	
	25			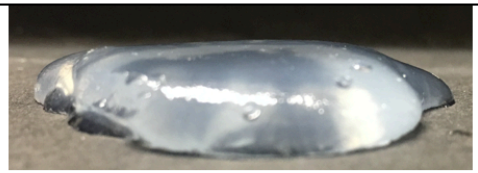
	50		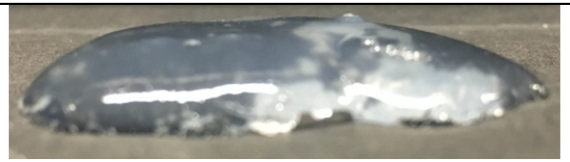	

Side view images of printed cylinders using a formulation of 5 % (w/w) gelatin with 1 % (w/w) agar at various printing temperatures and speeds

		Temperature (˚C)		
		45	50	55
Speed (mm/s)	10		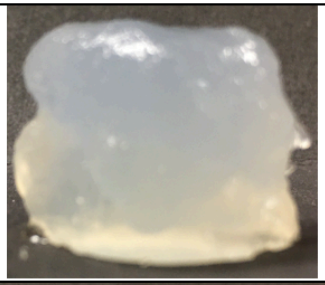	
	25		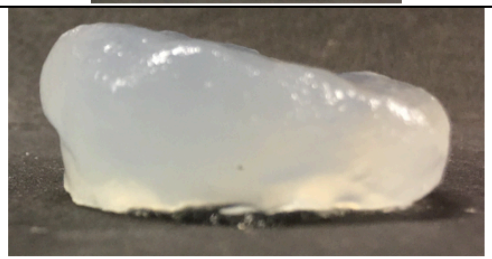	
	50	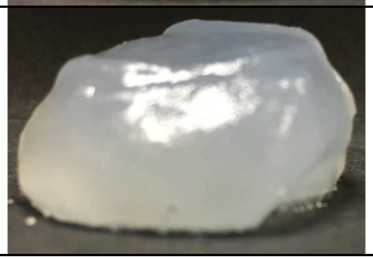		

Side view images of printed cylinders using a formulation of 5 % (w/w) gelatin with 2 % (w/w) agar at various printing temperatures and speeds

		Temperature (°C)		
		45	50	55
Speed (mm/s)	10	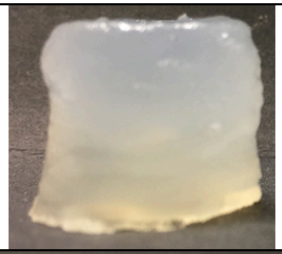		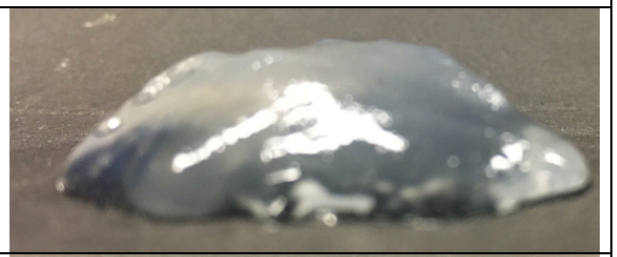
	25		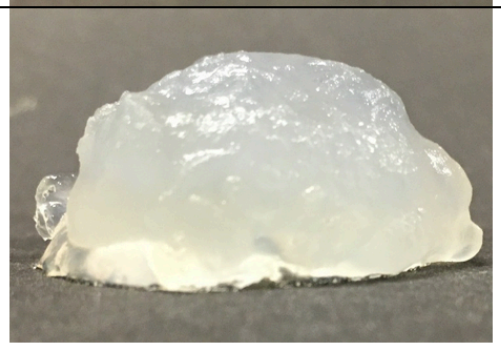	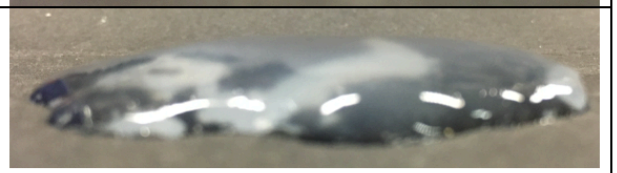
	50	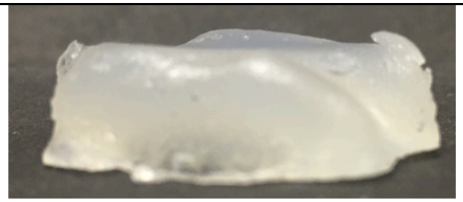	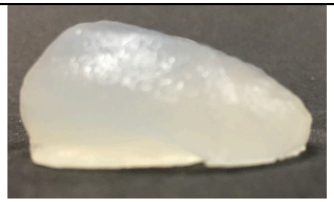	

Side view images of printed cylinders using a formulation of 5 % (w/w) gelatin with 3 % (w/w) agar at various printing temperatures and speeds